Deactivation of SCR catalysts in biomass fired power plants

Olsen, Brian Kjærgaard

Publication date:
2015

Document Version
Peer reviewed version

Deactivation of SCR catalysts in biomass fired power plants

Ph.D. Thesis

Brian Kjærgaard Olsen

Department of Chemical and Biochemical Engineering
Technical University of Denmark

2015

Preface

This thesis is written in accordance with the partial requirements for the Ph.D. degree at the Technical University of Denmark (DTU). The work has been carried out at the CHEC (Combustion and Harmful Emission Control) research center at the Department of Chemical and Biochemical Engineering (KT), DTU, under the supervision by Professor Anker Degn Jensen from KT and Principal Research Engineer Francesco Castellino from Haldor Topsøe A/S (HTAS). The project is a part of the GREEN Research Center (Center for Power Generation from Renewable Energy) which is funded by the former Danish Council for Strategic Research, now Innovation Fund Denmark.

First and foremost, I want to express my sincere gratitude to both of my supervisors for their guidance and input to this work. I am especially grateful to Anker Degn Jensen for his confidence in me and for giving me the opportunity to work on this project. Furthermore, I would like to thank Francesco Castellino for providing me with catalysts and for receiving exposed samples for analysis at HTAS.

For her valuable contribution to the K_2SO_4 exposure campaigns and pellet experiments, I would like to thank Bachelor student Frauke Kügler. I also want to thank Leonhard Schill, from the Department of Chemistry, DTU, for providing me with Hollandite manganese oxide. Likewise, I owe a special thanks to Bente Davidsen and Anna Katerinopoulou, from the microscopy department of HTAS, for carrying out SEM-WDS analysis of numerous samples.

I am grateful to the technical staff at CHEC, especially Anders Tiedje, for assisting me when help was needed.

Finally, thanks to my family, friends and colleagues at CHEC for supporting me during this endeavor.

Brian Kjærgaard Olsen

Kgs. Lyngby, Denmark
April 2015

Summary

In order to meet national and European targets regarding reduction of the emission of greenhouse gases, fossil fuels are gradually being substituted with biomass, such as straw, wood chips and wood pellets, in Danish combined heat and power plants. The release of inorganic elements, present in such biomass fuels, however, causes enhanced strain on the different equipment in these power plants. One of the affected units is the catalyst for selective catalytic reduction (SCR) of nitrogen oxides, which undergoes accelerated deactivation due to deposition of potassium rich particles and subsequent poisoning. The potassium poisoning of commercial vanadia based SCR catalysts have been studied for more than two decades, and a broad understanding have been obtained. However, more detailed information on the overall mechanism of deposition, reaction and transport of potassium, and its function of catalyst composition and operating conditions, is not available. The main objective of the work presented in this thesis has been to conduct an in depth investigation of the deactivation mechanism of vanadia based SCR catalysts, when subjected to potassium rich aerosols. It has furthermore been a goal to suggest and test new alkali resistant catalyst formulations, coatings and/or improved means of operation which can extend the life-time of SCR catalysts in biomass fired power plants.

Plate-type V_2O_5-(WO_3)/TiO_2 SCR catalysts have been exposed to KCl and K_2SO_4 aerosols in a bench-scale reactor at 150, 300 or 350 °C for up to 600 hours. The activity of fresh and exposed catalysts was measured in the temperature range 250-400 °C in a laboratory-scale reactor. All samples exposed for more than 240 hours proved to have deactivated significantly, however, catalysts exposed at 150 °C showed higher remaining activity compared to samples exposed at 300-350 °C. This indicates that the deactivation rate increases with the exposure/operating temperature. The majority of the catalysts exposed to KCl aerosols at high temperatures had lost more than 90 % of their initial activity. Increasing the mode of the mass based KCl particle size distribution, from an aerodynamic diameter of 0.12 to 2.6 μm, showed no effect on the catalyst deactivation rate. This may be attributed to a continued presence of a significant number of ultrafine KCl particles in the flue gas. The K_2SO_4 aerosols caused a slower rate of deactivation compared to the KCl aerosols. This indicates that potassium bound in K_2SO_4 deposits, on the catalyst surface, is less mobile than that bound KCl. However, an effect of particle size on the catalyst deactivation cannot be excluded, as the obtained K_2SO_4 aerosols generally were shifted towards larger particles (mass based distribution mode: 1.3 μm) compared to the KCl aerosols. Activity measurements on the exposed

catalyst plates indicated that WO_3 promoted samples, which in general showed higher NH_3 adsorption capacities, had lost larger fractions of their initial activities compared to unpromoted ones. This is likely due to the enhanced Brønsted acidity which appears to facilitate the transport of potassium in SCR catalysts.

The potassium mobility has further been studied using a new experimental protocol. This involves two-layer pellets of vanadia based SCR catalysts, where one side has been impregnated with KCl or K_2SO_4. SEM-WDS measurements on pellets heat treated at 350 °C showed that potassium bound in KCl readily left its counter ion, causing a faster transport into the undoped catalyst compared to potassium from K_2SO_4. Furthermore, only half of the sulfate bound potassium seemed to be able to leave its solid matrix. These observations are in agreement with the results from the plate exposure experiments. Likewise as indicated by the bench-scale experiments, the presence of WO_3 in the two-layer pellets appeared to facilitate the potassium transport. The potassium blocking abilities of potential coating materials have been tested using three-layer pellets. Here, layers of MgO, sepiolite, a mixture of the two, or Hollandite manganese oxide have been introduced in between the two (respectively potassium impregnated and undoped) catalyst layers. Pure MgO proved to be the most effective barrier of the tested candidates, and was able to retain the potassium in the impregnated side of the pellet, even after 7 days of exposure at SCR conditions. Partial or full potassium penetration of layers of the other tested materials was observed.

Half-length monoliths have been exposed to KCl aerosols in the bench-scale setup at 350 °C for up to 1100 hours, and their activities were followed by *in situ* measurements. A $3\%V_2O_5$-$7\%WO_3/TiO_2$ reference catalyst deactivated with a rate of 0.91 %/day during 960 hours of exposure, and a subsequent SEM-EDS analysis showed complete potassium penetration of the catalyst wall with average K/V molar ratios of 0.38-0.51. During 1100 hours of exposure, a similar monolith coated with 8.06 wt.% MgO deactivated with a rate of 0.24 %/day, relative to the fresh activity of the reference, but showed a 42 % lower start activity due to enhanced transport limitations. The MgO coat proved to have protected the SCR catalyst against potassium poisoning, however, SEM-EDS analysis showed that some potassium had penetrated the coat. The SEM analysis also indicated that the MgO coat was rather fragile and adhered weakly to the catalyst substrate, indicating the need for a binder material. A catalyst coated with a 1:1 mixture of MgO and TiO_2 showed insufficient start activity (30 % of that of the reference) when tested in the bench-scale setup, likely due to a low porosity of the coat.

A deactivation model describing the potassium poisoning of an SCR monolith catalyst has been derived. The model accounts for deposition and consumption of potassium rich particles on the external catalyst surface, the build-up of potassium, bound to Brønsted acid sites, throughout the catalyst wall, and the resulting loss in SCR activity. Simulations show that the particle deposition rate, and hence the deactivation rate, decreases if the particle size of the incoming aerosol is increased.

The results obtained in this work indicate that the life-time of SCR catalysts used in biomass fired power plants can be improved by ensuring a high conversion of KCl to K_2SO_4 aerosols, by reducing the operating temperature, and by increasing the size of the incoming, potassium rich aerosol particles to above 200 nm. While it may not be mechanically durable in its current state of development, applying an MgO coat to the SCR catalyst will also protect it against potassium poisoning.

Resumé (Summary in Danish)

I danske kraftvarmeværker bliver fossile brændsler i stigende grad udskiftet med biomasse såsom halm, træflis og træpiller, for at opfylde nationale og europæiske mål for reduktion af udledningen af drivhusgasser. Frigivelsen af uorganiske elementer, som findes i disse biobrændsler, medfører imidlertid øget belastning af diverse udstyr i kraftværkerne. En af de berørte enheder er katalysatoren til selektiv katalytisk reduktion (SCR) af kvælstofoxider, som undergår accelereret deaktivering på grund af aflejring af kaliumholdige partikler og efterfølgende forgiftning. Kaliumforgiftning af kommercielle SCR katalysatorer, baseret på vanadiumpentaoxid, er blevet studeret i mere end to årtier, og en bred forståelse er opnået herigennem. Mere detaljerede oplysninger om den overordnede mekanisme for aflejring, reaktion og transport af kalium, og dennes afhængighed af katalysatorsammensætning og driftsbetingelser, er dog ikke tilgængelige. Hovedformålet med arbejdet præsenteret i denne afhandling har været at foretage en dybtgående undersøgelse af deaktiveringsmekanismen for vanadiumpentaoxid-baserede SCR-katalysatorer, når disse udsættes for kaliumholdige aerosoler. Det har endvidere været et mål at foreslå og afprøve nye alkaliresistente katalysatorformuleringer, belægninger og/eller forbedrede driftsbetingelser, som kan forlænge levetiden af SCR-katalysatorer i biomassefyrede kraftværker.

V_2O_5-(WO_3)/TiO_2 SCR pladekatalysatorer blev eksponeret mod KCl- og K_2SO_4-aerosoler i en pilot-skala reaktor ved 150, 300 eller 350 °C i op til 600 timer. Aktiviteten af friske og eksponerede katalysatorer blev målt i temperaturområdet 250-400 °C i en laboratorie-skala reaktor. Alle prøver som var blevet eksponeret i mere end 240 timer havde deaktiveret betydeligt, men katalysatorer eksponeret ved 150 °C havde højere tilbageværende aktivitet sammenlignet med prøver eksponeret ved 300-350 °C. Dette indikerer, at deaktiveringshastigheden stiger med eksponerings/ driftstemperaturen. Størstedelen af de katalysatorer som blev udsat for KCl-aerosoler ved høj temperatur havde mistet mere end 90 % af deres oprindelige aktivitet. En forøgelse af modus for den massebaserede KCl-partikelstørrelsesfordeling, fra en aerodynamisk diameter på 0.12 til 2.6 µm, havde ingen indflydelse på deaktiveringshastigheden. Dette kan skyldes en fortsat tilstedeværelse af et betydeligt antal ultrafine KCl-partikler i røggassen. K_2SO_4-aerosolerne forårsagede en langsommere deaktivering sammenlignet med KCl-aerosolerne. Dette indikerer, at kalium bundet i K_2SO_4-aflejringer på katalysatoroverfladen er mindre mobilt end det bundet i KCl. Dog kan en effekt af partikelstørrelse på katalysatordeaktiveringen ikke udelukkes, da de dannede K_2SO_4-aerosoler generelt var forskudt mod større partikler (massebaseret fordelingsmodus: 1.3 µm)

sammenlignet med KCl-aerosolerne. Aktivitetsmålinger på de eksponerede pladekatalysatorer indikerede, at WO_3-holdige prøver, der generelt udviste højere NH_3-adsorptionskapacitet, havde mistet en større del af deres oprindelige aktivitet sammenlignet med WO_3-fri katalysatorer. Dette skyldes sandsynligvis den forøgede Brønsted-surhed som synes at fremme transporten af kalium i SCR-katalysatorer.

Kaliummobiliteten blev yderligere undersøgt ved anvendelse af en ny forsøgsprotokol. Denne involverer to-lags-piller af vanadiumpentaoxid-baserede SCR-katalysatorer, hvor den ene side er blevet imprægneret med KCl eller K_2SO_4. SEM-WDS-målinger på piller varmebehandlet ved 350 °C viste, at kalium bundet i KCl hurtigt forlod sin mod-ion, hvilket medførte en hurtigere transport ind i det uinprægnerede katalysatorlag sammenlignet med kalium fra K_2SO_4. Endvidere syntes kun halvdelen af det sulfatbundne kalium at være i stand til at forlade sin faststofmatrice. Disse observationer er i overensstemmelse med resultaterne fra plade-eksponeringsforsøgene. Tilstedeværelsen af WO_3 i to-lags-pillerne lod til at fremme kaliumtransporten, ligeledes som indikeret af pilot-forsøgene. Potentielle belægningsmaterialers evne til at skærme mod kalium blev testet ved brug af tre-lags-piller. Her blev lag af MgO, sepiolit, en blanding af de to, eller Hollandit manganoxid ført ind mellem de to (hhv. kaliumimprægneret og kaliumfri) katalysatorlag. Ren MgO viste sig at være den mest effektive barriere ud af de testede kandidater, og var i stand til at tilbageholde kalium i den imprægnerede side af pillen, selv efter 7 dages eksponering ved SCR-betingelser. Delvis eller fuld kaliumgennemtrængning blev observeret i de andre testede materialer.

Monolitter af halv længde blev eksponeret mod KCl-aerosoler i piloten ved 350 °C i op til 1100 timer, og deres aktiviteter blev fulgt med *in situ* målinger. En $3\%V_2O_5$-$7\%WO_3/TiO_2$ referencekatalysator deaktiverede med en hastighed på 0.91 %/dag i løbet af 960 timers eksponering, og en efterfølgende SEM-EDS-analyse viste fuldstændig kaliumgennemtrængning af katalysatorvæggen med gennemsnitlige K/V molforhold på 0.38-0.51. En lignende monolit, belagt med 8.06 vægt% MgO, deaktiverede med en hastighed på 0.24 %/dag, i forhold referencens friske aktivitet, i løbet af 1100 timers eksponering. Denne udviste dog en 42 % lavere startaktivitet på grund af øgede transportbegrænsninger. Selvom MgO-belægningen havde beskyttet SCR-katalysatoren mod kaliumforgiftning, viste en SEM-EDS analyse, at noget kalium var trængt gennem belægningen. SEM-analysen antydede også, at MgO-belægningen var temmelig skrøbelig og bandt svagt til katalysatoren. Dette indikerer et behov for et bindemiddel. En katalysator belagt

med en 1:1 blanding af MgO og TiO_2 udviste en utilstrækkelig startaktivitet (30 % af referencens), under test i piloten, angiveligt som følge af en lav porøsitet af belægningen.

En deaktiveringsmodel, der beskriver kaliumforgiftningen af en SCR-monolitkatalysator, er blevet udledt. Modellen redegør for aflejring og forbrug af kaliumrige partikler, på den ydre katalysatoroverflade, ophobning af Brønsted-syrebundet kalium gennem katalysatorenvæggen, og det deraf følgende tab i SCR-aktivitet. Modelsimuleringer viser, at partikelafsætningshastigheden, og dermed deaktiveringshastigheden, falder, hvis partikelstørrelsen af den indkommende aerosol øges.

Resultaterne opnået i dette arbejde indikerer, at levetiden af SCR-katalysatorer, der anvendes i biomassefyrede kraftværker, kan forbedres ved at sikre en høj omdannelse af KCl- til K_2SO_4-aerosoler, ved at sænke driftstemperaturen, og ved at øge størrelsen af de indkommende, kaliumholdige aerosolpartikler til over 200 nm. En MgO-belægning kan også beskytte SCR-katalysatoren mod kaliumforgiftning, selvom den, på sit nuværende udviklingsstadie, måske ikke er mekanisk holdbar.

Table of contents

Nomenclature

$A_{p,i}$ = total projected area of deposited particles from size class *i* [m^2]

A_{surf} = external catalyst surface area [m^2]

C_c = Cunningham slip correction factor

C_i = gas phase concentration of component *i* [mol/m^3]

C_{K} = surface concentration of potassium [mol/m^2]

$C_{\mathrm{K},p,i}$ = surface concentration of potassium bound in particles from size class *i* [mol/m^2]

C_{OH} = surface concentration of Brønsted sites [mol/m^2]

d = distance [m]

d_h = hydraulic diameter [m]

d_p = particle diameter [m]

$d_{p,a}$ = aerodynamic particle diameter [m]

$d_{p,i}$ = diameter of particle from size class *i* [m]

D_{AB} = binary diffusivity of component A in B [m^2/s]

$D_{e,i}$ = effective diffusivity of component *i* [m^2/s]

$D_{K,j,i}$ = Knudsen diffusivity of component *i* in pore system *j* [m^2/s]

D_i = diffusivity of component *i* [m^2/s]

D_j = diffusivity of component *i* in pore system *j* [m^2/s]

$D_{p,i}$ = diffusivity of particles in size class *i* [m^2/s]

D_s = surface diffusion coefficient of potassium [m^2/s]

E_a = activation energy [J/mol]

F_{gas} = volumetric gas flow rate [m^3/s]

ΔH_{ad} = enthalpy of adsorption [J/mol]

k' = pseudo first order rate constant [$m^3/kg/s$]

k_0 = pre-exponential factor [1/s]

k_0' = pseudo first order rate constant of fresh catalyst [$m^3/kg/s$]

$k_{g,i}$ = mass transfer coefficient of component *i* [m/s]

$k_{\mathrm{K_2SO_4}}$ = rate constant for the reaction between K_2SO_4 and -M-OH sites [1/s]

k_{KCl} = rate constant for the reaction between KCl and -M-OH sites [1/s]

$k_{\mathrm{KHSO_4}}$ = rate constant for the reaction between $KHSO_4$ and -M-OH sites [1/s]

$k_{p,i}$ = mass transfer coefficient of particles in size class *i* [m/s]

k_r = intrinsic rate constant [m^3/kg/s]

k_s = intrinsic rate constant [1/s]

K_0 = pre-exponential factor [m^3/mol]

K_{NH_3} = NH_3 adsorption equilibrium constant [m^3/mol]

Kn = Knudsen number

L = monolith channel length [m]

m_{cat} = catalyst mass [kg]

M = mass based aerosol concentration [kg/Nm^3]

M_i = molar mass of component *i* [kg/mol]

N = number based aerosol concentration [#/Nm^3]

N_A = Avogadro's number ($6.02214 \cdot 10^{23}$) [1/mol]

N_i = molar flux of component *i* [mol/m^2/s]

$N_{p,i}$ = flux of particles in size class *i* [#/m^2/s]

P = pressure [Pa]

$r_{c,j}$ = pore radius in pore system *j* [m]

$-r_i$ = reaction rate of component *i* [mol/kg/s]

$-r_i'$ = reaction rate of component *i* [mol/m^3/s]

R = gas constant (8.31447) [J/mol/K]

Re = Reynolds number

S_{surf} = internal volume specific surface area [m^2/m^3]

$Sc_{p,i}$ = Schmidt number of particles in size class *i*

Sh = Sherwood number

$Sh_{p,i}$ = Sherwood number of particles in size class *i*

t = time [s] or [h]

T = temperature [°C] or [K]

U = gas velocity [m/s]

$V_{m,KCl}$ = molar volume of KCl [m^3/mol]

$V_{p,i}$ = volume of particle from size class *i* [m^3]

V/S = half thickness of monolith wall [m]

w_i = mass fraction of component *i*

W_i = concentration of particles in size class *i* [#/m^3]

X_{NO} = conversion of NO

x = radial distance [m]

y_i = mole fraction of component *i*

z = axial distance [m]

Greek letters

α_f = flux ratio

ε = catalyst porosity

ε_j = volume fraction of pore system *j*

ϵ_{AB} = Lennard-Jones parameter (geometric mean) [J]

ϵ_i = Lennard-Jones parameter [J]

η_g = flue gas viscosity [Pa·s]

$\eta_{overall}$ = overall effectiveness factor

κ = Boltzmann's constant ($1.38 \cdot 10^{-23}$) [J/K]

λ = mean free path of air

$\Omega_{D,\mathrm{AB}}$ = collision integral

ρ_{cat} = catalyst density [kg/m^3]

ρ_g = gas density [kg/m^3]

σ_{AB} = collision diameter [Å]

σ_i = molecular radius of component *i* [Å]

φ = fraction of available Brønsted sites

Accents

~ = dimensionless

Subscripts

∞ = asymptotic

b = bulk

obs = observed

ref = reference

s = surface

Superscripts

* = dimensionless

0 = initial/inlet

ads = adsorbed

ss = steady-state

1. Introduction

1.1. Background

The European Union has defined a set of main climate and energy targets to be reached by 2020 – the so called "20-20-20" targets. These involve a reduction of the greenhouse gas emissions to 20 % below the 1990 levels, an increase in the share of the energy consumption produced from renewable recourses to 20 %, and a 20 % increase in the energy efficiency [1]. In order to meet these targets, Denmark is obligated to have renewable energy to account for more than 30 % of the final energy consumption by 2020 [2]. This requires an increase in the production of wind power as well as a transition from the use of fossil fuels, such as coal, oil and natural gas, to alternative fuels such as biomass (straw, wood chips, etc.), waste and biogas. On a short term, one of the most effective ways of utilizing biomass is to use it as fuel in the already existing, highly efficient combined heat and power plants.

As the supply of biomass may vary within a diverse range of organic, plant-based substances, a 100 % bio-dust fired power plant needs to have high fuel flexibility. Furthermore, the energy efficiency should be comparable to that of coal firing in order to be competitive. The use of biomass in the current heat and power plants, which were initially designed specifically for coal firing, introduces a range of challenges closely related to the properties of the biomass, which are very different from those of coal. These challenges include various combustion related issues, as well as a range of fly ash related problems such as increased deposit formation, corrosion of super heater surfaces and accelerated deactivation of the catalyst for selective catalytic reduction of nitrogen oxides.

Selective catalytic reduction (SCR) of nitrogen oxides (NO_x) with ammonia (NH_3) is a well established method for controlling the NO_x emissions from stationary sources such as coal fired heat and power plants [3,4]. Unfortunately, alkali and alkaline earth metals, which can be present in biomass in high concentrations (e.g. about in 1 wt.% cereal straw) [5], may act as poisons to the vanadia (V_2O_5) based, industrially applied SCR catalysts and can reduce their life-time dramatically, especially when the catalysts are used in high-dust configuration [6]. Potassium, released e.g. during firing of straw, may form submicron aerosols of potassium chloride (KCl) and/or potassium sulfate (K_2SO_4) [7,8] which can deposit on the external catalyst surface. Likely by titration of -V-OH sites and subsequent surface diffusion, potassium can reach in interior of the

catalyst. While the effect of potassium on commercial SCR catalysts is generally well understood, a detailed understanding of the overall mechanism for the deposition and transport of potassium is not available.

1.2. Objectives

The overall objective of the work presented in this thesis has been to conduct an in depth investigation of the deactivation mechanism of vanadia based SCR catalysts, when subjected to aerosols of KCl or K_2SO_4. This involves a study of the influence of catalyst composition on the deactivation rate, in an attempt to clarify the role of the -OH sites, as well as the influence of the operation temperature and of the characteristics of the incoming aerosol. It has furthermore been a goal to use the improved understanding to suggest and test new catalyst formulations or coatings, and/or improved means of operation, in order to extend the lifetime of SCR catalysts used in biomass fired power plants.

The experimental work has consisted of both bench-scale and lab-scale experiments. A bench-scale setup has been used to expose V_2O_5-(WO_3)/TiO_2 plate-type SCR catalysts to aerosols of KCl and K_2SO_4 under realistic SCR operating conditions, while the catalytic activity of fresh and exposed catalysts have been measured in a lab-scale reactor. Through this work, which is presented in section 4, it has been possible to study the potassium poisoning of SCR catalysts as a function of exposure temperature and catalyst composition. The work on plate-type catalysts constitutes a part of an article manuscript, found in Appendix A, to be submitted for publication.

In order to study the potassium mobility in SCR catalysts as a function of catalyst composition as well as operating temperature, a new experimental protocol have been developed. This involves pellets consisting of two layers of SCR catalysts, where one layer has been impregnated with a potassium salt (KCl or K_2SO_4). After treatment at SCR conditions for a given period of time, the pellets are analyzed by wavelength dispersive X-ray spectroscopy. By looking at how potassium has moved from the impregnated layer into the other (undoped) layer, detailed information on the rate of potassium diffusion in SCR catalysts can be obtained. This experimental method has also been applied to test materials (magnesium oxide, sepiolite and Hollandite manganese oxide) which potentially may act as diffusion barriers for potassium, by introducing a third pellet layer in between the catalyst layers. Ultimately, such materials may be used as a coatings for traditional SCR catalysts, enhancing their alkali resistance (and hence their life-time) when used in biomass fired power plants. The work conducted on these multi-layer pellets is presented in section 5. The first

part of this work, involving the two-layer pellets, is furthermore reported in the article manuscript in Appendix A.

Section 6 reports a work in which two coated 3%V_2O_5-7%WO_3/TiO_2 monoliths (one coated with magnesium oxide and one coated with a mixture of magnesium oxide and titania) have been exposed to KCl aerosols in the bench-scale setup. By following the deactivation using *in situ* activity measurements, the performance of the coated catalysts, with respect to SCR activity as well as alkali resistance, is compared to that of an uncoated reference monolith, which has undergone the same treatment. The potassium uptake of exposed catalysts has been measured by inductively coupled plasma optical emission spectrometry and energy dispersive X-ray spectroscopy.

Another objective of this Ph.D. project has been to develop a model, based on the experimental investigations, which can help predicting the activity loss of SCR catalysts exposed to potassium rich aerosol at given conditions. The work regarding the development of such a deactivation model is reported in section 7.

2. Literature survey

2.1. Introduction

This section consists of a short introduction of the SCR process as well a literature survey on deactivation of SCR catalysts for stationary applications. While the various routes of deactivation are touched upon, the main emphasis is put on poisoning of SCR catalysts by alkali and alkaline earth metals, and the numerous studies on this issue which have been carried out over the past decades. Recent studies on alternative, alkali resistant catalyst are also addressed.

2.2. The selective catalytic reduction of NO_x by NH_3

2.2.1. General

The selective catalytic reduction of NO_x by NH_3 is one of the most widely applied secondary measures for limiting the NO_x emission from stationary sources [4]. In the presence of oxygen (O_2), the overall reactions considered in the SCR process, which is typically carried out at temperatures between 300 and 400 °C, are given as follows [9]:

$$4NO + 4NH_3 + O_2 \rightarrow 4N_2 + 6H_2O \quad (2.1)$$

$$2NO_2 + 4NH_3 + O_2 \rightarrow 3N_2 + 6H_2O \quad (2.2)$$

Typically, most of the NO_x in the flue gas will be in the form of nitrogen monoxide (NO, around 95 %), thus only reaction 2.1 is generally considered [3]. Unwanted side reactions are the direct oxidation of ammonia into molecular nitrogen (N_2), nitrogen oxide or nitrous oxide [9]:

$$4NH_3 + 3O_2 \rightarrow 2N_2 + 6H_2O \quad (2.3)$$

$$4NH_3 + 5O_2 \rightarrow 4NO + 6H_2O \quad (2.4)$$

$$2NH_3 + 2O_2 \rightarrow N_2O + 3H_2O \quad (2.5)$$

The selectivity of SCR catalysts refers to their ability to favor the catalysis of the NO_x reduction rather than the oxidation of ammonia. During firing of sulfur rich fuels, sulfur dioxide (SO_2) will be released to the flue gas. This may lead to another unwanted side reaction over the catalyst – the oxidation of sulfur dioxide to sulfur trioxide (SO_3), which is catalyzed by vanadia [10- 13]:

$$SO_2 + ½O_2 \rightarrow SO_3 \quad (2.6)$$

In the presence of water (H_2O), the formed SO_3 may react with unreacted ammonia forming ammonium bisulfate (NH_4HSO_4). Below 300 °C condensation of NH_4HSO_4 may either deposit in the catalyst pores, causing plugging and deactivation, or on downstream equipment, causing corrosion [10-15].

2.2.2. Catalysts

Catalyst systems consisting of V_2O_5 supported on the anatase form of titania (TiO_2), typically promoted with tungsten oxide (WO_3) or molybdenum oxide (MoO_3) [16,17], have proved to be very active in the selective catalytic reduction of NO_x in a wide temperature range around 400 °C [3], and are the most widely used catalyst systems for removal of NO_x from stationary sources. In these catalysts, V_2O_5 is regarded as the active phase while WO_3 or MoO_3 serves to increase the surface acidity, selectivity as well of the stability of the system [16,18-20], however, higher activities of ternary systems (V, W and Ti), compared to binary systems (V and Ti) have also been reported [21-23]. The V_2O_5 loading in commercial catalyst can vary, but is typically below 2 wt.%. This relatively low loading of the active component is applied in order to minimize the undesired oxidation of SO_2 to SO_3 [10,16,22]. When used in biomass fired applications, the V_2O_5 content can be higher due to the lower SO_2 content in the flue gas [24]. Depending on the loading, supported vanadium oxide can exist as several different species on the support. These include [25,26]:

- isolated vanadium species
- dimeric or polymeric species
- two-dimensional vanadium oxide layer
- three-dimensional vanadium oxides, crystalline or amorphous of nature
- mixed metal oxide with the support

The best catalysts have proved to be those that contain well dispersed vanadium oxide and tungsten oxide (or molybdenum oxide), i.e. less than a monolayer, on the support. A monolayer is defined at the maximum amount of amorphous or two-dimensional vanadia in contact the oxide support [27]. For a sub-monolayer coverage of vanadia, the vanadium oxide will be present as monomeric vanadyl and polymeric vanadate species [16,28,29]. The polymeric species have been reported more reactive than the monomeric, and the fraction of polymeric species increases upon increasing V_2O_5 loading until the point where three-dimensional species (e.g. V_2O_5 crystallites) start to form,

that is, when monolayer coverage is exceeded [29]. For V_2O_5 supported on TiO_2, a monolayer typically corresponds to a surface concentration of about 7-10 V atoms per nm^2 [25,30-32].

Even though TiO_2 has poor SCR activity by its own, the anatase form of TiO_2 is preferred as support due to its high surface area, which secures a high dispersion of the active phase. The anatase form of TiO_2 is, however, thermodynamically unstable and tends to convert into rutile, which has a much lower specific surface area [33]. In fact, V_2O_5 even promotes the anatase-to-rutile transformation (rutilization) as well as sintering of anatase [34,35]. The addition of WO_3 or MoO_3 helps preserving the surface area by stabilizing the anatase phase and preventing the sintering process. In V_2O_5-WO_3/TiO_2 systems, up to 10 wt.% WO_3 is typically used [16].

2.2.3. Reaction mechanism

Based on *in situ* Fourier transform infrared spectroscopy (FTIR), Topsøe *et al*. [36-38] proposed the following widely accepted mechanism for the SCR reaction over TiO_2 supported V_2O_5 catalysts:

$$NH_3 + V^{5+}OH \rightleftarrows V^{5+}ONH_4 \quad (2.7)$$

$$V^{5+}ONH_4 + V^{5+}{=}O \rightleftarrows V^{5+}ONH_3^+V^{4+}OH \quad (2.8)$$

$$V^{5+}ONH_3^+V^{4+}OH + NO \rightarrow N_2 + H_2O + V^{5+}OH + V^{4+}OH \quad (2.9)$$

$$2V^{4+}OH \rightarrow H_2O + V^{3+} + V^{5+}{=}O \quad (2.10)$$

$$O_2 + 2V^{3+} \rightarrow 2V^{5+}{=}O \quad (2.11)$$

$$H_2O + V^{5+}OH \rightleftarrows V^{5+}OH_3O \quad (2.12)$$

Ammonia is adsorbed on V^{5+}-OH sites, which are generally associated with Brønsted acid sites (reaction 2.7), and the adsorbed ammonia is then activated by vanadyl species (V^{5+}=O) (reaction 2.8). The activated ammonia complex reacts with gaseous or weakly adsorbed NO to form molecular nitrogen, water as well as the reduced species V^{4+}-OH (reaction 2.9). This step is unlikely an elementary step since the reverse reaction is improbable. For this reason, the reaction with NO is assumed to be irreversible. Reduced hydroxyl surface species are partly re-oxidized to vanadyl by reaction 2.10. This step might be reversible at high water partial pressures; however, at industrial SCR conditions the catalyst is fully oxidized. The re-oxidation of the catalyst by gaseous oxygen is accounted for in reaction 2.11. Finally, reaction 2.12 describes the competitive adsorption of water

[38]. The proposed mechanism can be shown schematically in two catalytic cycles – an acid and a redox cycle, as illustrated in Figure 2.1:

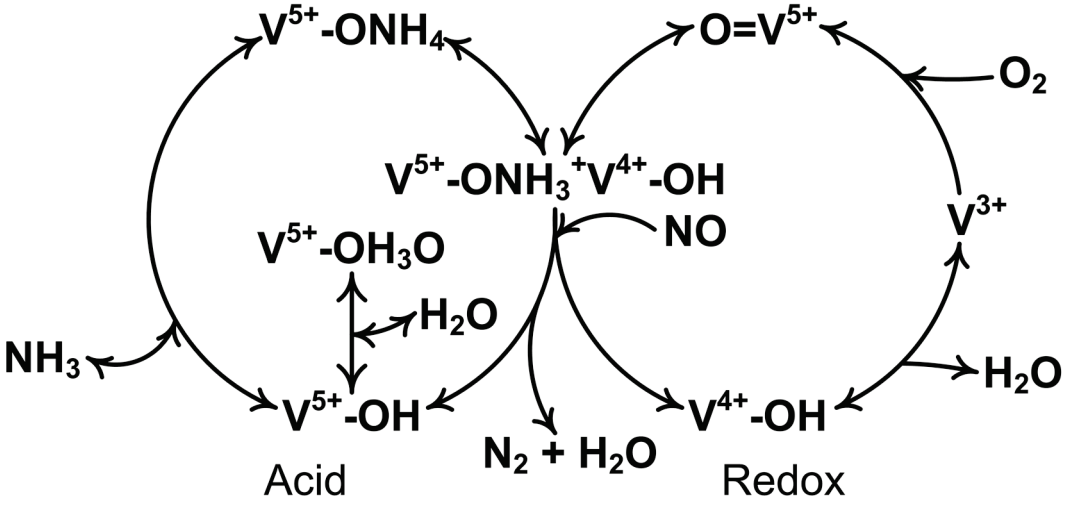

Figure 2.1: The proposed mechanism for the reduction of NO by NH_3 over V_2O_5 based catalysts. Adapted from [38].

Reaction 2.7 and 2.12 constitute the acid part of the cycle while reactions 2.10 and 2.11 make up the redox part. The two parts are coupled by reaction 2.8 and 2.9.

2.3. Deactivation of SCR catalysts

2.3.1. General

During operation, a catalyst will gradually lose some or all of its activity and/or selectivity due to various factors regarding the environment in which it is operated. This phenomenon is generally referred to as catalyst deactivation, and can be chemical or physical of nature. A catalyst may deactivate steadily over several years or within a few seconds. An example of the latter is the catalyst for fluid catalytic cracking of oil which deactivates rapidly due to formation of coke. This catalyst is, however, regenerated continuously by burning off the deposited coke [39]. For processes where replacement or regeneration of the catalyst is costly, vast effort should be put in the development of resistant catalysts and/or optimization of the process conditions. This generally requires knowledge on the cause and mechanism of the deactivation. The several means of deactivation can roughly be categorized into poisoning, fouling, sintering and phase transformation [40].

Catalyst poisoning is the strong chemisorption of components in the reaction mixture i.e. reactants, products or feed impurities. The poisoning effect of an adsorbed species can be due to occupation of

active sites, or by altering the nature of the catalyst surface. If the poison adsorbs uniformly over the entire catalyst surface, it is said to be non-selective. In this case, the activity loss will be proportional to the amount of adsorbed poison. A selective poison, on the other hand, prefers certain active sites over others (e.g. the most active sites), which may lead to a more complicated correlation between the loss of activity and amount of adsorbed poison.

Fouling is the physical blockage of the catalyst surface or pores caused by deposition of solid or liquid components from the fluid phase. Fouling hinders the reactants from reaching the active sites (and the products from leaving them), thereby causing a loss in observed activity. Extensive fouling may also cause an increased pressure drop over the catalytic unit.

Sintering is the loss of active surface area by agglomeration and coalescence of small crystallites into larger ones. The sintering process typically occurs at elevated temperatures, e.g. above 500 °C, and is usually accelerated in the presence of water vapor.

Phase transformation is the change from one crystalline phase to another. This could be a change of a catalytic active phase to an inactive one, or the change of a high surface area support phase, to one with a significantly lower surface area. As for sintering, phase transformation usually occurs at elevated temperatures [39-41].

Other routes of deactivation are the loss of active material by attrition, erosion or formation and vaporization of volatile compounds. For SCR catalysts, especially if located at high dust positions, attrition constitutes a relevant issue.

In the following, the deactivation of V_2O_5 based SCR catalysts by poisoning, fouling, and thermal degradation is discussed. High emphasis is put on studies on the deactivating effect of alkali and alkaline earth metals.

2.3.2. Poisoning

The main poisons for vanadia based SCR catalysts during biomass firing is alkali and alkaline earth metals. Phosphorous has also been reported to cause poisoning of SCR catalysts [42- 48], e.g. during co-firing of phosphorous rich secondary fuels such as sewage sludge and meat and bone meal [49,50], but also during combustion of certain coal types such as Powder River Basin coal [48]. Lead and zinc, which may be released to the flue gas during waste incineration [51-53], may

likewise cause poisoning of the SCR catalyst [42,45,51-56], while arsenic constitute a main poison during coal firing [42,57- 66].

In the case of alkali and alkaline earth metals, the poisoning strength of the individual metal is usually associated with the basicity of the given metal [17,42,47,67]. Reduced acidity of alkali poisoned SCR catalysts has been reported throughout the literature [6,17,42,44,45,47,67- 74]. Both Lewis and Brønsted acid sites contribute to the total acidity of a SCR catalyst, and, as mentioned previously, the adsorption of ammonia on the Brønsted acid sites of vanadia is regarded as a crucial step in the catalytic reduction of NO. Thus, a reduction of the total acidity results in a reduction of active sites and hence activity. Reducibility of vanadia based SCR catalysts have also been reported to be influenced by alkali poisoning [17,68,71,74-77]. Another important part of the catalytic cycle is the activation of adsorbed ammonia by a V^{5+}=O site, which is reduced to a V^{+4}-OH species and further to V^{+3} by desorption of water. If the reduction of V^{+5} to V^{+3} is hindered by the poison, the activity of the catalyst will decrease. One method to reduce the rate of (non-selective) poisoning (and thus deactivation) is to alter the combustion process in such a way that the amount of poison released from the fuel is limited, or so that poisons are captured upstream the SCR unit, either by constituents in the flue gas or by the fly ash, such that harmless components are formed. This could in practice be done by using fuel additives [78,79]. Another way is to modify the catalyst in such a manner that poisonous components preferably adsorb at none active sites. In the case of alkaline poisons this may be done by increasing the total acidity of the catalyst system e.g. by using a highly acidic support. If poisoning cannot be avoided, regeneration may still be feasible compared to the cost of replacing the catalyst.

2.3.3. Fouling

Phenomena such as fouling of the external surface and blocking of channels or pores of the SCR catalysts are caused by deposits on the catalyst, and will usually be accompanied by an increased pressure drop over the SCR section. During combustion of conventional fuels such as coal, calcium compounds typically contribute to the fouling and pore blocking of the system [33]. Formation and deposition of ammonia salts, such as ammonium bisulfate, on the catalyst can in principle constitute a problem, however, at typical SCR temperatures this will not occur [60]. Temperature control is thus important in order to avoid such deposits. For combustion of phosphorous rich fuels such as sewage sludge or meat and bone meal, polyphosphoric acids may constitute a problem either as a fouling layer on the catalyst surface or as pore condensates (or even as poisons) [46,49]. The

accumulation of fouling and channel blocking deposits can be limited by choosing the right monolith cell opening as well as frequent soot blowing [60].

2.3.4. Thermal degradation

The loss of surface area due to sintering or rutilization of titania is another common route for deactivation of SCR catalysts [33]. Alemany *et al.* [34] studied the structural changes of titania in V_2O_5/TiO_2 systems with different vanadia loadings and thermal treatments. Pure TiO_2 was studied as well. The various samples were calcined at temperatures between 110 and 800 °C. Both the size of the titania crystallites and the amount of rutile was found to increase with the calcination temperature. Furthermore, vanadia proved to enhance the crystal growth (sintering) as well as the rulitization. At a calcination temperature of 700 °C, only traces of rutile was found in the pure TiO_2 sample. For this calcination temperature, and a vanadia loading of 1.5 wt.%, 4 % of TiO_2 was identified as rutile. At a vanadia loading of 7.5 wt.% and a calcination temperature of 600 °C, 72 % of TiO_2 was found as rutile. The thermal stability of V_2O_5-WO_3/TiO_2 catalysts was studied by Madia *et al.* [35] using various vanadia loadings and increasingly harsher thermal aging procedures. In this study, vanadia was too found to decrease the thermal stability of the system by promoting anatase sintering. As a compromise between the activity gained by increasing the vanadia loading and the resulting decrease in thermal stability, an optimal vanadia loading of 2 wt.% was suggested. Thermal deactivation of a commercial V_2O_5-WO_3/TiO_2 catalyst, using calcination temperatures between 500 and 900 °C, was studied by Nova *et al.* [33]. The sintering of the TiO_2 anatase support, induced by high calcination temperatures, caused the isolated monomeric vanadyl species to agglomerate resulting in an increased SCR activity at lower temperatures, while the selectivity decreased at higher temperatures.

2.3.5. Deactivation by alkali and alkaline earth metals

2.3.5.1. Exposure and characterization methods

In most studies on poisoning of SCR catalysts, the poison is applied to catalyst by use of impregnation methods in the laboratory [6,17,42,44,45,47,67,68,69-71,73-77,80- 90]. Through impregnation, a very controlled poisoning can be carried out, and a wide range of samples, poisoned to various extents, can be prepared within a relatively short period of time. While the effect of the given poison, to some extent, may be deduced from characterization of impregnated samples, these catalysts hardly replicates the appearance (exterior as well as interior) of industrially exposed SCR catalysts. Under real SCR operating conditions, the poisons will likely be carried as aerosols in the

flue gas, which then deposits on the catalyst, or as gas phase components which condense or solidify on the surface or in the pores of the catalyst. This can in practice mean that the effect of a given poison, under realistic conditions, can be either less or even more severe than what is observed through impregnation experiments. Recently, some studies have been carried out on catalysts exposed to poison containing aerosols [47,54-56,72,91-94], e.g. formed by injecting a precursor solution into a hot flue gas upstream the catalyst. By analyzing the size distribution of the aerosols in the flue gas and the extent and composition of deposits on/in the catalyst, a more realistic depiction of the deactivation mechanism may be observed.

Activity measurements over SCR catalysts are typically carried out under conditions where a pseudo first order rate expression, with respect to the nitrogen oxide concentration, C_{NO}, can be assumed:

$$-r'_{NO} = k' C_{NO} \tag{2.13}$$

This assumption can be made when complete ammonia coverage on the catalytic surface is approached. In practice, this is true when the ratio between ammonia and nitrogen oxide at the inlet of the reactor is greater than or equal to 1. As the catalyst deactivates the rate constant, *k'*, decreases. However, since *k'* is an observed rate constant, which includes the effect of any mass transport limitations, the deactivation will be masked to a certain extent.

An important parameter, which is closely related to the activity of SCR catalysts, is the surface acidity. The surface acidity is typically measured through temperature programmed desorption of ammonia (NH_3-TPD) [17,44,47,68,70,71,74], or by chemisorption experiments where the catalyst surface is first saturated with ammonia followed by exposure to a NO containing gas [6,24,67,69,72,92]. The NO consumption is then related to the amount of ammonia chemisorbed on Brønsted and Lewis acid sites and thereby to the acidity of the catalyst. Another parameter, which has proved to be related to the activity, is the reducibility of V^{5+} to V^{3+} species. This can be studied by temperature programmed reduction, where the oxidized form of the catalyst is slowly heated up in a reducing atmosphere containing H_2 (H_2-TPR) [17,68,74-77]. Textural properties, measured before and after exposure to a given poison, can give an indication of the degree of physical deactivation due to a decrease in pore volume. Surface area and pore size distribution are usually determined by N_2 adsorption measurements, applying the BET (Brunauer-Emmett-Teller) method, or by Hg-porosimetry [6,24,55,69,72,77,81,91-93]. Deactivation due to sintering or rutilization of

the titania support can be measured by X-ray diffraction (XRD) [21,33]. This is also used to determine the dispersion of vanadia over the support. For a well dispersed active phase, no crystalline V_2O_5 should be apparent from the diffractogram (i.e. only the support phase(s) should be visible) [70]. The accumulation of poison in the bulk catalyst can e.g. be determined by inductively coupled plasma optical emission spectrometry (ICP-OES) [55,56,77,91-93] while scanning electron microscopy (SEM) in combination with energy dispersive X-ray spectroscopy (EDS) or wavelength dispersive X-ray spectroscopy (WDS) provide visuals of the state of the catalyst surface/nature of deposits as well as local compositions, e.g. at the surface or through a cross section, of the sample [24,55,56,70,72,92-96].

2.3.5.2. Investigations on the effect of alkali and alkaline earth metals

Alkali metals, such as sodium and potassium, have a poisoning effect on vanadia based SCR catalysts. While these elements may only play a minor role in the deactivation of the catalysts during coal combustion, they constitute a serious problem during (co-)firing of biomass [6,24,95]. This section presents a review over the many studies on the deactivation of vanadia based catalysts, by alkali and alkaline earth metals, which have been carried out in the recent years.

Chen *et al*. [42,67] studied the poisoning effect of various alkali oxides as well as CaO on a TiO_2 supported V_2O_5 catalyst (with a rather high loading of 5 wt.% V_2O_5 with respect to the weight of TiO_2). Doped catalysts were prepared by incipient wetness impregnation of the fresh catalyst with aqueous solutions of LiAc, $NaNO_3$, KNO_3, RbAc, CsAc and $CaAc_2$ respectively, which decomposed into their corresponding metal oxides upon calcination at 450 °C. The catalysts showed maximum activities in the temperature range 200-300 °C, while lower activities were observed at higher temperatures due to the oxidation of ammonia. The activities of the poisoned catalysts were measured at different dopant levels (i.e. at different ratios of dopant metal atoms and vanadium atoms), see Figure 2.2. In all cases, the activity of a doped catalyst decreased with increasing amount of dopant. The poisonous strength of the five alkali metal oxides as well as CaO proved to follow the basicity of the oxides, that is:

$$Cs_2O > Rb_2O > K_2O > Na_2O > Li_2O > CaO$$

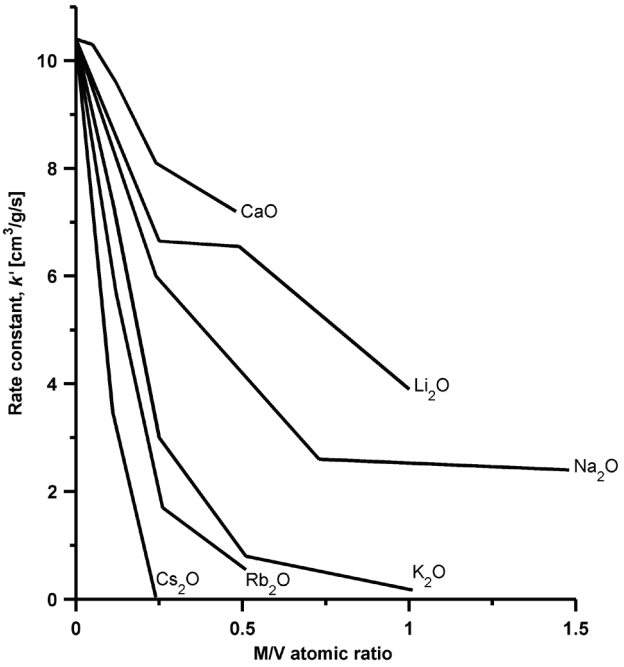

Figure 2.2: SCR activities of a 5 wt.% V_2O_5/TiO_2 catalyst doped to different extents with various alkali metal oxides. Conditions: $[NH_3] = [NO] = 1000$ ppmv, $[O_2] = 2$ %, balance N_2, $T = 300$ °C, gas hourly space velocity (GHSV) = 15000 h^{-1}. Adapted from [42].

At 300 °C, the K_2O poisoned catalyst had lost half of its initial activity at a K/V atomic ratio of 0.14. In comparison, the Cs_2O poisoned catalyst had deactivated 50 % at a Cs/V ratio of only 0.07. The results of these activity tests indicate that the deactivation is related to the electron donating ability of the dopant, hence not solely due to blocking of active sites. NH_3 chemisorption measurements were carried out at 200 °C for the fresh and the alkali doped samples using 1000 ppmv NH_3 in N_2. A direct correspondence between the SCR activity and NH_3 chemisorption capacity of poisoned samples was observed. The amount of NH_3 adsorbed on the undoped catalyst was 1.93 cm^3 STP/g (STP, Standard Temperature and Pressure) while only 0.33 cm^3 STP/g was adsorbed on a sample doped with K_2O at an atomic ratio of K/V = 0.13. The nature of the NH_3 chemisorption sites was elucidated by IR spectra of NH_3 adsorbed on the fresh and K_2O poisoned catalysts. The IR spectrum of the fresh sample showed a strong band at 1415 cm^{-1}. This arises from protonated ammonia, and is characteristic for NH_3 chemisorbed at Brønsted acid sites. Also, a weak band in the range 1640-1660 cm^{-1}, associated with NH_3 chemisorbed at Lewis acid sites, was observed. The spectrum of a K_2O doped sample (K/V = 0.13) indicated a decrease in the amount of ammonia adsorbed at Brønsted sites, while the Lewis sites remained largely unaffected. Based on this it was concluded that Brønsted acid sites are responsible for the SCR reaction and that alkali metals decrease the acidity of these sites.

Lietti *et al.* [73] also studied the effect of potassium on V_2O_5/TiO_2 catalysts (with V_2O_5 concentrations of 1.47 and 3.56 wt. %). In this study, the doped samples were prepared by dry impregnation with KOH or K_2CO_3 solutions followed by calcination at 500 °C for 2 hours. From FTIR characterization it was concluded that both isolated vanadyl and polymeric metavanadate species are present on a sub-monolayer V_2O_5/TiO_2 catalyst and that both types increases with increasing V_2O_5 loading. At high V_2O_5 loadings, a different type of isolated vanadyl species was observed which was characterized by slightly higher V=O stretching frequencies and higher Lewis acidity. Ammonia was found to adsorb at vanadium sites both in protonated and coordinated form, in agreement of what was observed by Chen and Yang [67]. It was also observed that the adsorption strength of both species increases with the V_2O_5 loading, and that the coordinated species are more thermally stable than protonated species. Potassium doping proved to reduce both the amount and the thermal stability of the two species. This observation contradicts that of Chen and Yang [67] who only observed a significant decrease in the amount of protonated ammonia species (i.e. ammonia adsorbed at Brønsted acid sites) upon potassium doping. By temperature programmed surface reaction experiments it was found that while potassium reduces the amount of active sites, their reactivity is largely unaltered. It was also found that potassium preferably interacts with vanadium sites rather than titanium sites. Temperature programmed reaction experiments showed that the re-oxidation of active sites is hindered by potassium doping.

Bulushev *et al.* [80] studied the influence of potassium on the formation of vanadia species on TiO_2 supported V_2O_5 catalysts. Potassium doped catalysts were prepared by co-impregnation with potassium oxalate during the impregnation with vanadia. FT-Raman spectroscopy of a potassium free catalyst with a vanadium loading of 1.2 wt.% (corresponding to about 2.1 wt%. V_2O_5) showed peaks characteristic for monomeric and polymeric vanadium species. TPR proved that both species are easily reduced on the undoped catalyst with a peak H_2-consumption at 494 °C. Potassium doping at a K/V atomic ratio of 0.25 resulted in a shift of the band characteristic for monomeric species in the Raman spectrum. The band was observed at a slightly lower wave number (1020 cm^{-1} vs. 1033 cm^{-1}), indicating a lengthening of the V=O bond. The band characteristic for polymeric species completely disappeared, indicating that potassium inhibits the formation of such species. A new band was observed (at 999 cm^{-1}) which was accredited to potassium doped monomeric species. The TPR peak of this potassium doped sample was broader compared to the one for the undoped. This indicates reduction of a multitude of species. Further potassium doping (K/V = 1) resulted in the disappearance of the band characteristic for monomeric species, while the band for the

potassium doped species moved towards lower frequencies in the Raman spectrum. A new, broad band appeared at 940 cm^{-1}. This was ascribed to the formation of amorphous-like KVO_3. The Raman spectrum of an undoped sample with a high vanadium loading (8.1 wt.% V, corresponding to about 14.5 wt.% V_2O_5) proved that crystalline V_2O_5 had formed on the catalyst surface. The characteristic peaks of monomeric and polymeric species were too present in the spectrum. A large TPR peak was observed at 567 °C and a smaller one at 690 °C. The 690 °C peak was assigned to the reduction of bulk crystalline V_2O_5 while the 567 °C peak was assigned to the reduction of amorphous-like V_2O_5 either in the form of a thin layer or as small particles. Potassium doping at a K/V atomic ratio of 0.05 resulted in a shift of the band characteristic for monomeric species towards lower wave numbers and the disappearance of the band for polymeric species in the Raman spectrum. A sample with a V_2O_5 loading of about 13 wt.% and doped to a K/V ratio of 1 showed Raman bands similar to that of the low vanadia sample with the same K/V ratio. For the high vanadia sample, however, also bulk crystalline KVO_3 was apparent. While the study show how the morphology of V_2O_5/TiO_2 catalysts is perturbed by the presence of potassium, it is important to note that the doped samples were prepared by co-impregnating vanadia and potassium onto the support, instead of potassium impregnation of existing V_2O_5/TiO_2 catalysts. The method/sequence in which potassium is introduced to the catalyst system may have influence on the formed surface species [97].

Tang *et al.* [68] have reported a study in which they investigated the effect of sodium and calcium ions on the surface acidity and reducibility of a V_2O_5/TiO_2 catalyst. A laboratory prepared 3.87 wt.% V_2O_5/TiO_2 catalyst was impregnated with aqueous solutions of $NaNO_3$ or $Ca(NO_3)_2$ in various concentrations, in order to obtain catalysts doped to different molar ratios of Na/V or Ca/V. Activity tests showed that both sodium and calcium ions significantly poisons the catalyst at a Na/V or Ca/V molar ratio of 0.2. While the activity gradually dropped upon increasing sodium doping, it was nearly unchanged for Ca/V ratios below 0.05, in line with the observations by Chen *et al.* [42,67]. IR measurements of NH_3 on fresh as well as doped catalyst showed that sodium ions reduce the acidity of Brønsted sites as well as Lewis sites, while calcium ions reduce the Brønsted acidity to a lower extent. NH_3-TPD indicated the presence of weak as well as strong acid sites (corresponding to ammonia desorption peaks at 270 and 450 °C respectively) on the catalyst surface. Upon doping with sodium ions, both the amount of weak and strong sites was reduced. Doping with calcium ions resulted in a reduction of strong sites while the amount of weak sites increased. This indicates that calcium preferably reacts with strong sites, reducing their acidity. It is

has been found that strong acid sites adsorbing ammonia above 350 °C are not involved in the SCR reaction at lower temperatures [70]. Hence, it is apparent that the effect of doping with alkaline metal ions cannot solely be explained by surface acidity. H_2-TPR profiles were obtained for fresh and doped catalysts in order to study the effect of sodium and calcium ions on the reducibility of dispersed vanadia species. From these profiles it was observed that increased loadings of sodium or calcium decreased the reducibility of dispersed vanadia, and that the reducibility generally was higher for the calcium doped catalyst. This correlates well with their activity measurements. XPS (X-ray photoelectron spectroscopy) studies have previously shown that sodium stabilizes V^{5+} species on V_2O_5/TiO_2 catalysts [98].

Si-Ahmed *et al.* [75] studied the effect of potassium on the structure and reducibility of a V_2O_5/TiO_2 catalyst, both through experimental studies and by density functional theory (DFT) calculations. Potassium doped catalysts were prepared by impregnation of TiO_2 with an aqueous solutions of KOH before the impregnation with a V_2O_5 precursor was carried out. The undoped catalyst contained 9.1 wt.% V_2O_5 while the potassium containing catalysts were doped to K/V atomic ratios of 0.075, 0.15, 0.30 and 0.45 respectively. The catalysts were characterized by Raman spectroscopy and H_2-TPR. The Raman spectrum of fresh, dehydrated catalyst showed the presence of isolated monovanadates, polyvanadates as well as some nanocrystalline V_2O_5. In line with the observations of Bulushev *et al.* [80], a weakening and a shift toward lower wave numbers of the characteristic band for the V=O vibration was observed with increasing potassium loading. As the potassium loading was further increased, formation of bulk potassium vanadates was apparent. TPR profiles showed a decreased reducibility of surface vanadium oxide species upon increasing potassium loading. The experimental findings were supported by DFT calculations where an increase in hydrogen adsorption energy was found for potassium doped models, indicating a weakened reducibility of poisoned vanadia sites. Doping the titania carrier with potassium before applying the vanadia hardly resembles potassium deposition on a SCR catalyst and the observed vanadium containing species on the doped samples may be specific to this preparation method [97].

In a related work, Lewandowska *et al.* [76] too used DFT calculations, Raman spectroscopy as well as H_2-TPR to study the effect of potassium, as well as sodium and lithium, on a V_2O_5/TiO_2 catalyst. Similar to the observations by Si-Ahmed *et al.* [75], the Raman spectra showed a red shift of the V=O vibration frequency for alkali doped samples, and from the H_2-TPR experiments and the DFT calculations the reducibility of the catalyst system was found to decrease according to the series:

undoped > Li > Na > K

The same relation between the reducibility of a fresh, Na doped (Na/V = 0.5), and K doped (K/V = 0.5), 1%V_2O_5/TiO_2 catalyst was recently found by Du *et al.* [74], also using both DFT calculations and H_2-TPR experiments. They moreover confirmed the stabilization of V^{5+} species, upon alkali doping, by XPS, as done by Martín *et al.* [98]. Furthermore, the Brønsted acidity of alkali doped catalysts was found to decrease, both through calculations and through NH_3-TPD experiments.

Gao *et al.* [81] studied the combined effect of K and Ca on a 1 wt.% V_2O_5/TiO_2 catalyst. The catalyst was doped to different extents with K and/or Ca by wet impregnation with aqueous solutions of KNO_3 and $Ca(NO_3)_2$. The alkali (or alkaline earth) metal to vanadium molar ratio of all the doped samples was kept at 1:1. Using a GHSV of 15000 h^{-1}, activity measurements at dry conditions, carried out over fresh catalyst in the temperature range 200-500 °C, showed maximum activity at 350 °C where more than 95 % of the NO was converted. The NO conversion at 350 °C over the doped samples was in all cases below 80 %, however, no clear relation between the K and Ca levels was observed. The BET surface area and pore volume of the doped catalysts did, in most cases, not decrease upon K or Ca poisoning and it was thus concluded that the observe decrease in activity was due to chemical poisoning. SEM images indicated that K_2O and CaO can affect the surface morphology of the catalyst by worsen the dispersion of active phase. However, this was not further investigated or discussed.

Kamata *et al.* [69] studied the effect of K_2O on a commercial V_2O_5-WO_3/TiO_2 catalyst. Powder samples from a V_2O_5-WO_3/TiO_2 monolith (1 wt.% V_2O_5, 8 wt.% WO_3) were impregnated with aqueous solutions of KNO_3, dried and then calcined in air at 450 °C for 4 hours in order to obtain K_2O doped catalysts. Activity measurements of fresh and doped catalysts showed that the NO conversion decreased in the entire investigated temperature range (260 to 400 °C) upon K_2O doping. The negative effect on the conversion increased with increasing K_2O level, and at 2 wt.% loading (corresponding to a K/V atomic ratio of 3.9) the conversion was almost zero at all tested temperatures. An evaluation of the BET surface area and average pore diameter indicated that the textural properties of the catalyst were nearly unaltered by K_2O for loadings up to 1 wt.% (K/V = 2.0). For this reason it was concluded that the observed deactivation was due to chemical interaction between K_2O and catalyst and not pore plugging. As observed for V_2O_5/TiO_2 catalysts [75,76,80], Raman spectroscopy showed that the band assigned to the symmetric stretching of V=O

was shifted (from 983 cm^{-1}) towards lower wave numbers upon increasing K_2O loading. At 1 wt.% loading, a split in the V=O band was observed (at 982 and 979 cm^{-1}), indicating a change in the structure of the surface vanadium induced by K_2O. At 2 wt.% loading, a band at 946 cm^{-1} appeared which was assigned to the formation of KVO_3. IR spectroscopy indicated that K_2O preferentially coordinates to the V-OH (and likely also to W-OH) groups on the catalyst and, upon increased loading, also to Ti-OH groups. IR spectra of NH_3 adsorption on the catalyst showed that NH_3 is both adsorbed as NH_4^+ on Brønsted sites and as coordinated NH_3 on Lewis sites. It was observed that the number and strength of Brønsted acid sites on V_2O_5 (and possibly on WO_3) decreased upon increasing K_2O loading, while the number of Lewis sites was largely unaffected, in line with the observations by Chen and Yang [67] for a V_2O_5/TiO_2 catalyst. Compared to the loss of activity, it was suggested that NH_4^+ ions on Brønsted acid sites is a major intermediate in the reduction of NO, in agreement with the mechanism proposed by Topsøe *et al.* [36-38]. Volumetric measurements of chemisorbed NH_3 showed that the amount of adsorbed NH_3 decreased with increasing K_2O loading. Based on the observations from the IR investigations, it was speculated mainly to be due to decreased NH_3 adsorption at Brønsted sites. It was furthermore found that the strength of acid sites decreased with increasing K_2O loading.

Zheng *et al.* [6] studied the deactivation of V_2O_5-WO_3/TiO_2 catalysts by potassium compounds and possible methods for regeneration. Plates of commercial catalysts with various V_2O_5 and WO_3 loadings (1-3 wt.% and 5-13 wt.% respectively) were doped to different extents with KCl or K_2SO_4 by wet impregnation. After drying at 150 °C for 15 hours, some samples were heat treated at 400 °C for 2 hours. Activity measurements at 250 °C showed that most of the activity was lost at a K/V atomic ratio of 1.5 for both KCl and K_2SO_4 doping, see Figure 2.3. A weak tendency towards KCl being the strongest poison of the two was observed. While deactivation of the SCR catalyst may be expected for all fuels releasing potassium in the form of KCl or K_2SO_4, it was pointed out than the mechanism by which potassium penetrates the catalyst in full-scale plants may differ from what is observed through impregnation studies. The BET surface area and pore volume of the doped catalysts proved to be lower than those for fresh samples, while an increase of the average pore diameter was apparent. The changes in textural properties were, however, not enough to explain the severe deactivation observed. A further elucidation of the deactivation mechanism was carried out through NH_3 chemisorption experiments. These showed that the amount of adsorbed ammonia decreases almost linearly with K/V atomic ratios below 0.5, and levels off, at just above zero, upon further potassium doping. The decreased amount of adsorbed NH_3 was speculated to explain the

decrease in the observed rate constant, possibly by reaction between potassium and Brønsted acid V-OH sites. IR spectra of a fresh and a doped (K/V = 1) 1 wt.% V_2O_5-WO_3/TiO_2 catalyst illustrated the disappearance of characteristic V-OH bands upon potassium doping and it was thus proposed that potassium coordinates to the -OH groups, corresponding to titration of the active sites for NH_3 chemisorption. Based on the temperature dependency of the Arrhenius rate constant in the rate expression for the NO reduction, it was speculated that raising the operation temperature of poisoned catalysts could counter the loss of activity. It was likewise speculated that an increased V_2O_5 loading might increase the potassium tolerance of the catalyst system. It was, however, found that raising the operation temperature of heavily poisoned catalysts (K/V > 1.37) to 450 °C hardly had any effect on the NO conversion. Furthermore, increasing the V_2O_5 loadings (to 2.6 and 7.3 wt.%) proved to promote the oxidation of NH_3 to NO, while the potassium tolerance did not necessarily increase.

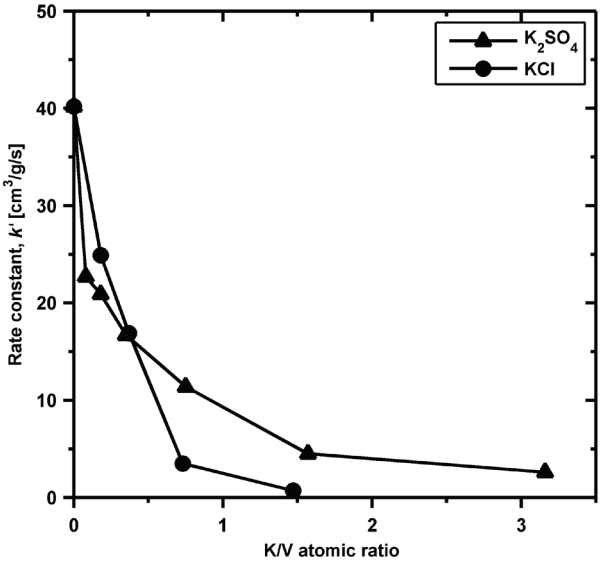

Figure 2.3: SCR activities of a 3 wt.% V_2O_5-WO_3/TiO_2 catalyst as function of potassium loading. Conditions: [NH_3] = 600 ppmv, [NO] = 500 ppmv, [O2] = [H_2O] = 5 %, balance N_2, *T* = 250 °C, Flow rate = 1.2 NL/min. Adapted from [6].

Lisi *et al.* [70] studied the deactivating effect of Na, K as well as HCl vapors on two commercial V_2O_5-WO_3/TiO_2 catalysts (with V contents of 0.55 and 1.8 wt.% respectively), both individually and in combination (Na + HCl and K + HCl respectively). Powder samples from both catalysts were respectively doped with 0.3, 0.7 and 1 wt.% K (corresponding to K/V ratios of 0.7, 1.7 and 2.4, or 0.2, 0.5 and 0.7, depending on the vanadia loading) or 0.18, 0.41 and 0.58 wt.% Na (resulting in similar alkali metal to vanadium ratios) by impregnation in KNO_3 or $NaNO_3$ solutions. To study the effect of HCl, both fresh samples and samples poisoned with the maximum amount of K or Na were

exposed to a 10 % HCl/He mixture at 300 °C for 12 hours. This HCl concentration is much higher than what SCR catalysts will experience during operation. XRD patterns of fresh catalysts only showed signals from the crystalline TiO_2 (anatase) phase. The lack of signals from V_2O_5 and WO_3 aggregates indicated a good dispersion. Comparable XRD patterns were observed for the poisoned samples, suggesting that no crystalline metal oxides or chlorides had formed on a detectable scale. No significant effect of the poisoning agents on the textural properties was found, and SEM-EDS on samples doped with the maximum level of K or Na showed no morphological changes compared to fresh samples. For the catalyst with the highest V loading, a significant drop in the V content (from 1.88 to 1.07 wt.%) was observed after the HCl exposure. This suggests the formation and removal of volatile vanadium chlorides. NH_3-TPD profiles were recorded in the temperature range 100 to 650 °C. Broad NH_3 desorption signals between 150 °C and 450-500 °C as well as a signal at 460-560 °C or 500-600 °C were observed for fresh catalysts. Poisoning by K or Na completely eliminated the latter peak (which is attributed to strong acid sites) in most cases. The effect on the total amount of desorbed NH_3 was most pronounced upon potassium doping. For V_2O_5/TiO_2 catalysts this has previously been accredited to the stronger bacisity of K compared to Na [42,67]. A significant amount of weaker acid sites were, however, still present after alkali poisoning. It was speculated that stronger Lewis wolframyl sites are neutralized by alkali metals while the weaker acid sites of vanadium oxide are preserved. Thermo gravimetric analyses (TGA) on fresh and poisoned samples were carried out in order to measure the water release as a function of temperature. Water leaving a sample at temperatures above 180 °C was accredited to -OH condensation and was thus correlated with the concentration of hydroxyl groups on the sample. The TGA experiments confirmed that alkali metals neutralizes surface hydroxyl groups and that the effect of K is stronger than Na. TPD showed that HCl exposure of fresh catalysts causes a slight quantitative increase in the total amount of acid sites. HCl treatment of alkali poisoned catalysts resulted in a significant increase in surface acidity; however, the profiles suggested that this was due to formation of new hydroxyl groups rather than restoration of the initial ones. Alkali poisoning had a significant negative effect on the catalytic activity of the two catalyst systems. The poisoning effect of K was stronger than for Na in the entire temperature range (200-400°C), in agreement with the previous observations. The activation energy was estimated to 14 kcal/mol for all samples (fresh as well as poisoned), indicating that alkali poisoning does not change the mechanism of the SCR reaction. For the sample with the highest vanadia loading, the pre-exponential factor decreased uniformly with increasing alkali loading while a clear trend was not observed for the other sample.

This suggests a significant interaction between alkali metals and non active sites in the latter case. HCl exposure proved to increase the activity of the sample with the lowest vanadia loading, at higher temperatures, while a substantial loss of activity was apparent in the whole temperature range for the catalyst with the high vanadia loading. This suggests that polyvanadates are less stable than monovanadates, i.e. that they more easily form volatile vanadium chlorides. Combined alkali and HCl poisoning resulted in a severe loss of activity, more pronounced than poisoning with alkali metals only. The activation energy after HCl poisoning was estimated to 17 kcal/mol, which suggests that HCl modifies the active sites, as indicated by the TPD results.

Nicosia *et al.* [44,45] studied the poisoning effect of potassium and calcium on V_2O_5-WO_3/TiO_2 catalysts. Monolithic metal substrates were coated with 1.3 g of commercial V_2O_5-WO_3/TiO_2 and impregnated with aqueous solutions of potassium or calcium salts. The maximum obtained loading of these dopants was 0.4 mole% with respect to the sum of titanium, tungsten and vanadium (corresponding to Ca/V or K/V ratios of 0.25). Of the investigated samples, the fresh catalyst showed the highest activity in the temperature range 200-450 °C. Calcium caused a strong deactivation when the anion of the dopant solution was acetate, while impregnation with various inorganic calcium salts, i.e. $CaSO_4$ (obtained from impregnation with $Ca(Ac)_2$ followed by treatment with SO_2), $Ca_3(PO_4)_2$ and $Ca(BO_3)_2$, only caused negligible deactivation. Potassium doping caused very strong deactivation even at 0.2 mole% loading. Only at a potassium loading of 0.1 mole%, the extent of deactivation was moderate in the entire temperature range. NH_3-TPD curves of fresh, calcium doped as well as potassium doped samples were recorded in the temperature range 100-525 °C. All curves showed two distinct peaks associated with desorption of weakly and strongly bound ammonia respectively. The NH_3 desorption in the temperature range 100-200 °C was similar for fresh and potassium doped samples while much less NH_3 desorbed from the calcium doped sample in this range. Less ammonia desorbed from the potassium doped samples at higher temperatures. The ammonia had fully desorbed from the calcium doped sample at 450 °C and between 400 and 450 °C for the potassium doped sample. DRIFT (diffusive reflectance infrared Fourier transform) spectra were recorded in order to investigate the stability of the adsorbed ammonia species on doped samples. From the spectra, two types of adsorbed species were apparent – i.e. ammonia adsorbed as ammonium on Brønsted acid sites and ammonia species coordinated on Lewis acid sites. For the potassium doped sample, the Brønsted peak showed significantly lower intensity compared to fresh catalyst indicating that potassium had strongly affected the formation of ammonium ions. The calcium doped sample showed intermediate behavior.

In a related study, Nicosia *et al.* [71] applied a series of characterization methods on V_2O_5-WO_3/TiO_2 powders doped with K and Ca by impregnation. Fresh and poisoned catalysts were characterized by NH_3-TPD, DRIFT spectroscopy and XPS. NH_3-desorption curves similar to those from their previous study were obtained. The total NH_3 adsorption capacity was 3.4, 2.0 and 1.4 mg NH_3/g catalyst for fresh, Ca doped and K doped sample respectively. DRIFT characterization of adsorbed NH_3 species on the different samples confirmed that the NH_3 adsorption capacity decreases upon doping with Ca or K. It was found that mainly Brønsted sites were affected by the respective dopant while Lewis sites were largely unaffected. A weakening of the reactivity of V^{5+}=O sites was furthermore observed for poisoned samples. XPS results showed that Ca and K had no influence on the dispersion of V and W. It was found that the given metal dopant interacts with surface oxygen centers. Moreover it was found that K and Ca mainly interact with oxygen in the vanadia phase and not in the tungsta or titania phase. It was speculated that the poisonous element occupies the non-atomic holes in the (0 1 0) V_2O_5 surface thus affecting both Brønsted acid sites as well as V^{5+}=O sites (up to four adjacent, active vanadium centers), both important in the catalytic reduction of NO [36-38]. These speculations were further strengthened by DFT calculations. This deactivation model can explain the heavy deactivation observed for catalysts doped with very small amounts of potassium.

Chen *et al.* [17] too studied the effect of alkali and alkaline earth metals on a V_2O_5-WO_3/TiO_2 catalyst (1 wt.% V_2O_5 and 9 wt.% WO_3 on nano TiO_2). Catalyst powder was doped to different extents with respectively Na_2O, K_2O, MgO as well as CaO. Activity measurements of the fresh catalyst showed a NO conversion of nearly 100 % in the range 300 to 450 °C. The poisoning effect of the respective dopants (with respect to the NO conversion) seemed to follow the basicity of the individual metal oxides (K_2O > Na_2O > CaO > MgO), in agreement with what has previously been observed for poisoning of V_2O_5/TiO_2 catalysts [42,67]. The surface acidity of fresh and doped samples was studied by NH_3-TPD in the temperature range 30 to 500 °C. All desorption curves showed two distinct peaks corresponding to desorption of NH_3 bonded to weak and strong acid sites respectively. Both the amount of weak as well as strong acid sites decreased when the samples were doped with 1 wt.% of the respective metal oxides. The amount of weak acid sites on doped catalysts, found from the TPD curves, decreased as follows:

$$Na_2O > CaO > MgO > K_2O$$

Similarly, the amount of strong acid sites decreased as:

$$MgO > CaO > Na_2O > K_2O$$

The effect of the individual dopants on the amount of strong acid sites thus correlates well with their effect on the catalyst activity. It may be problematic to deduce the relative poisoning effect of the individual element, with respect to the others, due to different loadings on an atomic basis (i.e. Na/V ≈ 3.0, K/V ≈ 2.0, Mg/V ≈ 2.3 and Ca/V ≈ 1.6); however, similar results have been obtained by Klimczak *et al.* [47]. NH_3 adsorption was studied for fresh and poisoned samples by DRIFT spectroscopy. The recorded spectra showed bands associated with NH_4^+ chemisorbed on Brønsted acid sites as well as NH_3 coordinated to Lewis acid sites, the first, however, being the most intensive for fresh catalyst. A reduction of the intensity of the bands assigned to the Brønsted acid sites was observed upon alkali doping. By carrying out the DRIFT measurements at temperatures of up to 300 °C, it was found that alkali metals also affect the stability of the Brønsted acid sites on the catalysts. The reducibility of vanadium and tungsten species on alkali doped catalysts was investigated by H_2-TPR in the temperature range 50 to 1000 °C. Two reduction peaks were observed for all samples, corresponding to the reduction of V^{5+} to V^{3+} and W^{6+} to W^0 (located around 520 and 796 °C for fresh catalyst) respectively. For K and Na doped samples the vanadium reduction peak shifted towards higher temperatures, while the tungsten reduction peaks shifted to lower temperatures – the higher the loading, the greater the shift. For Ca and Mg doped samples only the vanadium reduction peak showed a notable shift, and not as pronounced as for Na and K. The results showed that alkali poisoning could decrease the reduction degree of vanadium species and the K and Na seem to alter the environment around of tungsten species such that any Brønsted acid sites coordinated with these species might be affected. The latter somewhat disagrees with the observations by Nicosia *et al.* [71] who mainly observed interaction between potassium and the vanadia phase.

In a recent publication, Wu *et al.* [77] studied 1%V_2O_5-10%WO_3/TiO_2 catalysts impregnated with NH_4Cl, KCl and KOH respectively. The aim of this study was to look at the effect of chloride as well as potassium. Activity measurements showed barely any difference between the fresh and NH_4Cl impregnated catalyst at 250 and 300 °C, while NH_4Cl seemed to have a promoting effect at 350 °C. The activities of the KCl and KOH impregnated samples were in all cases low and did not seem to change much as the temperature increased. The activity of the KOH impregnated sample was slightly higher than that of the KCl doped one. No new crystalline phases in the impregnated catalysts were detected by XRD and no change in the pore size distribution was observed by N_2

physisorption. The total pore volume of the NH_4Cl impregnated sample had, however, increased. This was accredited to a corroding effect of chloride. ICP analysis showed that while the KCl impregnated sample had obtained 0.66 wt.% potassium, only 0.014 wt.% chlorine was present in the catalyst. Similarly, the NH_4Cl impregnated sample only contained 0.003 wt.% chlorine. Hence, chlorine had almost completely left the samples during the 2 hours of calcination at 400 °C upon the impregnation procedure. Raman spectroscopy indicated the presence of KVO_3 in KOH and KCl doped samples, while NH_4Cl seemed to have promoted the change of surface VO_x species from metavanadate into decavanadate. This was further indicated by UV-vis spectroscopy. It was speculated to be due to redispersion of the vanadia by formation of vanadium chloride during the impregnation. FTIR measurements at 200 °C on samples saturated with NH_3 showed a decrease in both the amount of Lewis and Brønsted acid sites for KOH and KCl doped samples, while NH_4Cl impregnation had no significant effect on the amount and stability of the acid sites. Similar to the observations by Chen *et al.* [17], H_2-TPR measurements showed a decrease in the reducibility of V^{5+} species of potassium impregnated catalysts. The TPR curve of the NH_4Cl doped sample showed the presence of a new, more reducible vanadium species formed during the redispersion by chloride. A weak indication of this species was also present in the KCl impregnated sample. The study shows that the anion, in this case chloride, plays a less significant role during poisoning of SCR catalysts by impregnation with potassium salts. The redispersion of vanadia species by the formation of vanadium chloride, which occurred during the impregnation, is unlikely to occur during poisoning by deposited KCl particles in a real case scenario.

Zheng *et al.* [24,72] studied the deactivation of V_2O_5-WO_3/TiO_2 monoliths in a Danish CHP (combined heating and power) plant (Masnedø) as well as in a pilot setup. Three 75 mm x 75 mm x 500 mm monoliths with a V_2O_5 loading of 3 wt.% were exposed to the flue gas from a grate fired CHP plant during biomass combustion (20 % wood chips and 80 % straw on energy basis) in up to 1600 hours [24]. The mass based distribution of aerosols in the flue gas, measured by a low pressure cascade impactor (LPI), showed a unimodal distribution with a geometric mean mass diameter of 0.7 μm, and a total aerosol concentration of 579 mg/Nm^3 (415 mg/Nm^3 consisting of particles below 1 μm). This distribution is shown in Figure 2.5. SEM-EDS of the collected aerosol particles showed that they had crystalline nature and mainly consisted of K, Cl and S, originating from KCl and K_2SO_4. Activity measurements were carried out *in situ* during the exposure. Two of the monoliths were operated at 350 °C while the last element was operated at 250 °C. All tested catalysts showed a loss in relative activity of 52-53 % after exposure of about 1200 hours,

corresponding to a deactivation rate of about 1 %/day. This indicates that operating the SCR catalyst at lower temperatures (e.g. at 250 °C instead of 350 °C) does not change the rate of deactivation during biomass firing. *In situ* NH_3 chemisorption tests indicated that the observed deactivation was due poisoning by chemical alteration of the active sites rather than physical deactivation such as pore blocking. This was further signified by BET measurements which only showed slight differences in surface area and total micro pore volume between fresh and exposed samples. SEM-EDS analysis of one of the catalyst operated at 350 °C showed that the deposited aerosols mainly contained K and S indicating that KCl aerosols from the flue gas had been sulfated on the catalyst surface. Measurements of the potassium inside the catalyst wall showed an average K/V molar ratio of 0.5. High K/V ratios of about 2.3 were found inside the other catalyst exposed at 350 °C, and the ratios were even higher (4-6) at its surfaces, see Figure 2.4. For the catalyst exposed at 250 °C, the K/V molar ratio decreased from 0.5, close to the surface, to 0.3 at the centre of the wall. A K/V ratio of 0.3 could not explain the observed deactivation (laboratory studies show a relative activity loss of 40 % at K/V = 0.3 [6]) thus it was concluded that this catalysts had also been subjected to channel blocking and surface fouling. Washing of one of the catalyst in 20 L of a 0.5 M H_2SO_4 solution proved to restore most of its original activity at temperatures above 300 °C. A second regeneration resulted in activities higher than those observed for the fresh catalyst at high temperatures. This was accredited to formation of surface sulfates.

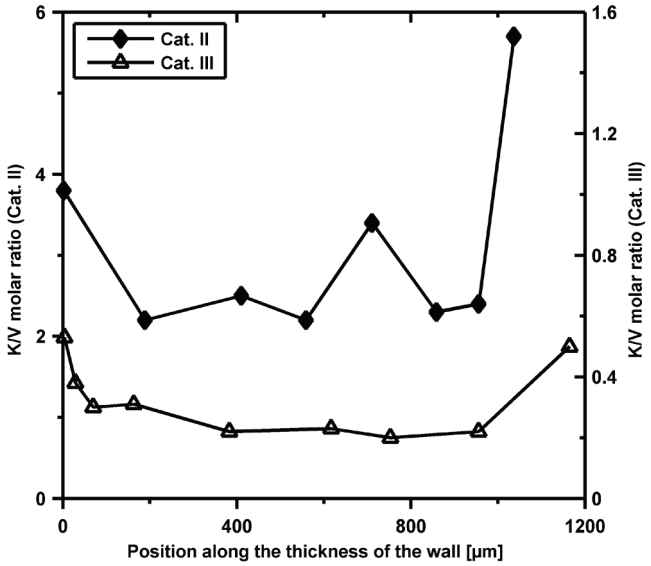

Figure 2.4: K/V molar ratio along the thickness of flue gas exposed V_2O_5-WO_3/TiO_2 catalysts operated at 350 °C (Cat. II) and 250 °C (Cat. III) respectively. Adapted from [24].

A further investigation on the deactivation mechanism was carried out in a pilot plant where full-length V_2O_5-WO_3/TiO_2 monoliths, similar to those tested at the CHP plant, were subjected to aerosols of KCl and K_2SO_4 respectively at 350 °C for up to 2700 hours [72]. The aerosols were generated by injecting an aqueous solution of the respective potassium salt into the hot flue gas from a natural gas burner. The geometric mean mass diameter of the KCl particles, measured by LPI, was 0.3 μm, which was smaller than the particles measured at the CHP plant (0.7 μm). While the mass size distribution of the KCl particles (aerosol concentration: 20-40 mg/Nm^3) showed unimodal behavior, the K_2SO_4 particles (aerosol concentration: 20-30 mg/Nm^3) had a bimodal size distribution with peaks at 0.07 μm and 1.05 μm and a mass mean diameter of 0.55 μm, see Figure 2.5. Activity tests of the monoliths were carried out *in situ*. Exposure of monoliths to KCl aerosols for 715 and 1830 hours resulted in a decrease of relative activities corresponding to roughly 1 %/day which is similar to what was observed at the CHP plant. The deactivation of the monolith exposed to K_2SO_4 aerosols was less severe. After an initial fast deactivation during the first 300 hours (accredited to residual KCl in the system), the loss of relative activity was only around 0.4 %/day. *In situ* NH_3 chemisorption tests showed that the NH_3 adsorption capacity decreased faster than the activity both during KCl and K_2SO_4 aerosol exposure. This was accredited to mass transfer limitations which dampens the observed rate of deactivation. The BET surface area of exposed samples showed a slight decrease compared to fresh ones. Also the total pore volume and average pore diameter (measured by Hg-porosimetry) decreased upon KCl exposure, indicating plugging of macro pores. SEM images of the first KCl aerosol exposed monolith surface showed loose particle deposits and partly filling of the large pores. The K/V atomic ratio dropped steeply from the surface to the inside of the catalyst. At 200 μm from the surface, the average K/V value was 0.75 which from laboratory tests is known to be enough to cause severe deactivation [6]. Likewise, lose particle deposits were found on the K_2SO_4 exposed monolith. The sulfur level inside the catalyst was not found to increase. The average K/V through this catalyst was 0.49. Fouling and channel blocking was accredited to contribute to the deactivation to a limited extent, since frequent soot blowing was carried out.

In the same study, Zheng *et al.* [72] also exposed 1.3 mm x 10 mm x 20 mm pieces of 1%V_2O_5-7%WO_3/TiO_2 catalyst plates to layers of pure KCl particles (with an average diameter of 360 μm) as well as fly ash (consisting of 55 wt.% KCl and 44 wt. % K_2SO_4) collected during their experiments at the CHP plant [24]. A 2 mm layer of the respective deposit was applied to the plate pieces, and the catalysts were heat treated at 350 °C in a flow of 200 NmL/min air saturated with

H_2O for up to 2970 hours. During the first 670 hours of the exposure of the KCl covered plates, 1000 ppmv SO_2 was added to the gas mixture as well. Activity measurements on the exposed plate pieces showed an activity loss of 13 % at 350 °C after exposure to KCl particles for 2397 hours, while no activity loss was observed for samples exposed to fly ash for 2970 hours. The modest deactivation rates of these catalysts, compared to those of their aerosol exposed monoliths [24,72], indicate that the deactivation is mainly caused by potassium from the ultrafine particles in aerosol. From the experimental results it was hence concluded that the deactivation of the SCR catalysts is caused by diffusion of fine, potassium containing aerosols (< 100 nm) into the larger pores of the catalyst (> 1 μm) and reaction with -V-OH sites to form -V-O-K. The further penetration of potassium into the catalyst was speculated to be due to surface diffusion. The fact that deactivation by KCl aerosols was faster than by K_2SO_4 was explained by the difference in the mass mean diameter of the aerosols as well as the respective differences between the Tamman and Hüttig temperatures of the two salts. KCl has lower Hüttig and Tamman temperatures than K_2SO_4 (40 °C and 249 °C compared to 129 °C and 397 °C) which implies that the mobility of KCl at 350 °C is higher than that of K_2SO_4.

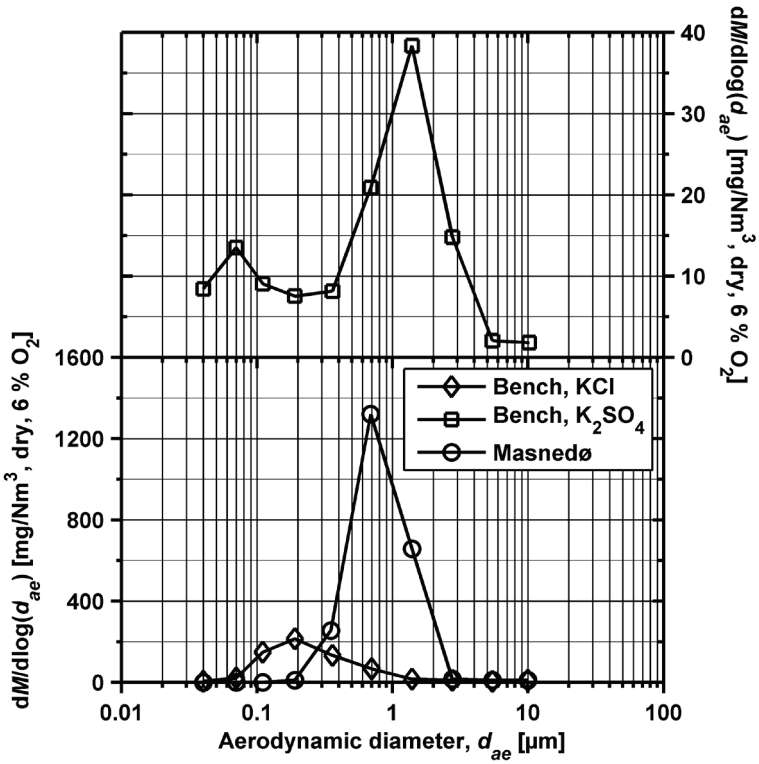

Figure 2.5: Aerosol mass size distributions measured by a low pressure impactor, converted to a reference state of dry gas at 273.15 K, 101.3 kPa, and a O_2 concentration of 6 vol.%. Upper figure: K_2SO_4 aerosol produced by adding 436 mL/h of a 7.4 g/L solution to a hot flue gas. Lower figure: KCl aerosol produced by adding 420 mL/h of a 37.3 g/L KCl solution to a hot flue gas and aerosol measured at the Masnedø plant. Adapted from [72].

Moradi *et al.* [54] studied the respective effect of KCl and K_2SO_4 aerosols on vanadia based catalysts as well. In their study, the catalysts were supported on monolithic or wire-mesh substrates. The aerosols were generated by atomization of an aqueous solution of the given salt (25 g/L) followed by mixing with dry air in order to reduce the relative humidity. The air stream with the generated aerosol was passed through a deactivation reactor, loaded with either the monolith or the wire-mesh catalysts, which was operated at 340 °C. Each catalyst was exposed for 31 hours. Aerosols were characterized by a scanning mobility particle sizer (SMPS) and an APS (Aerodynamic Particle Sizer). The number based mean particle size, as measured by SMPS, was found to be around 66 nm for all the generated aerosols. On a mass basis, the average diameter was 500 nm. The activity of fresh and exposed catalysts was measured in a laboratory reactor in the temperature range 200-450 °C. For monolithic catalysts, little to no effect on the activity was observed upon KCl aerosol exposure, while a slightly promoting effect of the K_2SO_4 aerosol exposure was observed at temperatures above 250 °C. The latter was accredited to increased activity due to sulfate groups. The minute effects of the potassium rich aerosols on the exposed monoliths may be due to the fairly short exposure period. For wire-mesh catalyst KCl had a stronger deactivating effect than K_2SO_4 which was correlated with its lower melting point.

Larsson *et al.* [55,56,91] studied and compared 1%V_2O_5-WO_3/TiO_2 monolith type catalysts which had been subjected to potassium by three different means. One mean of exposure was in a pilot-scale setup, where an electrostatic field was used to accelerate the deposition of aerosol particles of KCl and K_2SO_4 in the channels the catalysts. Here, the aerosols were generated by atomizing aqueous solutions of the respective salts which were then passed through an oven heated to 300 °C. An electric field was applied over the catalyst, which was operated at 200 °C, by applying an electrical potential over an aluminum foil covering the catalyst, and a steel wire located inside a catalyst channel. Each catalyst was exposed for 10 hours. Other monoliths were wet impregnated with aqueous solutions of KCl or K_2SO_4. For each salt, both low concentration (1 g/L) and high concentration (10 g/L) solutions were used respectively. Finally, the analysis results were compared to those of a similar monolith which had been operating at 350 °C for 6500 hours in a commercial biomass combustion plant firing wood chips (90 %) and peat (10 %) in a circulating fluidized bed (CFB) boiler. During the electrostatic aerosol deposition, aerosol size distributions were measured at the outlet of the catalyst by an SMPS and an ELPI (Electrical Low Pressure Impactor). Both the total number concentration and the mean diameter of the KCl and the K_2SO_4 aerosol were comparable ($5.7 \cdot 10^6$ versus $6.0 \cdot 10^6$ #/Ncm^3 and 104 versus 103 nm). In comparison, the catalyst

which had been used in the commercial plant had been exposed to particles with a total number concentration of $1.2 \cdot 10^7$ #/Ncm^3 and a mean diameter of 68 nm. For the catalysts which underwent electrostatic deposition, the bulk concentration of potassium, measured by ICP-OES, was 0.4 wt.% in the sample exposed to KCl and 0.2 wt.% in the one exposed to K_2SO_4. The plant exposed catalyst contained 0.5 wt.% potassium. The KCl impregnated catalysts contained 0.2 and 0.8 wt.% potassium while the K_2SO_4 impregnated samples contained 0.1 and 0.4 wt.%. BET measurement showed a slight decrease in the surface area and pore volume of particle exposed samples. The plant exposed catalyst had lost some of its original pore volume, while both surface area and pore volume were largely unaffected for impregnated samples. The potassium penetration profiles across the catalysts were measured by WDS. In the sample from the commercial exposure, potassium had penetrated the entire thickness (about 1 mm) of the catalyst, assuming a level above 1 wt.% across the center. In the KCl and K_2SO_4 particle exposed samples, the potassium penetration depth was 0.35 and 0.65 mm respectively. These samples had, however, only been exposed to particles from one side of the catalyst wall. Where present, potassium assumed similar levels as in the catalyst from the commercial exposure. Constant, low potassium levels of about 0.2 wt.% were measured through the catalysts doped with 1 g/L solutions of either KCl or K_2SO_4. Activity measurements at 300 °C, see Figure 2.6, showed a relative activity loss of 9 % for the KCl exposed catalyst, 4 % for the K_2SO_4 exposed sample and 15 % for catalyst from the commercial exposure. The slightly lower deactivation of K_2SO_4 aerosol exposed samples is in agreement with the observations by Zheng *et al.* [72].

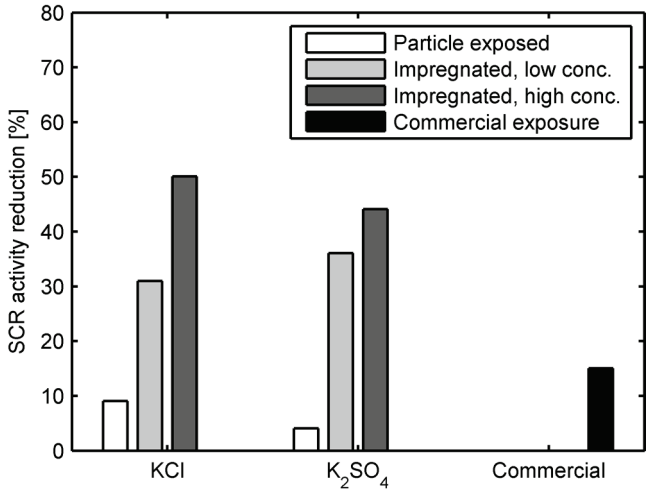

Figure 2.6: SCR activity reduction at 300 °C for particle exposed, salt impregnated and commercial exposed catalysts. Adapted from [91].

The KCl impregnated catalysts had lost 31 and 50 % of their initial activity while the K_2SO_4 doped samples had lost 36 and 44 %. Hence the slight tendency of KCl being the stronger poison, observed by Zheng *et al.* [6] in their impregnation study, was not apparent here. The authors made no attempt to explain the lower activity loss of the particle exposed catalysts, compared to the impregnated samples, even though the potassium levels inside the first mentioned were significantly higher.

Klimczak *et al.* [47,82] studied the poisoning effect of K, Na, Ca and Mg on the activity of V_2O_5-WO_3/TiO_2 monoliths – both by impregnation and by aerosol exposure. In case of impregnation, each channel in the tested monoliths was doped with aqueous solutions of the individual poison precursor (metal nitrates were used in all cases), using a pipetting robot. Activity tests were carried out at 250-450 °C over every individual channel, keeping the remaining channels in a N_2 atmosphere. Other monoliths were exposed to aerosols, generated by injection of respective precursor solutions upstream the monoliths, at 500 °C for 50 hours. Activity measurements of these monoliths were carried out at 200 to 450 °C. For catalyst impregnated with alkali and alkaline earth metals, the deactivating effect of the individual metals followed their basicity, i.e. K > Na > Ca > Mg, similar to what has been observed by other authors for both V_2O_5/TiO_2 and V_2O_5-WO_3/TiO_2 catalysts, prior to and after this study [17,42,67]. In the case of K and Na, almost complete deactivation was observed at 350 °C for theoretical metal loadings above 0.25 mmol/g washcoat. NH_3-TPD analyses, carried out over impregnated catalyst powders, showed that the ammonia adsorption capacity decreased in the Mg > Ca > Na > K, again in accordance with the basicity of the individual poison. The activity measurements of the aerosol exposed monoliths confirmed the order of the deactivating effect with respect to K, Na and Ca. DRIFT spectroscopy on fresh and Ca doped powder samples confirmed the reduction of ammonia adsorption capacity upon poisoning. These measurements also showed weakening of the signal from the first overtone vibration of V^{5+}=O indicating a reduced reactivity of these sites [71].

Kling *et al.* [95] investigated the deactivation of three V_2O_5/TiO_2 catalysts, with varying vanadia loading, in three Swedish CHP plants (Johannes, Brista and Uppsala) during combustion of biomass such as peat, wood, bark, forest residues and demolition wood. The amount of alkali metals (being mainly potassium) accumulated on the exposed samples proved to correlate linearly with the exposure time and the relative activity of the catalysts decreased upon increasing alkali accumulation. Catalysts with high vanadia loadings proved to be more resistant. It was found that

mainly particles in the flue gas smaller than 100 nm contributed to the alkali buildup on the catalysts, in line with was later signified by the studies of Zheng *et al.* [72]. SEM-EDS showed that potassium was evenly distributed throughout the walls of exposed catalyst instead of being accumulated at the outer surface, as reported by other researchers [24,72,55]. This either indicates that ultrafine potassium containing particles can penetrate deep into the pore system of the catalyst and/or that potassium bound in these particles is highly mobile.

In a Danish study [96], commercial SCR elements from two different vendors were exposed for 5000 to 19000 hours in a power plant (Studstrup) during co-firing of coal and straw (up to 10 % on an energy basis). After correcting the activity measurements for channel blocking, an average rate of deactivation (decrease in relative activity) of only 1.6 % per 1000 hours was observed. SEM-EDS showed that the surfaces of the exposed catalysts were mainly covered with coal ash and that potassium was primarily bound in silicates. No potassium sulfate deposits were found. It was concluded that the observed deactivation was due to physical deposition rather than chemical poisoning by alkali, and hence that co-combustion of straw, with a share of up to 10 % on an energy basis, does not enhance the deactivation of the SCR catalyst.

Castellino *et al.* [92,93] studied the influence of the products formed by reaction between phosphor and calcium based fuel additives and the potassium salts in the flue gas on commercial V_2O_5-WO_3/TiO_2 catalysts. These additives are thought to bind potassium in higher melting compounds, thus protecting the super heaters in power plants against sticky, corrosive depositions. The resulting compounds may, however, influence downstream equipment such as the SCR catalyst. Full-length monoliths were exposed to potassium containing aerosols, created by injection of aqueous salt solutions into the hot flue gas from a natural gas burner, in a pilot-scale setup. In one study [92], two monoliths were exposed to 100 mg/Nm^3 and 200 mg/Nm^3 K_3PO_4 for 720 and 189 hours respectively. The number based particle size distribution of the aerosol, measured by SMPS, showed a peak around 30 nm during addition of 100 mg/Nm³ K_3PO_4. For the volume based distribution, an indication of a second peak, outside the upper detection limit of the SMPS was observed. The peak for larger diameter particles was estimated by assuming a lognormal distribution resulting in a mean diameter of 1.25 μm. Particles collected by an LPI were analyzed by EDS. A K/P molar ratio between 3 and 3.5 was found, and it generally increased with the collected particle size (49 to 1488 nm). The bulk content of K in exposed samples, measured by ICP-OES, varied between 0.8 and 2.5 wt.%, while the P content varied between 0.4 and 0.8 wt.%.

About twice as much K was found in the "100 mg/Nm³" sample compared to the "200 mg/Nm³" sample while the P content was more or less the same. The bulk K/P ratio varied between 0.85 and 2.52, which is lower than the ratio introduced to the system, indicating different paths for the K and P accumulation in the catalyst walls. Very high P concentrations, of up to 12.6 wt.%, were observed on the surface of the "200 mg/Nm³" sample by SEM-EDS. EDS analyses on cross sections of the catalysts showed that both the K and P content dropped throughout the monolith wall, indicating a diffusion limited process. While the K concentration seemed to level off to a finite value of around 0.7 wt.%, the P concentration dropped to zero at a given distance (100-300 μm) inside the wall. This indicates that K penetrates and stays in the catalyst wall, while the P penetration is either slower or is counter balanced by evaporation of phosphorous species from the surface. Activity measurements were carried out *in situ* at 350 °C during the aerosol exposure. The two elements (exposed to 100 and 200 mg/Nm³ K_3PO_4) lost respectively 26 and 31 % of their initial activity during the first 72 hours of exposure and continued to deactivate at a significant rate. Also NH_3 chemisorption tests were carried out *in situ* at 350 °C. After 408 hours of exposure to 100 mg/Nm³ K_3PO_4, the amount of chemisorbed NH_3 was only half of the amount for a fresh catalyst. The decrease in chemisorbed NH_3 was seen as an indicator for deactivation by removal of NH_3 chemisorption sites. Based on the dual-mode particle size distribution, measured by SMPS, it was assumed that the smaller particles (mean diameter of 30 nm) were formed by homogenous nucleation in the gas phase, while the larger particles were formed by crystallization due to water evaporation. It was likewise assumed that the deposition rate of smaller particles is faster due to higher diffusion coefficients. It was speculated that the particles found at the inlet of the SCR reactor consisted of K_3PO_4, K_2CO_3, H_3PO_4, KPO_x and PO_x species. The K gradient in the catalyst was speculated to be due to solid-state acid-base reactions on the catalyst surface, followed by K penetration due to surface diffusion of K atoms into the catalyst wall. The P-gradient was expected to be controlled by capillary forces applied on liquid polyphosphoric acids as well as K-P solid particle diffusion. The "zero concentration" at a certain distance in the wall was speculated to be due to simultaneous P evaporation, by hydrolysis, of polyphosphoric acids on the surface. The observed deactivation was found to be partly due to physical blocking of the catalyst pores and surface, which was reversed by soot blowing in the absence of aerosols. The main mechanism of the deactivation was, however, concluded to be poisoning by K.

In a similar study [93], a commercial V_2O_5-WO_3/TiO_2 catalyst was exposed to aerosols, formed by simultaneous injection of KCl (10 mg/Nm^3), $Ca(OH)_2$ (13 mg/Nm^3), H_3PO_4 (26 mg/Nm^3) and

H_2SO_4 (20 mg/Nm^3) for 1000 hours. The number based particle size distribution (measured by SMPS) showed a peak around 9 nm. Again, the volume base distribution showed two distinct peaks – one around 12 nm and one around 300 nm. The second peak represented about 94 % of the total volume of the distribution. Results from LPI tests (in the range 25 to 11391 nm) showed a mass based particle size distribution centered around 200 nm. The deviation from the SMPS analysis was accredited to experimental uncertainties associated with the different measuring principles. EDS analyses of the LPI foils showed no Cl in the deposits, indicating that Cl is released to the gas phase upstream the reactor. P and Ca were not found in particles larger than 3000 nm (in which only K and S were found). ICP-OES analyses showed that P was the element that had accumulated the most in the bulk catalyst, while no significant accumulation of Ca and S was detected. Also EDS analyses of the catalyst surface showed highest accumulation of P, at even higher levels than found in the bulk. Ca and S were found on the surface of exposed catalyst indicating some deposition of these elements, while K was found in both the bulk and on the surface of exposed catalyst. SEM images showed that the spent catalyst had a 2-3 µm thick layer deposited on the surface. EDS on cross sections of the catalyst showed diffusion limited penetration of P in the catalyst wall, with a constant P level after the first 100 µm. K and Ca were not found inside the wall. The deactivation of the catalyst was monitored by *in situ* activity measurements. The majority of the total activity loss, which amounted to 19 % of the original activity, occurred during the first 191 hours of exposure, indicating that the components causing the initial fast deactivation did not cause any further deactivation throughout the rest of the exposure period. *In situ* NH_3 chemisorption experiments showed that only 16 % of the initial chemisorption capacity was lost after 260 hours of exposure. It was estimated that only 8 % (out of the 19 %) of the lost activity was due to poisoning by K and Ca, and that the remaining 11 % was due to physical pore blocking or surface masking. The relative NH_3 adsorption improved at higher exposure times (> 600 hours) due to formation of P-sites from polyphosphoric acids. These sites, however, were inactive with respect to the SCR reaction, or less active than the sites they replaced. Hg-porosimetry confirmed the physical deactivation by formation of an external layer. While the total intrusion volume did not differ significantly between fresh and spent catalyst, the spent catalyst had no (externally exposed) pores in the range 0.3-8 µm. Based on the observations, the formation of polyphosphoric acids was confirmed and the small particle class, found by SMPS, was associated with these. At SCR temperatures, polyphosphoric acids will be liquid and their penetration will thus be driven by capillary forces. The absence of Ca and K in the catalyst walls was taken as an indication of that these elements are tightly bound in

larger particles which both have slower deposition rates and are unable to penetrate the catalyst. This again indicates that potassium present in the deposited particles on the catalyst surface needs to be released from the particles on atomic scale in order to diffuse into the catalyst walls.

Alkali metals and, to a lesser extent, alkaline earth metals constitute serious poisons to the SCR catalyst in applications, such as biomass firing, where these may be present in the flue gas, in large amounts, in the form of aerosols. Impregnation studies on V_2O_5/TiO_2 as well as V_2O_5-WO_3/TiO_2 catalysts have shown that the relative poisonous strength of alkali and alkaline earth metals follows their basicity. While it is generally agreed that the amount and strength of Brønsted acid sites are reduced upon alkali poisoning, it is still unclear whether a similar, direct interaction with Lewis sites occurs. Several studies have shown that the reducibility of V^{5+} species decreases upon alkali poisoning. The alkali metals seem preferably to interact with V (or W) rather than Ti. Aerosol characterization in a full-scale, biomass fired power plant has shown that potassium is mainly present in the form of KCl and K_2SO_4 aerosols. Bench-scale as well as laboratory studies indicate that KCl is slightly more poisonous to the SCR catalyst compared to K_2SO_4. SEM-EDS analyses of aerosol exposed SCR monoliths show that potassium penetrates the entire thickness of the catalyst wall. It is believed that the deactivation of the SCR catalyst is caused by diffusion of potassium containing aerosols, in the submicron range, into the pores of the catalyst, followed by reaction with the Brønsted acid sites. Subsequent surface diffusion of potassium poisons the interior of the catalyst. Co-combustion with coal, and/or the use of additives such as $Ca(OH)_2$ and H_3PO_4 may slow down or even completely hinder the potassium poisoning of SCR catalysts.

2.3.6. Alternative catalyst formulations

One issue is the vulnerability towards potassium poisoning of commercially applied, vanadia based SCR catalysts during biomass combustion, others are their toxicity and activity for the oxidation of SO_2. These matters have lead to continuing studies on alternative SCR catalysts.

Long and Yang [99,100] have reported high activity and selectivity for the SCR reaction for a Fe-exchanged ZSM-5 zeolite catalyst, with a Si/Al ratio of 10, in the temperature range 400-550 °C. Furthermore, the selectivity for the SO_2 oxidation was remarkably lower than for a V_2O_5-WO_3/TiO_2 catalyst. However, in a review article by Brandenberger *et al.* [101] it was concluded that Fe-ZSM-5 zeolite based catalysts have insufficient hydrothermal stability and low temperature activity.

Kern *et al.* [83] exposed Fe-MFI and Fe-BETA zeolite based catalysts, supported on monolithic substrates, to solutions of Na, K, Ca, and Mg nitrates by impregnation. While the alkali and alkaline earth metals proved to deactivate the Fe-zeolite catalysts, the alkali resistance was higher compared to that of a standard V_2O_5-WO_3/TiO_2 monolith catalyst as seen in Figure 2.7:

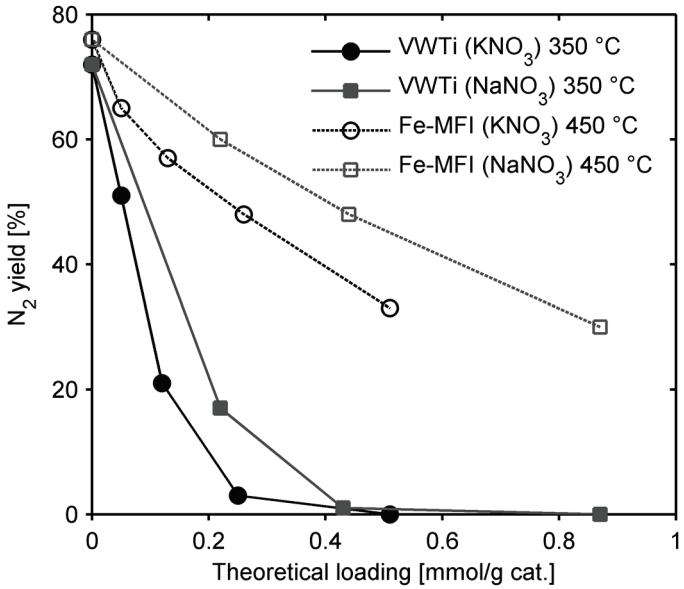

Figure 2.7: N_2 yield as a function of K and Na loading. Conditions: [NO] = [NH_3] = [CO] = 1000 ppmv, [CO_2] = [H_2O] = 5 %, [O_2] = 8 %, balance N_2, GHSV = 50000 h^{-1}. Data from [47,82,83].

Figure 2.7 shows the N_2 yields obtained by Kern *et al.* [47,82,83] from activity measurements on alkali doped V_2O_5-WO_3/TiO_2 (VWTi) and Fe-MFI monoliths. The N_2 yield is defined as the fraction of NO at the inlet converted into N_2 at the outlet of the monolith. The activity measurements on alkali doped V_2O_5-WO_3/TiO_2 monoliths were carried out at 350 °C, while the measurements on Fe-MFI monoliths were carried out at 450 °C. The conditions, including the dimensions of the monoliths, were otherwise the same. The main deactivation mechanism of zeolite catalysts was accredited pore blocking/narrowing by uptake of alkaline metals on cationic positions [83].

The potassium resistance of Fe-BETA as well as Fe-ZSM-5 and Fe-Mordenite zeolite catalysts was also studied by Putluru *et al.* [84,102]. The peak activity of the zeolites was obtained in the temperature range 425-575 °C. All three zeolites proved to be more alkali resistant compared to a V_2O_5-WO_3/TiO_2 (3 wt.% V_2O_5, 9 wt.% WO_3) catalysts, however, Fe-Mordenite and Fe-ZSM-5 were more resistant than Fe-BETA. When impregnated with KNO_3 to a potassium loading of 100 μmol/g catalyst (corresponding to K/Fe values of 0.10-0.19, depending on the Fe loading of the

given catalyst) the relative activity at 400 °C of the zeolites was 90 % or above. In comparison, the relative activity of the V_2O_5-WO_3/TiO_2 reference sample was 40 % at the same potassium loading (a K/V ratio of 0.3). At a K loading of 500 μmol/g (K/Fe = 0.93) the Fe-Mordenite still retained 44 % of its initial activity at its optimal operating temperature (500 °C). At the same loading (K/V = 1.52), the V_2O_5-WO_3/TiO_2 catalysts only showed a relative activity of 10 % at 400 °C. The alkali resistance of the zeolites proved to follow their surface acidities (Fe-Mordenite > Fe-ZSM-5 > Fe-BETA).

Based on the same zeolites (H-Mordenite, H-ZSM-5 and H-BETA), Putluru *et al.* [85,102] studied the SCR activity and potassium resistance of Cu-zeolites. Optimized (with respect to Cu loading) Cu-zeolites showed very high activities of 2300-2650 $cm^3/g/s$, significantly higher than what they observed for a commercial-type, vanadia based catalyst (i.e. about 1000 $cm^3/g/s$). The activities of the individual Cu-zeolites peaked at temperatures in the range 425-500 °C. The for the H-Mordenite, the optimal Cu loading was 4 wt.% while it was 5 wt.% for the H-ZSM-5 and H-BETA. A much higher potassium resistance was observed for the zeolite samples. Doping the catalysts with potassium (using KNO_3) at K/Cu atomic ratios below 0.20 had no influence on the activity in the whole tested temperature range (200-600 °C). At a potassium loading of 100 μmol/g catalysts (corresponding to K/Cu values of 0.13-0.16), the relative activity at 400 °C of all three zeolites was 90 %, similar to what was observed for the Fe-zeolites [84]. At higher potassium loadings, the Cu-H-Mordenite sample showed the highest resistance of the three zeolite catalysts. The improved alkali resistance was accredited to the high surface area and acidity of the zeolites.

Plates of 4 wt.% Cu on H-ZSM-5 and H-Mordenite, reinforced with ceramic fibers, were exposed to KCl aerosols at 350 °C for 1200 hours by Putluru *et al.* [103], in the same setup as was used by Zheng *et al.* [72]. A 3%V_2O_5-7%WO_3/TiO_2 reference catalyst was also exposed. X-ray powder diffraction (XRPD) measurements on the fresh zeolite catalysts only showed the patterns characteristic for the zeolite supports, indicating that CuO in both cases was amorphous and highly dispersed. No significant changes in the patterns were found for the exposed samples, showing that the catalysts were thermally stable. Both zeolite catalysts had significantly larger BET surface areas (338 m^2/g for Cu-H-ZSM-5 and 312 g/m^2 for Cu-H-Mordenite) compared to the vanadia based reference (64 m^2/g). Some decrease in the surface area of the exposed samples was observed. This was accredited to interactions between potassium and the support as well as blocking of pores. The total acidity of catalyst samples was measured by NH_3-TPD. For both fresh and exposed catalysts,

Cu-H-Mordenite was the most acidic catalyst (fresh acidity: 1590 μmol/g, exposed acidity: 1399 μmol/g) followed by Cu-H-ZSM-5 (fresh acidity: 1349 μmol/g, exposed acidity: 1052 μmol/g). The least acidic catalyst was the vanadia based reference which also lost a substantial amount of its initial acidity upon exposure (fresh acidity: 364 μmol/g, exposed acidity: 160 μmol/g). EDS measurements of the potassium content on the surface as well as inside the exposed samples showed that the diffusion of potassium, across the catalyst wall, was faster for the vanadia based reference compared to the Cu-zeolites. As observed for the potassium impregnated Cu-zeolites [85], the KCl aerosol exposed zeolite catalysts showed improved alkali resistance compared to the vanadia based reference. At 350 °C, the Cu-H-Mordenite and Cu-H-ZSM-5 respectively retained 59 and 37 % of their initial activity upon exposure, while only 5 % of the activity of the reference catalyst remained. Furthermore, the absolute activity of the fresh Cu-zeolite catalysts was 2-3 times as high as that of the reference. Again, the better alkali resistance of the Cu-zeolites was ascribed to the higher surface areas and acidities of these samples.

In another study, Putluru *et al.* [86,102] investigated the catalytic behavior of V_2O_5 wet impregnated onto various zeolites (H-ZSM-5, H-BETA, H-Mordenite and H-Y). The optimal vanadia loadings were found to be 10 to 16 wt.% depending on the support. XRD analyses verified good dispersion of vanadia and showed no crystalline V_2O_5 phases. The H-Mordenite supported catalyst proved to have the highest activity and acidity of all the investigated samples. Maximum activities of the individual samples were observed between 460 and 480 °C. The potassium resistance of the H-Modernite supported samples was found to be the greatest of them all. At a potassium loading of 100 μmol/g catalyst (corresponding to a K/V ratio of 0.08), obtained from wet impregnation with KNO_3, only 9 % of the original activity was lost at 500 °C, and even less at lower temperatures.

Promising results, with respect to alkali resistance, have been obtained from studies on vanadia supported on sulfated zirconia [87,88,102,104]. Sulfated V_2O_5/ZrO_2 catalysts have shown high surface acidities even after being doped with K_2O (to a K/V ratios of 0.4-0.5) and have also expressed higher activities than potassium doped V_2O_5/TiO_2 and V_2O_5-WO_3/TiO_2 catalysts [87,88,104]. However, the surface sulfates, which provide the enhanced alkali resistance [88], have proved to decompose over time in a flue gas without SO_2 [87]. This may be problematic during combustion of straw and wood based fuels which generally results in flue gases with low SO_2 contents [105]. Furthermore, the potassium hosted at acid sites on the zirconia support have proved

to become mobile at temperatures above 375 °C, resulting in irreversible poisoning of the active vanadia phase [104]. At 300 °C and in the presence of SO_2 in the gas (1000 ppmv), the sulfates were stable and the activity of fresh and potassium doped catalysts were comparable [87].

The effect of promoting V_2O_5/TiO_2 catalysts with heteropoly acids, in order to gain higher alkali resistance, was studied by Putluru *et al.* [89,102]. TiO_2 anatase powder was promoted with three different heteropoly acids, i.e. $H_3PW_{12}O_{40}$, $H_3SiW_{12}O_{40}$ and $H_3PMoW_{12}O_{40}$ respectively, before impregnation with a vanadia precursor. The resulting vanadia loading was 3 wt.%. XRD proved that heteropoly acids as well as vanadia were well dispersed over the support. Some rutile phase in the catalysts was identified by XRD. An increase in the rutile phase was found for catalysts impregnated with KNO_3 to a potassium level of 100 μmol/g catalyst (K/V = 0.3). NH_3-TPD showed higher acidity and potassium resistance of heteropoly acid promoted catalysts compared to a commercial V_2O_5-WO_3/TiO_2 catalyst. While the acid promoted catalysts lost 38-43 % of their initial acidity upon K doping, the commercial catalyst lost 75 % of its acidity. The acidity of the heteropoly acid promoted catalysts decreased with increasing calcination temperature above 400 °C. This was accredited to phase transformation of the titania support (from anatase to rutile) and decomposition of the heteropoly acids. Also the activity of the acid promoted catalysts peaked at a calcination temperature of 400 °C. The activity measurements were carried out in the temperature range 200 to 540 °C. Maximum activities of the acid promoted catalysts were observed between 440 and 460 °C. In the case of $H_3PW_{12}O_{40}$ and $H_3SiW_{12}O_{40}$ doped samples, the maximum activity was higher than that for the commercial catalyst. The three acid promoted catalysts showed high potassium resistance. Between 71 and 88 % of the initial activity at 400 °C was still left upon doping with 100 μmol potassium per gram catalyst. In comparison, the potassium doped commercial catalyst only retained around 30 % of its original activity.

The same heteropoly acid promoted TiO_2 supports (i.e. $H_3PW_{12}O_{40}$, $H_3SiW_{12}O_{40}$ and $H_3PMoW_{12}O_{40}$ promoted TiO_2) were used as carriers for Cu and Fe based SCR catalysts by Putluru *et al.* [102,106]. By wet impregnation with the respective metal nitrate, 3 wt.% of the given metal was loaded onto the individual heteropoly acid promoted TiO_2 carrier. Unpromoted Cu/TiO_2 and Fe/TiO_2 catalysts were prepared as well. Potassium doped versions of the same catalysts were prepared by co-impregnation with KNO_3 so that the final potassium loading was 100 μmol/g catalyst. The acidities of the fresh and potassium doped catalysts were measured by NH_3-TPD. In all cases, the catalysts on heteropoly acid promoted TiO_2 supports showed higher acidities than

those supported on pure TiO_2. Some loss of acidity was recorded for all alkali doped catalysts, however, while the Cu/TiO_2 and Fe/TiO_2 catalysts respectively lost 61 and 55 % of their initial acidity, all the acid promoted catalysts retained about 67 % of their acidity upon alkali doping. The heteropoly acid containing catalysts also showed better alkali resistance with respect to their catalytic activity. Furthermore, the absolute activities of these samples were in all cases higher than that of their unpromoted counterparts at temperatures above 300 °C. For the Cu based catalysts, the maximum activity was reached in the temperature range 350-400 °C, with the $H_3PMoW_{12}O_{40}$ and the $H_3SiW_{12}O_{40}$ promoted catalysts being the most active. After potassium doping, the relative activity at 400 °C of the Cu/TiO_2 catalyst was 23 %, while the acid promoted Cu-catalysts retained 59-72 % of their initial activity. The activity of the fresh Fe based catalysts peaked at temperatures between 440-480 °C. Here, the $H_3PW_{12}O_{40}$ promoted catalyst was the most active. The potassium doped Fe/TiO_2 catalyst retained 25 % of its original activity at 400 °C, while the acid promoted Fe-catalysts still possessed a relative activity of 45-60 %. Hence, TiO_2 supports doped with heteropoly acids, whether they are used with vanadia [89], as in traditional SCR catalysts, or in Cu and Fe based catalysts [106], can enhance the alkali resistance as well as the absolute activity of the resulting catalyst system.

Kristensen *et al.* [107] prepared V_2O_5/TiO_2 catalysts using a sol-gel, co-precipitation method. Through this technique, they were able to obtain high loadings of up to 20 wt.% V_2O_5 on anatase nanocrystals, without exceeding monolayer coverage. The high dispersion of vanadia was confirmed by XRPD, TEM (transmission electron microscopy) and FTIR spectroscopy. The acidity of the catalysts was measured by NH_3-TPD. While the amount of desorbed ammonia below 500 °C increased with increasing V_2O_5 loading in the range 5-20 wt.%, from 18-30 cm^3/g, the specific acidity (NH_3 molecules/nm^2) was largely unaffected by the V_2O_5 content since also the surface area increased accordingly with the vanadia loading. In comparison, the amount of ammonia which desorbed from a $3\%V_2O_5$-$7\%WO_3/TiO_2$ reference catalyst was 12 cm^3/g. By sulfating the catalysts using sulfuric acid during their preparation, the total acidities of the obtained catalysts were increased with up to a factor 3, compared to their unsulfated counterparts. The activity of the catalysts was measured at dry conditions in the temperature range 200-450 °C. The peak activity moved towards lower temperatures as the vanadia content increased. The optimal V_2O_5 loading was found to be 20 wt.%. For this catalyst, the activity at 380 °C was nearly twice as high as for the $3\%V_2O_5$-$7\%WO_3/TiO_2$ reference (about 1620 vs. 850 $cm^3/g/s$). For the sulfated catalysts the activity was even higher (about 1900 $cm^3/g/s$). The potassium resistance of the catalysts was tested

by measuring the activity of samples doped with K_2O to a potassium level of 280 μmol/g catalyst. V_2O_5/TiO_2 catalysts with vanadia loadings of 10, 15, 20 and 25 wt.% (corresponding to K/V ratios of 0.25, 0.17, 0.13 and 0.10) all showed higher potassium resistance at 380 °C compared to the $3\%V_2O_5$-$7\%WO_3/TiO_2$ reference catalyst (K/V ratio: 0.85) which was almost completely deactivated. The sample with 20 wt.% V_2O_5 proved to be the most potassium resistant catalyst retaining 36 % of its initial activity at 380 °C. The sulfated sample deactivated even less and kept 60 % of its fresh activity. One concern of having such high vanadia loadings is the risk of facilitating the SO_2 oxidation. The sulfated 20 wt.% V_2O_5/TiO_2 catalyst, however, showed similar SO_2 oxidation behavior as the $3\%V_2O_5$-$7\%WO_3/TiO_2$ reference. Another concern is the fact that vanadia promotes the sintering and rutilization of the support [16]. While this issue was mentioned by the authors, suggesting the addition of WO_3, it was not further addressed in this work.

In a related study, Kristensen [108] prepared extrudates of the sulfated 20 wt.% V_2O_5/TiO_2 catalyst mixed with sepiolite and various H_2SO_4 solutions (0 M, 0.05 M and 0.25 M). The optimal catalyst, based on activity and NH_3-TPD measurements, was found to be one extruded with pure water and 20 wt.% sepiolite. Based on this formulation, a fiber reinforced catalyst plate was prepared and exposed to KCl aerosols at 350 °C in the setup previously used by Zheng *et al.* [72]. After 632 hours of exposure, activity measurements on fractionated plate catalyst showed an activity loss of 32 % at 380 °C. In comparison, a $3\%V_2O_5$-$7\%WO_3/TiO_2$ reference catalyst, from the same exposure campaign, had lost 84 % of its initial activity. SEM-EDS measurements on a cross section of the exposed V_2O_5/TiO_2-sepiolite plate showed that potassium was mainly present on surface and had only penetrated the outer layer of the catalyst to a moderate extent. The improved potassium resistance of the V_2O_5/TiO_2-sepiolite catalyst was accredited to the porous structure of the sepiolite which physically prevents the deposited potassium in reaching the active sites. This conclusion was signified by the fact that potassium impregnated 20 wt.% V_2O_5/TiO_2 catalysts, with and without sepiolite, deactivated to similar extents.

Putluru and Jensen [94] attempted to improve the alkali resistance by adding a protective barrier to the surface of the catalyst. Plates of commercial V_2O_5-WO_3/TiO_2 catalysts were spray coated with aqueous suspensions of various zeolites as well as magnesium oxide. The plates were then exposed to KCl aerosols at 350 °C for 650-1200 hours. Activity measurements were carried out over 17 mm x 17 mm bits of exposed plates, as well as over unexposed counterparts at 350 °C. The activity of the fresh, coated plates was generally lower than that of an uncoated plate due to increased diffusion

limitations. However, exposed catalysts coated with H-BETA-25, H-Mordenite-10, H-ZSM-5-15 as well as MgO all showed promising alkali resistance compared to the uncoated catalyst, both regarding the catalytic activities and with respect to the potassium levels through the thickness of the plates, as measured by SEM-EDS. The protective effect of the zeolite coatings (H-BETA-25, H-Mordenite-10 and H-ZSM-5-15) was accredited to their high acidity, while that of MgO was accredited to its slightly alkaline nature which hinders the diffusion of potassium. Ultimately, magnesium based coatings were deemed the best choice due to their lack of Brønsted acid sites which may facilitate the diffusion of potassium. This work ultimately led to the filing of a patent application [109].

Huang *et al.* [90] have developed a highly alkali resistant SCR catalyst based on Hollandite manganese oxide. The catalyst was impregnated with solutions of various potassium salts (KCl, KNO_3, KOH, K_2SO_4 and K_2CO_3) to obtain potassium loadings of up to 1150 µmol/g catalyst. The initial activity at 350 °C of the Hollandite catalyst was comparable to that of a commercial type V_2O_5-WO_3/TiO_2 (3% V_2O_5, 7 % WO_3). While the vanadia based catalyst had lost nearly all of its initial activity at potassium loadings above 200 µmol/g (K/V = 0.61) the activity of the Hollandite catalyst had only dropped slightly a potassium loading of 1150 µmol/g. The high alkali resistance of the Hollandite catalyst was explained by it having two types of active sites – one type with SCR activity and one which can trap alkali atoms. TEM and XRD investigations on KCl doped catalysts indicated that the SCR reaction takes place on the external {110} facets of the Hollandite nanorods while alkali metal ions are captured inside the tunnels of the nanorods. Temperature programmed activity measurements supported by XRD analyses confirmed that potassium ions, bound in KCl crystals on the external surface of the catalyst at room temperature, migrates spontaneously into the tunnels of the nanorods when the temperature is raised above 230 °C.

2.4. Conclusion

Selective catalytic reduction of NO_x by ammonia over vanadia based catalyst has proved to be an effective method for reducing the NO_x emissions from stationary, coal fired sources. However, during firing biomass catalysts have proved to deactivate faster than during firing of conventional fuels. This is due to the release of alkali and alkaline earth metals from the biomass and the subsequent deposition of inorganic components, containing these elements, on the surface or in the pores of the SCR catalyst. These may poison the catalyst by reacting with the active sites or physically mask the active surface. Since the use of alternative sustainable fuels is an attractive

mean of reducing the net CO_2 emissions from power plants, the deactivation SCR catalysts, due to e.g. alkali poisoning, have been studied intensively in the literature during the past years. It is apparent that the study and understanding of the deactivation mechanism is essential to the development of new catalyst formulations, or the implementation of new operating conditions, which can improve the resistance towards deactivation of the SCR catalyst during e.g. biomass firing.

Most investigations on the poisonous effect of alkali and alkaline earth metals have been carried out through impregnation studies. In the recent years, however, several studies using aerosols as the mean of exposure have been performed. Such studies may provide a more realistic picture of the deactivation mechanism. The activity of vanadia based SCR catalysts is closely linked with its surface acidity, which again relates to the ammonia adsorption capacity. While the acidity is provided by Brønsted and Lewis acid sites on the various metal oxides in the system (e.g. V_2O_5, WO_3 and TiO_2), only ammonia adsorbed at the V-OH Brønsted sites is regarded as active in the reduction of NO. Alkaline elements such as potassium are believed to react with these sites thus rendering them inactive. Furthermore, research has shown the reducibility of V^{+5} species is inhibited upon alkali poisoning. Despite the numerous studies, the mechanism of which alkali containing compounds deactivates the SCR catalysts upon contact is not fully understood. Potassium, for instance, has proved to be able to fully penetrate the walls of SCR monoliths; however, the mechanism of which potassium is transported into the catalyst has not been fully investigated. Studies on how the size of deposited particles and/or the temperature, at which the catalyst is operated, influence the activity of, and potassium distribution in, exposed SCR catalysts may facilitate this understanding.

Several studies on how to improve or alter the formulation of SCR catalysts, in order to increase the alkali resistance, have been conducted. The general approach so far has been to increase the total acidity of the catalyst system, e.g. by the use of zeolites or acid promoted supports. Both the alkali resistance and the overall activity of the alternative catalysts have generally proved to correlate well with the enhanced acidity. None of these studies have, however, led to new catalyst formations which have been adopted by the industry.

3. Experimental

3.1. Catalysts

Two types of SCR catalysts have been used in this study, both of which were supplied by Haldor Topsøe A/S. One type consisted of plates of V_2O_5 based SCR catalysts, with approximate loadings of 1, 3 and 6 wt.%, on a fiber reinforced TiO_2 carrier. Some plates were promoted with about 7 wt.% WO_3. Upon delivery, the plates had dimensions (thickness x width x height) of 1 mm x 50 mm x 148-166 mm. The other type of catalyst consisted of high-dust corrugated monoliths of fiber reinforced $3\%V_2O_5$-$7\%WO_3/TiO_2$. The monoliths had a size of 72 mm x 72 mm x 250-500 mm, a hydraulic channel diameter of 6.5 mm and a wall thickness of about 1 mm. One of the monoliths was coated with 8.06 wt.% magnesium oxide (MgO) while another was coated with 8.36 wt.% of a 1:1 mixture of MgO and TiO_2.

3.2. Bench-scale aerosol exposures

3.2.1. The SCR exposure pilot

Catalysts (plates or monoliths) have been exposed to aerosols of KCl or K_2SO_4 in a bench-scale reactor previously used for a similar study by Zheng *et al.* [72]. The setup, illustrated in Figure 3.1, consists of a natural gas burner, a flue gas duct perpendicular to the burner outlet, a heat exchanger section where the reactor temperature can be controlled, and the reactor itself. The reactor can house a full-length (50 cm) SCR monolith or a set of up to nine plate-type catalysts placed in a steel cassette in the top part of the reactor. A second heat exchanger cools the flue gas further before it is led to the stack. A water cooled injector probe, equipped with a two-fluid nozzle, can be introduced into the flue gas duct at the end adjoining the burner outlet. At the opposite end of the duct, a bayonet heat exchanger can be inserted for further cooling. NH_3 can be supplied to the burner in order to increase the NO level in the flue gas, and upstream the reactor to carry out the NO reduction over the catalyst. Aerosols of either KCl or K_2SO_4 were generated by pumping an aqueous solution of the respective salt (with a concentration of 0.1 M with respect to potassium ions) through the injector probe, at a rate of 420 mL/h, and injecting it into the hot flue gas by the aid of pressurized air through the two-fluid nozzle.

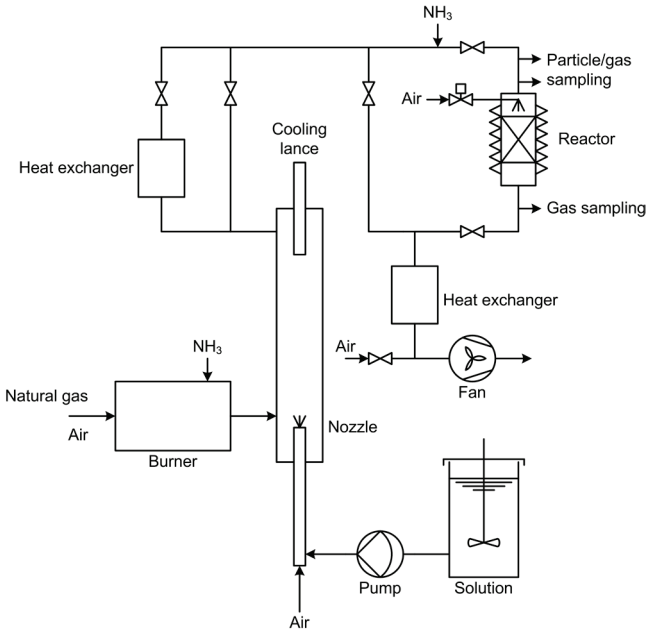

Figure 3.1: Schematic drawing of the bench-scale setup for aerosol exposure of SCR catalyst plates.

3.2.2. Exposure of catalyst plates

Six exposure campaigns have been conducted on plate shaped catalysts and up to nine plates were exposed in each experiment. Pieces with dimensions of 36 mm x 98 mm were cut from the individual plates and placed in a steel cassette which was subsequently mounted in the top of the reactor. The exposure campaigns differed by the injected salt solution (KCl or K_2SO_4), the SCR reactor temperature (150-350 °C), the total exposure time (72-600 hours) and the position of the injector nozzle (40 or 142 cm from the insertion port) leading to different temperatures for the aerosol particle formation. In addition to being heated by the flue gas, the SCR reactor was heated from the outside by an electrical heating cable and insulated by a mantle of mineral wool in order to minimize radial temperature gradients. The axial temperature gradient over the catalysts was always within 5 °C. In order to avoid build-up of particles on top of the catalyst cassette, a burst of pressurized air from a soot blower, located above the reactor, was released for approximately 1 second every 30 minutes. The total gas flow through the reactor was 35-45 Nm^3/h corresponding to a linear gas velocity of 1.7-2.2 Nm/s (0 °C, 1 atm, empty reactor).

3.2.3. Exposure of monoliths

Three monoliths have been exposed to KCl aerosols at 350 °C for up to 1100 hours. It was decided to use half-length monoliths in these experiments in order to ensure a reasonable degree of deactivation within the exposure period. Hence, each monolith was, when necessary, reduced to a

length of 250 mm and placed in the reactor. As during the plate exposures, the reactor was equipped with an electrical heating cable and an insulating mantel. The position of the injector probe was in all cases kept at 40 cm from the insertion port. The total gas flow through the reactor was 40-55 Nm^3/h (2.0-2.7 Nm/s), and the temperature gradient over the reactor was below 8 °C. During the monolith exposure campaigns, the soot blower was activated every 4 hours.

3.3. Aerosol measurement

3.3.1. Low pressure impactor

Mass based particle size distributions were measured by a 10-stage Berner-type low pressure impactor (LPI, Hauke Ges.m.b.H. & Co.KG) with an aerodynamic diameter range of 0.03-12.7 μm. The gas was sampled above the reactor inlet through a straight, cylindrical tube perpendicular to the main flow at a flow rate of 23.11 NL/min. In order to avoid water condensation, the sampling tube and the impactor were heated to 90 °C. The sampling time was 60 minutes. The particles were collected on aluminum foils coated with a thin film of Apiezon H vacuum grease. The grease was added by applying a thin layer of a dilute solution of the grease in toluene onto the foils. In order to remove the toluene, the foils were dried in an oven at 140 °C for several hours.

3.3.2. Scanning mobility particle sizer

Number based particle size distributions were measured by a scanning mobility particle sizer (SMPS, TSI Inc.) which consisted of an Electrostatic Classifier (Model 3080), equipped with an impactor nozzle with a diameter of 0.071 cm and a Long DMA (Differential Mobility Analyzer, Model 3081), and a Condensation Particle Counter (CPC, Model 3775). The aerosol containing flue gas samples were taken just above the inlet of the reactor. In order to avoid condensation of water as well as an overflow of particles to the particle counter, the samples were diluted 45-55 times using an injector diluter driven by dry, particle free air. The dilution ratio was calculated by measuring the CO_2 concentration of the flue gas before and after dilution. The sample flow rate through the classifier and the CPC was 1.5 L/min and the classifier was operated with a sheath air flow of 15 L/min. With the given configuration, the SMPS could measure the particle size distributions in the range 5.83 to 228.8 nm.

3.4. Activity measurements

3.4.1. Laboratory

The catalytic activities of the exposed plates, as well as unexposed counterparts, were measured in a laboratory setup, illustrated in Figure 3.2, at temperatures between 250 and 400 °C. The samples were crushed to a powder, diluted with sand and loaded into a quartz reactor, with an internal diameter of 10 mm, between two layers of quartz wool. A typical reactor loading contained 50-100 mg catalyst. A total flow of about 2800 NmL/min was used during the measurements and the gas was composed of 500 ppmv NO, 600 ppmv NH_3, 5 vol.% O_2, about 1.4 vol.% H_2O and balance N_2. The H_2O content was obtained by saturating a stream of N_2 at room temperature by passing it through a bubble flask with water. The dry NO concentration at the reactor outlet was measured by a Rosemount NGA 2000 analyzer.

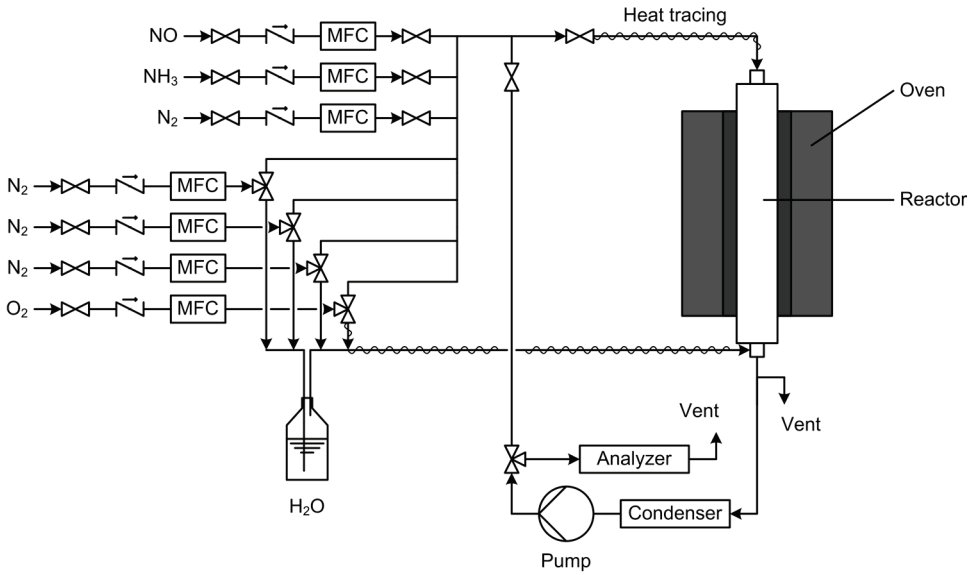

Figure 3.2: Schematic drawing of the laboratory flow setup for measurements of catalytic activity (MFC = mass flow controller).

The reactor itself, which was placed in a three-zone oven, is illustrated in Figure 3.3. NO, NH_3 and part of the N_2 were fed through a tube in the top of the reactor (1 in Figure 3.3), while O_2, H_2O and the remaining N_2 were fed through an inlet tube at the bottom (2). The two inlet streams were mixed above the catalyst bed, which was placed on a porous quartz plate, and the product gas exited through another tube at the bottom of the reactor (3). The reactor temperature was measured below the porous plate by a thermocouple inserted into a quartz tube (4 in Figure 3.3).

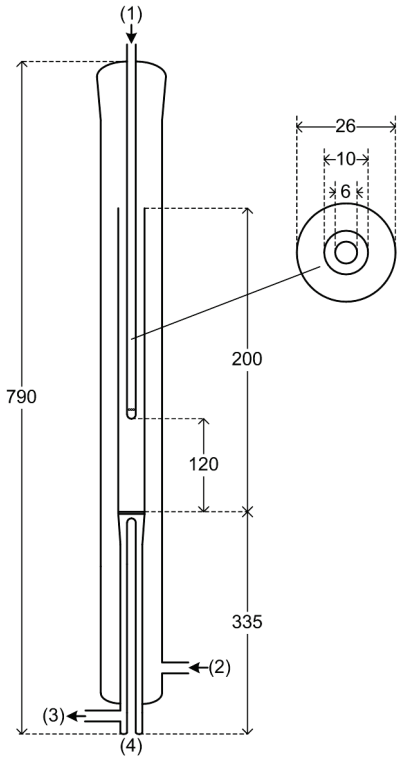

Figure 3.3: Illustration of the laboratory reactor. (1) Top gas inlet. (2) Bottom gas inlet. (3) Gas outlet. (4) Thermocouple insertion tube. All measures in millimetres.

3.4.2. Pilot plant

During the monolith exposures, frequent activity measurements were carried out *in situ* at 350 °C, in a flue gas consisting of about 500 ppmv NO, 600 ppmv NH_3, 10 vol.% O_2, 6 vol.% CO_2 and around 10 vol.% H_2O. The reduction agent, NH_3, was added to the flue gas upstream the reactor. As the NO level generated from the natural gas combustion was only about 100-120 ppmv, NH_3 was also added to the burner in order to enhance the NO production. During the activity measurements, the dry NO concentration in the flue gas was sequentially measured at the inlet and outlet of the reactor by a Rosemount NGA 2000 analyzer.

3.4.3. Activity calculation

The NO reduction in the SCR reaction can be described by an Eley-Rideal rate expression where NH_3 adsorbs on the catalyst surface while NO reacts from the gas phase with the adsorbed species [110-112]. This mechanism leads to the following rate expression:

$$-r_{\mathrm{NO}}\left[\frac{\mathrm{mol}}{\mathrm{kg{\cdot}s}}\right] = k_r C_{\mathrm{NO}} \frac{K_{\mathrm{NH3}} C_{\mathrm{NH3}}}{1+K_{\mathrm{NH3}} C_{\mathrm{NH3}}} \qquad (3.1)$$

Where k_r (in m^3/kg/s) is the intrinsic rate constant, C_i (in mol/m^3) is the concentration of component i in the gas phase, while K_{NH3} (in m^3/mol) is the NH_3 adsorption equilibrium constant. When NH_3 is in excess, equation 3.1 can be reduced to a pseudo first order expression with respect to NO:

$$-r_{NO} = k' C_{NO} \tag{2.13}$$

The observed rate constant, *k'*, which includes any external and external mass transfer limitations, can then be calculated by equation 3.2:

$$k' \left[\frac{m^3}{kg \cdot s}\right] = -\frac{F_{gas}}{m_{cat}} \ln(1 - X_{NO}) \tag{3.2}$$

Where F_{gas} (m^3/s) is the volumetric gas flow rate at reactor conditions, m_{cat} (kg) is the catalyst mass and X_{NO} is the NO conversion:

$$X_{NO} = \frac{C_{NO,in} - C_{NO,out}}{C_{NO,in}} \tag{3.3}$$

In the following sections, all measured activities/rate constants of exposed catalyst samples (plates as well as monoliths) will be reported relative to that of their fresh state, k'_0, i.e.:

$$\text{Relative activity} = \frac{k'}{k'_0} \tag{3.4}$$

This is done 1) in order not to disclose any absolute activities, as a courtesy to the catalyst supplier, Haldor Topsøe A/S, and 2) in order to be able to compare the deactivation rates of the exposed monoliths.

3.5. Ammonia chemisorption

In order to have a measure of the amount of active acid sites as a function of catalyst composition, NH_3 chemisorption measurements, similar to those carried out by Zheng *et al.* [6] have been performed on fresh catalyst plates, in the setup depicted in Figure 3.2. Pieces of 16 mm x 16 mm (corresponding to 0.62-0.68 g) were cut from the individual catalyst plates and placed in a quartz reactor which was heated to 250 °C. A gas mixture of 600 ppmv NH_3, 5 vol.% O_2 and about 1.5 vol.% H_2O in N_2 was passed over the catalyst at a flow rate of about 2740 NmL/min for 30 minutes, which was found sufficient in order to saturate the active sites with NH_3. The NH_3 flow was then shut off and about 500 ppmv NO was added to the reactor shortly after. The amount of

ammonia adsorbed on active sites could then directly be correlated to the amount of NO reduced by NH_3, assuming that the reaction followed the standard SCR reaction:

$$4NO + 4NH_3 + O_2 \rightarrow 4N_2 + 6H_2O \qquad (2.1)$$

3.6. Pellet experiments

The pellet experiments described below constitute a newly devised method for studying the transport of potassium in SCR catalysts. Using two-layer pellets consisting of SCR catalysts, where one side is impregnated with e.g. KCl or K_2SO_4, it is possible to study the potassium mobility as a function of catalyst composition as well as the applied potassium salt. By adding a third layer in between, it is possible to probe potential coating materials which may hinder the diffusion of potassium into the fresh catalyst.

3.6.1. Two-layer pellets

Pellets consisting of two layers of crushed plate catalyst in close contact have been produced. One layer was made from a fresh V_2O_5-(WO_3)/TiO_2 catalyst, while the other layer was made of the same catalyst doped with either KCl or K_2SO_4 to a potassium level of 0.8-1.6 wt.%. The potassium doping was achieved by wet impregnation of whole catalyst plates which were subsequently dried at 80 ºC, crushed, and (in some cases) calcined at 400 °C overnight. Initially, one side of the pellet was made by partial compression of the powder in a pellet die. The powder of the other side was then added to the die and a final compression pressure of 60 bar was applied for 1 minute. Each pellet consisted of about 600 mg of pulverized catalyst (300 mg in each layer) and had a diameter of 13 mm and a thickness of around 2.3 mm. A principle sketch of a two-layer pellet is shown in Figure 3.4. A pellet composed of a layer of pure KCl salt, crushed and sieved to a fraction below 250 µm, and a layer of fresh 3%V_2O_5-7%WO_3/TiO_2 catalyst powder was also produced.

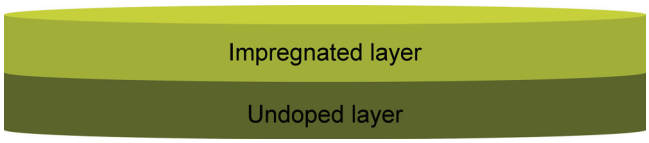

Figure 3.4: Principle sketch of two-layer pellet.

3.6.2. Three-layer pellets

Pellets with three layers have been produced following a similar procedure as with the two-layer pellets. Apart from containing two catalyst layers, one of fresh 3%V_2O_5-7%WO_3/TiO_2 and one

impregnated with either KCl or K_2SO_4 to a potassium level of 0.8-1.6 wt.%, a central barrier layer was introduced. The following materials have been used for the barrier layer:

- MgO
- Sepiolite
- A mixture of MgO and sepiolite (4:1 on weight basis)
- Hollandite manganese oxide

MgO has previously proved to be a promising coating material for improving the alkali resistance of SCR catalysts [94,109]. Kristensen [108] obtained improved alkali resistance of a catalyst plate containing 20 wt.% sepiolite, which is a hydrated magnesium silicate based clay mineral [113,114], and mainly observed potassium on the external surface of the plate after exposure to a KCl aerosol. Hence, sepiolite may serve as a separate barrier/coating material or perhaps as a binder for e.g. MgO. A 4:1 mixture of MgO and sepiolite was prepared by grinding the two materials together in a mortar. Hollandite manganese oxide (HMO) can by its own act as an SCR catalyst and has shown excellent alkali resistance due to being able to trap alkali ions at positions different from its SCR active sites [90,115]. The HMO, which was prepared following the synthesis route described by Hu *et al.* [115], was generously supplied by the Department of Chemistry, Technical University of Denmark.

As for the two-layer pellets, 300 mg catalyst (fresh and K-doped respectively) was used for each of the outer layers, while 150-300 mg material was used for the barrier layer. The total thickness of a pellet varied between 3.0 and 3.7 mm, depending on the total amount of material used. A principle sketch of a three-layer pellet is shown in Figure 3.5.

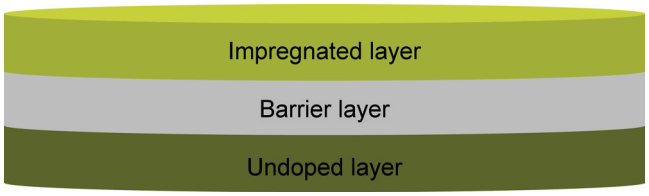

Figure 3.5: Principle sketch of three-layer pellet.

3.6.3. Pellet exposure

The two-layer and three-layer pellets were exposed at 150 °C or 350 °C for up to 7 days in a horizontal lab-scale reactor, illustrated in Figure 3.6. During the exposure, a gas mixture of 6 vol.% O_2 and 3 vol.% H_2O in N_2 was passed through the reactor at a flow rate of about 1000 NmL/min.

The H_2O content was achieved by saturating the O_2/N_2 mixture in a water filled bubble flask at room temperature.

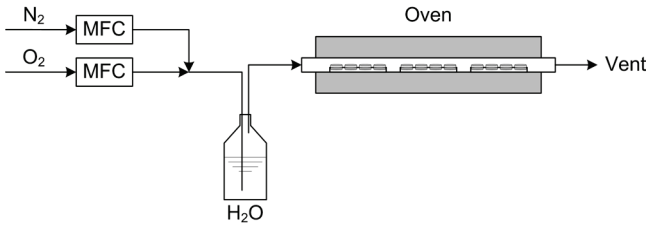

Figure 3.6: Schematic drawing of the lab-scale setup for exposure of two-layer pellets.

3.7. Catalyst characterization

3.7.1. Scanning electron microscopy

For samples exposed in the SCR pilot (plates and monoliths), the distribution of potassium through cross sections of the catalyst walls was measured at Haldor Topsøe A/S using SEM-EDS (Philips XL30 ESEM-FEG). Sections from three parts of the monoliths (top, middle and bottom) and single pieces from each analyzed plate were embedded in epoxy and polished with SiC-paper without using water. In order to avoid charging in the microscope, the specimens were coated with a conductive layer of carbon. In a similar fashion, the potassium profiles across the layers of exposed pellets were measured using SEM-WDS (JEOL JXA-8530F HyperProbe). Each pellet was halved, after being cast into epoxy, so that the potassium profile inside the pellet was measured.

3.7.2. Chemical analysis

For two of the exposed monoliths, the bulk potassium uptake in three sections of each catalyst (top, middle and bottom) has been measured by ICP-OES at Haldor Topsøe A/S.

4. Bench-scale exposure of catalyst plates

4.1. Introduction

This section contains a work in which the potassium poisoning of V_2O_5-(WO_3)/TiO_2 plate-type catalysts, of various composition, has been studied. The plates have been exposed to KCl or K_2SO_4 aerosols of different particle size at various temperatures in a bench-scale setup, and tested for remaining activity in a lab-scale reactor. The purpose has been to investigate the influence of catalyst composition, operating temperature as well as characteristics of the incoming aerosol on the degree of deactivation of the exposed samples.

4.2. Aerosol characterization

To study the potassium poisoning as a function of aerosol size distribution, the position of the injector probe was varied between exposure campaigns. Two fixed positions were used – one close to the burner outlet (40 cm from the probe insertion point), where the flue gas temperature was 1050-1100 °C, and one further downstream (142 cm from the insertion point), where the temperature at the injection point was about 550 °C. Figure 4.1 shows the mass based size distribution, measured by the LPI during injection of KCl solution, at the two respective probe positions. Injecting the solution at the burner outlet resulted in a size distribution with a peak at about 0.12 µm and a geometric mass mean diameter of around 0.15 µm. This mean diameter is only half of that observed by Zheng *et al.* [72] during KCl injection in the same bench-scale setup at a similar temperature (see Figure 2.5). This may be related to a significant difference in the concentration of the injected KCl solution between the two LPI measurements (7.4 g/L vs. 37.3 g/L). In the present study, the salt concentration was kept relatively low in order to avoid clogging of the two-fluid nozzle. An aerodynamic (mass mean) diameter of 0.15 µm roughly corresponds to a Stokes diameter of 0.1 µm for a KCl aerosol. Christensen and co-workers [7,8] measured the size distributions of the aerosols in the flue gas from two different straw fired boilers. Through several measurements the authors obtained mass mean Stokes diameters of 0.2-0.6 µm which are 2-6 times larger than we observed in the bench-scale setup at the given probe position. While the particles obtained in the setup were rather small, particles in this size range are indeed present in the flue gas from full-scale biomass fired power plants [95]. The measured distribution (Burner outlet, Figure 4.1) corresponds to a total aerosol concentration of 9.5 mg/Nm^3, which again corresponds about 12 % of the total injected amount of KCl. The majority of the injected KCl has hence deposited or condensed on surfaces upstream the reactor. The concentration of submicron

particles, measured at the reactor inlet, amounts to 9.0 mg/Nm^3. In the flue gas from a straw and wood chip fired boiler, Zheng *et al.* [24] measured a mass concentration of submicron particles of 415 mg/Nm^3, while Christensen and co-workers [7,8] observed 3-2000 mg/Nm^3 of submicron particles during their particle measuring campaigns. Hence, the particle mass concentration, which the plates have been subjected to in the bench-scale reactor, is rather low in comparison. Injecting the KCl solution further downstream the burner resulted in a particle size distribution peaking at 2.6 µm and with a geometric mass mean (aerodynamic) diameter of 1.1 µm, corresponding to a Stokes diameter of around 0.8 µm. At the lower flue gas temperature at this injection point, the aerosol particles will form by drying of the droplets created at the two-fluid nozzle rather than nucleation of particles from KCl molecules in the gas phase, resulting in particles which are somewhat larger than those observed by Christensen and co-workers [7,8] in full-scale plants. This distribution corresponds to an aerosol concentration of 14.8 mg/Nm^3 (about 19 % of the total injected KCl) with 4.2 mg/Nm^3 being submicron particles.

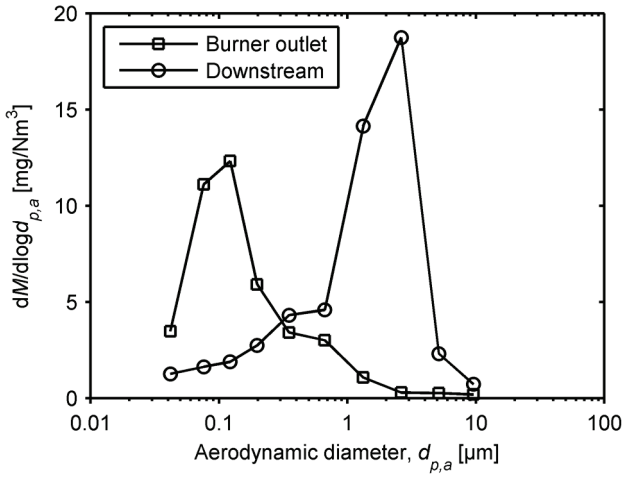

Figure 4.1: Mass based size distributions obtained during injection of a 0.1 M KCl solution at 420 mL/h at the burner outlet (flue gas temperature ≈ 1075 °C) as well as downstream the burner (flue gas temperature ≈ 550 °C).

When injecting a K_2SO_4 solution at the two different positions, no significant difference between the particle size distributions were obtained, as seen in Figure 4.2. Both distributions peak at 1.3 µm and the geometric mass mean (aerodynamic) diameters are 1.2 µm (burner outlet) 1.0 µm (downstream) respectively, corresponding to Stokes diameters of approximately 0.7 and 0.6 µm for K_2SO_4 aerosols. Due to the low vapor pressure of K_2SO_4, the aerosol was thus mostly formed by drying of droplets at both probe positions. The mass based particle concentration of the two distributions is 24.1 and 20.8 mg/Nm^3 respectively (around 27 and 23 % of the total injected K_2SO_4). Submicron aerosols constitute 7.9 and 7.4 mg/Nm^3 of the respective particle concentration.

The distributions measured for the K_2SO_4 aerosols correlate well with the results by Zheng *et al.* [72], obtained at similar conditions in the same setup.

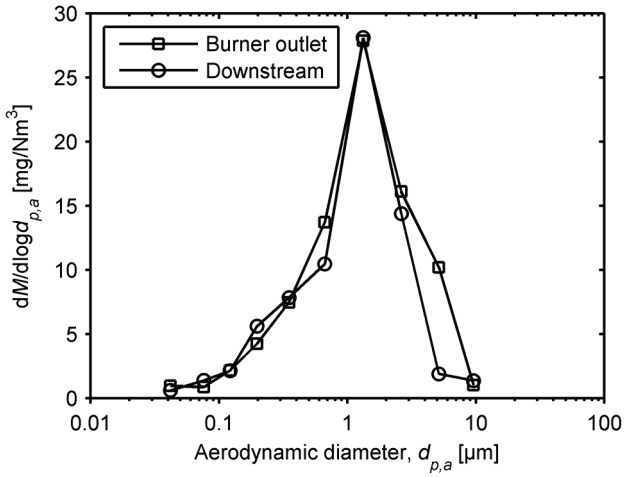

Figure 4.2: Mass based size distributions obtained during injection of a 0.05 M K_2SO_4 solution at 420 mL/h at the burner outlet (flue gas temperature ≈ 1075 °C) as well as downstream the burner (flue gas temperature ≈ 550 °C).

4.3. Ammonia chemisorption on fresh plate catalysts

The measured NH_3 chemisorption capacities of fresh SCR catalyst plates are listed in Table 4.1. Each value in the table is an average of at least two successive chemisorption measurements. The repeatability was in all cases excellent, as illustrated in Figure 4.3. For catalysts which have not been promoted with WO_3, the NH_3 chemisorption capacity, and thereby the amount of active acid sites, increases with the V_2O_5 content, however only slightly when going from 3 to 6 wt.% (from 66 to 70 µmol/g). For catalysts promoted with 7 wt.% WO_3 the NH_3 chemisorption capacity does not seem to depend on the V_2O_5 content. Both the promoted samples with 1 wt.% and the one 6 wt.% V_2O_5 showed an NH_3 chemisorption capacity of 81 µmol/g. This value was in both cases higher than that of the unpromoted counterpart of the respective sample. The NH_3 chemisorption capacity of the 3 wt.% V_2O_5 sample was 66 µmol/g both with and without WO_3 promotion. In general, the results indicate that WO_3 promotion increases the total amount of active acid sites and that this amount will be more or less constant, for the given WO_3 loading, regardless of the V_2O_5 content.

Table 4.1: NH_3 chemisorption capacities of V_2O_5-(WO_3)/TiO_2 catalysts measured at 250 °C.

V_2O_5 content [wt. %]	NH_3 chemisorption capacity [µmol/g]	
	0 wt.% WO_3	7 wt.% WO_3
1	41	81
3	66	66
6	70	81

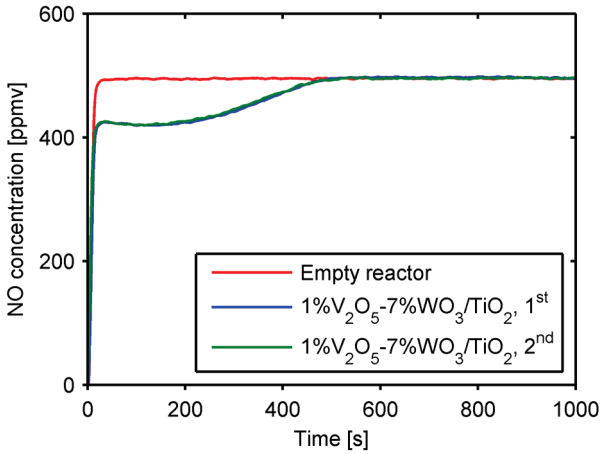

Figure 4.3: NO response during NH_3 chemisorption test in an empty reactor as well as during 2 successive measurements over a 1%V_2O_5-7%WO_3/TiO_2 catalyst. Measurement conditions: [NO] = 500 ppmv, [O_2] = 5 vol.%, [H_2O] ≈ 1. 5 vol.%, balance N_2. Temperature = 250 °C. Total flow = 2730 mL/min. Catalyst mass = 0.64 g.

4.4. Deactivation of aerosol exposed plates

The absolute activity of fresh, unexposed catalyst plates, not reported here, was generally higher (by a factor of 1.2-12.6 at 350 °C) for WO_3 promoted samples as reported by other researchers [21-23]. Furthermore, the activity increased with the V_2O_5 content at temperatures below 400 °C.

Figure 4.4 shows the relative activities of 3%V_2O_5-7%WO_3/TiO_2 catalysts exposed to KCl aerosols in four different campaigns, as a function of temperature. In three of the campaigns the two-fluid nozzle was positioned close to the burner outlet in order to ensure evaporation of the injected KCl solutions and the subsequent formation of submicron aerosol particles. In one of the campaigns the solution was injected into a colder flue gas (downstream burner position) in order to create larger particles (> 1 μm). We speculate larger particles to be less harmful to the SCR catalyst since the deposition rate is lower [72,95] and since the contact area between catalyst surface and potassium rich particles, deposited on the catalyst exterior, will be lower. As seen from the figure, the catalysts exposed in the four campaigns all show significant deactivation. The relative activity of the catalysts exposed at 350 °C for 600 or 300 hours is comparable and very low (< 5 %). The sample exposed at 150 °C for 300 hours shows higher relative activity compared to the above mentioned samples which indicates that the mobility of potassium is lower at reduced temperature. To some extent, this contradicts the observations by Zheng *et al.* [24], who did not see an effect of lowering the operating temperature, from 350 to 250 °C, on the deactivation rate of catalysts exposed to the flue gas from a straw and wood fired boiler. However, in our case the temperature was lowered even further (to 150 °C), which may be the reason for the improved relative activity. In Figure 4.4,

the relative activity of the given sample, exposed at 150 °C for 300 hours, decreases with increasing temperature which may indicate a shift in the selectivity towards ammonia oxidation. Another explanation could be further deactivation of the sample as the temperature was increased during the activity test. This is, however, unlikely since activity at 350 °C was measured twice, first when stepwise increasing the temperature from 250 to 400 °C and once more after the 400 °C measurement had been carried out. As seen from Figure 4.4, the catalyst activity at 350 °C is unchanged after having been operated at 400 °C. The sample exposed to large aerosol particles at 300 °C for 300 hours is only slightly more active than the catalysts exposed to the aerosol of smaller particles. While the LPI measurements (Figure 4.1) showed a clear shift in the particle size distribution towards larger particles when injecting the KCl solution into a colder flue gas, the catalyst may still have been subjected to a significant number of ultrafine particles (on a mass basis: < 1 mg/Nm^3 according to the LPI measurement), e.g. due to re-entrainment of KCl from old wall deposits in the high temperature zone of the setup. While the major part of these deposits had been removed before the experiment with large particles was initiated, the presence of a minor residue cannot be excluded.

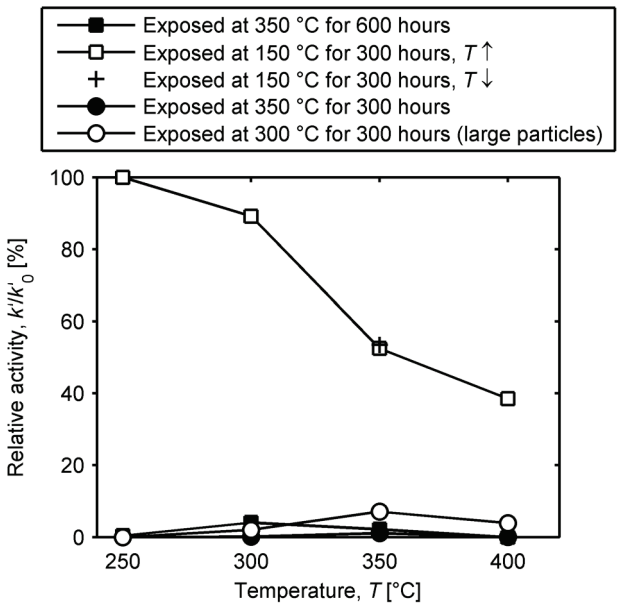

Figure 4.4: Relative catalytic activities of KCl exposed 3%V_2O_5-7%WO_3/TiO_2 catalysts as functions of temperature. Measurement conditions: [NO] = 500 ppmv, [NH_3] = 600 ppmv, [O_2] = 5 vol.%, [H_2O] ≈ 1.4 vol.%, balance N_2. Total flow = 2800 mL/min.

Relative activities, measured at 350 °C, of exposed samples of other compositions are given in Table 4.2. These show similar deactivation trends as the 3%V_2O_5-7%WO_3/TiO_2 samples. The relative activity of the respective samples exposed at 350 °C for either 600 or 300 hours (entries 1a-

3b and 7a-9b in Table 4.2) are generally low and counter intuitively tends to be lowest for samples exposed for 300 hours. This may, however, be accredited to measurement uncertainties which are enhanced when the activities of the exposed samples are very low. For the 1%V_2O_5/TiO_2 sample exposed at 350 °C for 300 hours (7a), no SCR activity could be measured. The same catalyst exposed for 600 hours (1a) shows a remaining activity of 24 % at 350 °C. This may again be due to uncertainties caused by the fact that the initial activity of the given catalyst is fairly low. There may also be variations in the amount of aerosol each plate has been exposed to, depending on its position in the cassette.

Table 4.2: Exposure conditions and relative activities of V_2O_5-(WO_3)/TiO_2 catalysts.

Entry no.	V_2O_5 content [wt. %]	Potassium source	Temperature [°C]	Time [h]	Aerosol distribution mode [µm]	Relative activity at 350 °C [%]	
						a) 0 wt.% WO_3	b) 7 wt.% WO_3
1	1	KCl	350	600	0.12	24	11
2	3	KCl	350	600	0.12	19	2
3	6	KCl	350	600	0.12	1	4
4	1	KCl	150	300	0.12	77	29
5	3	KCl	150	300	0.12	32	52
6	6	KCl	150	300	0.12	47	34
7	1	KCl	350	300	0.12	0	6
8	3	KCl	350	300	0.12	14	1
9	6	KCl	350	300	0.12	2	3
10	3	KCl	300	300	2.6	n.p.[a)]	7
11	6	KCl	300	300	2.6	n.p.	1
12	3	K_2SO_4	150	72	1.3	n.p.	84
13	3	K_2SO_4	150	240	1.3	77	64
14	3	K_2SO_4	300	72	1.3	n.p.	95
15	3	K_2SO_4	300	240	1.3	37	50

a) *n.p.:* Experiment not performed.

As was the case for the 3%V_2O_5-7%WO_3/TiO_2 sample exposed to KCl at 150 °C for 300 hours (Figure 4.4, 5b in Table 4.2), the other samples exposed in this campaign (4a-5a, 6a and 6b in Table 4.2) also show higher remaining activities compared to those exposed at higher temperatures, again indicating reduced mobility of potassium at 150 °C compared to 350 °C. There does not seem to be a definite tendency between V_2O_5 content and the degree of deactivation. However, except for the aforementioned sample 7a, the 1 wt.% V_2O_5 catalysts without WO_3 (1a and 4a) retain a larger fraction of their initial activity compared to WO_3 free samples with higher V_2O_5 loadings. Furthermore, the relative activity of the unpromoted samples exposed at 350 °C for 600 hours (1-3a) decreases with increasing V_2O_5 content. The latter stands in contrast to the results by Kling *et*

al. [95] who generally observed increasing alkali resistance (also based on relative activities) of SCR catalysts, exposed in CHP plants during biomass firing, with increasing vanadia loading. Kling *et al.* [95], however, conducted their activity measurements over 20 mm x 20 mm x 90 mm catalyst elements, and hence their results cannot be directly compared to ours. Heavy external mass transfer limitations, which will decrease during the deactivation of the catalyst and thereby disguise the poisonous effect of potassium, are to be expected during such measurements. Such transport limitations will increase with the intrinsic activity of the tested catalyst, which again is expected to increase with the vanadia content. In our experiments, which were carried out over catalyst powder, the external effectiveness factor at 350 °C, for the most active of the tested catalysts, has been estimated to be above 93 %, while the overall effectiveness factor is above 71 %. The increased deactivation rate of the samples with high V_2O_5 loadings, as observed in our study, may be caused by an increased abundance of active Brønsted acid sites, as indicated by the NH_3 chemisorption data in Table 4.1, over which potassium may diffuse. A similar trend cannot be observed for WO_3 promoted samples, indicating that any effect on the deactivation rate by variations in the V_2O_5 loading is masked by the relatively high content of WO_3. This too correlates with the observations from the chemisorption measurements. In five out of the six cases where the activity of KCl exposed samples have been measured for catalysts both with and without WO_3, and where relative activity at 350 °C is above 10 % for at least one of the samples in the $0\%WO_3/7\%WO_3$ pair (1ab, 2ab, 4ab-6ab and 8ab), the WO_3 promoted samples have lost a larger fraction of their initial activity compared to the unpromoted ones. This is e.g. the case for the $1\%V_2O_5$-$(7\%WO_3)/TiO_2$ catalysts exposed at 150 °C for 300 hours where the unpromoted sample (4a) has retained 77 % of its initial activity, while the promoted sample (4b) only has retained 29 %. This indicates that the increased Brønsted acidity provided by the WO_3 [18,19,116,117], apart from enhancing the initial activity, facilitates the transport of potassium in the catalysts, in a similar fashion as the Brønsted acid sites from V_2O_5, accelerating the poisoning.

The relative activities of $3\%V_2O_5$-$7\%WO_3/TiO_2$ catalysts exposed to K_2SO_4 aerosols are shown in Figure 4.5. As seen from the figure, the sample exposed at 300 °C for 72 hours shows the highest relative activity of the four samples, only deviating from 100 % at temperatures above 300 °C. The sample exposed at 150 °C for the same amount of time has lost a slightly larger fraction of its initial activity. The fact that the sample exposed at the highest temperature has deactivated the least contradicts the observations from the KCl exposed catalysts. This might be due to an initial activity drop during the first hours of exposure which may vary from catalyst to catalyst, and which is less

dependent on exposure conditions. Furthermore, small variations in the amount of aerosol the individual catalyst have been exposed to, e.g. due to being positioned differently in the cassette, may have a relatively large effect on the activity in the beginning of an exposure campaign. After 240 hours of exposure, both samples have deactivated further, and the sample exposed at 150 °C shows higher relative activity than that subjected to a K_2SO_4 aerosol at 300 °C, as expected. The K_2SO_4 exposed catalysts have deactivated significantly less compared to samples exposed to KCl at similar conditions, and the deactivation seem to be less temperature dependant. This indicates that K_2SO_4 is less poisonous compared to KCl, as previously reported by Zheng *et al.* [6,72]. However, as explained earlier, the particles generated during K_2SO_4 injection tended to be larger than those formed under KCl injection. Thus, an effect of particle size on the degree of deactivation cannot be excluded.

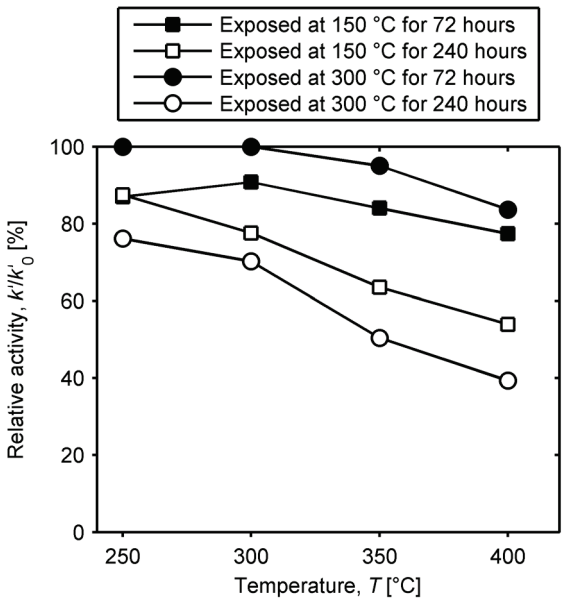

Figure 4.5: Relative catalytic activities of K_2SO_4 exposed $3\%V_2O_5$-$7\%WO_3/TiO_2$ catalysts as functions of temperature. Measurement conditions: [NO] = 500 ppmv, [NH_3] = 600 ppmv, [O_2] = 5 vol.%, [H_2O] ≈ 1.4 vol.%, balance N_2. Total flow = 2800 mL/min.

Table 4.2 lists relative activities (measured at 350 °C) of both unpromoted and WO_3 promoted $3\%V_2O_5/TiO_2$ catalysts exposed to K_2SO_4 aerosols (entries 12b-15b). As for the WO_3 promoted samples (Figure 4.5, 13b and 15b in Table 4.2) the unpromoted samples exposed for 240 hours show lower activity at the higher exposure temperature of 300 °C compared to exposure at 150 °C, once again indicating that the mobility of potassium is reduced at lower operating temperatures.

The significant deactivation observed for the catalyst plates, after only a few hundred hours of exposure in the bench-scale setup, is more severe than what is observed in full-scale biomass fired plants [24,95,118]. One explanation could be that the particles produced in the bench-scale setup, in several of the experiments, were smaller than those observed in full-scale plants, as previously discussed. Furthermore, the catalysts exposed in the bench-scale reactor were subjected to the pure potassium salts. In a full-scale plant, the deposited particles may contain other elements such as silicon and calcium [7,95,118]. The presence of compounds containing these elements may, to some extent, delay the potassium poisoning of the catalyst, either by dilution or by binding [119] a fraction of the potassium as inert species.

4.5. Potassium profiles in exposed plates

Figure 4.6 shows the SEM-EDS measured K/V molar ratios across the wall of three 3%V_2O_5-7%WO_3/TiO_2 catalyst plates exposed to either KCl or K_2SO_4 aerosols at various temperatures and exposure times. As seen from the figure, the thickness of the individual plates varied between 900 to about 1400 μm. The plate exposed to KCl at 350 °C for 600 hours has the highest K/V ratio, throughout its thickness, of the three specimens. Very high K/V ratios can be observed near the edges of the samples which drop steeply to a near constant level inside the catalyst. The average K/V ratio calculated at the distance from 100 to 800 μm is 0.60. For a 3%V_2O_5-WO_3/TiO_2 catalyst impregnated with KCl to a K/V ratio of 0.4, Zheng *et al.* [6] reported a remaining activity of about 40 % at 250 °C, while a K/V ratio of 0.7 reduced activity to around 10 % of its original value. Chen and co-workers [42,67] reported an activity loss of approximately 90 % at 300 °C for a 5%V_2O_5/TiO_2 catalyst impregnated with KNO_3 to a K/V ratio of about 0.5, while data from Kamata *et al.* [69] show a decrease in activity of nearly 70 % at 360 °C for a 1%V_2O_5-8%WO_3/TiO_2 catalyst containing 0.3 wt.% K_2O (from KNO_3 impregnation), corresponding to a K/V molar ratio of about 0.6. While these catalysts and/or test conditions are not entirely comparable to those in the present study, a K/V ratio of 0.60 does not seem to fully explain the complete deactivation observed for the given catalyst, as illustrated in Figure 4.4. The slight discrepancy between the activity and the K/V ratio of the catalyst may have arisen during the preparation of the activity measurement. When a section of the catalyst plate was crushed down, KCl particles deposited on the external surface of that section will be mixed into the catalyst powder possibly allowing for further potassium spreading and deactivation of the catalyst, either during the crushing procedure and/or during the

actual activity measurement where the catalyst powder is heated. No further deactivation of the catalysts over time was, however, observed during the performed activity measurements.

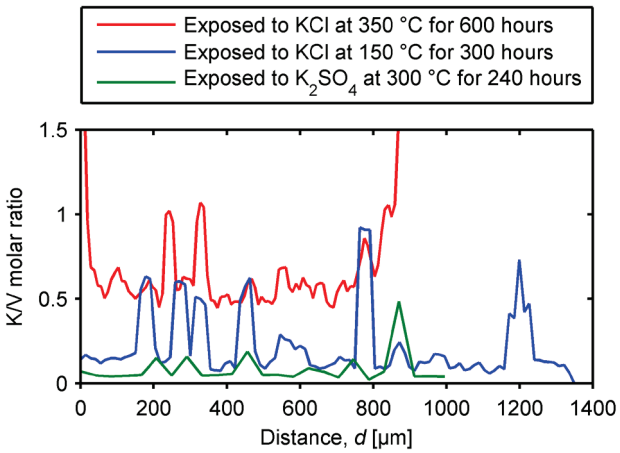

Figure 4.6: K/V molar ratios across the thickness of 3%V_2O_5-7%WO_3/TiO_2 catalyst plates exposed to aerosols of KCl or K_2SO_4.

The K/V ratios through the two remaining samples, i.e. the one exposed to KCl at 150 °C for 300 hours and the one exposed to K_2SO_4 at 300 °C for 240 hours, are low, around or below 0.1. Some peaks in the K/V ratio can be observed inside the first of the two, however, these are artifacts from where the electron beam hits a ceramic fiber. The low K/V ratios in the two latter samples are in good agreement with their higher remaining activity compared to the first sample although they might not explain the observed deactivation of about 50 % at 350 °C. At lower temperatures, however, these specimens retained most of their initial activity as seen from Figure 4.4 and 4.5.

4.6. Conclusion

Plates of industrial type V_2O_5-(WO_3)/TiO_2 SCR catalysts have been exposed to KCl or K_2SO_4 aerosols in a bench-scale reactor in order to investigate catalyst deactivation (by potassium poisoning) under biomass firing conditions. All catalysts exposed for 240 hours or longer showed significant deactivation. Samples exposed at 150 °C rather than 300/350 °C, however, showed higher remaining activity indicating decreased potassium mobility with decreasing temperature. Increasing the particle size of the KCl aerosol did not seem to reduce the deactivation rate of the exposed samples. This may, however, be due a sustained presence of ultrafine KCl particles in the flue gas, e.g. released from old KCl deposit in the high temperature zone of the setup. The K_2SO_4 exposed catalysts had deactivated considerably less than the KCl exposed ones. This could be due to K_2SO_4 being less mobile once deposited on the catalyst. However, measurements showed that the

particle size distribution of the K_2SO_4 aerosol obtained in the setup was shifted towards larger particles compared to that of the KCl aerosol, which may lead to a slower deposition rate of particles on the external surface of each catalyst plate. Hence, an effect of particle size on the catalyst deactivation cannot be excluded.

The relative activity of the exposed catalysts indicates that WO_3 promoted samples, which in general have higher NH_3 adsorption capacities, have lost a larger fraction of their initial activity compared to unpromoted ones. This implies that increased Brønsted acidity facilitates the potassium transport in the catalyst as well as leads to a higher equilibrium uptake, which supports the proposed theory of diffusion of potassium ions via Brønsted acid sites. It should, however, be noted that the absolute activity of promoted catalysts in general is significantly higher than for unpromoted samples and so it may not be favorable to use unpromoted catalysts in biomass fired systems. The results indicate that a lower operating temperature and high conversion of KCl to K_2SO_4 will enhance the life-time of an SCR catalyst.

5. Multi-layer pellet experiments

5.1. Introduction

A study on the potassium mobility in SCR catalysts has been carried out using a newly conceived experimental protocol. This involves pellets consisting of one undoped layer and one layer of potassium impregnated SCR catalyst. By heat treatment of the pellets, followed by measurement of the resulting potassium profiles across the pellet width, using SEM-WDS, detailed information on the rate of potassium diffusion in SCR catalysts can be obtained. The purpose of this work has been to investigate the mobility of potassium as a function of the salt used as dopant (KCl or K_2SO_4), catalyst composition, as well as operating temperature. By introducing a third layer in between the two catalyst layers, it has also been possible to screen for materials which can hinder the diffusion of potassium, from one catalyst layer to the other. Such a material may ultimately be used as a protective coating for an alkali resistant SCR catalyst.

5.2. Potassium mobility in two-layer pellets

5.2.1. The influence of dopant salt

Figure 5.1 shows the potassium profiles in an unexposed two-layer pellet as well as in pellets exposed for 2 and 7 days, measured by SEM-WDS analysis. The impregnated layer in these pellets was made from a $3\%V_2O_5$-WO_3/TiO_2 catalyst doped with an aqueous KCl solution to a potassium level of about 1.6 wt.%, corresponding to a molar K/V ratio of 1.2 (nominal). In this particular case, the powdered catalyst had not been calcined subsequent to the KCl impregnation. Even for the unexposed pellet, potassium has, surprisingly, partly diffused into the undoped layer, as seen from the figure. The potassium concentration in the pellets exposed for 2 and 7 days are comparable. While the concentration drops through the impregnated layer, it seems to be leveling out at around 0.6 wt.% potassium in the undoped layer, corresponding to a K/V ratio of about 0.5. This K/V ratio is comparable to that found in the catalyst plate exposed to KCl aerosols at 350 °C for 600 hours (see Figure 4.6), which indicates that there exists a saturation level at which potassium does no longer diffuse into the SCR catalyst. This level would be expected to correspond to the concentration of Brønsted acid sites.

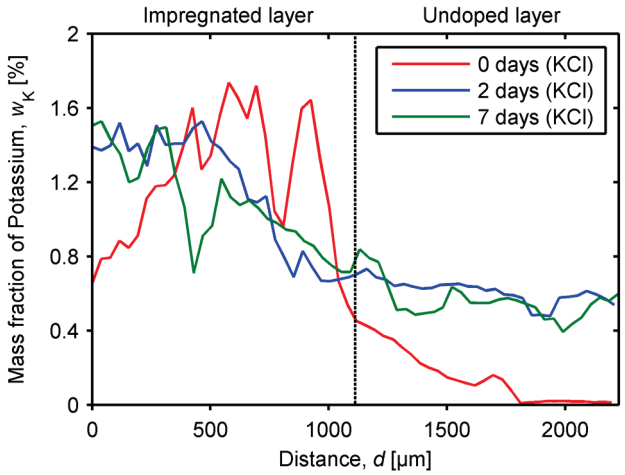

Figure 5.1: Potassium profiles in KCl impregnated (1.6 wt.% K, nominal) two-layer pellets of 3%V_2O_5-WO_3/TiO_2 catalyst, exposed to a flow (1000 NmL/min) of 6 vol.% O_2 and 3 vol.% H_2O in N_2 at 350 °C for 0-7 days.

Figure 5.2 shows the chlorine level in the same three pellets. As seen from the figure, a significant amount of chlorine is present in the impregnated layer of the unexposed pellet, which correlates well with the amount of potassium in the specimen. No chlorine is present in the undoped layer. The two exposed samples, however, are chlorine free all the way through, indicating that chlorine readily leaves the sample (likely as HCl) when exposed to a flow of N_2, O_2 and H_2O at 350 °C. This is in agreement with the observations by Wu *et al.* [77] who on found a minute chlorine level in a KCl impregnated SCR catalyst after calcination at 400 °C for 2 hours. This implies that potassium has to coordinate to something else when left behind by its counter ion, most likely being the Brønsted acid sites on the catalyst [67,72].

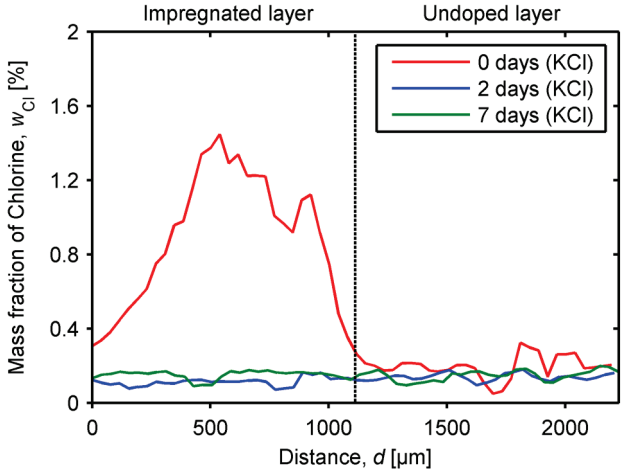

Figure 5.2: Chlorine profiles in KCl impregnated (1.6 wt.% K, nominal) two-layer pellets of 3%V_2O_5-WO_3/TiO_2 catalyst, exposed to a flow (1000 NmL/min) of 6 vol.% O_2 and 3 vol.% H_2O in N_2 at 350 °C for 0-7 days.

The above indicates that the potassium transport in SCR catalysts involves two steps: 1) reaction between salt bound potassium and catalyst surface, and 2) diffusion of potassium over the surface. The latter appears to be fast, judging from the rather flat potassium profiles in the undoped layers of the exposed pellets in Figure 5.1. Before heat treatment of a pellet, potassium is present in the impregnated layer as salt particles, in intimate contact with the catalyst material, and possibly also as surface bound potassium. The latter may explain the movement of potassium into the undoped layer before heat treatment. For an aerosol exposed SCR catalyst, only the external surface will be in close contact with ultrafine potassium salt particles, and thus the potassium transport, into the catalyst, will be slower. Figure 5.3 shows the potassium profile in a two-layer pellet consisting of a layer of pure KCl (particles size < 250 µm) and a layer of $3\%V_2O_5$-$7WO_3/TiO_2$ catalyst, exposed for 7 days. As seen from the figure, no potassium has moved into the catalyst layer. This implies that the salt particles not only have to be in close contact with the catalyst, in order for potassium to leave the salt in reaction with the surface, the particles also need to be very small – most likely in the submicron range. A similar conclusion was obtained by Zheng *et al.* [72]. They exposed catalyst plates with deposits of KCl particles (with a mean diameter of 350 µm) to 200 NmL/min of air with about 3 vol.% H_2O and 1000 ppmv SO_2 at 350 °C. After exposure for nearly 2400 hours, the catalysts had only lost 13 % of their initial activity at 350 °C. The reason for the much slower transport of potassium from the pure KCl layer, into the catalyst, is probably due to a lower contact area between the particles and the catalyst, despite the compression during the pellet formation.

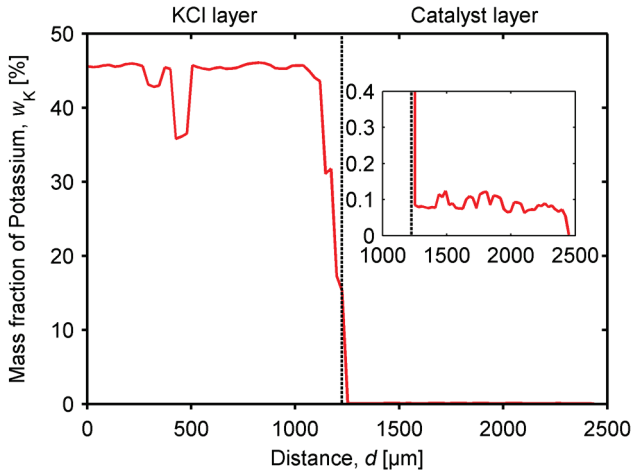

Figure 5.3: Potassium profiles in a two-layer pellet containing a layer of pure KCl and a layer of a $3\%V_2O_5$-$7WO_3/TiO_2$ catalyst, exposed to a flow (1000 NmL/min) of 6 vol.% O_2 and 3 vol.% H_2O in N_2 at 350 °C for 7 days.

The potassium level in three two-layer pellets of $3\%V_2O_5$-WO_3/TiO_2 catalyst with K_2SO_4 impregnated layers are shown in Figure 5.4. Two of the pellets have impregnated layers initially

containing about 0.8 wt.% potassium (K/V ≈ 0.6), while the third pellet has a layer doped to a potassium level of approximately 1.6 wt.%. One pellet is unexposed while two others have been exposed for 8 hours. For comparison, the potassium profile in a pellet with a KCl impregnated layer (0.8 wt.% potassium), also exposed for 8 hours, has been included as well. Similar to the impregnation with KCl, some potassium has moved into the undoped layer prior to exposure. Looking at the exposed pellets with impregnated layers containing 0.8 wt.% potassium from either K_2SO_4 or KCl, there is a significant difference in the potassium level in the undoped layers. For the pellet with the K_2SO_4 impregnated layer the potassium concentration has increased slightly compared to that in the unexposed pellet, and is essentially zero half way through the undoped layer, while the potassium level in the undoped layer of the pellet with the KCl impregnated layer is considerably higher. In the case of the pellet with the impregnated layer doped with 1.6 wt.% potassium from K_2SO_4, the potassium level in the undoped side, upon exposure for 8 hours, is comparable to that of the KCl impregnated pellet. Hence, potassium from K_2SO_4 appears to be half as mobile as that of KCl.

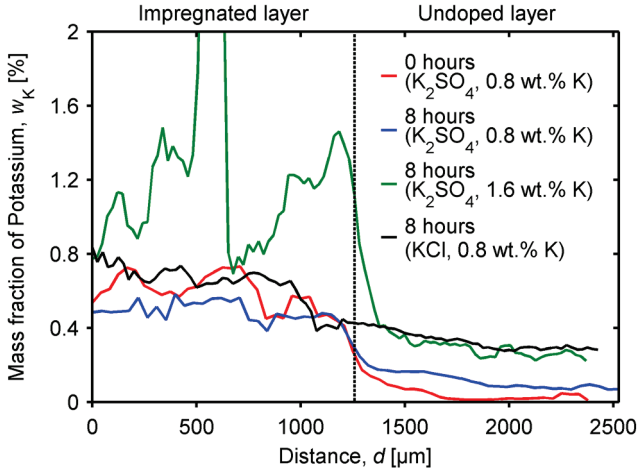

Figure 5.4: Potassium profiles in K_2SO_4 or KCl impregnated (0.8-1.6 wt.% K, nominal) two-layer pellets of 3%V_2O_5-WO_3/TiO_2 catalyst, exposed to a flow (1000 NmL/min) of 6 vol.% O_2 and 3 vol.% H_2O in N_2 at 350 °C for 0-8 hours.

Figure 5.5 shows the sulfur level in the two pellets with K_2SO_4 impregnated layers. Unlike chlorine, the sulfur stays in the impregnated layer both before and after exposure. These observations may explain the apparent difference in mobility between potassium bound in KCl and K_2SO_4.

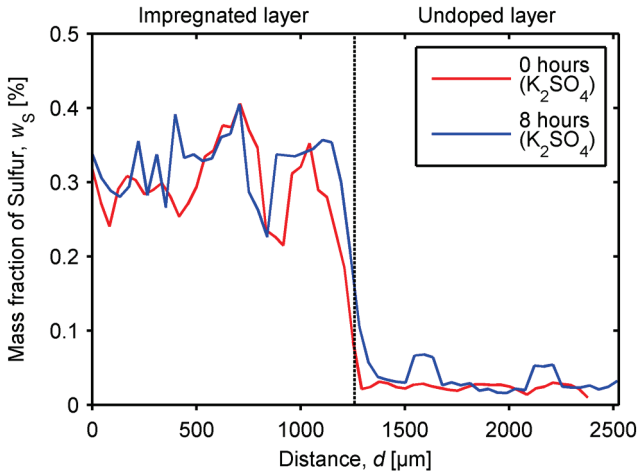

Figure 5.5: Sulfur profiles in K_2SO_4 impregnated (0.8 wt.% K, nominal) two-layer pellets of 3%V_2O_5-WO_3/TiO_2 catalyst, exposed to a flow (1000 NmL/min) of 6 vol.% O_2 and 3 vol.% H_2O in N_2 at 350 °C for 0-8 hours.

It is speculated that in order for salt bound potassium to diffuse into the undoped layer, it first needs to react with a Brønsted acid site on the catalyst, e.g. through the following reactions [6]:

$$\text{-M-OH} + \text{KCl} \overset{k_{\text{KCl}}}{\rightarrow} \text{-M-OK} + \text{HCl} \tag{5.1}$$

$$\text{-M-OH} + \text{K}_2\text{SO}_4 \overset{k_{\text{K}_2\text{SO}_4}}{\rightleftarrows} \text{-M-OK} + \text{KHSO}_4 \tag{5.2}$$

$$\text{-M-OH} + \text{KHSO}_4 \overset{k_{\text{KHSO}_4}}{\rightleftarrows} \text{-M-OK} + \text{H}_2\text{SO}_4 \tag{5.3}$$

Where -M-OH is either a vanadium or tungsten Brønsted acid center. A difference between KCl and K_2SO_4, as indicated by the results in Figure 5.2 and 5.5, is that the reaction product of the counter ion for KCl (HCl) is gaseous and thus leaves the sample, in this way pulling the reaction towards the right. The sulfur species are either non-volatile at the reaction conditions or significantly less volatile than HCl, which in principle could allow for the reverse reactions. Consequently, potassium bound in KCl can more easily escape its solid matrix compared to that bound in K_2SO_4 which may partly explain why potassium in KCl acts as a more efficient poison than K_2SO_4. $KHSO_4$, which is the product of reaction 5.2, melts at around 215 °C and may to some extent convert into $K_2S_2O_7$ at temperatures above 300 °C [120,121]. However, if salt melts were formed during exposure of the K_2SO_4 impregnated pellets, the sulfur would likely have diffused, into the undoped layer, together with potassium. The fact that chlorine leaves the sample upon short time exposure while sulfur stays in the specimen, as well as the apparent twofold difference in the mobility of potassium from K_2SO_4 and KCl, observed in Figure 5.4, suggest that only the first potassium atom in K_2SO_4 has a

reactivity comparable to that of KCl, while the reaction between $KHSO_4$ and -M-OH sites (5.3) is much slower, i.e.:

$$k_{KCl} \geq k_{K_2SO_4} \gg k_{KHSO_4} \quad (5.4)$$

5.2.2. The influence of catalyst composition

A series of two-layer pellets was produced from V_2O_5-WO_3/TiO_2 catalysts with 0, 1, 3 and 6 wt.% V_2O_5 and 7 wt.% WO_3. Furthermore, a two-layer pellet of WO_3 free 3%V_2O_5/TiO_2 catalyst and one of pure fiber reinforced TiO_2 carrier were produced. In all cases the impregnated layer was made from the respective catalyst doped with KCl to a potassium level of about 1.6 wt.%, corresponding to nominal K/V ratios of 3.7, 1.2 and 0.6 for the three different (nonzero) V_2O_5 loadings. Figure 5.6 shows the potassium profiles in these pellets after exposure for 7 days.

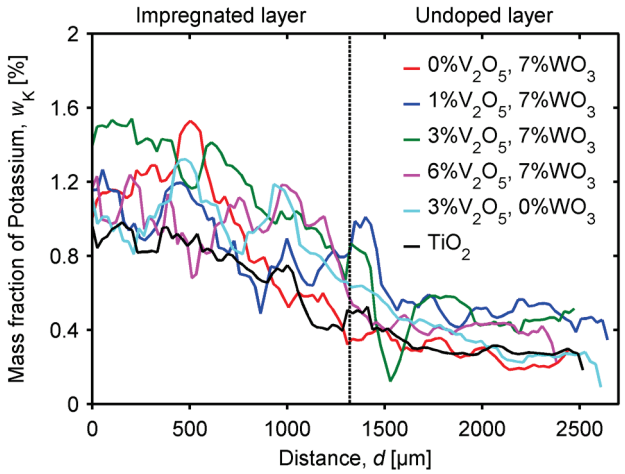

Figure 5.6: Potassium profiles in KCl impregnated (1.6 wt.% K, nominal) two-layer pellets of V_2O_5-(WO_3)/TiO_2 catalysts, exposed to a flow (1000 NmL/min) of 6 vol.% O_2 and 3 vol.% H_2O in N_2 at 350 °C for 7 days.

For the three pellets of catalyst containing both V_2O_5 and WO_3 the potassium concentration has reached comparable levels of 0.4-0.5 wt.% in the undoped layer. Hence, there does not seem to be a connection between potassium mobility and V_2O_5 loading for catalysts with relatively high WO_3 loadings. For the 3%V_2O_5/TiO_2 sample the potassium diffusion seem to have proceeded at a slower rate reaching a potassium level of about 0.25 wt.% far inside the undoped layer. Similar levels are found in the 7%WO_3/TiO_2 pellet and the pellet made from TiO_2 carrier. As indicated by plate exposure experiments, the two-layer pellet data further indicate that WO_3 promotion facilitates the potassium transport in the SCR catalyst. Furthermore, the higher potassium mobility in V_2O_5-WO_3/TiO_2 catalysts seems to be due to some interaction between V_2O_5 and WO_3 which is

independent on the V_2O_5 content. The latter is also in good agreement with the observations from the activity measurements as well as the NH_3 chemisorption study on the exposed plates.

5.2.3. The influence of exposure temperature

Figure 5.7 shows the potassium profiles in four two-layer pellets (of a 3%V_2O_5-7%WO_3/TiO_2 catalyst) which have been exposed at either 150 or 350 °C for 7 days. In two of the pellets, the impregnated layer was doped with KCl, while K_2SO_4 was used in the two other pellets. In all cases the original, nominal potassium concentration in the impregnated layer was 1.6 wt.%. The profiles confirm what was indicated by the plate exposure experiments, i.e. that the mobility of potassium increases with the exposure temperature. In the undoped layer, the highest potassium level, by a considerable margin, is found for the KCl impregnated pellet exposed at 350 °C – once again indicating that potassium bound KCl is more mobile that that bound in K_2SO_4. The potassium level in the undoped layer of the pellet with K_2SO_4, exposed at 350 °C, is comparable to that of the pellet with KCl, exposed at 150 °C. As expected, based on the previous observations, the lowest potassium concentration is found in the K_2SO_4 impregnated pellet which was exposed at 150 °C. Both the rate of reaction between particle bound potassium and surface sites, and the surface diffusivity of potassium are expected to increase with the temperature. However, as potassium bound to Brønsted acid sites appears to diffuse already at room temperature (as seen from Figure 5.1), it is likely the prior that is the most temperature dependant.

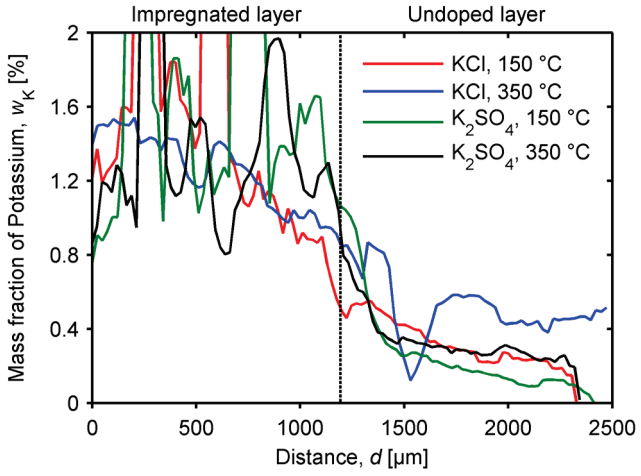

Figure 5.7: Potassium profiles in KCl/K_2SO_4 impregnated (1.6 wt.% K, nominal) two-layer pellets of 3%V_2O_5-7%WO_3/TiO_2 catalyst, exposed to a flow (1000 NmL/min) of 6 vol.% O_2 and 3 vol.% H_2O in N_2 at 150 or 350 °C for 7 days.

5.3. Screening of barrier materials in three-layer pellets

5.3.1. Magnesium oxide

Figure 5.8 shows the potassium profiles in two three-layer pellets exposed for 32 hours, measured by SEM-WDS analysis. The impregnated layer was made from a 3%V_2O_5-7%WO_3/TiO_2 catalyst doped with KCl to a potassium level of about 0.8 %, while the central layer (named "X" in Figure 5.8) was either made from undoped catalyst or MgO.

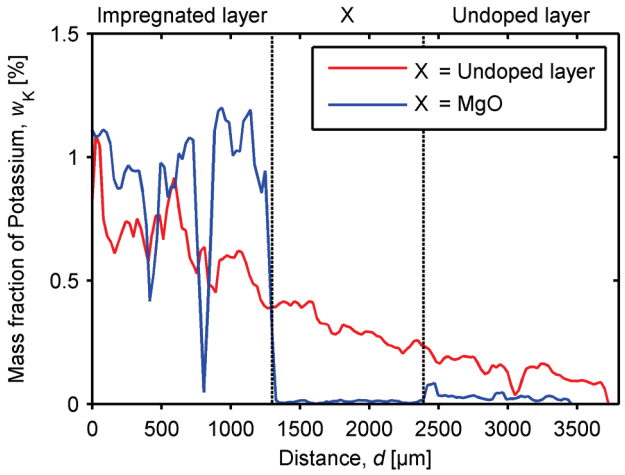

Figure 5.8: Potassium profiles in KCl impregnated (0.8 wt.% K, nominal) three-layer pellets of 3%V_2O_5-7%WO_3/TiO_2 catalyst, exposed to a flow (1000 NmL/min) of 6 vol.% O_2 and 3 vol.% H_2O in N_2 at 350 °C for 32 hours.

As seen from the figure, potassium has diffused seamlessly through the entire pellet in the sample with two undoped layers, while it is retained in the impregnated layer of the sample with the MgO barrier. The slight potassium level found in the undoped side of the latter pellet is likely to originate from the fiber support of the original catalyst. The figure illustrates: 1) That the preparation method ensures a continuous pellet in which potassium may diffuse freely, unless it is chemically blocked by the barrier layer, and 2) That MgO can effectively block the diffusion of potassium, likely due to its own alkaline nature, and may thus be applicable as a coating material for SCR catalysts as stated in a patent application by Jensen *et al.* [109]. One concern is that magnesium itself is a weak poison for SCR catalysts [17,47,82], which may diffuse into the catalyst causing deactivation. However, from Figure 5.9, which shows the SEM-WDS measured profiles of vanadium and magnesium in the pellet with the MgO layer, it is apparent that magnesium has not moved into either of the catalyst layers, and vise versa for vanadium. This indicates that the diffusion of magnesium in SCR catalysts is at least much slower than that of potassium and that magnesium poisoning of a coated catalyst can be avoided – at least if it is applied by a dry coating method as used here.

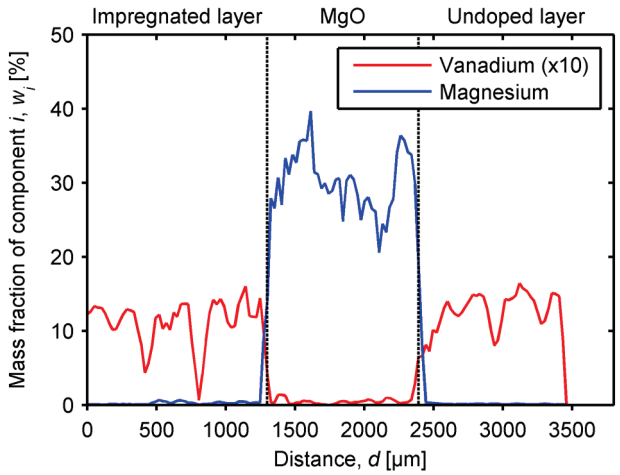

Figure 5.9: Vanadium and magnesium profiles in a Catalyst/MgO/Catalyst three-layer pellet, exposed to a flow (1000 NmL/min) of 6 vol.% O_2 and 3 vol.% H_2O in N_2 at 350 °C for 32 hours. Catalyst = 3%V_2O_5-7%WO_3/TiO_2.

To keep the transport limitations at a minimum, the MgO layer on a coated catalyst should be significantly thinner (1-100 µm [109]) than the one simulated by the pellet in Figure 5.8 and 5.9. Figure 5.10 shows the potassium profile in a three-layer pellet, exposed for 7 days, with an MgO barrier layer of about one third of the thickness of that in the previous sample (i.e. around 300 µm), which is about the thinnest practically achievable in the pellet die.

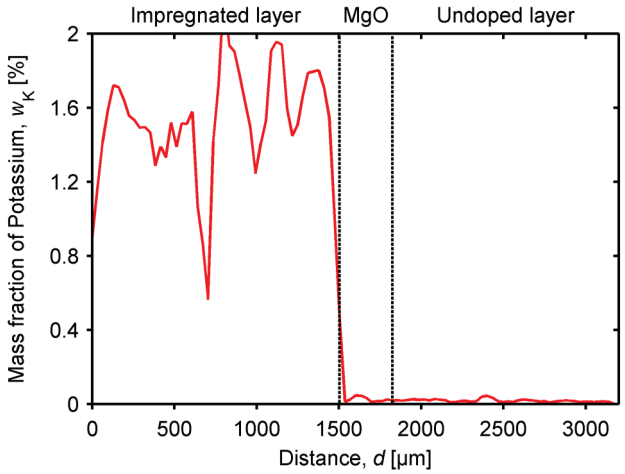

Figure 5.10: Potassium profile in a KCl impregnated (1.6 wt.% K, nominal) Catalyst/MgO/Catalyst three-layer pellet, exposed to a flow (1000 NmL/min) of 6 vol.% O_2 and 3 vol.% H_2O in N_2 at 350 °C for 7 days. Catalyst = 3%V_2O_5-7%WO_3/TiO_2.

In this pellet, the impregnated layer was doped with KCl to a nominal level of 1.6 wt.% potassium. As with the previous pellet, the MgO layer has blocked the diffusion of potassium, retaining it in the impregnated layer. Not only does the thinner MgO layer performs just as well, in keeping the

potassium from the undoped catalyst, as the one in Figure 5.8, it is also apparent that the MgO layer is still potassium free even after one week of exposure. This further signifies that MgO is a good candidate for a potassium resistant coating material for SCR catalysts.

5.3.2. Sepiolite

A three-layer pellet consisting of a KCl impregnated 3%V_2O_5-7%WO_3/TiO_2 catalyst layer (1.6 wt.% potassium, nominal), a sepiolite barrier layer, and a fresh catalyst layer was exposed for 7 days. As seen from the potassium profile in Figure 5.11, potassium appears to have diffused unhindered through the central layer. Sepiolite hence appears as being a poor chemical potassium barrier. This is in agreement with the research by Kristensen [108] which indicates that sepiolite mainly acts as a physical barrier, preventing deposited potassium in reacting with active sites. In the case of the three-layer pellet, the reaction between salt bound potassium and active sites occurs in the impregnated layer, at some distance from the sepiolite interface. While sepiolite clearly facilitates the surface diffusion of potassium, it may thus still be applicable as a coating material for SCR catalysts exposed to salt bound potassium.

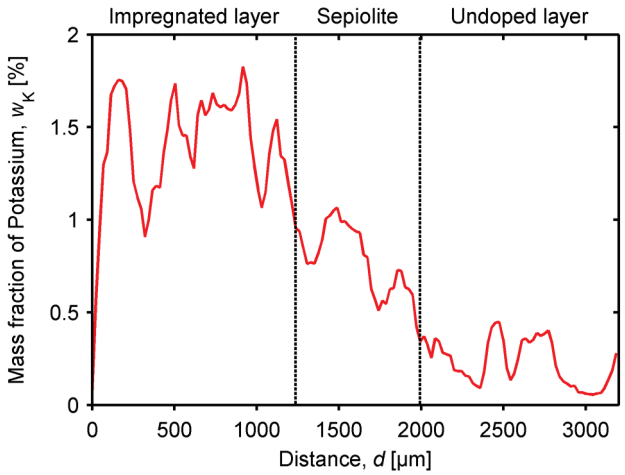

Figure 5.11: Potassium profile in a KCl impregnated (1.6 wt.% K, nominal) Catalyst/Sepiolite/Catalyst three-layer pellet, exposed to a flow (1000 NmL/min) of 6 vol.% O_2 and 3 vol.% H_2O in N_2 at 350 °C for 7 days. Catalyst = 3%V_2O_5-7%WO_3/TiO_2.

Another possibility is to use the soft sepiolite clay as a binder for the protective coating material. A coating based on MgO might benefit from a binder since MgO, on its own, is rather brittle [122] and may lead to fragile coatings that do not adhere well to the substrate. Figure 5.12 shows the potassium profile in a three-layer pellet with a KCl impregnated 3%V_2O_5-7%WO_3/TiO_2 catalyst layer (1.6 wt.% potassium, nominal), a barrier layer consisting of a 4:1 mixture (on weight basis) of MgO and sepiolite ("MgO + Sep." in the figure), and a layer of fresh catalyst. The pellet was

exposed for 7 days. As seen from the figure, the MgO + sepiolite barrier has prevented potassium in reaching the undoped layer, however, some potassium seem to have accumulated in the central layer. This is likely due to ability of sepiolite to facilitate the potassium transport, as apparent from Figure 5.11. This effect might be reduced by decreasing the sepiolite fraction in the barrier layer.

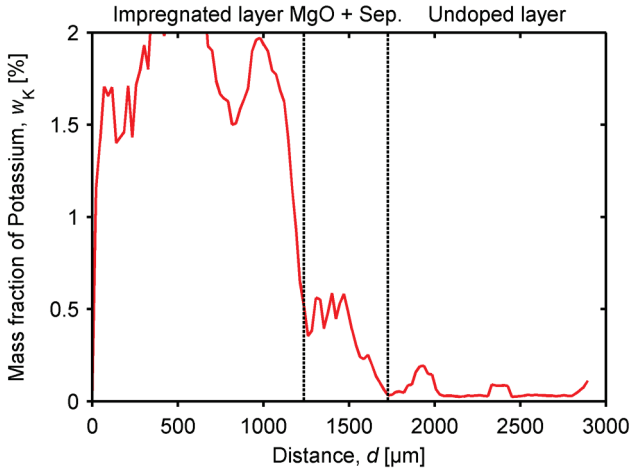

Figure 5.12: Potassium profile in a KCl impregnated (1.6 wt.% K, nominal) Catalyst/MgO + Sepiolite/Catalyst three-layer pellet, exposed to a flow (1000 NmL/min) of 6 vol.% O_2 and 3 vol.% H_2O in N_2 at 350 °C for 7 days. Catalyst = 3%V_2O_5-7%WO_3/TiO_2.

5.3.3. Hollandite manganese oxide

Figure 5.13 shows the potassium profiles in three three-layer pellets with HMO barrier layers, exposed for either 32 hours or 7 days. In all cases the catalyst layers were made from a 3%V_2O_5-7%WO_3/TiO_2 catalyst. In the pellets exposed for 32 hours, the impregnated layer was doped with either KCl or K_2SO_4 to a level of about 0.8 wt.% potassium. In the pellet exposed for 7 days, the impregnated layer was doped with KCl to a nominal potassium level of 1.6 wt.%. As seen from the figure, potassium is in all cases kept from the undoped layer, although it seems to have penetrated into the HMO layer, to a small extent, after 32 hours of exposure. The potassium diffusion in the HMO layer is, however, significantly slower than that in a vanadia based catalyst (as seen in Figure 5.8). Furthermore, potassium from the KCl impregnated pellet seem to have diffused slightly further into the HMO layer, which is in agreement with the observations from the two-layer pellets. After 7 days of exposure, the diffusion of potassium in the HMO layer is more evident and about half of the 600 µm thick layer has been penetrated. The fact that potassium diffuses into the barrier layer may not be surprising since the HMO contains internal tunnels which can accommodate potassium ions [90]. If HMO is to be used as a coating material, it will have to be synthesized in large quantities e.g. using manganese sulfate ($MnSO_4$) and ammonium persulfate ($(NH_4)_2S_2O_8$) [115] as

raw materials. Hence, while the HMO can protect the catalyst by slowing the potassium diffusion, it may not be a feasible coating material.

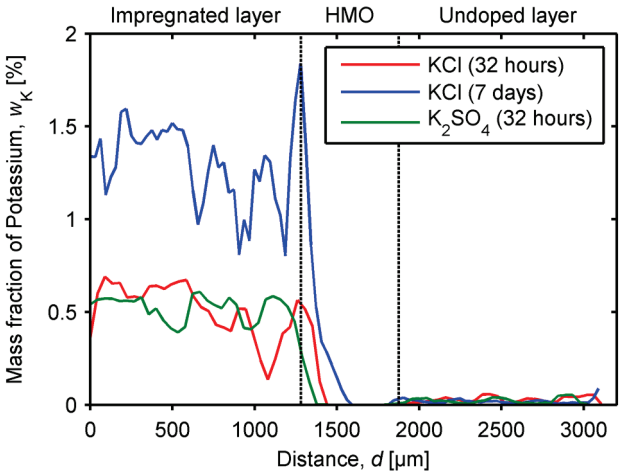

Figure 5.13: Potassium profiles in KCl or K_2SO_4 impregnated (0.8 or 1.6 wt.% K, nominal) Catalyst/HMO/Catalyst three-layer pellets, exposed to a flow (1000 NmL/min) of 6 vol.% O_2 and 3 vol.% H_2O in N_2 at 350 °C for 32 hours or 7 days. Catalyst = 3%V_2O_5-7%WO_3/TiO_2.

5.4. Conclusion

The potassium mobility in SCR catalysts was studied using a novel experimental method in which pellets composed of two similar layers of catalyst were heat treated. One of the layers was impregnated with KCl or K_2SO_4 while the other layer was undoped. These investigations clearly showed that potassium bound in KCl has a much higher mobility in SCR catalysts compared to that in K_2SO_4, where only one of the potassium atoms essentially is able to leave the solid matrix. While chlorine completely left the catalyst pellet upon treatment at SCR conditions (350 °C, 6 vol.% O_2 and 3 vol.% H_2O in N_2) sulfur stayed in the sample and was immobile. A study on the potassium mobility in two-layer pellets as a function of catalyst composition indicates that the presence of WO_3 facilitates the potassium transport, which was also indicated by the results from the plate exposure campaigns in the previous section. It was furthermore found that the potassium mobility in SCR catalysts increases with the exposure temperature, likewise in agreement with the observations from the plate exposures. The results support a view where potassium reacts with and subsequently diffuses over Brønsted acid sites in the catalyst, and that the reaction rate of salt bound potassium (KCl of K_2SO_4) is related to how strongly potassium is bound to its counter ion.

One possible method of protecting the SCR catalyst against alkali poisoning, during biomass firing, is to apply a suitable coating to its external surface. Such a coating should be of a material that can

effectively act as a barrier for the alkali metals, and have a structure that allows for gas to pass through. By the use of three-layer pellets, three materials, i.e. magnesium oxide, sepiolite and Hollandite manganese oxide, have been tested with respect to their ability to block the diffusion of potassium. Pure MgO proved to be the most effective potassium barrier of the three tested candidates. No potassium was detected by SEM-WDS in a 300 μm thick MgO layer, upon exposure to SCR conditions for 7 days. Pure sepiolite was unable to delay the surface diffusion of potassium from the impregnated to the undoped layer; however, it may still act as a physical potassium barrier or as a binder for e.g. an MgO based coating. Hollandite manganese oxide proved to reduce the diffusion rate of potassium across the three-layer pellets, however, is unfeasible as a coating material due to its subpar performance compared to MgO, and to its potentially expensive synthesis route. While not very comprehensive, this study serves as a proof of concept for fast screening of potential (chemical) alkali barriers, before extensive tests of application methods as well as long term alkali exposure experiments, of coated SCR catalysts, are commenced.

6. Bench-scale exposure of monolith catalysts

6.1. Introduction

This section reports a work in which two differently coated 3%V_2O_5-7%WO_3/TiO_2 monoliths have been exposed to KCl aerosols in the bench-scale setup. By following the deactivation using *in situ* activity measurements, the performance of the coated catalysts, with respect to SCR activity as well as alkali resistance, is compared to that of an uncoated reference monolith, which has undergone the same treatment. The potassium uptake of exposed catalysts has been measured by ICP-OES and SEM-EDS.

6.2. Aerosol characterization

Figure 6.1 shows two number based size distributions obtained by the SMPS during injection of the KCl solution at two different days. Both distributions are unimodal, #1 peaking at 31.1 nm while distribution #2 peaks at 30.0 nm. The geometric mean diameters are 29.1 and 29.4 nm respectively. These mean particle diameters are an order of magnitude smaller than those measured by Christensen and co-workers [7,8] in the flue gas from straw fired boilers. The total number concentration varies significantly between the two distributions in Figure 6.1, i.e. distribution #1 corresponds to a concentration of $3.0 \cdot 10^8$ particles/Ncm^3 while #2 corresponds to a concentration of $1.2 \cdot 10^8$ particles/Ncm^3. The total number concentrations obtained in the bench-scale setup are up to 150 times larger than those reported by Christensen and co-workers [7,8] who also observed large variations in the total number concentration over time. Although the total amount of particles observed in our setup is significantly larger than what has been observed in straw fired boilers, the smaller particles results in low total mass concentrations of 15.2 and 5.4 mg/Nm^3 for distribution #1 and 2 respectively, assuming a particle density of 1.988 g/cm^3 (the density of KCl [123]). These concentrations correlate well with the 9.0 mg/Nm^3, reported in section 4, which was measured using an LPI during KCl exposure of catalyst plates. In comparison, mass concentrations of 3-2000 mg/Nm^3 were measured by Christensen and co-workers [7,8], while Zheng *et al.* [24] observed a mass concentration of submicron particles of 415 mg/Nm^3 in the flue gas from a boiler firing straw and wood chips. Despite these differences, catalysts exposed to potassium rich aerosols in our bench-scale setup have showed deactivation rates similar to catalyst exposed in full-scale, biomass fired power plants [72].

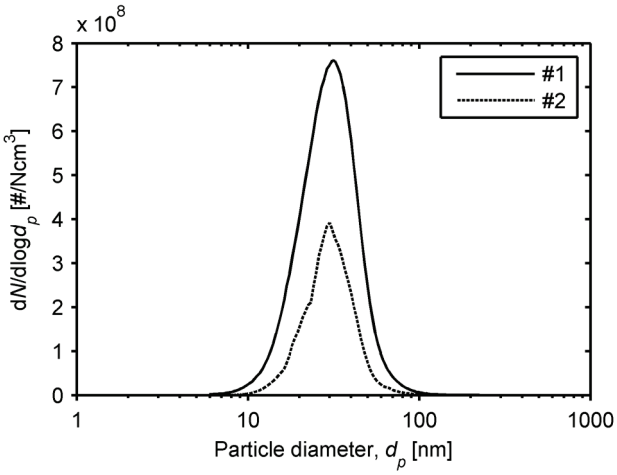

Figure 6.1: Number based particle size distributions measured by SMPS at the reactor inlet during injection of a 0.1 M KCl solution at 420 mL/h.

6.3. Deactivation of exposed monoliths

The relative activity of an uncoated 3%V_2O_5-7%WO_3/TiO_2 reference monolith, measured during exposure to a KCl aerosol at 350 °C, is plotted in Figure 6.2 as a function of time. As seen from the figure, the activity decreases almost linearly from 100 % to 63 % during 960 hours of KCl exposure. This corresponds to a deactivation rate of 0.91 %/day which correlates well with previous studies in both the bench-scale setup and in a straw and wood chip fired power plant, where deactivation rates of about 1 %/day have been observed [24,72]. This confirms that even though the particle load, on a mass basis, may be significantly lower than what can be observed in the flue gas from actual biomass fired boilers, realistic deactivation rates can still be achieved in the bench-scale setup.

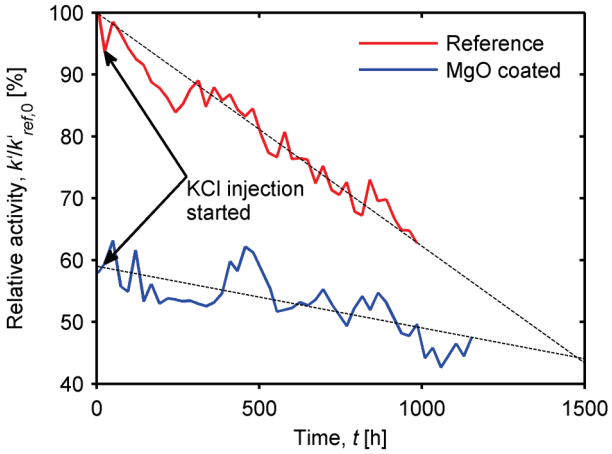

Figure 6.2: Relative activity of a 3%V_2O_5-7%WO_3/TiO_2 reference monolith, and a monolith coated with 8.06 wt.% MgO, during exposure to a KCl aerosol at 350 °C as a function of time.

Figure 6.2 also shows the activity as a function of time of a monolith coated with 8.06 wt.% MgO, during exposure to a KCl aerosol. Here, the activity is reported relative to the that of the fresh, uncoated reference, $k'_{ref,0}$. As seen from the figure, the initial observed activity of the coated monolith is only about 58 % of that of the uncoated reference. The lower start activity is likely due to increased diffusion limitations caused by the MgO coat, slight magnesium poisoning of the outermost active sites during application of the coat, or a combination thereof. The deactivation rate of the MgO coated monolith is notably slower than that of the reference. During 1100 hours of KCl exposure, the relative activity drops from 58 to 47 %, corresponding to a deactivation rate of 0.24 %/day, relative to the fresh activity of the uncoated reference. The large fluctuations in the observed relative activity of the MgO coated monolith may be caused by enhance measurement uncertainties due to the lower start activity. The experiment shows that an MgO coat can significantly reduce the deactivation rate of a catalyst exposed to a potassium rich aerosol, however, at the expense of a lower initial activity. Extrapolation of the near linear deactivation trends of two catalysts indicates that the MgO coated monolith will retain a higher absolute activity after about 1500 hours of exposure to the KCl aerosol, as shown in Figure 6.2.

A 3%V_2O_5-7%WO_3/TiO_2 monolith coated with 8.36 wt.% of a 1:1 mixture of MgO and TiO_2 was also exposed to a KCl aerosol, however, the observed start activity of this catalyst system was only 30 % of that of the uncoated reference, and it was ultimately decided to terminate the experiment after only 100 hours of exposure. No further investigations on this catalyst were performed. It is not clear why the start activity was so low, but it may be speculated that the coating had a lower porosity leading to further mass transfer restrictions.

6.4. Characterization of the reference monolith

Table 6.1 states the bulk composition of three sections (denoted top, middle and bottom) of the exposed reference monolith, with respect to potassium, vanadium and tungsten. As expected, the vanadium and tungsten levels are fairly constant through the three sections, although they seem to decrease slightly along the monolith. The potassium concentration decreases slightly from 1.45 wt.% in the top to 1.38 wt.% in the middle section, followed by a significant drop to 0.76 wt.% in the bottom section. Based on the potassium and vanadium content, bulk molar K/V ratios have been calculated, also stated in Table 6.1. In the top and middle section the ratio is 1.1 while it has dropped to 0.6 in the bottom section. The fact that the potassium level is lower at the bottom of the

monolith may be due a change in the velocity profile from turbulent, at the inlet, to laminar along the catalyst channels, leading to lower mass transfer of particles to the catalyst surface [124].

Table 6.1: Bulk chemical composition of a 3%V_2O_5-7%WO_3/TiO_2 reference monolith, exposed to a KCl aerosol at 350 °C for 960 hours.

	Potassium [wt.%]	Vanadium [wt.%]	Tungsten [wt.%]	K/V molar ratio
Top	1.45	1.73	5.94	1.1
Middle	1.38	1.66	5.67	1.1
Bottom	0.76	1.59	5.34	0.6

Figure 6.3 shows the K/V molar ratios across the thickness of the catalyst wall, measured by SEM-EDS analysis in the three sections of the exposed reference monolith. Similar to previous observations [24,72,95], potassium has in all cases penetrated the entire wall, and all profiles are rather flat, indicating a fast diffusion of potassium. The K/V profile measured in the top section of the monolith assumes a value of about 0.90 at the surface and drops to an average of 0.51 inside the wall (calculated at the distance from 100 to 500 µm). For the middle and bottom part of the monolith, the average K/V ratio in the wall (i.e. 100 µm from each surface) is 0.38 and 0.44 respectively. As stated above, the higher potassium level at the inlet of the monolith may be due to the flow development in the channels which leads to a faster mass transfer in the top section.

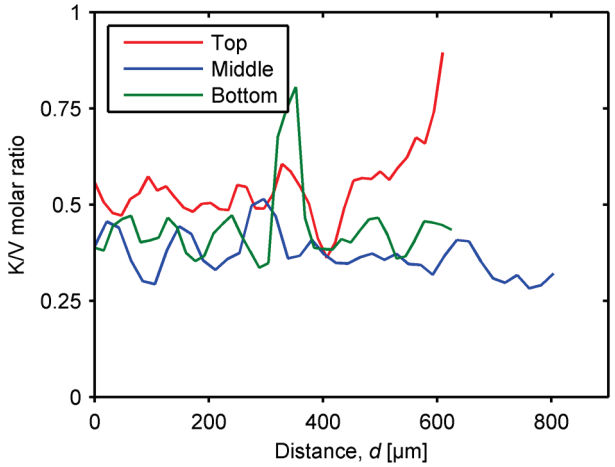

Figure 6.3: K/V molar ratios across the thickness of the catalyst wall of a 3%V_2O_5-7%WO_3/TiO_2 reference monolith, exposed to a KCl aerosol at 350 °C for 960 hours.

In section 4, a K/V molar ratio of 0.60 in a KCl aerosol exposed plate catalyst, of similar composition, was reported. This catalyst had lost nearly all of its initial activity, which does not seem to correlate with the 37 % activity loss and K/V ratios of 0.38-0.51 for the exposed monolith. This can, however, be explained by the two different methods of which the activity was measured. In section 4, the relative activity of the exposed plate was measured on powder in a lab-scale reactor. Here, the overall effectiveness is expected to be high (above 71 % at 350 °C for a fresh

catalyst, and even higher for a poisoned sample). During activity measurements over monolith elements, as done in the work reported in this section, significantly lower effectiveness factors are to be expected. More specifically, an overall effectiveness factor of 3-9 %, for activity measurements over the fresh monolith, has been estimated. As the monolith deactivates, the effectiveness factor increases, thereby disguising the activity loss due to potassium poisoning.

In the catalyst wall of a 3%V_2O_5-WO_3/TiO_2 monolith, exposed to a potassium rich aerosol in a straw and wood chip fired power plant at 350 °C for 1140 hours, Zheng *et al*. [24] measured a K/V molar ratio of 0.5. In another catalyst, exposed at 250 °C for 1620 hours, a K/V ratio of 0.3 was observed. The two catalysts respectively retained 48 and 47 % of their initial observed activity [24]. In a bench-scale study, Zheng *et al.* [72] measured an average K/V molar ratio of 0.49 in the wall of a 3%V_2O_5-7%WO_3/TiO_2 monolith, exposed to a K_2SO_4 aerosol for 2700 hours, which retained about 53 % of its initial observed activity. In a laboratory study, Zheng *et al.* [6] reported an intrinsic activity loss of about 60 % for a 3%V_2O_5-WO_3/TiO_2 catalyst impregnated with KCl to a K/V ratio of 0.4. Larsson and co-workers [55,56,91] respectively subjected 1%V_2O_5-WO_3/TiO_2 monoliths to generated aerosols of KCl and K_2SO_4 at 200 °C for 10 hours, accelerating the particle deposition by applying an electrostatic field to the catalyst channels. While SEM-WDS analysis in both cases showed high potassium concentrations above 1 wt.% (corresponding to K/V molar ratios above 2.3) at penetration depths of 350 and 650 μm (out of a total wall thickness of about 800 μm), the observed relative activity at 350 °C was about 86 % and 98 % for the KCl and K_2SO_4 exposed catalysts respectively [55]. A similar observation was made by the authors for a catalyst exposed for 6500 hours at 350 °C to K, S and Cl rich particles in a commercial biomass combustion plant firing 90 % wood chips and 10 % peat [55,56,91]. Likewise, Moradi *et al.* [54] only observed minute effects on the SCR activity after respectively exposing vanadia based monoliths to generated aerosols of KCl and K_2SO_4 at 340 °C for 31 hours. By wet impregnation of 1%V_2O_5-WO_3/TiO_2 monoliths with 1 g/L solutions of KCl and K_2SO_4, Larsson and co-workers [55,91] obtained potassium concentrations of about 0.2 wt.% (corresponding to K/V molar ratios of around 0.5) inside the catalyst walls, as measured by SEM-WDS – i.e. significantly lower concentrations than what they observed in particle exposed monoliths. Even so, the observed relative activity at 350 °C was 50 % and 56 % for the KCl and K_2SO_4 impregnated sample respectively [55]. Kern and co-workers [47,82], on the other hand, observed significant deactivation of V_2O_5-WO_3/TiO_2 monoliths both after exposure to potassium rich aerosols, at 500 °C for 50 hours, and upon wet impregnation with KNO_3 solutions. The K/V molar ratios of 0.38-0.51 and the observed activity loss of 37 %,

measured for the exposed reference monolith in this study, correlate well with the studies by Zheng and co-workers [6,24,72], Kern and co-workers [47,82], as well as the impregnation study by Larsson and co-workers [55,91]. However, some discrepancy exists between the results from our KCl exposure campaign and the particle exposures by Larsson and co-workers [55,56,91], as well as Moradi *et al.* [54].

6.5. Characterization of the MgO coated monolith

Table 6.2 shows the bulk composition of the exposed, MgO coated monolith. As with the reference monolith, both the vanadium and the tungsten concentration decrease slightly along the MgO coated catalyst. The potassium concentration drops to around half from the top to the middle section, corresponding to a drop in the K/V molar ratio from 0.6 to 0.3, while the potassium concentration increases slightly from the middle to the bottom section (to a K/V ratio of 0.4). The bulk potassium uptake of the top and bottom section is only about half of that of the corresponding sections of the reference monolith, while it is less than one fourth for the middle section. This is in accordance with the significantly lower deactivation rate of the MgO coated monolith.

Table 6.2: Bulk chemical composition of a 3%V_2O_5-7%WO_3/TiO_2 monolith coated with 8.06 wt.% MgO, exposed to a KCl aerosol at 350 °C for 1100 hours.

	Potassium [wt.%]	Vanadium [wt.%]	Tungsten [wt.%]	K/V molar ratio
Top	0.67	1.42	4.58	0.6
Middle	0.30	1.36	4.43	0.3
Bottom	0.39	1.32	4.28	0.4

Figure 6.4 shows the K/V molar ratios across the thickness of the catalyst wall, in three sections of the exposed, MgO coated monolith. No significant differences between the K/V profile measured in the top, middle and bottom section of the catalyst can be observed. In all cases the K/V ratio drops from a high value in the outer 50-200 μm of the wall to a rather constant level in the center of the sample. The average K/V ratio calculated 200 μm from each surface is 0.17, 0.21 and 0.18 for the sample from the top, middle and bottom section respectively. The values are 2-3 times smaller than those for the corresponding sections in the reference monolith.

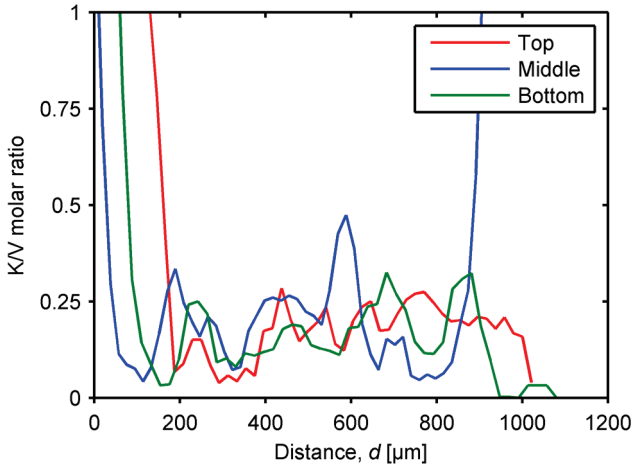

Figure 6.4: K/V molar ratios across the thickness of the catalyst wall of a 3%V_2O_5-7%WO_3/TiO_2 monolith coated with 8.06 wt.% MgO, exposed to a KCl aerosol at 350 °C for 1100 hours.

The relative mass fractions of potassium, vanadium, tungsten and magnesium across the sample from the bottom section, calculated from SEM-EDS measurements, are shown in Figure 6.5. For each metal, the mass fraction at a given position is taken as a relative to the maximum mass fraction of the metal, measured in the entire profile.

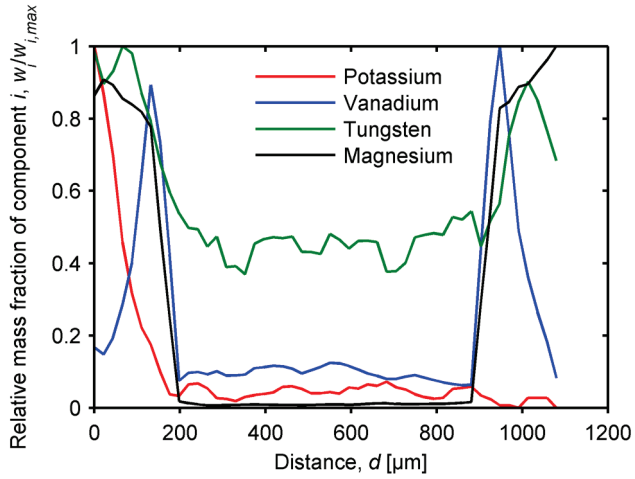

Figure 6.5: Relative potassium, vanadium, tungsten and magnesium profiles in a sample from the bottom section of a 3%V_2O_5-7%WO_3/TiO_2 monolith coated with 8.06 wt.% MgO, exposed to a KCl aerosol at 350 °C for 1100 hours.

As seen from the figure, the coat, represented by the magnesium concentration, is about 200 µm thick on both sides of the catalyst. No magnesium appears to have penetrated the catalyst. On the contrary, relatively large amounts of both vanadium and tungsten have diffused into the coating, likely during the application. The loss of active material to the coat may partially explain the lower observed start activity of the coated monolith (together with the increased mass transfer limitations). While the coat, to a great extent, has protected the catalyst, potassium has clearly been able to

penetrate the MgO layer, unlike what was observed in the three-layer pellet experiments. Figure 6.6 shows a SEM image of the same cross section. The consistent gap of about 10-40 µm between the MgO coat and the catalyst indicates that the adhesion between the two is rather weak. This is further indicated by the fact that a segment of the coating is missing in the bottom left part of the image. The loss of coating material may have happed before or during the KCl exposure, or during the preparation of the sample for the SEM analysis.

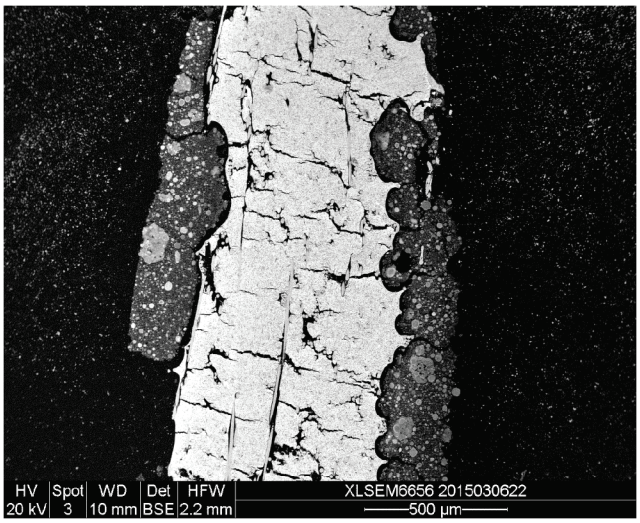

Figure 6.6: SEM image of a wall cross section from the bottom part of the MgO coated monolith.

The SEM image shown in Figure 6.7 depicts a part of the catalyst where most of the coat is missing, and the K/V molar ratios across this section are shown in Figure 6.8. As seen from the latter, the K/V ratios reached in this part of the catalyst are significantly higher than those reported in Figure 6.4. The average K/V ratio across the center of the wall, calculated 100 µm from each surface, is 0.66 which is comparable to and even larger than those measured in the exposed reference monolith. This confirms that the MgO coat has been missing from this area of the monolith at least during part of the exposure period. The observed deactivation of the MgO coated monolith may hence both be due to potassium penetration of the coat, as observed in Figure 6.5, and to poisoning of various parts of the catalyst where to coat is lost.

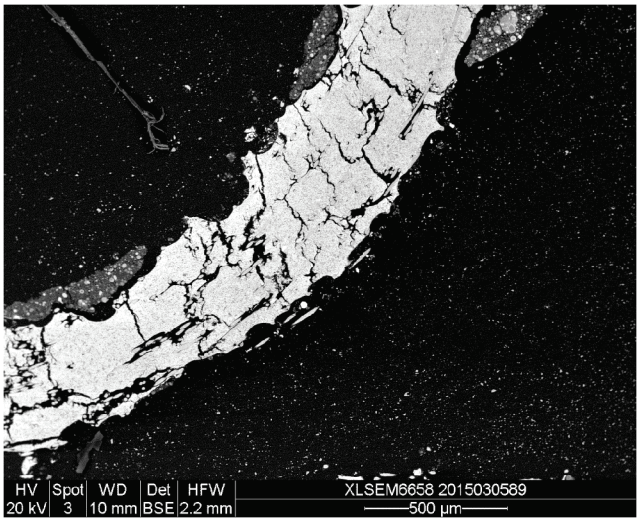

Figure 6.7: SEM image of a wall cross section of the MgO coated monolith where the coat is missing.

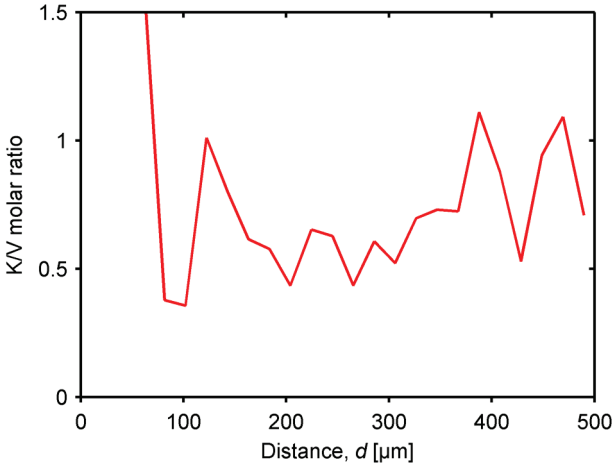

Figure 6.8: K/V molar ratios in a coating-less wall cross section of a 3%V_2O_5-7%WO_3/TiO_2 monolith coated with 8.06 wt.% MgO, exposed to a KCl aerosol at 350 °C for 1100 hours.

6.6. Conclusion

Three half-length monoliths have been exposed to KCl aerosols at 350 °C in the bench-scale setup. A 3%V_2O_5-7%WO_3/TiO_2 reference catalyst deactivated with a rate of 0.91 %/day during 960 hours of exposure. SEM-EDS analysis on cross sections of the exposed monolith showed complete potassium penetration and average K/V molar ratios of 0.38-0.51 inside the catalyst wall. A similar monolith coated with 8.06 wt.% MgO deactivated with a rate of 0.24 %/day, relative to the fresh activity of the uncoated reference, during 1100 hours of exposure. The initial observed activity of the MgO coated catalyst was only 58 % of that of the reference, likely due to increased transport limitations, as well as loss of vanadium and tungsten to the coating during its application. SEM-EDS analysis showed that potassium had penetrated the MgO coat, however, the potassium

accumulation, inside the catalyst as well as on bulk basis, was 2-4 times lower than in the reference monolith. The SEM analysis also showed that the MgO layer was rather thick (200 μm), hence, there may be room for improving the mass transfer, and thereby the observed activity, by reducing the thickness of the coat. Furthermore, the SEM analysis indicated that the MgO coat adhered weakly to the catalyst and showed that the coating was missing in several places. The potassium accumulation in such a section of the catalyst proved to be comparable to that of the reference case. The characterization of the MgO coated monolith hence proves that a coat of MgO, at least to some extent, can protect the SCR catalyst against potassium poisoning. It is, however, also evident that a binder material should be considered, in order to obtain a stronger adhesion. Apart from sepiolite, which was tested in the three-layer experiments, a candidate could be TiO_2, which constitutes the majority of the catalyst system. However, an initial test with a catalyst coated with a 1:1 mixture of MgO and TiO_2 showed an insufficient start activity when tested in the bench-scale setup. It is hence apparent that more work is needed in order to develop a coating that, apart from acting as a potassium barrier, is both mechanically durable, and is thin and porous enough to allow for passage of gas species.

7. Deactivation model

7.1. Introduction

Khodayari and Odenbrand [125] have previously proposed a model for accumulation of poison in SCR catalysts and the resulting deactivation. This model, however, assumes the poison to be in the gas phase. For potassium poisoning during biomass firing, such an assumption is not very realistic since potassium will be bound in particles of KCl and/or K_2SO_4. At a typical SCR operating temperature of 350 °C, the vapor pressure of KCl is only about $3.6 \cdot 10^{-9}$ kPa [126] and will be even lower for K_2SO_4 due to its higher melting point (1069 °C for K_2SO_4 versus 771 °C for KCl, CRC [123]).

This section presents a model for the selective catalytic reduction of NO by NH_3, in a single catalyst channel of a monolith during deposition of KCl particles of a known size distribution, and the resulting continuous deactivation of the catalyst. The model calculates the NO and NH_3 concentrations along the monolith channel as well as inside the catalyst wall. Furthermore, the accumulation of potassium on the external surface and the subsequent transport into the wall by surface diffusion, causing deactivation of Brønsted sites inside the catalyst, are being accounted for. The solution procedure as well as simulation examples (including a parameter study) are also reported in the following.

7.2. Assumptions

The following assumptions have been made during the derivation and solution of the model:

- A developing laminar velocity profile exists along the catalyst channels.
- Complete mixing of NH_3 and flue gas at the catalyst inlet.
- A 1:1 reaction between NO and NH_3 following the reaction scheme:
  $4\ NO + 4\ NH_3 + O_2 \rightarrow 4\ N_2 + 6\ H_2O$
- The reaction between NO and NH_3 follows an Eley-Rideal mechanism where NH_3 adsorbs on the Brønsted acid sites of the catalyst and NO reacts from the gas phase.
- The change in adsorbed NH_3 during deactivation is slow.
- Isothermal operation – no significant production or consumption of heat during reaction.
- Particle deposition by film diffusion assuming a zero particle concentration in the gas phase at the wall.

- The flow pattern in the channel is unaltered by particle build-up on the wall.
- All the depositing particles are spherical and consist of KCl.
- Potassium bound in deposited particles reacts irreversibly with Brønsted sites on the catalyst surface:
  K-particles + H-O-surface → K-O-surface + HCl (g)
- Potassium is transported into the catalyst wall by surface diffusion over -OH sites.

7.3. The model

7.3.1. Gas phase species

7.3.1.1. Axial concentration profiles

We first consider the concentrations of NO and NH_3 in the bulk flue gas, flowing with a mean velocity of U (in m/s) along a single monolith channel of length L and hydraulic diameter d_h. The flow direction is denoted z in the following. The transient concentration profiles of NO and NH_3 in the axial direction are given by:

$$\frac{\partial C_{\mathrm{NO},b}}{\partial t} = -U\frac{\partial C_{\mathrm{NO},b}}{\partial z} - \frac{4k_{g,\mathrm{NO}}}{d_h}\left(C_{\mathrm{NO},b} - C_{\mathrm{NO},s}\right) \tag{7.1}$$

$$\frac{\partial C_{\mathrm{NH3},b}}{\partial t} = -U\frac{\partial C_{\mathrm{NH3},b}}{\partial z} - \frac{4k_{g,\mathrm{NH3}}}{d_h}\left(C_{\mathrm{NH3},b} - C_{\mathrm{NH3},s}\right) \tag{7.2}$$

Where $C_{i,b}$ is the bulk concentration and $C_{i,s}$ surface concentration of component i (both in mol/m^3), while $k_{g,i}$ is the mass transfer coefficient of component i (in m/s). Since the flow is assumed to develop from turbulent at the catalyst inlet, to laminar along the channel, the mass transfer coefficient will be a function of the axial position, z. At $t = t_0$, no deactivation has occurred and the system is assumed to be at steady-state. Hence, the steady-state concentrations, $C^{ss}_{i,b}$, at all axial positions are required as initial conditions:

$$C_{i,b}(t = t_0, z) = C^{ss}_{i,b}(z) \tag{7.3}$$

The inlet concentrations of NO and NH_3 are assumed to be constant at all times and are defined as:

$$C_{i,b}(t, z = 0) = C^0_{i,b} \tag{7.4}$$

By introducing a reference concentration C_{ref}, a reference distance z_{ref} and a reference time t_{ref}, the differential equations can be written in a dimensionless form:

$$\frac{\partial \tilde{C}_{\mathrm{NO},b}}{\partial \tilde{t}} = -\frac{Ut_{ref}}{z_{ref}}\frac{\partial \tilde{C}_{\mathrm{NO},b}}{\partial \tilde{z}} - \frac{4k_{g,\mathrm{NO}}t_{ref}}{d_h}(\tilde{C}_{\mathrm{NO},b} - \tilde{C}_{\mathrm{NO},s}) \quad (7.5)$$

$$\frac{\partial \tilde{C}_{\mathrm{NH},b}}{\partial \tilde{t}} = -\frac{Ut_{ref}}{z_{ref}}\frac{\partial \tilde{C}_{\mathrm{NH3},b}}{\partial \tilde{z}} - \frac{4k_{g,\mathrm{NH3}}t_{ref}}{d_h}(\tilde{C}_{\mathrm{NH3},b} - \tilde{C}_{\mathrm{NH3},s}) \quad (7.6)$$

With the initial and boundary conditions:

$$\tilde{C}_{i,b}(\tilde{t} = \tilde{t}_0, \tilde{z}) = \tilde{C}_{i,b}^{ss}(\tilde{z}) \text{ and } \tilde{C}_{i,b}(\tilde{t}, \tilde{z} = 0) = \tilde{C}_{i,b}^{0} \quad (7.7, 7.8)$$

Where:

$$\tilde{C}_i = \frac{C_i}{C_{ref}}, \tilde{z} = \frac{z}{z_{ref}} \text{ and } \tilde{t} = \frac{t}{t_{ref}} \quad (7.9, 7.10, 7.11)$$

The following will be used as reference parameters:

$$C_{ref} = C_{\mathrm{NO},b}^{0}, z_{ref} = L \text{ and } t_{ref} = \frac{L}{U} \quad (7.12, 7.13, 7.14)$$

7.3.1.2. Radial concentration profiles

We now consider the concentration of NO and NH_3 inside the catalyst wall which have the characteristic width (half thickness) V/S (in m). Symmetry is assumed at the centre of the wall ($x = 0$). The transient concentration profiles of the two gas phase components in the radial direction are given by:

$$\varepsilon \frac{\partial C_{\mathrm{NO}}}{\partial t} = D_{e,\mathrm{NO}} \frac{\partial^2 C_{\mathrm{NO}}}{\partial x^2} + r'_{\mathrm{NO}} \quad (7.15)$$

$$\varepsilon \frac{\partial C_{\mathrm{NH3}}}{\partial t} + (1-\varepsilon)\frac{\partial C_{\mathrm{NH3}}^{ads}}{\partial t} = D_{e,\mathrm{NH3}} \frac{\partial^2 C_{\mathrm{NH3}}}{\partial x^2} + r'_{\mathrm{NH3}} \quad (7.16)$$

Where C_i is the gas phase concentration of component i at a given position inside the wall (mol/m^3), C_{NH3}^{ads} is the amount of NH_3 adsorbed on the catalyst (mol/m^3), ε is the porosity of the catalyst wall, and $D_{e,i}$ is the effective diffusivity of component i (m^2/s), which is assumed to be constant throughout the catalyst wall. It is furthermore assumed that adsorbed NH_3 does not diffuse over the solid phase.

The reaction between NO and NH_3, with the rate $-r_i'$, is assumed to follow an Eley-Rideal expression [110-112,127]:

$$-r_i' = -r'_{\mathrm{NO}} = -r'_{\mathrm{NH3}} = -r' = k_s C_{\mathrm{NO}} \frac{K_{\mathrm{NH3}} C_{\mathrm{NH3}}}{1 + K_{\mathrm{NH3}} C_{\mathrm{NH3}}} \quad (7.17)$$

Where k_s is the rate constant (s^{-1}) while K_{NH3} is the adsorption equilibrium constant of NH_3 on Brønsted sites (in m^3/mol). These parameters are temperature dependant and can be expressed by a pre-exponential factor, k_0 or K_0, and an activation energy, E_a, or enthalpy of adsorption, ΔH_{ad}:

$$k_s = k_0 \cdot e^{-\frac{E_a}{RT}} \tag{7.18}$$

$$K_{NH3} = K_0 \cdot e^{-\frac{\Delta H_{ad}}{RT}} \tag{7.19}$$

Where R is the gas constant (in J/mol/K) and T is the temperature in Kelvin. Table 7.1 presents examples of the activation energy, adsorption enthalpy as well as the pre-exponential factors, reported in the literature:

Table 7.1: Activation energy, NH_3 adsorption enthalpy and pre-exponential factors.

Parameter	Value	Reference
E_a	79496 J/mol	Beeckman and Hegedus [127]
ΔH_{ad}	-137000 J/mol	Koebel and Elsener [112]
k_0	86.4 m/s *a)*	[127]
K_0	$3.0 \cdot 10^{-12}$ Pa^{-1}	[112]

a) Corresponding to $1.08 \cdot 10^{10}$ 1/s using a catalyst volume specific surface area of $1.25 \cdot 10^8$ m^2/m^3 as reported by Beeckman and Hegedus [127].

As the catalyst deactivates, less sites becomes available for NH_3 to adsorb on. In order to account for this, we now introduce the fraction of available Brønsted sites, φ, and modify the rate expression:

$$\varphi = \frac{C_{\mathrm{OH}}}{C^0_{\mathrm{OH}}} \tag{7.20}$$

$$-r' = k_s C_{\mathrm{NO}} \varphi \frac{K_{\mathrm{NH3}} C_{\mathrm{NH3}}}{1 + K_{\mathrm{NH3}} C_{\mathrm{NH3}}} \tag{7.21}$$

Where C^0_{OH} and C_{OH} are the initial and current surface concentration of Brønsted sites (in mol/m^2 internal surface) at a given position inside the wall. During the deactivation, the local rate of change in the NO and NH_3 concentrations are likely to be small. In the following we assume that the concentration of adsorbed NH_3 is at pseudo steady-state, i.e.:

$$\frac{\partial C^{ads}_{\mathrm{NH3}}}{\partial t}(t,x) \approx 0 \tag{7.22}$$

The gas phase concentrations of NO and NH_3 could in principle also be assumed to be in pseudo steady-state, however, it has been chosen to keep all differential equations in transient form to avoid mixed differential-algebraic equations.

The above changes yields the following set of partial differential equations which can describe the concentration profiles of NO and NH_3 inside the catalyst wall during depletion of Brønsted acid sites:

$$\varepsilon \frac{\partial C_{\mathrm{NO}}}{\partial t} = D_{e,\mathrm{NO}} \frac{\partial^2 C_{\mathrm{NO}}}{\partial x^2} - k_s C_{\mathrm{NO}} \varphi \frac{K_{\mathrm{NH3}} C_{\mathrm{NH3}}}{1+K_{\mathrm{NH3}} C_{\mathrm{NH3}}} \tag{7.23}$$

$$\varepsilon \frac{\partial C_{\mathrm{NH3}}}{\partial t} = D_{e,\mathrm{NH3}} \frac{\partial^2 C_{\mathrm{NH3}}}{\partial x^2} - k_s C_{\mathrm{NO}} \varphi \frac{K_{\mathrm{NH3}} C_{\mathrm{NH3}}}{1+K_{\mathrm{NH3}} C_{\mathrm{NH3}}} \tag{7.24}$$

As for the axial concentration profiles, the steady-state concentrations for a fresh catalyst, C^{ss}_i, are required as initial conditions:

$$C_i(t = t_0, x) = C_i^{ss}(x) \tag{7.25}$$

Since we assume symmetry at the center of the wall, the following boundary condition must be fulfilled:

$$\frac{\partial C_i}{\partial x}(t, x = 0) = 0 \tag{7.26}$$

The flux of component *i* from the surface ($x = V/S$), into the catalyst, is equal to the flux from the bulk gas to the surface:

$$D_{e,i} \frac{\partial C_i}{\partial x}\Big|_s = k_{g,i}\left(C_{i,b} - C_{i,s}\right) \tag{7.27}$$

The system can be written in a dimensionless form upon introduction of the reference distance $x_{ref} = V/S$:

$$\varepsilon \frac{\partial \tilde{C}_{\mathrm{NO}}}{\partial \tilde{t}} = \frac{D_{e,\mathrm{NO}} t_{ref}}{x_{ref}^2} \frac{\partial^2 \tilde{C}_{\mathrm{NO}}}{\partial \tilde{x}^2} - t_{ref} k_s \tilde{C}_{\mathrm{NO}} \varphi \frac{K_{\mathrm{NH3}} \tilde{C}_{\mathrm{NH3}}}{\frac{1}{C_{ref}}+K_{\mathrm{NH3}} \tilde{C}_{\mathrm{NH3}}} \tag{7.28}$$

$$\varepsilon \frac{\partial \tilde{C}_{\mathrm{NH3}}}{\partial \tilde{t}} = \frac{D_{e,\mathrm{NH3}} t_{ref}}{x_{ref}^2} \frac{\partial^2 \tilde{C}_{\mathrm{NH3}}}{\partial \tilde{x}^2} - t_{ref} k_s \tilde{C}_{\mathrm{NO}} \varphi \frac{K_{\mathrm{NH3}} \tilde{C}_{\mathrm{NH3}}}{\frac{1}{C_{ref}}+K_{\mathrm{NH3}} \tilde{C}_{\mathrm{NH3}}} \tag{7.29}$$

With the initial and boundary conditions:

$$\tilde{C}_i(\tilde{t} = \tilde{t}_0, \tilde{x}) = \tilde{C}_i^{ss}(\tilde{x}) \tag{7.30}$$

$$\frac{\partial \tilde{C}_i}{\partial \tilde{x}}(\tilde{t}, \tilde{x} = 0) = 0 \text{ and } \frac{D_{e,i}}{x_{ref}} \frac{\partial \tilde{C}_i}{\partial \tilde{x}}\bigg|_s = k_{g,i}\left(\tilde{C}_{i,b} - \tilde{C}_i(\tilde{t}, \tilde{x} = 1)\right) \tag{7.31, 7.32}$$

Where:

$$\tilde{x} = \frac{x}{x_{ref}} \tag{7.33}$$

7.3.2. Potassium accumulation

7.3.2.1. Particle deposition and external potassium accumulation

When an aerosol with a given size distribution passes through a catalyst channel, particles will diffuse towards and deposit on the channel walls. The flux of particles to the surface depends on their size as well as the flow conditions in the channel. In the following it is assumed that the axial concentration profile of each particle class in a discrete, polydisperse distribution is constant with respect to time (i.e. at steady-state). It is furthermore assumed that the particles are transported to the catalyst surface solely by film diffusion and that the particle flux is independent of the amount of particles already accumulated on the surface. The bulk concentration of particles in size class *i*, $W_{i,b}$ (in #/m^3), along a catalyst channel, is then described by the following differential equation:

$$\frac{dW_{i,b}}{dz} = -\frac{4k_{p,i}}{d_h U} W_{i,b} \tag{7.34}$$

Where $k_{p,i}$ is the mass transfer coefficient (in m/s) of particles in size class *i*. This differential equation has the following solution:

$$W_{i,b} = W_{i,b}^0 e^{-\frac{4}{d_h U}\int_0^z k_{p,i}(z\prime)dz\prime} \tag{7.35}$$

Where $W^0_{i,b}$ is the concentration of particles in size class *i* at the channel inlet. For each size class, the flux of particles to the surface at a given axial position, $N_{p,i}$ (in #/m^2), is given by:

$$N_{p,i} = k_{p,i} W_{i,b} \tag{7.36}$$

The rate of which particles of a given size accumulate on the channel wall is given by the particle flux to the surface minus the amount that is being consumed by reaction with surface -OH sites. We now introduce the surface concentration of potassium bound in particles of size *i*, $C_{K,p,i}$ (in mol/m^2 external surface). The accumulation rate of this parameter is given by:

$$\frac{\partial C_{\mathrm{K},p,i}}{\partial t} = \frac{V_{p,i}}{V_{m,\mathrm{KCl}}} N_{p,i} - k_{\mathrm{KCl}} C_{\mathrm{OH,s}} \frac{A_{p,i}}{A_{surf}} \tag{7.37}$$

Where $V_{p,i}$ is the volume of a particle from size class i and $V_{m,\mathrm{KCl}}$ is the molar volume of KCl ($3.7501 \cdot 10^{-5}$ m^3/mol [123]). The entity k_{KCl} is the rate constant (in 1/s) of the reaction between potassium bound in KCl particles and surface -OH sites, with the surface concentration $C_{\mathrm{OH},s}$ (in mol/m^2 internal surface). $A_{p,i}$ is the total projected area (in m^2) of deposited particles (of size i) while A_{surf} is the external surface area (m^2) of the catalyst. When the catalyst surface is fully covered, deposition of additional particles will have no influence on the reaction rate, thus the following constraint applies:

$$\frac{\sum_i A_{p,i}}{A_{surf}} \leq 1 \tag{7.38}$$

When this ratio reaches unity, the catalyst surface is saturated with particles and the continued particle deposition will replenish all particle bound potassium that reacts with surface sites, without increasing the total contact area between the catalyst and particles any further. In the model, the rate of change of $C_{\mathrm{K},p,i}$ is then set to zero. The ratio $A_{p,i}/A_{surf}$ can be expressed in terms of $C_{\mathrm{K},p,i}$:

$$\frac{A_{p,i}}{A_{surf}} = \frac{\pi}{4} d_{p,i}^2 \frac{V_{m,\mathrm{KCl}}\, C_{\mathrm{K},p,i}}{V_{p,i}} \tag{7.39}$$

Where $d_{p,i}$ is the particle diameter. While the particles likely are closer to being cubic [128], they are assumed spherical due to way they are characterized experimentally. The potassium accumulation rate then becomes:

$$\frac{\partial C_{\mathrm{K},p,i}}{\partial t} = \frac{\pi}{6V_{m,\mathrm{KCl}}} d_{p,i}^3 N_{p,i} - k_{\mathrm{KCl}} C_{\mathrm{OH,s}} \frac{3V_{m,\mathrm{KCl}}\, C_{\mathrm{K},p,i}}{2d_{p,i}} \tag{7.40}$$

At $t = t_0$, the catalyst surface is particle free, i.e.:

$$C_{\mathrm{K},p,i}(t = t_0, z) = 0 \tag{7.41}$$

We now define the fraction of available Brønsted sites at the external surface, φ_s:

$$\varphi_s = \frac{C_{\mathrm{OH},s}}{C_{\mathrm{OH}}^0} \tag{7.42}$$

The equation for the potassium accumulation rate can then be made dimensionless:

$$\frac{\partial \tilde{C}_{\mathrm{K},p,i}}{\partial \tilde{t}} = \frac{\pi}{6V_{m,\mathrm{KCl}}} \frac{t_{ref}}{C^0_{\mathrm{OH}} S_{surf} \frac{V}{S}} d^3_{p,i} N_{p,i} - t_{ref} k_{\mathrm{KCl}} C^0_{\mathrm{OH}} \varphi_s \frac{3V_{m,\mathrm{KCl}} \tilde{C}_{\mathrm{K},p,i}}{2d_{p,i}} \qquad (7.43)$$

Where S_{surf} is the internal volume specific surface area of the catalyst (in m^2/m^3) and:

$$\tilde{C}_{\mathrm{K},p,i} = \frac{C_{\mathrm{K},p,i}}{C^0_{\mathrm{OH}} S_{surf} \frac{V}{S}} \qquad (7.44)$$

7.3.2.2. Surface diffusion of potassium

The potassium that has reacted with -OH sites on the external catalyst surface is assumed to diffuse into the catalyst over Brønsted acid sites on the internal surface. The surface concentration profile of potassium poisoned sites through the catalyst wall, $C_{\mathrm{K}}(x)$ (in mol/m^2 internal surface), is given by:

$$\frac{\partial C_{\mathrm{K}}}{\partial t} = D_s \frac{\partial^2 C_{\mathrm{K}}}{\partial x^2} \qquad (7.45)$$

Where D_s is the surface diffusion coefficient (in m^2/s) of potassium (over Brønsted sites). Initially, the catalyst is assumed to be potassium free, i.e.:

$$C_{\mathrm{K}}(t = t_0, x) = 0 \qquad (7.46)$$

Due to the symmetry assumption, the flux is zero at the center of the wall ($x = 0$):

$$\frac{\partial C_{\mathrm{K}}}{\partial x}(t, x = 0) = 0 \qquad (7.47)$$

At the wall surface (x = V/S), potassium bound in deposited particles reacts irreversibly with Brønsted sites on the surface. The flux of potassium into the catalyst is equal to the total amount of potassium, bound in particles, that reacts with sites at the external surface:

$$D_s \frac{\partial C_{\mathrm{K}}}{\partial x}\Big|_s = \frac{k_{\mathrm{KCl}}}{S_{surf}} C_{\mathrm{OH},s} \frac{\sum_i A_{p,i}}{A_{surf}} = \frac{3k_{\mathrm{KCl}} V_{m,\mathrm{KCl}}}{2S_{surf}} C_{\mathrm{OH},s} \sum_i \frac{C_{\mathrm{K},p,i}}{d_{p,i}} \qquad (7.48)$$

The surface concentration of potassium is related to the concentration of Brønsted acid sites as follows:

$$C^0_{\mathrm{OH}} = C_{\mathrm{OH}} + C_{\mathrm{K}} \qquad (7.49)$$

Equations 7.45-7.48 are now rewritten in terms of φ and made dimensionless:

$$\frac{\partial \varphi}{\partial \tilde{t}} = \frac{D_s t_{ref}}{x_{ref}^2} \frac{\partial^2 \varphi}{\partial \tilde{x}^2} \tag{7.50}$$

$$\varphi(\tilde{t} = \tilde{t}_0, \tilde{x}) = 1 \tag{7.51}$$

$$\frac{\partial \varphi}{\partial \tilde{x}}(\tilde{t}, \tilde{x} = 0) = 0 \tag{7.52}$$

$$\frac{D_s}{x_{ref}} \frac{\partial \varphi}{\partial \tilde{x}}\bigg|_s = -\frac{3 k_{\mathrm{KCl}} V_{m,\mathrm{KCl}}}{2} C_{\mathrm{OH}}^0 \varphi_s \frac{V}{S} \sum_i \frac{\tilde{C}_{\mathrm{K},p,i}}{d_{p,i}} \tag{7.53}$$

7.4. Correlations

The various correlations which have been applied in order to estimate the gas and particle mass transfer coefficients and diffusivities, required in the model, are presented below.

The mass transfer coefficient of gas component A, $k_{g,\mathrm{A}}$, is given by:

$$k_{g,\mathrm{A}} = Sh \frac{D_{\mathrm{A}}}{d_h} \tag{7.54}$$

Where Sh is the Sherwood number and D_{A} is the diffusivity of component A. In the following, the diffusivity of component A in the bulk flue gas is approximated by the binary diffusion coefficient, D_{AB}, of component A in air (denoted component B) using the Chapman-Enskog kinetic theory for diffusivity [129]:

$$D_{\mathrm{AB}} = \frac{3}{16} \sqrt{\frac{2(RT)^3}{\pi} \left(\frac{1}{M_{\mathrm{A}}} + \frac{1}{M_{\mathrm{B}}} \right)} \frac{1}{N_A P \sigma_{\mathrm{AB}}^2 \Omega_{D,\mathrm{AB}}} \tag{7.55}$$

Where M_i is the molar mass of component i, P is the pressure and N_A is the Avogadro number. The collision diameter, σ_{AB}, is given by the sum of the radii of molecule A and B:

$$\sigma_{\mathrm{AB}} = \frac{1}{2}(\sigma_{\mathrm{A}} + \sigma_{\mathrm{B}}) \tag{7.56}$$

The collision integral, $\Omega_{D,\mathrm{AB}}$, is given by:

$$\Omega_{D,\mathrm{AB}} = \frac{1.06036}{T^{*0.15610}} + \frac{0.19300}{\exp(0.47635 T^*)} + \frac{1.03587}{\exp(1.52996 T^*)} + \frac{1.76474}{\exp(3.89411 T^*)} \tag{7.57}$$

$$T^* = \frac{\kappa T}{\epsilon_{\mathrm{AB}}} \tag{7.58}$$

Where T^* is the dimensionless temperature, κ is the Boltzmann constant ($1.38 \cdot 10^{-23}$ J/K) and ϵ_{AB} is the geometric mean of the corresponding Lennard-Jones parameters for the single components:

$$\epsilon_{AB} = \sqrt{\epsilon_A \epsilon_B} \tag{7.59}$$

Lennard-Jones parameters for air, NO and NH_3 from Poling *et al.* [130] are stated in Table 7.2 along with their molar mass:

Table 7.2: Lennard-Jones parameters [130] and molar mass of air, NO and NH_3.

Component	Lennard-Jones parameters [130]		Molar mass [g/mol]
	σ [Å]	ϵ_i/κ [K]	
Air	3.711	78.6	28.964
NO	3.492	116.7	31.010
NH_3	2.900	558.3	17.034

It is assumed that the flow is turbulent when the gas enters the monolith channel. As the gas moves along the channel, a laminar velocity profile is approached. Based on the work by Grigull and Tratz [131] as well as Shah and London [132], Tronconi *et al.* [111,133] suggested the following correlation for the Sherwood number in a monolith channel with a developing laminar velocity profile:

$$Sh = Sh_\infty + 8.827(1000z^*)^{-0.545} \exp(-48.2z^*) \tag{7.60}$$

Where Sh_∞ is the asymptotic Sherwood number, which depends on the channel geometry, and z^* is the dimensionless axial coordinate given by:

$$z^* = \frac{zD_{AB}}{Ud_h^2} \tag{7.61}$$

Table 7.3 states the asymptotic Sherwood numbers for different channel geometries [133]. In the following, circular channel geometry is assumed.

Table 7.3: Asymptotic Sherwood numbers for various channel geometries [133].

Channel geometry	Sh_∞
Circular	3.659
Square	2.977
Triangular	2.494

The effective diffusion coefficient of NO and NH_3 in the catalyst wall ($D_{e,NO}$ and $D_{e,NH3}$) can be calculated from a model for diffusion in bimodal pore structures [134]:

$$D_{e,\mathrm{A}} = \varepsilon_a^2 D_a + (1-\varepsilon_a)^2 D_i + 4\varepsilon_a(1-\varepsilon_a)\left(\frac{1}{D_a}+\frac{1}{D_i}\right)^{-1} \quad (7.62)$$

Where D_a and D_i are given by:

$$D_a = \left(\frac{1-\alpha_f y_{\mathrm{A}}}{D_{\mathrm{AB}}} + \frac{1}{D_{Ka,\mathrm{A}}}\right)^{-1} \quad (7.63)$$

$$D_i = \frac{\varepsilon_i^2}{(1-\varepsilon_a)^2}\left(\frac{1-\alpha_f y_{\mathrm{A}}}{D_{\mathrm{AB}}} + \frac{1}{D_{Ki,\mathrm{A}}}\right)^{-1} \quad (7.64)$$

Here, ε_a and ε_i are the volume fractions of macro and micro pores respectively, y_{A} is the mole fraction of component A while α_f is the flux ratio:

$$\alpha_f = 1 + \frac{N_{\mathrm{A}}}{N_{\mathrm{B}}} \quad (7.65)$$

For small mole fractions of NO and NH_3 (say below 1000 ppmv) the above expressions reduce to:

$$D_a = \left(\frac{1}{D_{\mathrm{AB}}} + \frac{1}{D_{Ka,\mathrm{A}}}\right)^{-1} \quad (7.66)$$

$$D_i = \frac{\varepsilon_i^2}{(1-\varepsilon_a)^2}\left(\frac{1}{D_{\mathrm{AB}}} + \frac{1}{D_{Ki,\mathrm{A}}}\right)^{-1} \quad (7.67)$$

The Knudsen diffusivity of component A in pore system j, $D_{Kj,\mathrm{A}}$, is given by [134]:

$$D_{Kj,\mathrm{A}} = \frac{8}{3} r_{c,j} \sqrt{\frac{RT}{2\pi M_{\mathrm{A}}}} \quad (7.68)$$

Where $r_{c,j}$ is the pore radius in the given pore system. The total porosity of the catalyst is the sum of the micro and macro pore volume factions:

$$\varepsilon = \varepsilon_i + \varepsilon_a$$

Based on Hg-porosimetry on material from a commercial SCR catalyst, the modeled catalyst is assumed to have the pore radii and porosities started in Table 7.4. As seen from the pore radii, the porosity of the "micro pores" actually covers both the micro and meso pores.

Table 7.4: Assumed macro and "micro" (micro + meso) pore radii and porosities of the SCR monolith.

$r_{c,a}$ [m]	$r_{c,i}$ [m]	ε_a	ε_i
$1500 \cdot 10^{-10}$	$146 \cdot 10^{-10}$	0.54	0.16

The mass transfer coefficient of particles in size class i, $k_{p,i}$, is given by:

$$k_{p,i} = Sh_{p,i} \frac{D_{p,i}}{d_h} \tag{7.69}$$

Where $D_{p,i}$ is the diffusivity of particles of size i. The correlation for the Sherwood number stated above (equation 7.60) is also applicable here. The particle diffusivity can be calculated from the following correlation [135]:

$$D_{p,i} = \kappa T \frac{C_c}{3\pi\eta_g d_{p,i}} \tag{7.70}$$

Where η_g is viscosity of the flue gas, which we in the following will assume has the properties of air, and C_c is the Cunningham slip correction factor, given by [135]:

$$C_c = 1 + Kn\left(1.142 + 0.558e^{-\frac{0.999}{Kn}}\right) \tag{7.71}$$

Kn is the Knudsen number [135]:

$$Kn = \frac{2\lambda}{d_{p,i}} \tag{7.72}$$

The mean free path of air, λ (in m), is given by [135]:

$$\lambda = 0.0664 \cdot \left(\frac{101000}{P}\right)\left(\frac{T}{293}\right)\left(\frac{1+\frac{110}{293}}{1+\frac{110}{T}}\right) \cdot 10^{-6} \text{ m} \tag{7.73}$$

The viscosity of air at the respective temperature and pressure can be found by interpolation between data from CRC [123]. It is, of course, an approximation to use the properties of air as a substitution for a more vaguely defined flue gas. Based on the ideal gas law, the density of air at 350 °C and 1 bar can be calculated to 0.557 kg/m^3, while the viscosity (based on data from [123]) is $3.16 \cdot 10^{-5}$ Pa·s. This corresponds to a kinematic viscosity of $5.67 \cdot 10^{-5}$ m^2/s. Lefers *et al.* [136] have reported a calculated density of 0.551 kg/m^3 and a kinematic viscosity of $5.25 \cdot 10^{-5}$ m^2/s (at 1 atm and 350 °C) of a flue gas from a natural gas fired boiler.

7.5. Solution procedure

In the solution of the system, the monolith channel is regarded as a series of n continuously stirred tank reactors with the heights Δz ($n \cdot \Delta z = L$). In practice, this is done by approximating the spatial differential quotient with the corresponding difference quotient:

$$\left.\frac{d\tilde{C}_{\mathrm{NO},b}}{d\tilde{t}}\right|_{\tilde{z}+\Delta\tilde{z}} \approx -\frac{Ut_{ref}}{z_{ref}}\frac{\tilde{C}_{\mathrm{NO},b}|_{\tilde{z}+\Delta\tilde{z}}-\tilde{C}_{\mathrm{NO},b}|_{\tilde{z}}}{\Delta\tilde{z}} - \frac{4k_{g,\mathrm{NO}}t_{ref}}{d_h}\left(\tilde{C}_{\mathrm{NO},b}\big|_{\tilde{z}+\Delta\tilde{z}} - \tilde{C}_{\mathrm{NO},s}\big|_{\tilde{z}+\Delta\tilde{z}}\right) \tag{7.74}$$

$$\left.\frac{d\tilde{C}_{\mathrm{NH3},b}}{d\tilde{t}}\right|_{\tilde{z}+\Delta\tilde{z}} \approx -\frac{Ut_{ref}}{z_{ref}}\frac{\tilde{C}_{\mathrm{NH3},b}|_{\tilde{z}+\Delta\tilde{z}}-\tilde{C}_{\mathrm{NH3},b}|_{\tilde{z}}}{\Delta\tilde{z}} - \frac{4k_{g,\mathrm{NH3}}t_{ref}}{d_h}\left(\tilde{C}_{\mathrm{NH3},b}\big|_{\tilde{z}+\Delta\tilde{z}} - \tilde{C}_{\mathrm{NH3},s}\big|_{\tilde{z}+\Delta\tilde{z}}\right) \tag{7.75}$$

Since the mass transfer coefficient is a function of z, an average value is calculated for each reactor:

$$\langle k_{g,i}\rangle = \frac{\int_z^{z+\Delta z} k_{g,i}(z\prime)dz\prime}{\Delta z} \tag{7.76}$$

The same is done for the particle mass transfer coefficient, $k_{p,i}$. In the first reactor (with inlet at $z = 0$ and outlet at $z = \Delta z$), the inlet concentrations are known:

$$\tilde{C}_{i,b}(t)\big|_{z=0} = \tilde{C}^0_{i,b} \tag{7.77}$$

The outlet concentrations of a reactor, which are the solutions to equation 7.74 and 7.75, will constitute of series of NO and NH_3 concentrations, given in each point in time, which will serve as input to the next reactor. Besides the inlet concentrations, the steady-state concentrations in each reactor are needed:

$$\tilde{C}_{i,b}(\tilde{t}=\tilde{t}_0)\big|_{\tilde{z}+\Delta\tilde{z}} = \tilde{C}^{ss}_{i,b}\big|_{\tilde{z}+\Delta\tilde{z}} \tag{7.78}$$

For the radial equations, the spatial derivative is approximated with a central finite difference:

$$\left.\frac{\partial\tilde{C}_{\mathrm{NO}}}{\partial\tilde{t}}\right|_{\tilde{x}} \approx \frac{D_{e,\mathrm{NO}}t_{ref}}{\varepsilon x^2_{ref}}\frac{\tilde{C}_{\mathrm{NO}}|_{\tilde{x}+\Delta\tilde{x}}-2\tilde{C}_{\mathrm{NO}}|_{\tilde{x}}+\tilde{C}_{\mathrm{NO}}|_{\tilde{x}-\Delta\tilde{x}}}{(\Delta\tilde{x})^2} - \frac{t_{ref}}{\varepsilon}k_s\tilde{C}_{\mathrm{NO}}\big|_{\tilde{x}}\varphi|_{\tilde{x}}\frac{K_{\mathrm{NH3}}\tilde{C}_{\mathrm{NH3}}|_{\tilde{x}}}{\frac{1}{C_{ref}}+K_{\mathrm{NH3}}\tilde{C}_{\mathrm{NH3}}|_{\tilde{x}}} \tag{7.79}$$

$$\left.\frac{\partial\tilde{C}_{\mathrm{NH3}}}{\partial\tilde{t}}\right|_{\tilde{x}} \approx \frac{D_{e,\mathrm{NO}}t_{ref}}{\varepsilon x^2_{ref}}\frac{\tilde{C}_{\mathrm{NH3}}|_{\tilde{x}+\Delta\tilde{x}}-2\tilde{C}_{\mathrm{NH3}}|_{\tilde{x}}+\tilde{C}_{\mathrm{NH3}}|_{\tilde{x}-\Delta\tilde{x}}}{(\Delta\tilde{x})^2} - \frac{t_{ref}}{\varepsilon}k_s\tilde{C}_{\mathrm{NO}}\big|_{\tilde{x}}\varphi|_{\tilde{x}}\frac{K_{\mathrm{NH3}}\tilde{C}_{\mathrm{NH3}}|_{\tilde{x}}}{\frac{1}{C_{ref}}+K_{\mathrm{NH3}}\tilde{C}_{\mathrm{NH3}}|_{\tilde{x}}} \tag{7.80}$$

$$\left.\frac{\partial\varphi}{\partial\tilde{t}}\right|_{\tilde{x}} = \frac{D_s t_{ref}}{x_{ref}^2}\frac{\varphi|_{\tilde{x}+\Delta\tilde{x}} - 2\varphi|_{\tilde{x}} + \varphi|_{\tilde{x}-\Delta\tilde{x}}}{(\Delta\tilde{x})^2} \tag{7.81}$$

At the catalyst center ($x = 0$), the following applies:

$$\frac{\tilde{C}_i|_{\tilde{x}+\Delta\tilde{x}} - \tilde{C}_i|_{\tilde{x}-\Delta\tilde{x}}}{2\Delta\tilde{x}} = 0 \tag{7.82}$$

$$\frac{\varphi|_{\tilde{x}+\Delta\tilde{x}} - \varphi|_{\tilde{x}-\Delta\tilde{x}}}{2\Delta\tilde{x}} = 0 \tag{7.83}$$

At the catalyst surface ($x = V/S$), the boundary conditions become:

$$\frac{\tilde{C}_i|_{\tilde{x}+\Delta\tilde{x}} - \tilde{C}_i|_{\tilde{x}-\Delta\tilde{x}}}{2\Delta\tilde{x}} = \frac{x_{ref} k_{g,i}}{D_{e,i}}\left(\tilde{C}_{i,b}\big|_{\tilde{z}+\Delta\tilde{z}} - \tilde{C}_i\big|_{\tilde{x}}\right) \tag{7.84}$$

$$\frac{\varphi|_{\tilde{x}+\Delta\tilde{x}} - \varphi|_{\tilde{x}-\Delta\tilde{x}}}{2\Delta\tilde{x}} = -\frac{3 x_{ref} k_{\mathrm{KCl}} V_{m,\mathrm{KCl}}}{2 D_S} C_{\mathrm{OH}}^0 \varphi|_{\tilde{x}} \frac{V}{S}\sum_i \frac{\tilde{C}_{\mathrm{K},p,i}\big|_{\tilde{z}+\Delta\tilde{z}}}{d_{p,i}} \tag{7.85}$$

At $t = t_0$, the concentrations of NO and NH_3, at each discrete point inside the wall are given by the respective steady-state concentrations, while the fraction of available Brønsted sites is equal to 1:

$$\tilde{C}_i(\tilde{t} = \tilde{t}_0)\big|_{\tilde{x}} = \tilde{C}_i^{ss}\big|_{\tilde{x}} \tag{7.86}$$

$$\varphi(\tilde{t} = \tilde{t}_0)|_x = 1 \tag{7.87}$$

For each reactor in the z direction, equations 7.74, 7.75, 7.77 and 7.78 together with equations 7.79-7.87 (for each discrete x value) and equation 7.43 (for each particle size class in a given distribution) constitute a system of ordinary differential equations with associated initial and boundary conditions. The steady-state concentrations of NO and NH_3 can in practice be found by respectively setting the NO and NH_3 concentration to $C^0_{\mathrm{NO},b}$ and $C^0_{\mathrm{NH3},b}$ at the inlet, and $C^0_{\mathrm{NO},b}$ and 0 everywhere else (in the channel as well as in the wall), and then solve the system without particle deposition for the time span $t = t_0$-t_{ss} to $t = t_0$. In the following, the model is solved using the ode15s solver in MATLAB [137].

7.6. Simulations

7.6.1. Operating conditions and catalyst shape parameters

The deactivation model is solved for a simulated particle exposure period of 1000 hours, with an initiation period, without particle deposition, of 1 hour, ($t_0 = 0$, $t_{ss} = 60 \cdot 60$ s, $t_{sim} = 1000 \cdot 60 \cdot 60$ s).

Correlations and parameters presented above as well as the operating and shape parameters of the catalyst, listed in Table 7.5 below, are used in the simulations if nothing else is stated.

Table 7.5: Operating conditions and catalyst shape parameters used in the simulations.

Parameter	Value	Parameter	Value	Parameter	Value
P	1 atm	U	6.9 m/s	S_{surf}	$6.81 \cdot 10^{7}$ m^2/m^3
T	350 °C	d_h	6.5 mm	C^0_{OH}	$2.6 \cdot 10^{-6}$ mol/m^2
$C^0_{NO,b}$	500 ppmv	L	25 cm		
$C^0_{NH3,b}$	600 ppmv	V/S	0.5 mm		

The operating and shape parameters have been chosen so that they closely resemble those of the $3\%V_2O_5$-$7\%WO_3/TiO_2$ monolith which was exposed to a KCl aerosol at 350 °C for 960 hours (discussed in section 6). From SEM-EDS analysis of KCl exposed SCR catalyst plates as well as SEM-WDS measurements on two-layer pellets (Figure 4.6 and Figure 5.1), there appears to exist a potassium saturation level at a K/V molar ratio of 0.5-0.6 (for $3\%V_2O_5$-$7\%WO_3/TiO_2$ catalysts). Assuming that the catalyst is saturated with potassium at a K/V molar ratio of 0.55 and that potassium only reacts with Brønsted acid sites, the initial concentration of Brønsted acid sites, C^0_{OH}, is 0.18 mol/kg catalyst. Zheng *et al.* [6] measured a BET surface area of 68.1 m^2/g for a similar catalyst, which gives a value for C^0_{OH} of $2.6 \cdot 10^{-6}$ mol/m^2. Assuming a catalyst density, ρ_{cat}, of 1000 kg/m^3, the internal specific surface are becomes $6.81 \cdot 10^{7}$ m^2/m^3. The observed start conversion of NO over the exposed monolith was 55 %. Using the Arrhenius parameters in Table 7.1, a simulated start conversion of 57 % is obtained. Hence, no attempt to adjust the kinetics has been made. For the first simulation (denoted "simulation #1"), the deactivation parameters k_{KCl} and D_s have been manually fitted in order to match the experimentally measured deactivation profile.

7.6.2. Particle size distribution and particle deposition flux

During exposure of the monolith, the number based particle size distribution of the KCl aerosol in the bulk gas was measured by an SMPS. This distribution, shown in Figure 7.1 (Inlet), consists of 102 discrete size classes, with mean particle diameters in the range 5.94 to 224.7 nm, and contains a total of $3.0 \cdot 10^{14}$ particles/Nm^3, corresponding to a volume based particle concentration of $7.6 \cdot 10^{-9}$ m^3/Nm^3. This distribution is used as input to the deactivation model if nothing else is stated. Using equation 7.35, the particle size distribution at the outlet of the monolith channel has been calculated and plotted in Figure 7.1 as well.

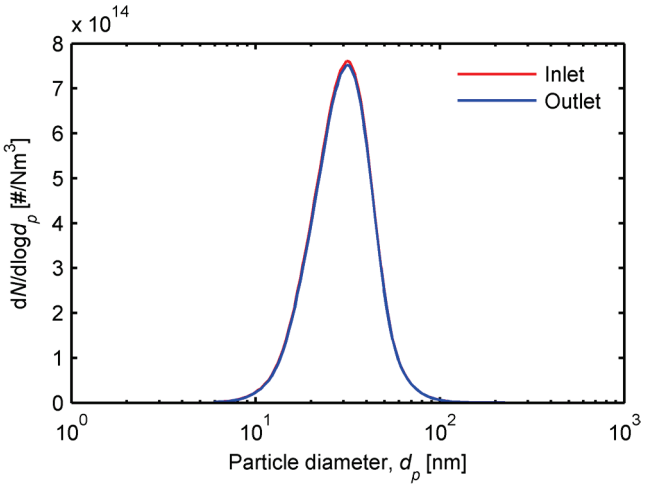

Figure 7.1: Number based particle size distribution used as input to the deactivation model (Inlet) and calculated size distribution of the particles that leave a 25 cm long monolith channel with a hydraulic diameter of 6.5 mm (Outlet).

As seen from the figure, a substantial amount of submicron particles are present at the inlet of the catalyst and only a very small fraction of the particles is lost to the catalyst surface during the passage. Both distributions peak at 31.1 nm.

Figure 7.2 shows the potassium deposition flux (in μmol/m^2/s) as a function of distance in the monolith channel, for particles with diameters of 5.94, 31.1 and 224.7 nm respectively.

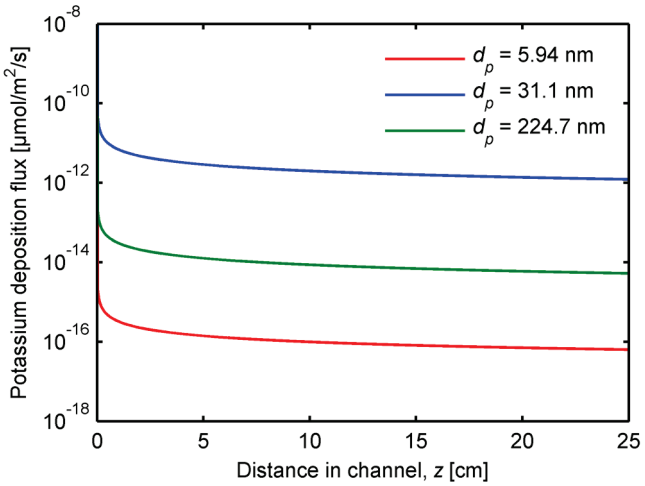

Figure 7.2: Potassium deposition flux of three particle size classes as a function of axial position. $W^0_{5.94\ nm,b} = 2.9 \cdot 10^{10}$ #/Nm^3, $W^0_{31.1\ nm,b} = 2.0 \cdot 10^{13}$ #/Nm^3, $W^0_{224.7\ nm,b} = 1.3 \cdot 10^9$ #/Nm^3.

At the inlet of the channel (z = 0), the flow is turbulent and the mass transfer coefficient, $k_{p,i}$, is infinitely high. The deposition flux decreases with the mass transfer coefficient and the slightly decreasing particle concentration along the channel. Although the 5.94 nm particles have the highest diffusivity, the potassium deposition flux is significantly lower than that of the 31.1 nm particles, due to their low volume based concentration. Conversely, the 224.7 nm particles have the

lowest diffusivity, while they have a higher volume based concentration compared to the 5.94 nm particles. A 224.7 nm particle takes up 54000 times the volume of a 5.94 nm particle. As a result, the potassium deposition flux of the 224.7 particles is higher than that of the smallest particles although still lower than the deposition flux of the 31.1 nm particles.

7.6.3. Preliminary results, simulation #1

Figure 7.3 shows the relative activity as a function of time, simulated by the deactivation model, together with that measured for the KCl exposed monolith. In order to compare it with the experimental results, the relative activity is calculated as a ratio between observed activities, in including mass transfer limitations, assuming a first order reaction with respect to NO and zero order with respect to NH_3:

$$\frac{k'_{obs}}{k'_{obs,0}} = \frac{\ln(1-X_{\mathrm{NO}}(t))}{\ln(1-X_{\mathrm{NO}}(t_0))} \tag{7.88}$$

Where the conversion, X, is given by:

$$X_{\mathrm{NO}}(t) = \frac{C^0_{\mathrm{NO},b} - C_{\mathrm{NO},b}(t,L)}{C^0_{\mathrm{NO},b}} \tag{7.89}$$

For the simulation, a resolution of 100 tank reactors in the z direction and 100 points inside the catalyst wall (x direction), for each reactor, was found to yield a sufficiently convergent solution. The results from this simulation, in the following referred to as "simulation #1", will form a basis for comparison for further simulations.

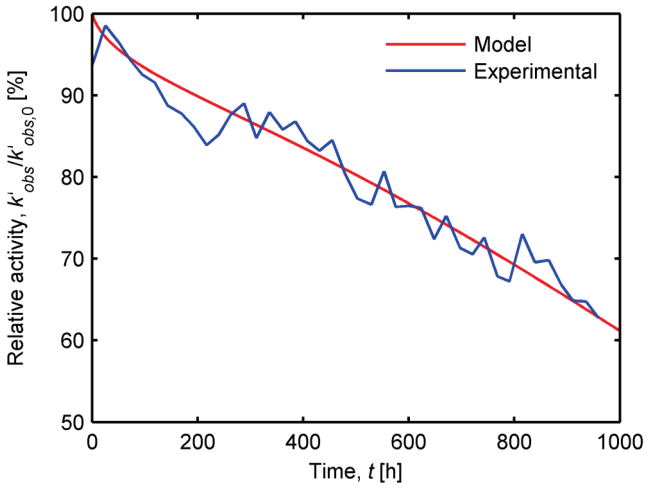

Figure 7.3: Simulated (Model) and experimental deactivation profile of a 3%V_2O_5-7%WO_3/TiO_2 monolith catalyst exposed to KCl aerosols for 960 hours. Values of fitted parameters: $k_{KCl} = 1.2 \cdot 10^{-1}$ 1/s, $D_s = 9.90 \cdot 10^{-14}$ m^2/s (simulation #1).

As seen from the figure, an adequate fit between the simulated and experimental deactivation profile was obtained by setting k_{KCl} to $1.2 \cdot 10^{-1}$ 1/s and D_s to $9.90 \cdot 10^{-14}$ m^2/s. Figure 7.4 shows the simulated NO and NH_3 concentrations from the surface to the center of the catalyst wall, at the inlet and outlet of the channel, at $t = t_0$.

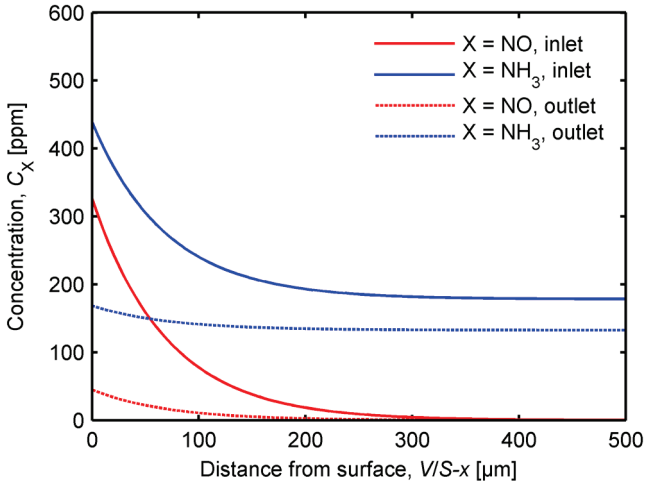

Figure 7.4: NO and NH_3 concentration profiles in the catalyst wall calculated at the inlet and outlet of the monolith channel at $t = t_0$. Bulk concentrations: $[NO]_{inlet}$ = 500 ppmv, $[NH3]_{inlet}$ = 600 ppmv, $[NO]_{outlet}$ = 214 ppmv, $[NH3]_{outlet}$ = 314 ppmv (simulation #1).

As seen from the figure, the SCR reaction takes place in the first 300 µm of the catalyst material at the inlet of the channel, and in about 200 µm at the outlet. As the catalyst deactivates, more of the catalyst is utilized, as apparent from Figure 7.5, which shows the same concentration profiles at $t = t_{sim}$ (= 1000 hours).

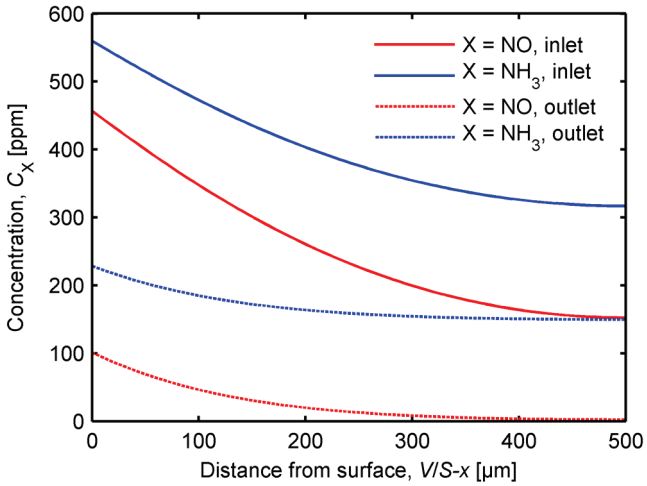

Figure 7.5: NO and NH_3 concentration profiles in the catalyst wall calculated at the inlet and outlet of the monolith channel at $t = t_{sim}$ (1000 h). Bulk concentrations: $[NO]_{inlet}$ = 500 ppmv, $[NH3]_{inlet}$ = 600 ppmv, $[NO]_{outlet}$ = 298 ppmv, $[NH3]_{outlet}$ = 398 ppmv (simulation #1).

Figure 7.6 shows the fraction of available Brønsted sites, φ, at the center ($x = 0$) of the catalyst wall, calculated for the inlet and outlet of the channel. After about 23 hours, potassium has penetrated into the center of the catalyst wall, at the inlet of the channel, and the Brønsted sites located here start to get poisoned. It takes additional 8 hours (31 hours in total) for potassium to reach the wall center at the outlet of the channel. As seen from the figure, the model predicts a significant difference, in the rate at which the center sites are consumed, between the top and bottom of the channel. At the channel inlet, 93 % of the active sites, at the center of the wall, have been poisoned, while this number is 66 % at the outlet, after 1000 hours of exposure.

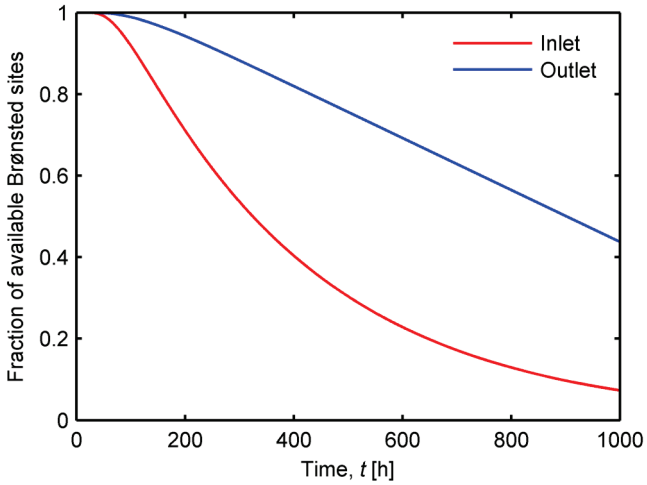

Figure 7.6: Fraction of available Brønsted sites at the center of the catalyst wall ($x = 0$) as a function of time calculated at the inlet and outlet of the monolith channel (simulation #1).

Figure 7.7 shows the K/V molar ratio across the half thickness of the catalyst wall calculated at the inlet and outlet of the monolith channel at $t = t_{sim}$, assuming that the catalyst contains 3 wt.% V_2O_5, corresponding to 0.33 mol V/kg. For comparison, the K/V molar ratios measured (by SEM-EDS) in the top and bottom section of the KCl exposed monolith are shown as well. The experimental data has been scaled in the x direction, assuming a wall thickness of exactly 1000 µm. As seen from the figure, the model predicts somewhat higher K/V molar ratios at the inlet of the channel compared to that in the outlet. At the channel inlet, the K/V molar ratio drops from 0.54 to 0.51 towards the center of the wall. The profile at the outlet of the channel is slightly steeper, dropping from 0.43 to 0.31. The profiles are still rather flat, indicating that the release of potassium from deposited particles, on the external surface, is slow compared to the diffusion of potassium from the external surface into the catalyst wall. The simulated profiles correlate well with the experimental K/V molar ratios, accounting for the difference between the profiles measured in the top and bottom section of the exposed monolith.

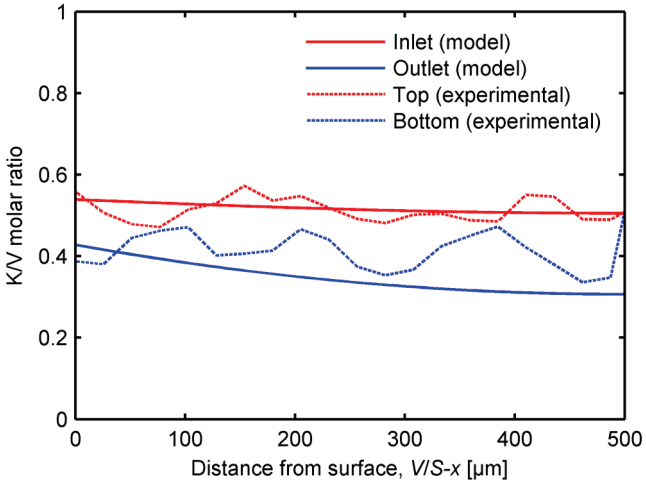

Figure 7.7: Simulated and experimentally measured K/V molar ratios across the half thickness of the catalyst wall of a 3%V_2O_5-7%WO_3/TiO_2 monolith after 960 hours of KCl exposure (simulation #1).

Figure 7.8 shows the overall effectiveness factor, $\eta_{overall}$, as a function of time, calculated at the inlet and outlet of the monolith channel.

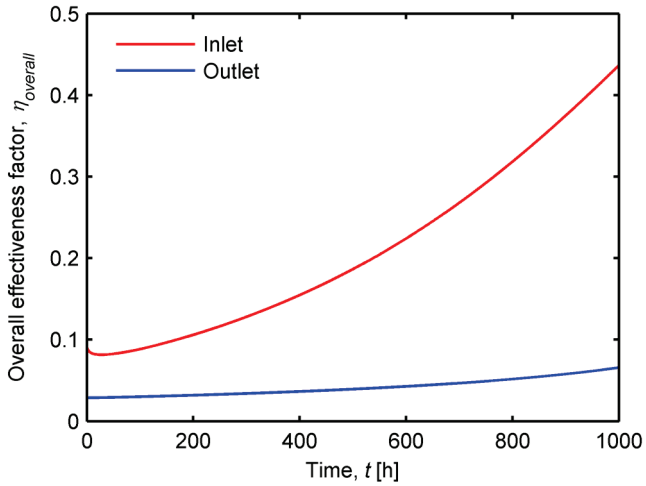

Figure 7.8: Overall effectiveness factor as a function of time calculated at the inlet and outlet of the monolith channel (simulation #1).

At $t = t_0$, the effectiveness factor is 0.09 close to the inlet and only 0.03 at the outlet. The catalyst is hence subjected to severe mass transfer limitations. As the catalyst deactivates, the effectiveness factor generally increases. However, during the first hours, a slight decrease can be observed at the inlet of the channel. This is likely due to a fast (and complete) deactivation of the active sites in the outermost layer of the catalyst wall, causing an initial increase in the transport limitations. As the internal sites start to deactivate (due to diffusion of potassium), the overall effectiveness factor increases. After 1000 hours it respectively assumes a value of 0.44 and 0.07 at the inlet and outlet.

The decreasing mass transfer limitations explain how the catalyst can retain an observed relative activity of 61 %, while only 7-44 % of the initial amount of Brønsted acid sites is available at the center of the catalyst wall.

7.6.4. Parameter study

A parameter study, investigating the influence of various input parameters on the solution of the deactivation model, has been carried out and is presented and discussed in the following. A total of 14 simulations, including the base case discussed above, have been conducted, and the parameter study is summarized in Table 7.6. Between simulation #1 and all subsequent simulations one of the following parameters have been changed in the model: The initial concentration of Brønsted acid sites, C^0_{OH}, the deactivation rate constant, k_{KCl}, the surface diffusion coefficient, D_s, the particle size distribution of the incoming aerosol, or the particle mass transfer coefficients, $k_{p,i}$. Apart from listing the input parameters used in the various simulations, Table 7.6 summarizes the simulation results in the form of the observed relative activity, $k'_{obs}/k'_{obs,0}$, and the fraction of available Brønsted sites at the center of the catalyst wall (near the inlet and outlet of the channel), $\varphi(x = 0)$, both taken at $t = t_{sim}$ (= 1000 hours).

Table 7.6: Summary of the parameter study. Cells which have been greyed out indicate the parameters that have been changed compared to the base case (#1).

#	C^0_{OH} [mol/m^2]	k_{KCl} [1/s]	D_s [m^2/s]	Distribution Type [a]	Distribution mode [nm]	$k_{p,i}$ mod [b]	$k'_{obs}/k'_{obs,0}$ [%] [c]	$\varphi(x = 0)$ inlet/outlet [c]
1	$2.6\cdot10^{-6}$	$1.2\cdot10^{-1}$	$9.90\cdot10^{-14}$	Poly	31.1	1	61	0.07/0.44
2	$9.7\cdot10^{-7}$	$1.2\cdot10^{-1}$	$9.90\cdot10^{-14}$	Poly	31.1	1	48	0.07/0.10
3	$2.6\cdot10^{-6}$	$1.2\cdot10^{-2}$	$9.90\cdot10^{-14}$	Poly	31.1	1	84	0.41/0.48
4	$2.6\cdot10^{-6}$	$1.2\cdot10^{0}$	$9.90\cdot10^{-14}$	Poly	31.1	1	56	0.04/0.44
5	$2.6\cdot10^{-6}$	$1.2\cdot10^{-1}$	$9.90\cdot10^{-15}$	Poly	31.1	1	76	0.88/0.90
6	$2.6\cdot10^{-6}$	$1.2\cdot10^{-1}$	$4.95\cdot10^{-14}$	Poly	31.1	1	67	0.26/0.51
7	$2.6\cdot10^{-6}$	$1.2\cdot10^{-1}$	$1.98\cdot10^{-13}$	Poly	31.1	1	53	0.01/0.40
8	$2.6\cdot10^{-6}$	$1.2\cdot10^{-1}$	$9.90\cdot10^{-13}$	Poly	31.1	1	44	0.00/0.37
9	$2.6\cdot10^{-6}$	$1.2\cdot10^{-1}$	$9.90\cdot10^{-14}$	Mono	224.7	1	89	0.08/0.87
10	$2.6\cdot10^{-6}$	$1.2\cdot10^{-1}$	$9.90\cdot10^{-14}$	Mono	2247	1	97	0.33/0.97
11	$2.6\cdot10^{-6}$	$1.2\cdot10^{-1}$	$9.90\cdot10^{-14}$	Poly	31.1	0.1	95	0.10/0.94
12	$2.6\cdot10^{-6}$	$1.2\cdot10^{-1}$	$9.90\cdot10^{-14}$	Mono	224.7	0.1	99	0.65/0.99
13	$2.6\cdot10^{-6}$	$1.2\cdot10^{-1}$	$9.90\cdot10^{-14}$	Poly	31.1	10	47	0.07/0.07
14	$2.6\cdot10^{-6}$	$1.2\cdot10^{-1}$	$9.90\cdot10^{-14}$	Mono	224.7	10	49	0.07/0.11

a) Poly = Polydisperse, Mono = Monodisperse.
b) $k_{p,i}$ modifier. All particle mass transfer coefficients are multiplied by this value.
c) At $t = t_{sim}$ (1000 h).

7.6.4.1. Initial concentration of Brønsted acid sites, simulation #2

The value for the initial concentration of Brønsted acid sites, used in simulation #1, is based on the K/V molar ratios measured in exposed catalyst plates and pellets. Another option is to base it on the NH_3 chemisorption capacity, previously measured for a $3\%V_2O_5$-$7\%WO_3/TiO_2$ catalyst (i.e. 0.066 mol/kg, section 4). This value, divided by the BET surface area measured by Zheng *et al.* [6] (68.1 m^2/g), gives an initial concentration of Brønsted acid sites of $9.7 \cdot 10^{-7}$ mol/m^2, which is used in simulation #2. Figure 7.9 shows the resulting K/V molar ratios across the half thickness of the catalyst wall.

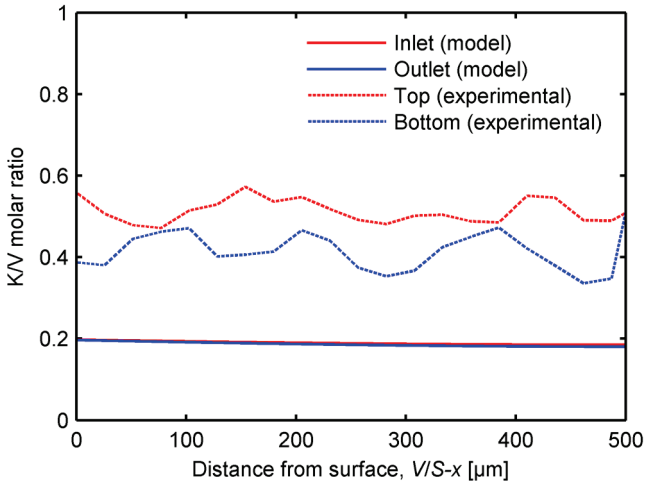

Figure 7.9: Simulated and experimentally measured K/V molar ratios across the half thickness of the catalyst wall of a $3\%V_2O_5$-$7\%WO_3/TiO_2$ monolith after 960 hours of KCl exposure (simulation #2).

As the total amount of Brønsted sites at $t = t_0$ is assumed be 0.066 mol/kg, the simulated K/V ratio (for a catalyst with a V_2O_5 content of 3 wt.%) can never exceed a maximum value of 0.2, which is approached at the external surface of the catalyst, both at the inlet and at the outlet of the channel, as seen in Figure 7.9. The profiles nearly overlap, unlike those in Figure 7.7. As C^0_{OH} is decreased, so is the maximum rate at which particle bound potassium reacts with Brønsted sites on the external surface, according to equation 7.43. The deactivation will hence, to a larger extent, be limited by the reaction on the external surface and the potassium profiles in the wall, at the inlet and outlet of the channel, becomes more flat and moves closer to each other. The applied method for measuring the NH_3 adsorption capacity, on which the C^0_{OH} value is based (in simulation #2), can only account for the acid sites which are active in the SCR reaction. In reality, the catalyst may have additional "non-active" Brønsted sites, which can still facilitate the potassium transport. Hence, it is reasonable to use the C^0_{OH} value from simulation #1, which gave a better agreement with experimental K/V profiles. Also the deactivation profile is changed upon decreasing C^0_{OH}, as indicated in Table 7.6.

For simulation #2, a lower relative activity of 48 % is obtained after 1000 hours of exposure. This may seem to contradict the observations from the plate exposure campaigns (section 4) as well as the two-layer experiments (section 5), where Brønsted acid sites appeared to enhance the potassium transport in SCR catalysts, and thereby the deactivation rate. However, in the current deactivation model, the possible influence of catalyst composition on the potassium surface diffusivity is not taken into account.

7.6.4.2. Deactivation rate constant, simulation #3 & 4

Figure 7.10 shows the deactivation profiles obtained by solving the model after respectively multiplying the deactivation rate constant, k_{KCl}, with a factor of 0.1 (simulation #3) and 10 (simulation #4) compared to the base case.

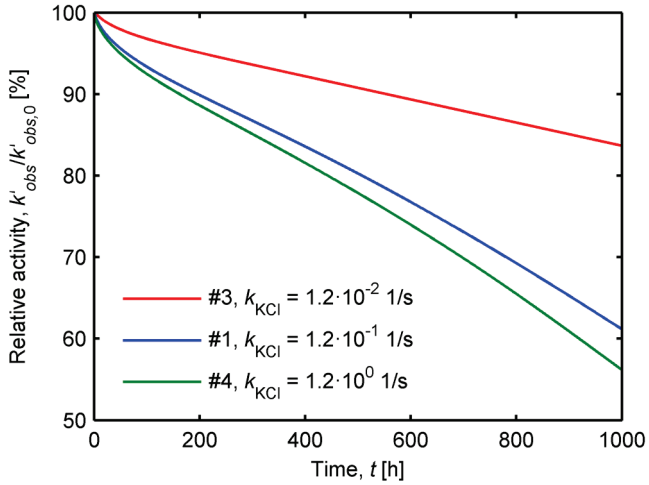

Figure 7.10: Simulated deactivation profiles obtained using k_{KCl} values of $1.2 \cdot 10^{-2}$, $1.2 \cdot 10^{-1}$ and $1.2 \cdot 10^{-0}$ 1/s.

As seen from the figure, the catalyst deactivates faster as k_{KCl} is increased, just as expected. However, the higher the value of k_{KCl} is, the less pronounced is the effect on the resulting deactivation profile. After 1000 hours of exposure, the relative activity of the catalyst is 84, 61 and 56 % depending on the value of k_{KCl}. For the lowest value of the deactivation rate constant (i.e. $1.2 \cdot 10^{-2}$ 1/s, simulation #3), the inlet and outlet values of φ, at the center of the catalyst wall, are similar (0.41 and 0.48, as seen from Table 7.6) due slow consumption of particle bound potassium at the catalyst surface. When the rate constant is increased, the inlet value of φ decreases rapidly (to 0.07 in simulation #1 and to 0.04 in simulation #4), as the high particle flux at the entrance ensures a fast saturation of the surface. The deactivation rate of the lower part of the catalyst will to an increasing extent be limited by the particle deposition rate. As a result, the outlet value of φ only decreases slightly for increasing values of k_{KCl} (0.48 → 0.44 → 0.44). It can hence be concluded

that the deactivation rate increases with k_{KCl}, and that the resulting deactivation profiles is mostly sensitive to low values of this parameter.

7.6.4.3. Surface diffusion coefficient, simulation #5-8

Figure 7.11 shows the deactivation profile from simulation #1, together with those obtained by solving the model after respectively multiplying the surface diffusion coefficient, D_s, with a factor of 0.1 (simulation #5), 0.5 (simulation #6), 2 (simulation #7) and 10 (simulation #8).

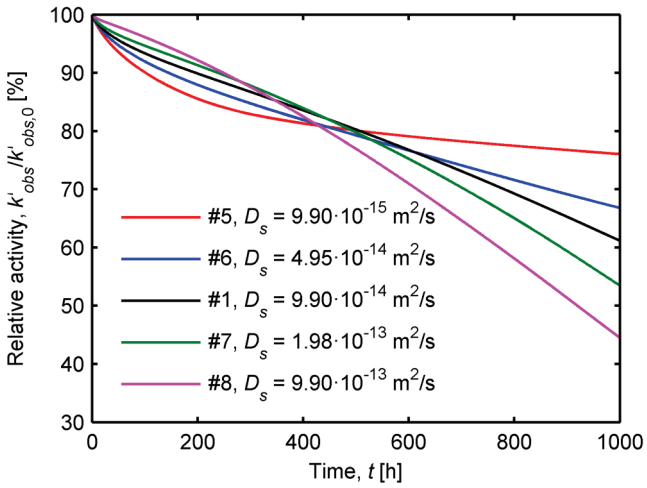

Figure 7.11: Simulated deactivation profiles obtained using D_s values of $9.90 \cdot 10^{-15}$, $4.95 \cdot 10^{-14}$, $9.90 \cdot 10^{-14}$, $1.98 \cdot 10^{-13}$ and $9.90 \cdot 10^{-13}$ m^2/s.

During the first hours, the degree of deactivation is largest for the catalyst from simulation #5 while it is lowest for the catalyst from simulation #8. After about 400 hours, the two deactivation profiles cross, and the catalyst from simulation #5 ends at a relative activity of 76 %, after 1000 hours, while that of simulation #8 ends at 44 %. When the surface diffusion coefficient is low, as in simulation #5, potassium will accumulate faster in the outermost layer of the catalyst, where the SCR reaction primarily takes place in the fresh catalyst. This is the reason for the initial fast deactivation seen in Figure 7.11. If the diffusion coefficient is high (simulation #8), the potassium is more evenly distributed throughout the catalyst, however, the total number of poisoned sites will be higher, leading to a larger degree of deactivation in the long run.

Figure 7.12 shows the K/V profiles after 1000 hours, calculated at the outlet of the channel, for the 5 simulations. As seen from the figure, the profiles become progressively more flat as the surface diffusion coefficient is increased. In simulation #5 the K/V molar ratio drops from 0.54 at the surface to 0.05 at the center of the catalyst. In simulation #8 the ratio assumes a near constant value of 0.36 at the surface and 0.34 center of the wall. In conclusion, the deactivation rate increases with D_s for long term exposures, and potassium becomes more evenly distributed in the catalyst. For

short term exposures, the deactivation rate is faster for low values of D_s due to potassium accumulation in outer part of the catalyst wall.

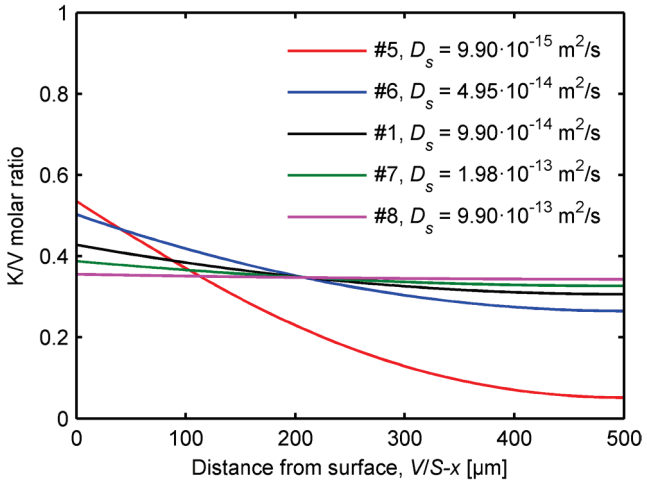

Figure 7.12: Simulated K/V molar ratios (after 1000 hours KCl exposure) across the half thickness of the catalyst wall, at the outlet of the monolith channel, using D_s values of 9.90·10^{-15}, 4.95·10^{-14}, 9.90·10^{-14}, 1.98·10^{-13} and 9.90·10^{-13} m^2/s.

7.6.4.4. Particle size distribution, simulation #9 & 10

In order to study the effect of particle size on the rate of deactivation, the size distribution of the incoming KCl aerosol has been assumed monodisperse, while maintaining the total volume based particle concentration (7.63·10^{-9} m^3/Nm^3). In simulation #9, all particles are assumed to have a diameter of 224.7 nm which yields a total number based concentration of 1.29·10^{12} particles/Nm^3. In simulation #10, the particles have a diameter of 2247 nm corresponding to 1.29·10^9 particles/Nm^3. Figure 7.13 shows the potassium deposition flux as a function of distance in the monolith channel, for the two monodisperse distributions from simulation #9 and 10. Furthermore, the figure shows the resulting potassium deposition flux from a particle size distribution consisting solely of 5.94 nm particles (with a total volume concentration of 7.63·10^{-9} m^3/Nm^3). As seen from the figure, the potassium deposition flux decreases with increasing particle size. As the total volume based concentration is kept constant, the deposition flux only depends on the mass transfer coefficient.

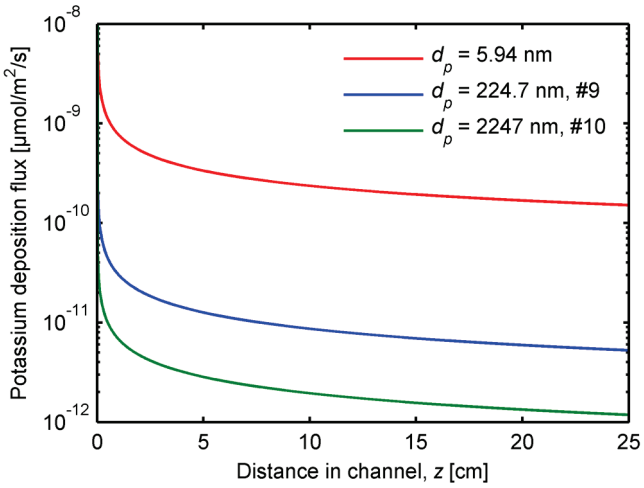

Figure 7.13: Potassium deposition flux of three monodisperse particle size distributions. $W^0_{5.94\ nm,b} = 7.0 \cdot 10^{16}$ #/Nm^3, $W^0_{224.7\ nm,b} = 1.3 \cdot 10^{12}$ #/Nm^3, $W^0_{2247\ nm,b} = 1.3 \cdot 10^{9}$ #/Nm^3.

The resulting deactivation profiles are shown in Figure 7.14.

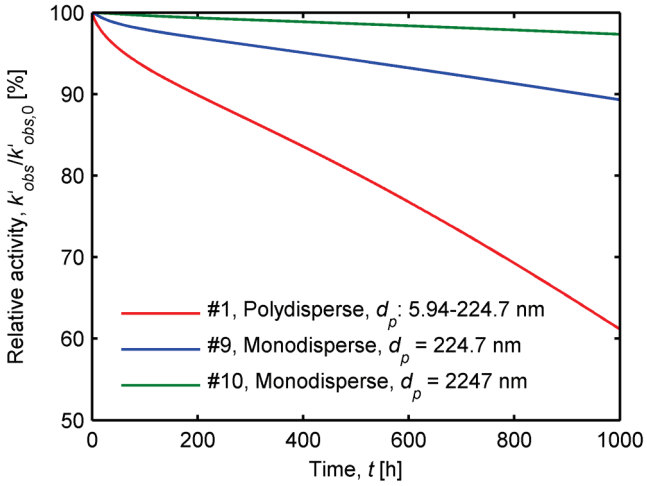

Figure 7.14: Simulated deactivation profiles obtained using polydisperse and monodisperse particle size distributions as input to the model.

The catalyst from simulation #9 deactivates significantly less compared to the one from simulation #1, ending at a relative activity of 89 % after 1000 hours. As seen from the φ values in Table 7.6, the deactivation of the top part of the catalyst is nearly unchanged compared to the base case, while nearly double the amount of Brønsted acid sites, at the center of the catalyst wall, remain unpoisoned at the outlet of the channel. In simulation #10, the particle deposition is so slow that not even the external surface at the very inlet of the monolith channel is fully covered with particles after 1000 hours of exposure. This is apparent from Table 7.6 where φ assumes a value of 0.33 at the channel inlet. As a result, the catalyst only loses 3 % of its initial observed activity. The results show that a way forward, to lower the rate of deactivation, would be to increase the size of the potassium rich aerosol particles. This correlates with the observations by Kling *et al.* [95] who

found that mainly particles below 100 nm contributed the alkali accumulation on SCR catalysts exposed to the flue gas from biomass fired boilers. In praxis, this might be achieved by the addition of seed particles to the hot flue gas.

7.6.4.5. Particle mass transfer coefficient, simulation #11-14

As stated earlier, the particle mass transfer coefficient is determined using a correlation for the Sherwood number in a monolith channel with a developing laminar velocity profile. The Sherwood number is generally given by some function of the Reynolds number, *Re*, and Schmidt number, $Sc_{p,i}$:

$$Sh_{p,i} = f\left(Re = \frac{\rho_g U d_h}{\eta_g}, Sc_{p,i} = \frac{\eta_g}{\rho_g D_{p,i}}\right) \tag{7.90}$$

Where ρ_g is the gas density. As the Schmidt number is inversely proportional to the particle diffusivity, the estimated Sherwood number, and hence the mass transfer coefficient, may be associated with significant uncertainties for large particles. In order to study the effect of $k_{p,i}$ on the resulting deactivation profile, all particle mass transfer coefficients have been multiplied with a factor 0.1 in simulation #11 and 12, and a factor 10 in simulation #13 and 14.

In simulation #11 and 13, the polydisperse particle size distribution from Figure 7.1 has been used. As seen from Table 7.6, reducing the particle mass transfer coefficients by a factor 10, in simulation #11, yields relative activity of 95 % after 1000 hours of exposure, which is a significant increase compared to simulation #1. As expected, increasing the mass transfer coefficients by a factor 10, as in simulation #13, accelerates the deactivation. After 1000 hours of exposure, the catalyst retains 47 % of its initial activity (compared to 61 % in the base case). As the particle deposition is faster, the entire surface along the catalyst becomes saturated with particles within 15 hours. As a result, φ assumes similar values at the inlet and outlet of the channel (i.e. 0.07 at the center of the catalyst wall, see Table 7.6). From simulation #11 and 13 it may thus be concluded that large uncertainties in the estimated values of $k_{p,i}$ may have a significant effect on the predicted deactivation profile, even when the particle size distribution primarily consists of particles below 224.7 nm.

Simulation #12 and 14 use the distribution from simulation #9, which solely consists of 224.7 nm particles. When the mass transfer coefficient is reduced by an order of magnitude (simulation #12), the relative activity after 1000 hours is 99 %, compared to 89 % in simulation #9. When the mass transfer coefficient conversely is increased by an order of magnitude (simulation #14), the resulting

deactivation profile approach that of simulation #13. Hence, for particles with diameters around 224.7 nm or higher, uncertainties in the estimation of the mass transfer coefficient can have tremendous impact on the predicted deactivation profile. This impact will increase with the particle size.

7.7. Model shortcomings

In simulation #1, the deactivation rate constant, k_{KCl}, and the potassium surface diffusion coefficient, D_s, have been fitted in order to match the modeled deactivation profile with that of a monolith exposed to KCl aerosols at 350 °C. In reality, both parameters are likely to have Arrhenius-type dependencies on the operating temperature, each involving a pre-exponential factor and an energy barrier. Taking these into account would thus have introduced two addition fitting parameters in the deactivation model, which cannot be estimated from our current experimental foundation. Furthermore, the surface diffusion coefficient may have some dependency on the initial concentration of Brønsted acid sites (i.e. the shorter the mean distance between two sites, the larger the potassium diffusivity).

In the model, a constant incoming particle size distribution is used. In reality, the aerosol characteristics, and especially the total particle concentration, may vary significantly over time, as apparent from Figure 6.1 as well as from the measurements by Christensen and co-workers [7,8]. As only a small fraction of the incoming particles deposit on the catalyst surface, reducing the total particle concentration by a given factor roughly corresponds to reducing all values of $k_{p,i}$ with the same factor. In the preceding parameter study, it has been shown that the model is rather sensitive to uncertainties in the values of $k_{p,i}$. Hence, the calculated deactivation profiles will also be sensitive to variations in the particle concentration; at least until the point where the entire catalyst surface is saturated with particles. In its current state, the model cannot account for transient variations in the concentration of incoming particles, and it is thus reasonable to use the measured size distribution which contains the largest amount of particles for the calculation of the deactivation profile.

The rate, at which particle bound potassium reacts with Brønsted sites on the external surface of the catalyst, is assumed to scale with the total projected particle area – no matter the particle size. The actual contact area between the individual particles and the catalyst surface will likely be more diverse due to the topography of external surface and agglomeration of particles. On one hand, smaller particles may effectively have access to a larger surface area since they, to a greater extent, are able to deposit in dents, pore mouths and cracks in the external surface. On the other hand, these

may form agglomerates such as dendrites in which the majority of the particles masks the external surface without being in contact with it. In the current model, the effect of the individual particle size classes on the deactivation rate may hence be too simplistic.

7.8. Conclusion

A transient model for the potassium poisoning of a single channel of a monolith catalyst for selective catalytic reduction of NO by NH_3 has been derived. The model accounts for deposition and consumption of KCl particles on the external catalyst surface, the build-up of potassium, bound to Brønsted acid sites, throughout the catalyst wall, and the resulting loss in SCR activity. By fitting the value of the rate constant for reaction between KCl particles and surface -OH groups, k_{KCl}, and the surface diffusion coefficient of potassium, D_s, it was possible to obtain a solution that resembled the experimental deactivation profile of a $3\%V_2O_5$-$7WO_3/TiO_2$ monolith catalyst, exposed to a KCl aerosol at 350 °C for about 1000 hours. Furthermore, the simulated K/V molar ratios were in good agreement with those measured in the exposed catalyst, and the model was able to account for the slight difference measured in the top and bottom parts of the monolith.

In the model, the rate at which particle bound potassium reacts with Brønsted acid sites at the external surface scales with the initial amount of -OH sites. As a result, the potassium profiles across the catalyst wall become more flat as C^0_{OH} is decreased, and the difference between inlet and outlet profiles diminishes. The deactivation rate increases upon decreasing C^0_{OH}. At first, this seems to contradict previous observations, which indicate that increased Brønsted acidity facilitates the deactivation. However, the surface diffusivity of potassium is most likely a function of the abundance of Brønsted sites in the given catalyst. Such a relation is not considered in this model. As expected, the deactivation rate increases with increasing values of k_{KCl}, while D_s directly affects both the shape of the deactivation profile as well as the K/V profiles. If the surface diffusion coefficient is low, an initial high deactivation rate is observed due to accumulation of potassium poisoned sites in the outer layer of the catalyst wall. Further deactivation is, however, limited by the slow diffusion of potassium. Increasingly more flat K/V profiles are obtained as the surface diffusion coefficient is increased. Simulations show that the deposition rate, and hence the deactivation rate, decreases if the particle size of the incoming, potassium rich, aerosol is increased. This might be practically achievable by addition of seed particles to the hot flue gas.

Due to the limited experimental foundation, the values of the fitted parameters are specific to the given catalyst and operating conditions, and may not apply for other temperatures and catalyst

compositions. In addition, a more detailed description of the available surface area as a function of particle size, including the possibility of particle agglomeration, may improve the accuracy of the model.

8. Final conclusion

The main objective of this Ph.D. project has been to conduct an in depth investigation of the deactivation mechanism of vanadia based SCR catalysts, when subjected to potassium rich aerosols, and more specifically to study the influence of catalyst composition, operating temperature and aerosol characteristics on the deactivation rate.

This objective has been approached by exposing plate-type V_2O_5-(WO_3)/TiO_2 SCR catalysts to aerosols of KCl and K_2SO_4 in a bench-scale reactor. All samples exposed for more than 240 hours showed significant deactivation, when tested for remaining activity in a laboratory-scale reactor. Catalysts exposed at a reduced temperature of 150 °C showed higher remaining activity compared to samples exposed at 300-350 °C. The majority of the catalysts exposed to KCl aerosols at high temperatures had lost more than 90 % of their initial activity. No effect on the catalyst deactivation was observed by increasing the particle size of the KCl aerosol. This could, however, be due a sustained presence of ultrafine KCl particles in the flue gas. Hence, it was not possible to obtain a clear understanding of the influence of the aerosol particle size distribution on the deactivation rate through the bench-scale experiments. Catalysts exposed to K_2SO_4 aerosols proved to deactivate considerably less than those exposed to KCl. This indicates that potassium bound in K_2SO_4 deposits, on the catalyst surface, is less mobile than that bound KCl. However, the K_2SO_4 aerosols obtained in the setup were generally shifted towards larger particles compared to the KCl aerosols. Hence, an effect of particle size on the catalyst deactivation cannot be excluded. The relative activity of the exposed catalyst plates indicated that WO_3 promoted samples, which in general showed higher NH_3 adsorption capacities, had lost a larger fraction of their initial activity compared to unpromoted ones. Furthermore, the relative activity of unpromoted samples generally decreased with increasing vanadia loading (and increasing NH_3 adsorption capacity), while no correlation between vanadia content and remaining activity could be found for WO_3 containing samples. These results imply that increased Brønsted acidity facilitates the potassium transport in the catalysts.

The mobility of potassium in SCR catalysts has further been studied using a newly conceived experimental protocol which involves so-called two-layer pellets. These investigations clearly showed that potassium bound in KCl reacts faster with the catalyst surface, compared to that bound in K_2SO_4, and thereby penetrates the SCR catalyst more rapidly by a fast surface diffusion mechanism (which naturally is independent on the potassium salt). The faster reaction rate is further

signified by the fact that KCl impregnated two-layer pellets were chlorine free upon treatment at SCR conditions (350 °C, 6 vol.% O_2 and 3 vol.% H_2O in N_2), while sulfur stayed immobile in K_2SO_4 impregnated samples. Furthermore, only half of the sulfate bound potassium proved to be able to leave its solid matrix. As indicated by the bench-scale exposures of catalyst plates, the potassium mobility in SCR catalysts increased with the exposure temperature. Also as indicated by the bench-scale experiments, the presence of WO_3 in the two-layer pellets appeared to facilitate the potassium transport, independently on the vanadia content.

The results from the plate exposures and the two-layer pellet experiments support a deactivation mechanism in which particle bound potassium reacts with the Brønsted acid sites on the catalyst and subsequently penetrates the catalyst system by diffusion over these. The rate of reaction between salt bound potassium and the Brønsted acid sites is related to how strongly potassium is bound to its counter ion and increases with the operating temperature. Also the surface diffusivity of potassium is likely to increase at elevated temperatures; however, potassium has proved to diffuse at a significant rate already at room conditions.

Another objective of this Ph.D. study has been to suggest and test new alkali resistant catalyst formulations or coatings. By the use of three-layer pellets, magnesium oxide, sepiolite and Hollandite manganese oxide have been tested with respect to their ability to block the diffusion of potassium. In general, this approach served as a useful method for fast screening of potential coating materials. Pure MgO proved to be the most effective potassium barrier of the three tested candidates. No potassium was detected by SEM-WDS in a 300 μm thick MgO layer, upon exposure to SCR conditions for 7 days. Pure sepiolite was unable to delay the surface diffusion of potassium from the impregnated to the undoped layer; however, it may still act as a binder for e.g. an MgO based coating. Hollandite manganese oxide proved to reduce the diffusion rate of potassium across the three-layer pellets, however, is unfeasible as a coating material due to its subpar performance compared to MgO, and to its potentially expensive synthesis route.

Two coated half-length monoliths, and one uncoated reference, have been exposed to KCl aerosols at 350 °C in the bench-scale setup. The $3\%V_2O_5$-$7\%WO_3/TiO_2$ reference catalyst deactivated with a rate of 0.91 %/day during 960 hours of exposure, and SEM-EDS analysis showed complete potassium penetration and average K/V molar ratios of 0.38-0.51 inside the catalyst wall. A similar monolith coated with 8.06 wt.% MgO deactivated with a rate of 0.24 %/day, relative to the fresh activity of the uncoated reference, during 1100 hours of exposure. The initial observed activity of

this catalyst was only 58 % of that of the reference, likely due to increased transport limitations, as well as loss of vanadium and tungsten to the coating during its application. SEM-EDS analysis showed that potassium had penetrated the MgO coat, however, to a lower extent compared to the reference monolith. The SEM analysis also showed that the MgO coat was 200 μm thick, adhered weakly to the catalyst, and that the coating was fragile. Overall, the MgO coat proved to have protected the SCR catalyst against potassium poisoning to some degree. A catalyst coated with a 1:1 mixture of MgO and TiO_2 showed insufficient start activity (30 % of that of the reference) when tested in the bench-scale setup, likely due to a low porosity of the coat.

A single channel model describing the potassium poisoning of an SCR monolith catalyst has been derived. The model accounts for the deposition and reaction of KCl particles on the external catalyst surface, and the subsequent surface diffusion of potassium, over Brønsted acid sites, into the catalyst wall. By fitting the value of the rate constant for reaction between KCl particles and surface -OH groups and the surface diffusion coefficient of potassium, it was possible to obtain a solution that resembled the experimental deactivation profile of the KCl exposed reference catalyst. Simulations show that the particle deposition rate, and hence the deactivation rate, decreases if the particle size of the incoming, potassium rich, aerosol is increased.

Overall, the results from the work conducted in this Ph.D. project indicate that the life-time of SCR catalysts used in biomass fired power plants can be improved by ensuring a high conversion of KCl to K_2SO_4 aerosols, and by reducing the operating temperature. Furthermore, increasing the size of the potassium rich aerosol particles, preferably to above 200 nm, may reduce the particle deposition as well as the deactivation rate. This might be practically achievable by addition of seed particles to the hot flue gas. Applying an alkaline coat, such as MgO, to the SCR catalyst will protect it against potassium poisoning, and within a few thousand hours of operation it may retain a higher activity compared to an uncoated catalyst. However, more work is needed in order to develop a mechanically durable coating. As indicated by the plate exposure campaigns and the two-layer pellet experiments, increased Brønsted acidity seems to facilitate the potassium transport in the SCR catalysts. Reducing the amount of Brønsted acid sites, e.g. by lowering the WO_3 content, is however not immediately recommended as this will lower the initial activity of the catalyst and likely also the thermal stability.

9. Suggestions for further work

The results from the plate exposure campaigns as well as the two-layer experiments indicate that potassium bound in KCl more easily can react with Brønsted acid sites, on the catalyst surface, compared to that bound in K_2SO_4, hence causing a faster deactivation rate. It would be of value to verify this by conducting an exposure campaign, similar to the one with the reference monolith, but with injection of a 0.05 M K_2SO_4 solution instead of 0.1 M KCl (i.e. the same amount of potassium). Such an experiment would also provide addition data to the deactivation model, which could then be expanded to work for K_2SO_4 aerosols as well. Further exposure experiments, carried out at temperatures other than 350 °C (e.g. at 150 and 250 °C), may supply the information necessary for deducing the temperature dependencies of the potassium surface diffusion coefficient and the rate constant for the reaction between particle bound potassium and Brønsted acid sites, used in the model.

More work can be done regarding catalyst coatings. While MgO seems to be a good candidate, the results from the exposure experiments indicate the need of a binder material, in order to avoid loss of the coating during handling or operation of the catalyst. Such a binder material should, however, still ensure a sufficiently porous coating, in order to limit the transport restrictions. As the two coated catalysts, tested in this work, were supplied by Haldor Topsøe A/S, possible application methods were not studied. Here, however, there may be room for improvement. First of all, the MgO coat proved to be rather thick, i.e. about 200 µm. It should be possible to reduce the thickness to at least 100 µm, which would limit the transport restrictions caused by the coat. Also, some vanadium and tungsten species had diffused from the catalyst into the MgO layer, likely due to dissolution during the application of the coat. Hence, other solvents, or even dry coating methods, should be considered. If an alkaline oxide based coating is to be used, its SO_2 stability at SCR conditions should be tested.

The two-layer pellet experiments proved to be a useful method for studying the behavior of potassium in SCR catalysts under controlled conditions. The water content in the gas, which is passed over the pellets, may have an influence on the potassium mobility. Hence, it might be worthwhile to conduct a series of experiments in which the water concentration is varied.

10. References

[1] European Commission, The 2020 climate and energy package, http://ec.europa.eu /clima/policies/package (accessed March 30, 2015).

[2] Energistyrelsen, Dansk klima- og energipolitik, http://www.ens.dk/politik/dansk-klima-energipolitik (accessed March 30, 2015).

[3] H. Bosch and F. Janssen. Catalytic reduction of nitrogen oxides – A review on the fundamentals and technology. *Catalysis Today*, 2(4):369-532, 1988.

[4] P. Forzatti. Present status and perspectives in de-NO_x SCR catalysis. *Applied Catalysis A: General*, 222:221-236, 2001.

[5] B. Sander. Properties of Danish Biofuels and the Requirements for Power Production. *Biomass and Bioenergy*, 12(3):177-183, 1997.

[6] Y. Zheng, A.D. Jensen, and J.E. Johnsson. Laboratory Investigation of Selective Catalytic Reduction Catalysts: Deactivation by Potassium Compounds and Catalyst Regeneration. *Industrial & Engineering Chemistry Research*, 43:941-947, 2004.

[7] K.A. Christensen, and H. Livbjerg. A Field Study of Submicron Particles from the Combustion of Straw. *Aerosol Science and Technology*, 25:185-199, 1996.

[8] K.A. Christensen, M. Stenholm, and H. Livbjerg. The Formation of Submicron Aerosol Particles, HCl and SO_2 in Straw-Fired Boilers. *Journal of Aerosol Science*, 29(4):421-444, 1998.

[9] V.I. Pârvulescu, P. Grange, and B. Delmon. Catalytic removal of NO. *Catalysis Today*, 46:233-316, 1998.

[10] J. Svachula, L.J. Alemany, N. Ferlazzo, P. Forzatti, and E. Tronconi. Oxidation of SO_2 to SO_3 over Honeycomb DeNoxing Catalysts. *Industrial & Engineering Chemistry Research*, 32:826-834, 1993.

[11] J.P. Dunn, P.R. Koppula, H.G. Stenger, and I.E. Wachs. Oxidation of sulfur dioxide to sulfur trioxide over supported vanadia catalysts. *Applied Catalysis B: Environmental*, 19:103-177, 1998.

[12] J.P. Dunn, H.G. Stenger Jr., and I,E, Wachs. Oxidation of sulfur dioxide over supported vanadia catalysts: molecular structure – reactivity relationships and reaction kinetics. *Catalysis Today*, 51:301-318, 1999.

[13] E. Tronconi, A. Cavanna, C. Orsenigo, and P. Forzatti. Transient Kinetics of SO_2 Oxidation Over SCR-DeNO_x Monolith Catalysts. *Industrial & Engineering Chemistry Research*, 38:2593-2598, 1999.

[14] R.G. Herman, J.W. Sale, H.G. Stenger Jr., C.E. Lyman, J.E. Agogliatti, Y. Cai, B. Ramachandran, and S. Choi. Monitoring aging and deactivation of emission abatement catalysts for selective catalytic reduction of NO_x. *Topics in Catalysis*, 18(3-4):251-257, 2002.

[15] J.R. Thøgersen, T. Slabiak, and N. White. Ammonium bisulphate inhibition of SCR catalysts. Haldor Topsøe A/S, http://www.topsoe.com/sites/default/files /ammonium_bisulphate_ inhibition_of_scr_catalysts.ashx__0.pdf (accessed March 30, 2015).

[16] G. Busca, L. Lietti, G. Ramis, and F. Berti. Chemical and mechanistic aspects of the selective catalytic reduction of NO_x by ammonia over oxide catalysts: A review. *Applied Catalysis B: Environmental*, 18:1-36, 1998.

[17] L. Chen, J. Li, and M. Ge. The poisoning effect of alkali metals doping over nano V_2O_5-WO_3/TiO_2 catalysts on selective catalytic reduction of NOx by NH_3. *Chemical Engineering Journal*, 170:531-537, 2011.

[18] J.P. Chen and R.T. Yang. Role of WO_3 in mixed V_2O_5-WO_3/TiO_2 catalysts for selective catalytic reduction of nitric oxide with ammonia. *Applied Catalysis A: General*, 80:135-148, 1992.

[19] G. Ramis, G. Busca, C. Cristiani, L. Lietti, P. Forzatti, and F. Bregani. Characterization of Tungsta-Titania Catalysts. *Langmuir*, 8:1744-1749, 1992.

[20] L.J. Alemany, M.A. Larrubia, M.C. Jiménez, F. Delgado, and J.M. Blasco. WO_3/TiO_2 catalysts: Morphological and structural properties. Reaction Kinetics and Catalysis Letters, 60(1):41-47, 1997.

[21] L.J. Alemany, L. Lietti, N. Ferlazzo, P. Forsatti, G. Busca, E. Giamello, and F. Bregani. Reactivity and Physicochemical Characterisation of V_2O_5-WO_3/TiO_2 De-NO_x Catalysts. *Journal of Catalysis*, 155:117-130, 1995.

[22] L. Lietti, P. Forzatti, and F. Bregani. Steady-State and Transient Reactivity Study of TiO_2-Supported V_2O_5-WO_3 $DeNO_x$ Catalysts: Relevance of the Vanadium-Tungsten Interaction on the Catalytic Activity. *Industrial & Engineering Chemistry Research*, 35:3884-3892, 1996.

[23] P.G.W.A. Kompio, A. Brückner, F. Hipler, G. Auer, E. Löffler, and W. Grünert. A new view on the relations between tungsten and vanadium in V_2O_5-WO_3/TiO_2 catalysts for the selective reduction of NO with NH_3. *Journal of Catalysis*, 286:237-247, 2012.

[24] Y. Zheng, A.D. Jensen, and J.E. Johnsson. Deactivation of V_2O_5-WO_3-TiO_2 SCR catalyst at a biomass-fired combined heat and power plant. *Applied Catalysis B: Environmental*, 60:253-264, 2005.

[25] B. Grzybowska-Świerkosz. Vanadia-titania catalysts for oxidation of *o*-xylene and other hydrocarbons. *Applied Catalysis A: General*, 157:263-310, 1997.

[26] B.M. Weckhuysen and D.E. Keller. Chemistry, spectroscopy and the role of supported vanadium oxides in heterogeneous catalysis. *Catalysis Today*, 78:25-46, 2003.

[27] I.E. Wachs and B.M. Weckhuysen. Structure and reactivity of surface vanadium oxide species on oxide supports. *Applied Catalysis A: General*, 157:67-90, 1997.

[28] G.T. Went, L.-J. Leu, and A.T. Bell. Quantitative Structural Analysis of Dispersed Vanadia Species in TiO_2(Anatase)-Supported V_2O_5. *Journal of Catalysis*, 134:479-491, 1992.

[29] G.T. Went, L.-J. Leu, R.R. Rosin, and A.T. Bell. The Effects of Structure on the Catalytic Activity and Selectivity of V_2O_5/TiO_2 for the Reduction of NO by NH_3. *Journal of Catalysis*, 134:492-505, 1992.

[30] G. Busca, G. Centi, L. Marchetti, and F. Trifiro. Chemical and Spectroscopic Study of the Nature of a Vanadium Oxide Monolayer Supported on a High-Surface-Area TiO_2 Anatase. *Langmuir*, 2:568-577, 1986.

[31] G.C. Bond and S.F. Tahir. Vanadium oxide monolayer catalysts: Preparation, characterization and catalytic activity. *Applied Catalysis*, 71:1-31, 1991.

[32] G. Deo and I.E. Wachs. Reactivity of Supported Vanadium Oxide Catalysts: The Partial Oxidation of Methanol. *Journal of Catalysis*, 146:323-334, 1994.

[33] I. Nova, L. dall'Acqua, L. Lietti, E. Giamello, and P. Forzatti. Study of thermal deactivation of a de-NO_x commercial catalyst. *Applied Catalysis B: Environmental*, 35:31-42, 2001.

[34] L.J. Alemany, M.A. Bañares, M.A. Larrubia, M.C. Jiménez, F. Delgado, and J.M. Blasco. Vanadia-titania systems: Morphological and structural properties. *Materials Research Bulletin*, 31(5):513-520, 1996.

[35] G. Madia, M. Elsener, M. Koebel, F. Raimondi, and A. Wokaun. Thermal stability of vanadia-tungsta-titania catalysts in the SCR prosess. *Applied Catalysis B: Environmental*, 39:181-190, 2002.

[36] N.-Y. Topsøe. Mechanism of the Selective Catalytic Reduction of Nitric Oxide by Ammonia Elucidated by in Situ On-Line Fourier Transform Infrared Spectroscopy. *Science*, 265(5176):1217-1219, 1994.

[37] N.-Y. Topsøe, J.A. Dumesic, and H. Topsøe. Vanadia/Titania Catalysts for Selective Catalytic Reduction of Nitric Oxide by Ammonia: II. Studies of Active Sites and Formulation of Catalytic Cycles. *Journal of Catalysis*, 151:241-252, 1995.

[38] J.A. Dumesic, N.-Y. Topsøe, H. Topsøe, Y. Chen, and T. Slabiak. Kinetics of Selective Catalytic Reduction of Nitric Oxide by Ammonia over Vanadia/Titania. *Journal of Catalysis*, 163:409-417, 1996.

[39] J.A. Moulijn, A.E. van Diepen, and F. Kapteijn. Catalyst deactivation: is it predictable? What to do? *Applied Catalysis A: General*, 212:3-16, 2001.

[40] P. Forzatti and L. Lietti. Catalyst deactivation. *Catalysis Today*, 52:165-181, 1999.

[41] C.H. Bartholomew. Mechanisms of catalyst deactivation. *Applied Catalysis A: General*, 212:17-60, 2001.

[42] J.P. Chen, M.A. Buzanowski, R.T. Yang, and J.E. Cichanowicz. Deactivation of the Vanadia Catalyst in the Selective Catalytic Reduction Process. *Journal of the Air & Waste Management Association*, 40:1403-1409, 1990.

[43] H. Kamata, K. Takahashi, and C.U.I. Odenbrand. Surface acid property and its relation to SCR activity of phosphorus added to commercial $V_2O_5(WO_3)/TiO_2$ catalyst. *Catalysis Letters*, 53:65-71, 1998.

[44] D. Nicosia, M. Elsener, O. Kröcher, and P. Jansohn. Basic investigation of the chemical deactivation of V_2O_5/WO_3-TiO_2 SCR catalysts by potassium, calcium, and phosphate. *Topics in Catalysis*, 42-43: 333-336, 2007.

[45] O. Kröcher and M. Elsener. Chemical deactivation of V_2O_5/WO_3-TiO_2 SCR catalysts by additives and impurities from fuels, lubrication oils, and urea solution: I. Catalytic studies. *Applied Catalysis B: Environmental*, 75:215-227, 2008.

[46] F. Castellino, S.B. Rasmussen, A.D. Jensen, J.E. Johnsson, and R. Fehrmann. Deactivation of vanadia-based commercial SCR catalysts by polyphosphoric acids. *Applied Catalysis B: Environmental*, 83:110-122, 2008.

[47] M. Klimczak, P. Kern, T. Heinzelmann, M. Lucas, and P. Claus. High-throughput study of the effects of inorganic additives and poisons on NH_3-SCR catalysts–Part I: V_2O_5-WO_3/TiO_2 catalysts. *Applied Catalysis B: Environmental*, 95:39-47, 2010.

[48] M. Gadgil. Deactivation of Selective Catalytic Reduction (SCR) Catalyst by Phosphorus: Proposed Mechanism and Solution. Presented at The International Pittsburgh Coal Conference, Pittsburgh, Pennsylvania, September 12-15 2011.

[49] J. Beck, J. Brandenstein, S. Unterberger, and K.R.G. Hein. Effects of sewage sludge and meat and bone meal Co-combustion on SCR catalysts. *Applied Catalysis B: Environmental*, 49:15-25, 2004.

[50] J. Beck, R. Müller, J. Brandenstein, B. Matscheko, J. Matschke, S. Unterberger, and K.R.G. Hein. The behaviour of phosphorus in flue gases from coal and secondary fuel co-combustion. *Fuel*, 84:1911-1919, 2005.

[51] R. Khodayari and C.U.I. Odenbrand. Deactivating Effects of Lead on the Selective Catalytic Reduction of Nitric Oxide with Ammonia over a $V_2O_5/WO_3/TiO_2$ Catalyst for Waste Incineration Applications. *Industrial & Engineering Chemistry Research*, 37:1196-1202, 1998.

[52] R. Khodayari. Selective Catalytic Reduction of NO_x: Deactivation and Regeneration Studies and Kinetic Modelling of Deactivation. PhD Thesis, Department of Chemical Engineering II, Lund University, Sweden, 2001 (ISBN: 917874122X).

[53] Y. Jiang, X. Gao, Y. Zhang, W. Wu, H. Song, Z. Luo, and K. Cen. Effects of $PbCl_2$ on selective catalytic reduction of NO with NH_3 over vanadia-based catalysts. *Journal of Hazardous Materials*, 274:270-278, 2014.

[54] F. Moradi, J. Brandin, M. Sohrabi, M. Faghihi, and M. Sanati. Deactivation of oxidation and SCR catalysts used in flue gas cleaning by exposure to aerosols of high- and low melting point salts, potassium salts and zinc chloride. *Applied Catalysis B: Environmental*, 46:65-76, 2003.

[55] A.-C. Larsson, J. Einvall, A. Andersson, and M. Sanati. Targeting by Comparison with Laboratory Experiments the SCR Catalyst Deactivation Process by Potassium and Zinc Salts in a Large-Scale Biomass Combustion Boiler. *Energy & Fuels*, 20:1398-1405, 2006.

[56] A.-C. Larsson, J. Einvall, and M. Sanati. Deactivation of SCR Catalysts by Exposure to Aerosol Particles of Potassium and Zinc Salts. *Aerosol Science and Technology*, 41:369-379, 2007.

[57] E. Hums and H.E. Göbel. Effects of As_2O_3 on the Phase Composition of V_2O_5-MoO_3-TiO_2 (Anatase) $DeNO_x$ Catalysts. *Industrial & Engineering Chemistry Research*, 30:1814-1818, 1991.

[58] E. Hums. Mechanistic Effects of Arsenic Oxide on the Catalytic Components of $DeNO_x$ Catalysts. *Industrial & Engineering Chemistry Research*, 31:1030-1035, 1992.

[59] E. Hums and G.W. Spitznagel. Deactivation Behavior of SCR DeNOx Catalysts - Basis for the Development of a New Generation of Catalysts. Symposium on NO_x Reduction, 207th National Meeting, American Chemical Society, San Diego, California, March 13-18 1994.

[60] S. Pritchard, C. DiFrancesco, S. Kaneko, N. Kobayashi, K. Suyama, and K. Iida. Optimizing SCR Catalyst Design and Performance for Coal-Fired Boilers. Presented at EPA/EPRI 1995 Joint Symposium on Stationary Combustion NO_x Control, May 16-19 1995.

[61] F.C. Lange, H. Schmelz, and H. Knözinger. Infrared-spectroscopic investigations of selective catalytic reduction catalysts poisoned with arsenic oxide. *Applied Catalysis B: Environmental*, 8:245-265, 1996.

[62] E. Hums. Understanding of Deactivation Behavior of DeNOx Catalysts: A Key to Advanced Catalyst Applications. *Kinetics and Catalysis*, 39(5):603-606, 1998.

[63] J.E. Staudt, T. Engelmeyer, W.H. Weston, and R. Sigling. The Impact Of Arsenic On Coal Fired Power Plants Equipped With SCR. Presented at ICAT Forum 2002, Houston, Texas, February 12-13 2002.

[64] M. Ichiki. Poisoning kinetics by arsenic on the De-NOx catalyst. Proceeding of the International Conference on Power Engineering-03, Kobe, Japan, November 9-13 2003.

[65] C.L. Senior, D.O. Lignell, A.F. Sarofim, and A. Mehta. Modeling arsenic partitioning in coal-fired power plants. *Combustion and Flame*, 147:209-221, 2006.

[66] J.R. Jensen, T. Slabiak, and N. White. Arsenic resistant SCR catalysts. Haldor Topsøe A/S, March 2009, http://www.topsoe.com/sites/default/files/arsenic_resistant_scr_catalyst_march_09.ashx__0.pdf (accessed March 30, 2015).

[67] J.P. Chen and R.T. Yang. Mechanism of Poisoning of the V_2O_5/TiO_2 Catalyst for the Reduction of NO by NH_3. *Journal of Catalysis*, 125:411-420, 1990.

[68] F. Tang, B. Xu, H. Shi, J. Qiu, and Y. Fan. The poisoning effect of Na^+ and Ca^{2+} ions doped on the V_2O_5/TiO_2 catalysts for selective catalytic reduction of NO by NH_3. *Applied Catalysis B: Environmental*, 94:71-76, 2010.

[69] H. Kamata, K. Takahashi, and C.U.I. Odenbrand. The role of K_2O in the selective reduction of NO with NH_3 over a $V_2O_5(WO_3)/TiO_2$ commercial selective catalytic reduction catalyst. *Journal of Molecular Catalysis A: Chemical*, 139:189-198, 1999.

[70] L. Lisi, G. Lasorella, S. Malloggi, and G. Russo. Single and combined deactivating effect of alkali metals and HCl on commercial SCR catalysts. *Applied Catalysis B: Environmental*, 50:251-258, 2004.

[71] D. Nicosia, I. Czekaj, and O. Kröcher. Chemical deactivation of V_2O_5/WO_3-TiO_2 SCR catalysts by additives and impurities from fuels, lubrication oils and urea solution: Part II. Characterization study of the effect of alkali and alkaline earth metals. *Applied Catalysis B: Environmental*, 77:228-236, 2008.

[72] Y. Zheng, A.D. Jensen, J.E. Johnsson, and J.R. Thøgersen. Deactivation of V_2O_5-WO_3-TiO_2 SCR catalyst at biomass fired power plants: Elucidation of mechanisms by lab- and pilot-scale experiments. *Applied Catalysis B: Environmental*, 83:186-194, 2008

[73] L. Lietti, P. Forzatti, G. Ramis, G. Busca, and F. Bregani. Potassium doping of vanadia/titania de-NO_xing catalysts: Surface characterisation and reactivity study. *Applied Catalysis B: Enviromental*, 3:13-35, 1993.

[74] X. Du, X. Gao, K. Qiu, Z. Luo, and K. Cen. The Reaction of Poisonous Alkali oxides with Vanadia SCR Catalyst and the Afterward influence: A DFT and Experimental Study. *The Journal of Physical Chemistry C*, 119:1905-1912, 2015.

[75] H. Si-Ahmed, M. Calatayud, C. Minot, E. Lozano Diz, A.E. Lewandowska, and M.A. Bañares. Combining theoretical description with experimental *in situ* studies on the effect of potassium on the structure and reactivity of titania-supported vanadium oxide catalyst. *Catalysis Today*, 126:96-102, 2007.

[76] A.E. Lewandowska, M. Calatayud, E. Lozano-Diz, C. Minot, and M.A. Bañares. Combining theoretical description with experimental *in situ* studies on the effect of alkali additives on the structure and reactivity of vanadium oxide supported catalysts. *Catalysis Today*, 139:209-213, 2008.

[77] X. Wu, W. Yu, Z. Si, and D. Weng. Chemical deactivation of V_2O_5-WO_3/TiO_2 SCR catalysts by combined effect of potassium and chloride. Frontiers of Environmental Science & Engineering, 7(3):420-427, 2013.

[78] J.H. Zeuthen, P.A. Jensen, J.P. Jensen, and H. Livbjerg. Aerosol Formation during the Combustion of Straw with Addition of Sorbents. *Energy & Fuels*, 21:699-709, 2007.

[79] H. Wu, P. Glarborg, F.J. Frandsen, K. Dam-Johansen, and P.A. Jensen. Dust-Firing of Straw and Additives: Ash Chemistry and Deposition Behavior. Energy & Fuels, 25:2862-2873, 2011.

[80] D.A. Bulushev, F. Rainone, L. Kiwi-Minsker, and A. Renken. Influence of Potassium Doping on the Formation of Vanadia Species in V/Ti Oxide Catalysts. *Langmuir*, 17:5276-5282, 2001.

[81] F. Gao, X. Gao, Y. Fu, Y. Zhang, Z. Luo, M. Ni, and K. Cen. Experimental study on combined deactivating effect of K and Ca on SCR catalysts. Proceedings of the 2011 International Conference on Electric Information and Control Engineering, Wuhan, China, April 15-17 2011.

[82] P. Kern, M. Klimczak, M. Lucas, A. Döring, and P. Claus. Entwicklung einer Technologieplattform zur Untersuchung der chemischen Vergiftung von NH_3-SCR- und NO-Oxidationskatalysatoren mit kombinatorischen und rationalen Mitteln. *Chemie Ingenieur Technik*, 81(3):289-296, 2009.

[83] P. Kern, M. Klimczak, T. Heinzelmann, M. Lucas, and P. Claus. High-throughput study of the effects of inorganic additives and poisons on NH_3-SCR catalysts. Part II: Fe-zeolite catalysts. *Applied Catalysis B: Environmental*, 95:48-56, 2010.

[84] S.S.R. Putluru, A.D. Jensen, A. Riisager, and R. Fehrmann. Alkali Resistant Fe-Zeolite Catalysts for SCR of NO with NH_3 in Flue Gases. *Topics in Catalysis*, 54:1286-1292, 2011.

[85] S.S.R. Putluru, A. Riisager, and R. Fehrmann. Alkali resistant Cu/zeolite deNO_x catalysts for flue gas cleaning in biomass fired applications. *Applied Catalysis B: Environmental*, 101:183-188, 2011.

[86] S.S.R. Putluru, A. Riisager, and R. Fehrmann. Vanadia supported on zeolites for SCR of NO by ammonia. *Applied Catalysis B: Environmental*, 97:333-339, 2010.

[87] A.L. Kustov, M.Y. Kustova, R. Fehrmann, and P. Simonsen. Vanadia on sulphated-ZrO_2, a promising catalyst for NO abatement with ammonia in alkali containing flue gases. *Applied Catalysis B: Environmental*, 58:97-104, 2005.

[88] J. Due-Hansen, S. Boghosian, A. Kustov, P. Fristrup, G. Tsilomelekis, K. Ståhl, C.H. Christensen, and R. Fehrmann. Vanadia-based SCR catalysts supported on tungstated and sulfated zirconia: Influence of doping with potassium. *Journal of Catalysis*, 251:459-473, 2007.

[89] S.S.R. Putluru, A.D. Jensen, A. Riisager, and R. Fehrmann. Heteropoly acid promoted V_2O_5/TiO_2 catalysts for NO abatement with ammonia in alkali containing flue gases. *Catalysis Science & Technology*, 1:631-637, 2011.

[90] Z. Huang, X. Gu, W. Wen, P. Hu, M. Makkee, H. Lin, F. Kapteijn, and X. Tang. A "Smart" Hollandite $DeNO_x$ Catalyst: Self-Protection against Alkali Poisoning. *Angewandte Chemie International Edition*, 52:660-664, 2013.

[91] A.-C. Larsson, J. Einvall, A. Andersson, and M. Sanati. Physical and chemical characterisation of potassium deactivation of a SCR catalyst for biomass combustion. Topics in Catalysis, 45(1-4):149-152, 2007.

[92] F. Castellino, A.D. Jensen, J.E. Johnsson, and R. Fehrmann. Influence of reaction products of K-getter fuel additives on commercial vanadia-based SCR catalyst. Part I. Potassium phosphate. *Applied Catalysis B: Environmental*, 86:196-205, 2009.

[93] F. Castellino, A.D. Jensen, J.E. Johnsson, and R. Fehrmann. Influence of reaction products of K-getter fuel additives on commercial vanadia-based SCR catalysts. Part II. Simultaneous addition of KCl, $Ca(OH)_2$, H_3PO_4 and H_2SO_4 in a hot flue gas at a SCR pilot-scale setup. *Applied Catalysis B: Environmental*, 86:206-215, 2009.

[94] S.S.R. Putluru and A.D. Jensen. Alternative alkali resistant $deNO_x$ technologies. Appendix-I. PSO Project 7318 2007-2010, Department of Chemical and Biochemical Engineering, Technical University of Denmark, 2011.

[95] Å. Kling, C. Andersson, Å. Myringer, D. Eskilsson, and S.G. Järås. Alkali deactivation of high-dust SCR catalysts used for NO_x reduction exposed to flue gas from 100 MW-scale biofuel and peat fired boilers: Influence of flue gas composition. *Applied Catalysis B: Environmental*, 69:240-251, 2007.

[96] W. Lin, A.D. Jensen, and J. Bjerkvig. Long Term Deactivation Test of High Dust SCR Catalysts by Straw Co-firing. Final report of CHEC part of PSO-project 5296, 2009.

[97] D. Courcot, A. Ponchel, B. Grzybowska, Y. Barbaux, M. Rigole, M. Guelton, and J.P. Bonnelle. Effect of the sequence of potassium introduction to V_2O_5/TiO_2 catalysts on their

physicochemical properties and catalytic performance in oxidative dehydrogeneation of propane. *Catalysis Today*, 33:109-118, 1997.

[98] C. Martín, V. Rives, and A.R. González-Elipe. Effect of Sodium on the Reducibility of V(V) Ions during Propene Adsorption on V_2O_5/TiO_2 Catalysts. *Journal of Catalysis*, 114:473-477, 1988.

[99] R.Q. Long and R.T. Yang. Superior Fe-ZSM-5 Catalyst for Selective Catalytic Reduction of Nitric Oxide by Ammonia. *Journal of the American Chemical Society*, 121:5595-5596, 1999.

[100] R.Q. Long and R.T. Yang. Catalytic Performance of Fe-ZSM-5 Catalysts for Selective Catalytic Reduction of Nitric Oxide by Ammonia. *Journal of Catalysis*, 188:332-339, 1999.

[101] S. Brandenberger, O. Kröcher, A. Tissler, and R. Althoff. The State of the Art in Selective Catalytic Reduction of NO_x by Ammonia Using Metal-Exchanged Zeolite Catalysts. *Catalysis Reviews*, 50:492-531, 2008.

[102] S.S.R. Putluru, S.B. Kristensen, J. Due-Hansen, A. Riisager, and R. Fehrmann. Alternative alkali resistant deNO_x catalysts. *Catalysis Today*, 184:192-196, 2012.

[103] S.S.R. Putluru, A.D. Jensen, A. Riisager, and R. Fehrmann. Alkali resistivity of Cu based selective catalytic reduction catalysts: Potassium chloride aerosol exposure and activity measurements. *Catalysis Communications*, 18:41-46, 2012.

[104] A.L. Kustov, S.B. Rasmussen, R. Fehrmann, and P. Simonsen. Activity and deactivation of sulphated TiO_2- and ZrO_2-based V, Cu and Fe oxide catalysts for NO abatement in alkali containing flue gases. *Applied Catalysis B: Environmental*, 76:9-14, 2007.

[105] R. Khodayari and C.U.I. Odenbrand. Regeneration of commercial TiO_2-V_2O_5-WO_3 SCR catalysts used in bio fuel plants. *Applied Catalysis B: Environmental*, 30:87-99, 2001.

[106] S.S.R. Putluru, S. Mossin, A. Riisager, and R. Fehrmann. Heteropoly acid promoted Cu and Fe catalysts for the selective catalytic reduction of NO with ammonia. *Catalysis Today*, 176:292-297, 2011.

[107] S.B. Kristensen, A.J. Kunov-Kruse, A. Riisager, and S. B. Rasmussen. High performance vanadia-anatase nanoparticle catalysts for the Selective Catalytic Reduction of NO by ammonia. *Journal of Catalysis*, 284:60-67, 2011.

[108] S.B. Kristensen. deNOx catalysts for biomass combustion. PhD Thesis, Department of Chemistry, Technical University of Denmark, Denmark, 2013.

[109] A.D. Jensen, F. Castellino, P.D. Rams, J.B. Pedersen, and S.S.R. Putluru. Deactivation-resistant catalyst for selective catalytic reduction of NO_x. U.S. Patent Application 20120315206. December 13, 2012.

[110] G. Ramis, G. Busca, F. Bregani, and P. Forzatti. Fourier Transform-Infrared Study of the Adsorption and Coadsorption of Nitric Oxide, Nitrogen Dioxide and Ammonia on Vanadia-Titania and Mechanism of Selective Catalytic Reduction. *Applied Catalysis*, 64:259-278, 1990.

[111] E. Tronconi, P. Forzatti, J.P. Gomez Martin, and S. Malloggi. Selective Catalytic Removal of NO_x: A Mathematical Model for Design of Catalyst and Reactor. *Chemical Engineering Science*, 47(9-11):2401-2406, 1992.

[112] M. Koebel, and M. Elsener. Selective catalytic reduction of NO over commercial $DeNO_x$-catalysts: experimental determination of kinetic and thermodynamic parameters. *Chemical Engineering Science*, 53(4):657-669, 1998.

[113] G. Tartaglione, D. Tabuani, and G. Camino. Thermal and morphological characterisation of organically modified sepiolite. *Microporous and Mesoporous Materials*, 107:161-168, 2008.

[114] R.L. Frost, J. Kristóf, and E. Horváth. Controlled rate thermal analysis of sepiolite. *Journal of Thermal Analysis and Calorimetry*, 98:423-428, 2009.

[115] P. Hu, Z. Huang, W. Hua, X. Gu, and X. Tang. Effect of H_2O on catalytic performance of manganese oxides in NO reduction by NH_3. *Applied Catalysis A: General*, 437-438:139-148, 2012.

[116] L.J. Alemany, F. Berti, G. Busca, G. Ramis, D. Robba, G.P. Toledo, and M. Trombella. Characterization and composition of commercial V_2O_5-WO_3-TiO_2 SCR catalysts. *Applied Catalysis B: Environmental*, 10:299-311, 1996.

[117] M.D. Amiridis, R.V. Duevel, and I.E. Wachs. The effect of metal oxide additives on the activity of V_2O_5/TiO_2 catalysts for the selective catalytic reduction of nitric oxide by ammonia. Applied Catalysis B: Environmental, 20:111-122, 1999.

[118] R. Khodayari, C. Andersson, C.U.I. Odenbrand, and L.H. Andersson. Deactivation and Regeneration of SCR Catalysts used in Bio Fuel Power Plants. Proceedings of the 5th European Conference on Industrial Furnace and Boilers, volume II, Espinho-Porto, Portugal, April 11-14, 2000.

[119] L. Wang, J.E. Hustad, Ø.Skreiberg, G. Skjevrak, and M. Grønli. A critical review on additives to reduce ash related operation problems in biomass combustion applications. *Energy Procedia*, 20:20-29, 2012.

[120] K.M. Eriksen, R. Fehrmann, G. Hatem, M. Gaune-Escard, O.B. Lapina, and V.M. Mastikhin. Conductivity, NMR, Thermal Measurements, and Phase Diagram of the $K_2S_2O_7$-$KHSO_4$ System. *The Journal of Physical Chemistry*, 100:10771-10778, 1996.

[121] C.B. Knudsen, A.G. Kalampounias, R. Fehrmann, and S. Boghosian. Thermal Dissociation of Molten $KHSO_4$: Temperature Dependence of Raman Spectra and Thermodynamics. *The Journal of Physical Chemistry B*, 112:11996-12000, 2008.

[122] K. Matsunaga, S. Li, C. Iwamoto, T. Yamamoto, and Y. Ikuhara. *In situ* observation of crack propagation in magnesium oxide ceramics. *Nanotechnology*, 15:S376-S381, 2004.

[123] W.M. Haynes, ed. CRC Handbook of Chemistry and Physics. 95nd Edition (Internet Version 2013), CRC Press/Taylor and Francis, 2015.

[124] M.L. Heiredal, A.D. Jensen, J.R. Thøgersen, F.J. Frandsen, and J.-U. Friemann. Pilot-Scale Investigation and CFD Modeling of Particle Deposition in Low-Dust Monolithic SCR DeNOx Catalysts. *AIChE Journal*, 59(6):1919:1933, 2013.

[125] R. Khodayari, and C.U.I. Odenbrand. Selective catalytic reduction of NO_x: a mathematical model for poison accumulation and conversion performance. *Chemical Engineering Science*, 54:1775-1785, 1999.

[126] B.H. Zimm, and J.E. Mayer. Vapor Pressures, Heats of Vaporization, and Entropies of Some Alkali Halides. *The Journal of Chemical Physics*, 12(9):362-369, 1944.

[127] J.W. Beeckman, and L.L. Hegedus. Design of Monolith Catalysts for Power Plant NO_x Emission Control. *Industrial & Engineering Chemistry Research*, 30:969-978, 1991.

[128] J.R. Jensen, L.B. Nielsen, C. Schultz-Møller, S. Wedel, and H. Livbjerg. The Nucleation of Aerosols in Flue Gases with a High Content of Alkali—A laboratory Study. *Aerosol Science and Technology*, 33:490-509, 2000.

[129] R.B. Bird, W.E. Stewart, and E.N. Lightfoot. Transport Phenomena. 2nd Edition, Wiley, 2007 (ISBN: 0470115394).

[130] B.E. Poling, J.M. Prausnitz, and J.P. O'Connell. The Properties of Gases & Liquids. 5th Edition, McGraw-Hill, 2001 (ISBN: 0070116822).

[131] U. Grigull, and H. Tratz. Thermischer Einlauf in Ausgebildeter Laminarer Rohrströmung. *International Journal of Heat and Mass Transfer*, 8:669-678, 1965.

[132] R.K. Shah, and A.L. London. Laminar Flow Forced Convection in Ducts. Academic Press, 1978 (ISBN: 0120200511).

[133] E. Tronconi, and P. Forzatti. Adequacy of Lumped Parameter Models for SCR Reactors with Monolith Structure. *AIChE Journal*, 38(2):201-210, 1992.

[134] R. Aris. The mathematical theory of diffusion and reaction in permeable catalysts, Volume 1: The theory of steady state. Oxford University Press, 1975 (ISBN: 0195198298).

[135] P.A. Baron, and K. Willeke, eds. Aerosol Measurement – Principles, Techniques and Applications. 2nd Edition, Wiley, 2001 (ISBN: 0471356360).

[136] J.B. Lefers, P. Lodder, and G.D. Enoch. Modelling of Selective Catalytic Denox Reactors – Strategy for Replacing Deactivated Catalyst Elements. *Chemical Engineering & Technology*, 14:192:200, 1991.

[137] MATLAB, Release 2013a, The MathWorks, Inc., Natick, Massachusetts, United States, 2013.

Appendix A

Potassium poisoning of vanadia based SCR catalysts: Influence of catalyst composition and potassium mobility

Brian K. Olsen,[†] Frauke Kügler,[†,‡] Francesco Castellino,[§] and Anker D. Jensen[,†]*

[†]Department of Chemical and Biochemical Engineering, Technical University of Denmark, Building 229, 2800 Kgs. Lyngby, Denmark

[§]Haldor Topsøe A/S, Nymøllevej 55, 2800 Kgs. Lyngby, Denmark

Abstract: The deactivation of V_2O_5-(WO_3)/TiO_2 catalysts for selective catalytic reduction (SCR) of NO_x upon exposure to aerosols of KCl or K_2SO_4, at different temperatures, has been studied. All samples exposed for more than 240 hours lost a substantial fraction of their initial activity although lower exposure temperatures slow down the deactivation. K_2SO_4 causes a lower rate of deactivation compared to KCl. This may be related to a faster transfer of potassium from the solid KCl matrix to the catalyst, however, it cannot be ruled out to also be caused by a significantly larger particle size of the K_2SO_4 aerosol (mass based distribution mode: 1.3 μm) compared to that of the KCl aerosol (mass based distribution mode: 0.12 μm). The relative activities of exposed catalysts indicate that WO_3 promotion of SCR catalyst accelerates the deactivation, likely due to the enhanced Brønsted acidity which appears to promote the transport of potassium. Using a newly developed experimental protocol consisting of two-layer pellets of SCR catalysts, where one side is impregnated with KCl or K_2SO_4, the potassium transport in such systems, which is assumed to take place through reaction and diffusion over acid sites, was investigated. SEM-WDS measurements on pellets heat treated at

350 °C show that potassium bound in KCl readily leaves its counter ion and thus moves faster into the catalyst compared to potassium from K_2SO_4, which is in agreement with results from the aerosol exposures.

1. Introduction

Selective catalytic reduction (SCR) of nitrogen oxides (NO_x) with ammonia (NH_3) is a well established method for controlling the NO_x emissions from stationary sources such as coal fired heat and power plants.[1,2] The most widely used catalysts for such applications consist of vanadia (V_2O_5) supported on titania (TiO_2), promoted with either tungsten oxide (WO_3) or molybdenum oxide (MoO_3), in the shape of honeycomb monoliths.[2] Topsøe and co-workers[3-5] proposed a mechanism for the SCR reaction over V_2O_5 based catalysts consisting of two catalytic cycles, involving Brønsted acid sites (V^{5+}-OH) and redox sites (V^{5+}=O).

In a time with great focus on decreasing the release of carbon dioxide (CO_2) to the atmosphere, firing (or co-firing) of biomass (straw, wood chips etc.) is being applied in order to reduce the net CO_2 emissions. Unfortunately, alkali and alkaline earth metals, which can be present in biomass in high concentrations[6], may act as poisons to the industrially applied SCR catalysts and can reduce their life-time dramatically, especially when the catalysts are used in high-dust configuration.[7] Potassium, released e.g. during firing of straw, may form submicron aerosols of potassium chloride (KCl) and/or potassium sulfate (K_2SO_4)[8,9] which can deposit on the external catalyst surface. Most likely through a surface diffusion mechanism, potassium subsequently diffuses into the catalyst wall[10-12]. It is believed that potassium, due to its alkaline nature, poisons the SCR catalyst by reacting with the acidic V^{5+}-OH sites.[7,11,13-17] Research has furthermore shown that the reducibility of V^{5+}=O species is inhibited upon alkali poisoning.[17-20] While the effect of potassium on commercial SCR catalysts is generally well understood, a more systematic study of the deactivation mechanism will provide useful information for development of new alkali resistant catalysts and/or

improved means of operation. To our knowledge, there are no systematic studies of the influence of catalyst composition on the rate of potassium uptake and associated deactivation. Furthermore, there are no systematic studies of the influence of the aerosol size distribution on the rate of deactivation. It is conceivable that the aerosol size distribution may significantly influence the rate of deactivation since: 1) The rate of deposition of aerosol particles increases with decreasing size due to their higher diffusion velocity and 2) The rate of potassium uptake is likely to depend on the volume (or mass) based contact area with the catalyst material which is smaller for larger particles (contact area/particle volume ~ $1/d_p$, with d_p being the aerosol particle diameter). Finally, the influence of catalyst operating temperature on the rate of deactivation has not previously been investigated in depth.

In this work, the deactivation by potassium poisoning of V_2O_5-(WO_3)/TiO_2 based catalyst plates, of various composition, have been studied. The plates have been exposed to KCl or K_2SO_4 aerosols of different particle size at various temperatures in a bench-scale setup, and tested for remaining activity in a lab-scale reactor. Furthermore, the mobility of potassium in SCR catalysts have been studied by a newly conceived experimental protocol in which pellets consisting of one undoped layer and one layer of potassium impregnated SCR catalyst are heat treated in a lab-scale oven, followed by measurement of the resulting potassium profiles across the pellet width using Scanning Electron Microscopy/Wavelength Dispersive X-ray Spectroscopy (SEM-WDS). These experiments provide detailed information on the rate of potassium diffusion in SCR catalysts.

2. Experimental section

2.1. Catalysts. Plate shaped catalysts supplied by Haldor Topsøe A/S were used in this study. The catalysts were based on V_2O_5, with approximate loadings of 1, 3 and 6 wt.%, on a fiber reinforced TiO_2 carrier. Some plates were promoted with about 7 wt.% WO_3. Upon delivery, the plates had dimensions (thickness x width x height) of 1 mm x 50 mm x 148-166 mm, from which pieces with

dimensions of 36 mm x 98 mm were cut from the individual plates and used for the bench-scale exposure campaigns.

2.2. Bench-scale aerosol exposure. The plates were exposed to aerosols of KCl or K_2SO_4 in a bench-scale reactor previously used for a similar study by Zheng et al.[11] The setup, illustrated in Figure 1, consists of a natural gas burner, a flue gas duct perpendicular to the burner outlet, a heat exchanger section where the reactor temperature can be controlled, and the reactor itself. The reactor can house a full-length (50 cm) SCR monolith or, as was the case in this study, a set of up to nine plate-type catalysts placed in a steel cassette in the top part of the reactor. A second heat exchanger cools the flue gas further before it is led to the stack.

A water cooled injector probe, equipped with a two-fluid nozzle, can be introduced into the flue gas duct at the end adjoining the burner outlet. At the opposite end of the duct, a bayonet heat exchanger can be inserted for further cooling. Aerosols of either KCl or K_2SO_4 were generated by pumping an aqueous solution of the respective salt (with a concentration of 0.1 M with respect to potassium ions) through the injector probe, at a rate of 420 mL/h, and injecting it into the hot flue gas by the aid of pressurized air through the two-fluid nozzle.

In addition to being heated by the flue gas, the SCR reactor was heated from the outside by an electrical heating cable and insulated by a mantle of mineral wool in order to minimize radial temperature gradients. The axial temperature gradient over the catalysts was always within 5 °C. In order to avoid build-up of particles on top of the catalyst cassette, a burst of pressurized air from a soot blower, located above the reactor, was released for approximately 1 second every 30 minutes. The total gas flow through the reactor was 35-45 Nm^3/h corresponding to a linear gas velocity of 1.7-2.2 Nm/s (0 °C, 1 atm, empty reactor). Six exposure campaigns have been conducted in this study. The campaigns differed by the injected salt solution, the SCR reactor temperature, the total

exposure time and the position of the injector nozzle leading to different temperatures for the aerosol particle formation. Up to nine catalyst plates were exposed in each campaign.

2.3. Aerosol measurement. The mass based particle size distribution was measured by a 10-stage Berner-type low pressure impactor (LPI, Hauke Ges.m.b.H. & Co.KG) with an aerodynamic diameter range of 0.03-12.7 μm. The gas was sampled above the reactor inlet through a straight cylindrical tube perpendicular to the main flow at a flow rate of 23.11 NL/min. In order to avoid water condensation, the sampling tube and the impactor were heated to 90 °C. The sampling time was 60 minutes. The particles were collected on aluminum foils coated with a thin film of Apiezon H vacuum grease. The grease was added by applying a thin layer of a dilute solution of the grease in toluene onto the foils. In order to remove the toluene, the foils were dried in an oven at 140 °C for several hours.

2.4. Activity measurement. The catalytic activities of the exposed samples, as well as unexposed counterparts, were measured in the laboratory at temperatures between 250 and 400 °C. The samples were crushed to a powder, diluted with sand and loaded into a quartz reactor between two layers of quartz wool. A typical reactor loading contained 50-100 mg catalyst. A total flow of about 2800 NmL/min was used during the measurements and the gas was composed of 500 ppmv NO, 600 ppmv NH_3, 5 vol.% O_2, about 1.4 vol.% H_2O and balance N_2. The H_2O content was obtained by saturating a stream of N_2 at room temperature by passing it through a bubble flask with water. The dry NO concentration at the reactor outlet was measured by a Rosemount NGA 2000 analyzer.

The NO reduction in the SCR reaction can be described by an Eley-Rideal rate expression where NH_3 adsorbs on the catalyst surface while NO reacts from the gas phase with the adsorbed species.[21-23] This mechanism leads to the following rate expression:

$$-r_{\mathrm{NO}}\left[\frac{\mathrm{kmol}}{\mathrm{kg{\cdot}s}}\right] = k_r C_{\mathrm{NO}} \frac{K_{\mathrm{NH_3}} C_{\mathrm{NH_3}}}{1+K_{\mathrm{NH_3}} C_{\mathrm{NH_3}}} \qquad (1)$$

Where k_r (m^3/kg/s) is the intrinsic rate constant, C_i (kmol/m^3) is the concentration of component i in the gas phase, while K_{NH_3} (m^3/kmol) is the NH_3 adsorption equilibrium constant. When NH_3 is in excess, equation 1 can be reduced to a pseudo first order expression with respect to NO:

$$-r_{NO} = k' C_{NO} \quad (2)$$

For a first order reaction with plug flow in a packed-bed reactor, the pseudo first order rate constant, k', can be calculated from equation 3:

$$k' \left[\frac{m^3}{kg \cdot s}\right] = -\frac{F_{gas}}{m_{cat}} \ln(1 - X_{NO}) \quad (3)$$

Where F_{gas} (m^3/s) is the gas flow rate at reactor conditions, m_{cat} (kg) is the catalyst mass and X_{NO} is the NO conversion. In the following the rate constant/catalytic activity of an exposed sample will be reported relative to that of the same catalyst in its fresh state, k'_0.

2.5. Ammonia chemisorption. In order to have a measure of the amount of active acid sites as a function of catalyst composition, NH_3 chemisorption measurements, similar to those carried out by Zheng et al.[7] have been performed on fresh catalysts. Pieces of 16 mm x 16 mm (corresponding to 0.62-0.68 g) were cut from the individual catalyst plates and placed in a quartz reactor which was heated to 250 °C. A gas mixture of 600 ppmv NH_3, 5 vol.% O_2 and about 1.5 vol.% H_2O in N_2 was passed over the catalyst for 30 minutes, which was found sufficient in order to saturate the active sites with NH_3. The NH_3 flow was then shut off and about 500 ppmv NO was added to the reactor shortly after. The amount of ammonia adsorbed on active sites could then directly be correlated to the amount of NO reduced by NH_3, assuming that the reaction followed the standard SCR reaction:

$$4NO + 4NH_3 + O_2 \rightarrow 4N_2 + 6H_2O \quad (4)$$

2.6. Two-layer pellet experiments. Pellets consisting of two layers of crushed plate catalyst in close contact have been produced. One layer was made from a fresh V_2O_5-(WO_3)/TiO_2 catalyst, while the other layer was made of the same catalyst doped with either KCl or K_2SO_4 to a potassium level of 0.8-1.6 wt.%. The potassium doping was achieved by wet impregnation of whole catalyst

plates which were subsequently dried at 80 ºC, crushed, and (in some cases) calcined at 400 °C overnight. Initially, one side of the pellet was made by partial compression of the powder in a pellet die. The powder of the other side was then added to the die and a final compression pressure of 60 bar was applied for 1 minute. Each pellet consisted of about 600 mg of pulverized catalyst (300 mg in each layer) and had a diameter of 13 mm and a thickness of 2.3 mm. A principle sketch of a two-layer pellet is shown in Figure 2. A pellet composed of a layer of pure KCl salt, crushed and sieved to a fraction below 250 µm, and a layer of fresh 3%V_2O_5-7%WO_3/TiO_2 catalyst powder was also produced. The pellets were exposed at 350 °C for up to 7 days in a horizontal lab-scale reactor, illustrated in Figure 3. During the exposure, a gas mixture of 6 vol.% O_2 and 3 vol.% H_2O in N_2 was passed through the reactor at a flow rate of about 1000 NmL/min. The H_2O content was achieved by saturating the O_2/N_2 mixture in a water filled bubble flask at room temperature.

2.7. Catalyst characterization. The distribution of potassium in exposed plates and pellets was measured at Haldor Topsøe A/S using SEM-EDS (Energy Dispersive X-ray Spectroscopy, Philips XL30 ESEM-FEG) and SEM-WDS (JEOL JXA-8530F HyperProbe) respectively. The samples (small plate bits or halved pellets) were embedded in epoxy and polished with SiC-paper without using water. In order to avoid charging in the microscope, the specimens were coated with a conductive layer of carbon.

3. Results and discussion

3.1. Characterization of aerosols in bench-scale reactor. To study the potassium poisoning as a function of aerosol size distribution, the position of the injector probe was varied between exposure campaigns. Two fixed positions were used – one close to the burner outlet, where the flue gas temperature was 1050-1100 °C, and one further downstream, where the temperature at the injection point was about 550 °C. Figure 4 shows the mass based size distribution, measured by the LPI during injection of KCl solution, at the two respective probe positions. Injecting the solution at the

burner outlet resulted in a size distribution with a peak at about 0.12 μm and a geometric mass mean diameter of around 0.15 μm. This mean diameter is only half of that observed by Zheng et al. during KCl injection in the same bench-scale setup at a similar temperature.[11] This may be related to a significant difference in the concentration of the injected KCl solution between the two LPI measurements (7.4 g/L vs. 37.3 g/L). In the present study, the salt concentration was kept relatively low in order to avoid clogging of the two-fluid nozzle. An aerodynamic (mass mean) diameter of 0.15 μm roughly corresponds to a Stokes diameter of 0.1 μm for a KCl aerosol. Christensen and co-workers[8,9] measured the size distributions of the aerosols in the flue gas from two different straw fired boilers. Through several measurements the authors obtained mass mean Stokes diameters of 0.2-0.6 μm which are 2-6 times larger than we observed in the bench-scale setup at the given probe position. While the particles obtained in the setup were rather small, particles in this size range are indeed present in the flue gas from full-scale biomass fired power plants.[12] Injecting the KCl solution further downstream the burner resulted in a particle size distribution peaking at 2.6 μm and with a geometric mass mean (aerodynamic) diameter of 1.1 μm, corresponding to a Stokes diameter of around 0.8 μm. At the lower flue gas temperature at this injection point, the aerosol particles will form by drying of the droplets created at the two-fluid nozzle rather than nucleation of particles from KCl molecules in the gas phase, resulting in particles which are somewhat larger than those observed by Christensen and co-workers[8,9] in full-scale plants.

When injecting a K_2SO_4 solution at the two different positions, no significant difference between the particle size distributions were obtained, as seen in Figure 5. Both distributions peak at 1.3 μm and the geometric mass mean (aerodynamic) diameters are 1.2 μm (burner outlet) 1.0 μm (downstream) respectively, corresponding to Stokes diameters of approximately 0.7 and 0.6 μm for K_2SO_4 aerosols. Due to the low vapor pressure of K_2SO_4, the aerosol was thus mostly formed by

drying of droplets at both probe positions. The distributions measured for the K_2SO_4 aerosols correlate well with the observations by Zheng et al.[11]

3.2. Ammonia chemisorption on fresh catalysts. The measured NH_3 chemisorption capacities of fresh SCR catalysts are listed in Table 1. Each value in the table is an average of at least two successive chemisorption measurements. The repeatability was in all cases excellent. For catalysts which have not been promoted with WO_3, the NH_3 chemisorption capacity, and thereby the amount of active acid sites, increases with the V_2O_5 content, however only slightly when going from 3 to 6 wt.% (from 66 to 70 μmol/g). For catalysts promoted with 7 wt.% WO_3 the NH_3 chemisorption capacity does not seem to depend on the V_2O_5 content. Both the promoted samples with 1 wt.% and the one 6 wt.% V_2O_5 showed an NH_3 chemisorption capacity of 81 μmol/g. This value was in both cases higher than that of the unpromoted counterpart of the respective sample. The NH_3 chemisorption capacity of the 3 wt.% V_2O_5 sample was 66 μmol/g both with and without WO_3 promotion. In general, the results indicate that WO_3 promotion increases the total amount of active acid sites and that this amount will be more or less constant, for the given WO_3 loading, regardless of the V_2O_5 content.

3.3. Deactivation of aerosol exposed plates. The absolute activity of fresh, unexposed catalysts, not reported here, was generally higher (by a factor of 1.2-12.6 at 350 °C) for WO_3 promoted samples as reported by other researchers.[24-26] Furthermore, the activity increased with the V_2O_5 content at temperatures below 400 °C.

Figure 6 shows the relative activities of $3\%V_2O_5$-$7\%WO_3/TiO_2$ catalysts exposed to KCl aerosols in four different campaigns, as a function of temperature. In three of the campaigns the two-fluid nozzle was positioned close to the burner outlet in order to ensure evaporation of the injected KCl solutions and the subsequent formation of submicron aerosol particles. In one of the campaigns the solution was injected into a colder flue gas (downstream burner position) in order to create larger

particles (> 1 μm). As discussed in the Introduction, we speculate larger particles to be less harmful to the SCR catalyst since the deposition rate is lower[11,12] and since the contact area between catalyst surface and potassium rich particles, deposited on the catalyst exterior, will be lower. As seen from the figure, the catalysts exposed in the four campaigns all show significant deactivation. The relative activity of the catalysts exposed at 350 °C for 600 or 300 hours is comparable and very low (< 5 %). The sample exposed at 150 °C for 300 hours shows higher relative activity compared to the above mentioned samples which indicates that the mobility of potassium is lower at reduced temperature. The relative activity of the given sample decreases with increasing temperature which may indicate a shift in the selectivity towards ammonia oxidation. Another explanation could be further deactivation of the sample as the temperature was increased during the activity test. This is, however, unlikely since activity at 350 °C was measured twice, first when stepwise increasing the temperature from 250 to 400 °C and once more after the 400 °C measurement had been carried out. As seen from Figure 6, the catalyst activity at 350 °C is unchanged after having been operated at 400 °C. The sample exposed to large aerosol particles at 300 °C for 300 hours is only slightly more active than the catalysts exposed to the aerosol of smaller particles. While the LPI measurements (Figure 4) showed a clear shift in the particle size distribution towards larger particles when injecting the KCl solution into a colder flue gas, the catalyst may still have been subjected to a significant amount of ultrafine particles due to deposits of KCl on the wall in the high temperature zone. While the major part of these deposits had been removed before the experiment with large particles was initiated, the presence of a minor residue cannot be excluded. A further investigation on this issue is needed.

Relative activities, measured at 350 °C, of exposed samples of other compositions are given in Table 2. These show similar deactivation trends as the 3%V_2O_5-7%WO_3/TiO_2 samples. The relative activity of the respective samples exposed at 350 °C for either 600 or 300 hours (entries 1a-3b and

7a-9b in Table 2) are generally low and counter intuitively tends to be lowest for samples exposed for 300 hours. This may, however, be accredited to measurement uncertainties which are enhanced when the activities of the exposed samples are very low.

For the 1%V_2O_5/TiO_2 sample exposed at 350 °C for 300 hours (7a), no SCR activity could be measured. The same catalyst exposed for 600 hours (1a) shows a remaining activity of 24 % at 350 °C. This may again be due to uncertainties caused by the fact that the initial activity of the given catalyst is fairly low. There may also be variations in the amount of aerosol each plate has been exposed to, depending on its position in the cassette.

As was the case for the 3%V_2O_5-7%WO_3/TiO_2 sample exposed to KCl at 150 °C for 300 hours (Figure 6, 5b in Table 2), the other samples exposed in this campaign (4a-5a, 6a and 6b in Table 2) also show higher remaining activities compared to those exposed at higher temperatures, again indicating reduced mobility of potassium at 150 °C compared to 350 °C. There does not seem to be a definite tendency between V_2O_5 content and the degree of deactivation. However, except for the aforementioned sample 7a, the 1 wt.% V_2O_5 catalysts without WO_3 (1a and 4a) retain a larger fraction of their initial activity compared to WO_3 free samples with higher V_2O_5 loadings. Furthermore, the relative activity of the unpromoted samples exposed at 350 °C for 600 hours (1-3a) decreases with increasing V_2O_5 content. The increased deactivation rate of the samples with high V_2O_5 loadings may be caused by an increased abundance of active Brønsted acid sites, as indicated by the NH_3 chemisorption data in Table 1, over which potassium may diffuse. A similar trend cannot be observed for WO_3 promoted samples, indicating that any effect on the deactivation rate by variations in the V_2O_5 loading is masked by the relatively high content of WO_3. This too correlates with the observations from the chemisorption measurements. In five out of the six cases where the activity of KCl exposed samples have been measured for catalysts both with and without WO_3, and where relative activity at 350 °C is above 10 % for at least one of the samples in the

0%WO_3/7%WO_3 pair (1ab, 2ab, 4ab-6ab and 8ab), the WO_3 promoted samples have lost a larger fraction of their initial activity compared to the unpromoted ones. This is e.g. the case for the 1%V_2O_5-(7%WO_3)/TiO_2 catalysts exposed at 150 °C for 300 hours where the unpromoted sample (4a) has retained 77 % of its initial activity, while the promoted sample (4b) only has retained 29 %. This indicates that the increased Brønsted acidity provided by the WO_3[27-30], apart from enhancing the initial activity, facilitates the transport of potassium in the catalysts, in a similar fashion as the Brønsted acid sites from V_2O_5, accelerating the poisoning.

The relative activities of 3%V_2O_5-7%WO_3/TiO_2 catalysts exposed to K_2SO_4 aerosols are shown in Figure 7. As seen from the figure, the sample exposed at 300 °C for 72 hours shows the highest relative activity of the four samples, only deviating from 100 % at temperatures above 300 °C. The sample exposed at 150 °C for the same amount of time has lost a slightly larger fraction of its initial activity. The fact that the sample exposed at the highest temperature has deactivated the least contradicts the observations from the KCl exposed catalysts. This might be due to an initial activity drop during the first hours of exposure which may vary from catalyst to catalyst, and which is less dependent on exposure conditions. Furthermore, small variations in the amount of aerosol the individual catalyst have been exposed to, e.g. due to being positioned differently in the cassette, may have a relatively large effect on the activity in the beginning of an exposure campaign. After 240 hours of exposure, both samples have deactivated further, and the sample exposed at 150 °C shows higher relative activity than that subjected to a K_2SO_4 aerosol at 300 °C, as expected. The K_2SO_4 exposed catalysts have deactivated significantly less compared to samples exposed to KCl at similar conditions, and the deactivation seem to be less temperature dependant. This indicates that K_2SO_4 is less poisonous compared to KCl, as previously reported by Zheng et al.[7,11] However, as explained earlier, the particles generated during K_2SO_4 injection tended to be larger than those

formed under KCl injection. Thus, an effect of particle size on the degree of deactivation cannot be excluded.

Table 2 lists relative activities (measured at 350 °C) of both unpromoted and WO_3 promoted $3\%V_2O_5/TiO_2$ catalysts exposed to K_2SO_4 aerosols (entries 12b-15b). As for the WO_3 promoted samples (Figure 7, 13b and 15b in Table 2) the unpromoted samples exposed for 240 hours show lower activity at the higher exposure temperature of 300 °C compared to exposure at 150 °C, once again indicating that the mobility of potassium is reduced at lower operating temperatures.

The significant deactivation observed for the catalyst plates, after only a few hundred hours of exposure in the bench-scale setup, is more severe than what is observed in full-scale biomass fired plants.[10,12,31] One explanation could be that the particles produced in the bench-scale setup, in several of the experiments, were smaller than those observed in full-scale plants, as previously discussed. Furthermore, the catalysts exposed in the bench-scale reactor were subjected to the pure potassium salts. In a full-scale plant, the deposited particles may contain other elements such as silicon and calcium.[8,12,31] The presence of compounds containing these elements may, to some extent, delay the potassium poisoning of the catalyst, either by dilution or by binding[32] a fraction of the potassium as inert species.

3.4. Potassium profiles in exposed plates. Figure 8 shows the SEM-EDS measured K/V molar ratios across the wall of three $3\%V_2O_5$-$7\%WO_3/TiO_2$ catalyst plates exposed to either KCl or K_2SO_4 aerosols at various temperatures and exposure times. As seen from the figure, the thickness of the individual plates varied between 900 to about 1400 μm. The plate exposed to KCl at 350 °C for 600 hours has the highest K/V ratio, throughout its thickness, of the three specimens. Very high K/V ratios can be observed near the edges of the samples which drop steeply to a near constant level inside the catalyst. The average K/V ratio calculated at the distance from 100 to 800 μm is 0.60. For a $3\%V_2O_5$-WO_3/TiO_2 catalyst impregnated with KCl to a K/V ratio of 0.4, Zheng et al.[7]

reported a remaining activity of about 40 % at 250 °C, while a K/V ratio of 0.7 reduced activity to around 10 % of its original value. Chen and co-workers[13,33] reported an activity loss of approximately 90 % at 300 °C for a 5%V_2O_5/TiO_2 catalyst impregnated with KNO_3 to a K/V ratio of about 0.5, while data from Kamata et al.[14] show a decrease in activity of nearly 70 % at 360 °C for a 1%V_2O_5-8%WO_3/TiO_2 catalyst containing 0.3 wt.% K_2O (from KNO_3 impregnation), corresponding to a K/V molar ratio of about 0.6. Larsson et al.[34] only observed small effects on the activity upon exposing 1%V_2O_5-WO_3/TiO_2 monoliths to aerosols of KCl and K_2SO_4. Even though the authors measured potassium concentrations above 1 wt.% (corresponding to K/V molar ratios above 2.3), at penetration depths of up to 650 µm, inside the catalyst walls, the KCl and K_2SO_4 aerosol exposed catalysts respectively retained 86 and 98 % of their initial activity at 350 °C. Conversely, Larsson et al.[34] observed relative activities of 50 and 56 % in similar catalysts, respectively impregnated with KCl and K_2SO_4, although lower potassium concentrations of about 0.2 wt.% (corresponding to K/V molar ratios of around 0.5) were detected in the catalysts. While the catalysts and/or test conditions in these studies are not entirely comparable to those in the present study, a K/V ratio of 0.60 does not seem to fully explain the complete deactivation observed for the given catalyst, as illustrated in Figure 6. The slight discrepancy between the activity and the K/V ratio of the catalyst may have arisen during the preparation of the activity measurement. When a section of the catalyst plate was crushed down, KCl particles deposited on the external surface of that section will be mixed into the catalyst powder possibly allowing for further potassium spreading and deactivation of the catalyst, either during the crushing procedure and/or during the actual activity measurement where the catalyst powder is heated. No further deactivation of the catalysts over time was, however, observed during the performed activity measurements.

The K/V ratios through the two remaining samples, *i.e.* the one exposed to KCl at 150 °C for 300 hours and the one exposed to K_2SO_4 at 300 °C for 240 hours, are low, around or below 0.1. Some

peaks in the K/V ratio can be observed inside the first of the two, however, these are artifacts from where the electron beam hits a ceramic fiber. The low K/V ratios in the two latter samples are in good agreement with their higher remaining activity compared to the first sample although they might not explain the observed deactivation of about 50 % at 350 °C. At lower temperatures, however, these specimens retained most of their initial activity as seen from Figure 6 and 7.

3.5. Potassium mobility in two-layer pellets. Figure 9 shows the potassium profiles in an unexposed two-layer pellet as well as in pellets exposed for 2 and 7 days, measured by SEM-WDS analysis. The impregnated layer in these pellets was made from a 3%V_2O_5-WO_3/TiO_2 catalyst doped with an aqueous KCl solution to a potassium level of about 1.6 wt.%, corresponding to a molar K/V ratio of 1.2 (nominal). In this particular case, the powdered catalyst had not been calcined subsequent to the KCl impregnation. Even for the unexposed pellet, potassium has, surprisingly, partly diffused into the undoped layer, as seen from the figure. The potassium concentration in the pellets exposed for 2 and 7 days are comparable. While the concentration drops through the impregnated layer, it seems to be leveling out at around 0.6 wt.% potassium in the undoped layer, corresponding to a K/V ratio of about 0.5. This K/V ratio is comparable to that found in the catalyst plate exposed to KCl aerosols at 350 °C for 600 hours (see Figure 8), which indicates that there exists a saturation level at which potassium does no longer diffuse into the SCR catalyst. This level would be expected to correspond to the concentration of Brønsted acid sites. Figure 10 shows the chlorine level in the same three pellets. As seen from the figure, a significant amount of chlorine is present in the impregnated layer of the unexposed pellet, which correlates well with the amount of potassium in the specimen. No chlorine is present in the undoped layer. The two exposed samples, however, are chlorine free all the way through, indicating that chlorine readily leaves the sample (likely as HCl) when exposed to a flow of N_2, O_2 and H_2O at 350 °C. This

implies that potassium has to coordinate to something else when left behind by its counter ion, most likely being the Brønsted acid sites on the catalyst.[11,13]

The above indicates that the potassium transport in SCR catalysts involves two steps: 1) reaction between salt bound potassium and catalyst surface, and 2) diffusion of potassium over the surface. The latter appears to be fast, judging from the rather flat potassium profiles in the undoped layers of the exposed pellets in Figure 9. Before heat treatment of a pellet, potassium is present in the impregnated layer as salt particles, in intimate contact with the catalyst material, and possibly also as surface bound potassium. The latter may explain the movement of potassium into the undoped layer before heat treatment. For an aerosol exposed SCR catalyst, only the external surface will be in close contact with ultrafine potassium salt particles, and thus the potassium transport, into the catalyst, will be slower. Figure 11 shows the potassium profile in a two-layer pellet consisting of a layer of pure KCl (particles size < 250 μm) and a layer of 3%V_2O_5-7WO_3/TiO_2 catalyst, exposed for 7 days. As seen from the figure, no potassium has moved into the catalyst layer. This implies that the salt particles not only have to be in close contact with the catalyst, in order for potassium to leave the salt in reaction with the surface, the particles also need to be very small – most likely in the submicron range. A similar conclusion was obtained by Zheng et al.[11] They exposed catalyst plates with deposits of KCl particles (with a mean diameter of 350 μm) to 200 NmL/min of air with about 3 vol.% H_2O and 1000 ppm SO_2 at 350 °C. After exposure for nearly 2400 hours, the catalysts had only lost 13 % of their initial activity at 350 °C. The reason for the much slower transport of potassium from the pure KCl layer, into the catalyst, is probably due to a lower contact area between the particles and the catalyst, despite the compression during the pellet formation.

The potassium level in three two-layer pellets of 3%V_2O_5-WO_3/TiO_2 catalyst with K_2SO_4 impregnated layers are shown in Figure 12. Two of the pellets have impregnated layers initially containing about 0.8 wt.% potassium (K/V ≈ 0.6), while the third pellet has a layer doped to a

potassium level of approximately 1.6 wt.%. One pellet is unexposed while two others have been exposed for 8 hours. For comparison, the potassium profile in a pellet with a KCl impregnated layer (0.8 wt.% potassium), also exposed for 8 hours, has been included as well. Similar to the impregnation with KCl, some potassium has moved into the undoped layer prior to exposure. Looking at the exposed pellets with impregnated layers containing 0.8 wt.% potassium from either K_2SO_4 or KCl, there is a significant difference in the potassium level in the undoped layers. For the pellet with the K_2SO_4 impregnated layer the potassium concentration has increased slightly compared to that in the unexposed pellet, and is essentially zero half way through the undoped layer, while the potassium level in the undoped layer of the pellet with the KCl impregnated layer is considerably higher. In the case of the pellet with the impregnated layer doped with 1.6 wt.% potassium from K_2SO_4, the potassium level in the undoped side, upon exposure for 8 hours, is comparable to that of the KCl impregnated pellet. Hence, potassium from K_2SO_4 appears to be half as mobile as that of KCl.

Figure 13 shows the sulfur level in the two pellets with K_2SO_4 impregnated layers. Unlike chlorine, the sulfur stays in the impregnated layer both before and after exposure. These observations may explain the apparent difference in mobility between potassium bound in KCl and K_2SO_4. It is speculated that in order for salt bound potassium to diffuse into the undoped layer, it first needs to react with a Brønsted acid site on the catalyst, e.g. through the following reactions:[7]

$$\text{-M-OH} + \text{KCl} \overset{k_{\text{KCl}}}{\rightarrow} \text{-M-OK} + \text{HCl} \quad (5)$$

$$\text{-M-OH} + \text{K}_2\text{SO}_4 \overset{k_{\text{K}_2\text{SO}_4}}{\rightleftarrows} \text{-M-OK} + \text{KHSO}_4 \quad (6)$$

$$\text{-M-OH} + \text{KHSO}_4 \overset{k_{\text{KHSO}_4}}{\rightleftarrows} \text{-M-OK} + \text{H}_2\text{SO}_4 \quad (7)$$

Where -M-OH is either a vanadium or tungsten Brønsted acid center. A difference between KCl and K_2SO_4, as indicated by the results in Figure 10 and 13, is that the reaction product of the counter ion for KCl (HCl) is gaseous and thus leaves the sample, in this way pulling the reaction towards the

right. The sulfur species are either non-volatile at the reaction conditions or significantly less volatile than HCl, which in principle could allow for the reverse reactions. Consequently, potassium bound in KCl can more easily escape its solid matrix compared to that bound in K_2SO_4 which may partly explain why potassium in KCl acts as a more efficient poison than K_2SO_4. $KHSO_4$, which is the product of reaction 6, melts at around 215 °C and may to some extent convert into $K_2S_2O_7$ at temperatures above 300 °C.[36,37] However, if salt melts were formed during exposure of the K_2SO_4 impregnated pellets, the sulfur would likely have diffused, into the undoped layer, together with potassium. The fact that chlorine leaves the sample upon short time exposure while sulfur stays in the impregnated layer, as well as the apparent twofold difference in the mobility of potassium from K_2SO_4 and KCl, observed in Figure 12, suggest that only the first potassium atom in K_2SO_4 has a reactivity comparable to that of KCl, while the reaction between $KHSO_4$ and -M-OH sites (7) is much slower, *i.e.* $k_{\mathrm{KCl}} \geq k_{\mathrm{K_2SO_4}} \gg k_{\mathrm{KHSO_4}}$.

In order to study the potassium mobility as a function of catalyst composition, a series of two-layer pellets was produced from V_2O_5-WO_3/TiO_2 catalysts with 0, 1, 3 and 6 wt.% V_2O_5 and 7 wt.% WO_3. Furthermore, a two-layer pellet of WO_3 free 3%V_2O_5/TiO_2 catalyst and one of pure fiber reinforced TiO_2 carrier were produced. In all cases the impregnated layer was made from the respective catalyst doped with KCl to a potassium level of about 1.6 wt.%, corresponding to nominal K/V ratios of 3.7, 1.2 and 0.6 for the three different (nonzero) V_2O_5 loadings. Figure 14 shows the potassium profiles in these pellets after exposure for 7 days. For the three pellets of catalyst containing both V_2O_5 and WO_3 the potassium concentration has reached comparable levels of 0.4-0.5 wt.% in the undoped layer. Hence, there does not seem to be a connection between potassium mobility and V_2O_5 loading for catalysts with relatively high WO_3 loadings. For the 3%V_2O_5/TiO_2 sample the potassium diffusion seem to have proceeded at a slower rate reaching a potassium level of about 0.25 wt.% far inside the undoped layer. Similar levels are found in the

7%WO_3/TiO_2 pellet and the pellet made from TiO_2 carrier. As indicated by the bench-scale tests, the two-layer pellet data further indicate that WO_3 promotion facilitates the potassium transport in the SCR catalyst. Furthermore, the higher potassium mobility in V_2O_5-WO_3/TiO_2 catalysts seems to be due to some interaction between V_2O_5 and WO_3 which is independent on the V_2O_5 content. The latter is also in good agreement with the observations from the activity measurements as well as the NH_3 chemisorption study.

4. Conclusion

Industrial type V_2O_5-$(WO_3)/TiO_2$ SCR catalysts have been exposed to KCl or K_2SO_4 aerosols in a bench-scale reactor in order to investigate catalyst deactivation (by potassium poisoning) under biomass firing conditions. All catalysts exposed for 240 hours or longer showed significant deactivation. Samples exposed at 150 °C rather than 300/350 °C, however, showed higher remaining activity indicating decreased potassium mobility with decreasing temperature. The K_2SO_4 exposed catalysts had deactivated considerably less than the KCl exposed ones. This could be due to K_2SO_4 being less mobile once deposited on the catalyst, which is supported by the observations from the pellet experiments. In addition, measurements showed that the particle size distribution of the K_2SO_4 aerosol obtained in the setup was shifted towards larger particles compared to that of the KCl aerosol, which may lead to a slower deposition rate of particles on the external surface of each catalyst plate. Hence, an effect of particle size on the catalyst deactivation cannot be excluded.

The relative activity of the exposed catalysts indicates that WO_3 promoted samples, which in general have higher NH_3 adsorption capacities, have lost a larger fraction of their initial activity compared to unpromoted ones. This implies that increased Brønsted acidity facilitates the potassium transport in the catalyst as well as leads to a higher equilibrium uptake, which supports the proposed theory of diffusion of potassium ions via Brønsted acid sites. This is further supported by the results

from a study on the potassium mobility in two-layer catalyst pellets of various compositions. It should, however, be noted that the absolute activity of promoted catalysts in general is significantly higher than for unpromoted samples and so it may not be favorable to use unpromoted catalysts in biomass fired systems.

The potassium mobility in SCR catalysts was studied using a novel experimental method in which pellets composed of two similar layers of catalyst were heat treated. One of the layers was impregnated with KCl or K_2SO_4 while the other layer was undoped. These investigations clearly showed that potassium bound in KCl has a much higher mobility in SCR catalysts compared to that in K_2SO_4, where only one of the potassium atoms essentially is able to leave the solid matrix. While chlorine completely left the catalyst pellet upon treatment at SCR conditions (350 °C, 6 vol.% O_2 and 3 vol.% H_2O in N_2) sulfur stayed in the sample and was immobile. The results support a view where potassium reacts with and subsequently diffuses over Brønsted acid sites in the catalyst, and that the reaction rate of salt bound potassium (KCl of K_2SO_4) is related to how strongly potassium is bound to its counter ion. The results indicate that a lower operating temperature and high conversion of KCl to K_2SO_4 will enhance the life time of an SCR catalyst.

AUTHOR INFORMATION

Corresponding Author

*Email: aj@kt.dtu.dk

Present Addresses

‡Department of Energy Process Engineering and Chemical Engineering, Technical University of Freiberg, Fuchsmühlenweg 9, 09596 Freiberg, Germany

ACKNOWLEDGMENTS

The Danish Council for Strategic Research is gratefully acknowledged for funding this work which is a part of the GREEN Research Center (DSF-10-093956).

NOMENCLATURE

C_{NH_3} = gas phase concentration of NH_3 (kmol/m^3)

C_{NO} = gas phase concentration of NO (kmol/m^3)

d = distance (m)

d_p = particle diameter (m)

$d_{p,a}$ = aerodynamic particle diameter (m)

F_{gas} = gas flow rate (m^3/s)

k' = pseudo first order rate constant (m^3/kg/s)

k'_0 = pseudo first order rate constant of fresh catalyst (m^3/kg/s)

$k_{K_2SO_4}$ = rate constant for the reaction between K_2SO_4 and -M-OH sites (1/s)

k_{KCl} = rate constant for the reaction between KCl and -M-OH sites (1/s)

k_{KHSO_4} = rate constant for the reaction between $KHSO_4$ and -M-OH sites (1/s)

K_{NH_3} = NH_3 adsorption equilibrium constant (m^3/kmol)

k_r = intrinsic rate constant (m^3/kg/s)

M = mass based aerosol concentration (kg/Nm^3)

m_{cat} = catalyst mass (kg)

$-r_{NO}$ = NO reduction rate (kmol/kg/s)

T = temperature (°C)

w_{Cl} = mass fraction of chlorine

w_K = mass fraction of potassium

w_S = mass fraction of sulfur

X_{NO} = conversion of NO

REFERENCES

(1) Bosch, H.; Janssen, F. Catalytic reduction of nitrogen oxides – A review on the fundamentals and technology. *Catal. Today* **1988,** *2*, 369-532.

(2) Forzatti, P. Present status and perspectives in de-NO_x SCR catalysis. *Appl. Catal. A* **2001,** *222*, 221-236.

(3) Topsøe, N.-Y. Mechanism of the Selective Catalytic Reduction of Nitric Oxide by Ammonia Elucidated by in Situ On-Line Fourier Transform Infrared Spectroscopy. *Science* **1994,** *265*, 1217-1219.

(4) Topsøe, N.-Y.; Dumesic, J. A.; Topsøe, H. Vanadia/Titania Catalysts for Selective Catalytic Reduction of Nitric Oxide by Ammonia – II. Studies of Active Sites and Formulation of Catalytic Cycles. *J. Catal.* **1995**, *151*, 241-252.

(5) Dumesic, J. A.; Topsøe, N.-Y.; Topsøe, H.; Chen, Y.; Slabiak, T. Kinetics of Selective Catalytic Reduction of Nitric Oxide by Ammonia over Vanadia/Titania. *J. Catal.* **1996,** *163*, 409-417.

(6) Sander, B. Properties of Danish Biofuels and the Requirements for Power Production. *Biomass Bioenergy* **1997,** *12*, 177-183.

(7) Zheng, Y.; Jensen, A. D.; Johnsson, J. E. Laboratory Investigation of Selective Catalytic Reduction Catalysts: Deactivation by Potassium Compounds and Catalyst Regeneration. *Ind. Eng. Chem. Res.* **2004,** *43*, 941-947.

(8) Christensen, K. A.; Livbjerg, H. A Field Study of Submicron Particles from the Combustion of Straw. *Aerosol Sci. Technol.* **1996,** *25*, 185-199.

(9) Christensen, K. A.; Stenholm, M.; Livbjerg, H. The Formation of Submicron Aerosol Particles, HCl and SO_2 in Straw-Fired Boilers. *J. Aerosol Sci.* **1998,** *29*, 421-444.

(10) Zheng, Y.; Jensen, A. D.; Johnsson, J. E. Deactivation of V_2O_5-WO_3-TiO_2 SCR catalyst at a biomass-fired combined heat and power plant. *Appl. Catal. B* **2005,** *60*, 253-264.

(11) Zheng, Y.; Jensen, A. D.; Johnsson, J. E.; Thøgersen, J. R. Deactivation of V_2O_5-WO_3-TiO_2 SCR catalyst at biomass fired power plants: Elucidation of mechanisms by lab- and pilot-scale experiments. *Appl. Catal. B* **2008,** *83*, 186-194.

(12) Kling, Å.; Andersson, C.; Myringer, Å.; Eskilsson, D.; Järås, S. G. Alkali deactivation of high-dust SCR catalysts used for NO_x reduction exposed to flue gas from 100 MW-scale biofuel and peat fired boilers: Influence of flue gas composition. *Appl. Catal. B.* **2007,** *69*, 240-251.

(13) Chen, J. P.; Yang, R. T. Mechanism of Poisoning of the V_2O_5/TiO_2 Catalyst for the Reduction of NO by NH_3. *J. Catal.* **1990,** *125*, 411-420.

(14) Kamata, H.; Takahashi, K.; Odenbrand, C. U. I. The role of K_2O in the selective reduction of NO with NH_3 over a $V_2O_5(WO_3)/TiO_2$ commercial selective catalytic reduction catalyst. *J. Mol. Catal. A: Chem.* **1999,** *139*, 189-198.

(15) Nicosia, D.; Elsener, M.; Kröcher, O.; Jansohn, P. Basic investigation of the chemical deactivation of V_2O_5/WO_3-TiO_2 SCR catalysts by potassium, calcium, and phosphate. *Top. Catal.* **2007,** *42-43*, 333-336.

(16) Klimczak, M.; Kern, P.; Heinzelmann, T.; Lucas, M.; Claus, P. High-throughput study of the effects of inorganic additives and poisons on NH_3-SCR catalysts–Part I: V_2O_5-WO_3/TiO_2 catalysts. *Appl. Catal. B* **2010,** *95*, 39-47.

(17) Chen, L.; Li, J.; Ge, M. The poisoning effect of alkali metals doping over nano V_2O_5-WO_3/TiO_2 catalysts on selective catalytic reduction of NOx by NH_3. *Chem. Eng. J.* **2011,** *170*, 531-537.

(18) Si-Ahmed, H.; Calatayud, M.; Minot, C.; Lozano Diz, E.; Lewandowska, A.E.; Bañares, M.A. Combining theoretical description with experimental *in situ* studies on the effect of potassium on the structure and reactivity of titania-supported vanadium oxide catalyst. *Catal. Today* **2007,** 126, 96-102.

(19) Nicosia, D.; Czekaj, I.; Kröcher, O. Chemical deactivation of V_2O_5/WO_3-TiO_2 SCR catalysts by additives and impurities from fuels, lubrication oils and urea solution: Part II. Characterization study of the effect of alkali and alkaline earth metals. *Appl. Catal. B* **2008,** *77*, 228-236.

(20) Tang, F.; Xu, B.; Shi, H.; Qiu, J.; Fan, Y. The poisoning effect of Na^+ and Ca^{2+} ions doped on the V_2O_5/TiO_2 catalysts for selective catalytic reduction of NO by NH_3. *Appl. Catal. B* **2010,** *94*, 71-76.

(21) Ramis, G.; Busca, G.; Bregani, F.; Forzatti, P. Fourier Transform-Infrared Study of the Adsorption and Coadsorption of Nitric Oxide, Nitrogen Dioxide and Ammonia on Vanadia-Titania and Mechanism of Selective Catalytic Reduction. *Appl. Catal.* **1990,** *64*, 259-278.

(22) Tronconi, E.; Forzatti, P.; Gomez Martin, J. P.; Malloggi, S. Selective Catalytic Removal of NO_x: A Mathematical Model for Design of Catalyst and Reactor. *Chem. Eng. Sci.* **1992,** *47*, 2401-2406.

(23) Koebel, M.; Elsener, M. Selective catalytic reduction of NO over commercial $DeNO_x$-catalysts: experimental determination of kinetic and thermodynamic parameters. *Chem. Eng. Sci.* **1998,** *53*, 657-669.

(24) Alemany, L. J; Lietti, L.; Ferlazzo, N.; Forzatti, P.; Busca, G.; Giamello, E.; Bregani, F. Reactivity and Physicochemical Characterisation of V_2O_5-WO_3/TiO_2 De-NO_x Catalysts. *J. Catal.* **1995,** *155*, 117-130.

(25) Lietti, L.; Forzatti, P.; Bregani, F. Steady-State and Transient Reactivity Study of TiO_2-Supported V_2O_5-WO_3 De-NO_x Catalysts: Relevance of the Vanadium-Tungsten Interaction on the Catalytic Activity. *Ind. Eng. Chem. Res.* **1996,** *35*, 3884-3892.

(26) Kompio, P. G. W. A.; Brückner, A.; Hipler, F.; Auer, G.; Löffler, E.; Grünert, W. A new view on the relations between tungsten and vanadium in V_2O_5-WO_3/TiO_2 catalysts for the selective reduction of NO with NH_3. *J. Catal.* **2012,** *286*, 237-247.

(27) Ramis, G.; Busca, G.; Cristiani, C.; Lietti, L.; Forzatti, P.; Bregani, F. Characterization of Tungsta-Titania Catalysts. *Langmuir* **1992,** *8*, 1744-1749.

(28) Chen, J. P.; Yang, R. T. Role of WO_3 in mixed V_2O_5-WO_3/TiO_2 catalysts for selective catalytic reduction of nitric oxide with ammonia. *Appl. Catal. A* **1992,** *80*, 135-148.

(29) Alemany, L. J.; Berti, F.; Busca, G.; Ramis, G.; Robba, D.; Toledo, G. P.; Trombetta, M. Characterization and composition of commercial V_2O_5-WO_3-TiO_2 SCR catalysts. *Appl. Catal. B* **1996,** *10*, 299-311.

(30) Amiridis, M. D.; Duevel, R. V.; Wachs, I. E. The effect of metal oxide additives on the activity of V_2O_5/TiO_2 catalysts for the selective catalytic reduction of nitric oxide by ammonia. *Appl. Catal. B* **1999,** *20*, 111-122.

(31) Khodayari, R.; Andersson, C.; Odenbrand, C. U. I.; Andersson, L. H. Deactivation and Regeneration of SCR Catalysts used in Bio Fuel Power Plants. *Proceedings of the 5th European*

Conference on Industrial Furnace and Boilers, volume II, Espinho-Porto, Portugal, April 11-14, 2000.

(32) Wang, L.; Hustad, J. E.; Skreiberg, Ø.; Skjevrak, G.; Grønli, M. A critical review on additives to reduce ash related operation problems in biomass combustion applications. *Energy Procedia*, **2012,** *20*, 20-29.

(33) Chen, J. P.; Buzanowski, M. A.; Yang, R. T.; Cichanowicz, J. E. Deactivation of the Vanadia Catalyst in the Selective Catalytic Reduction Process. *J. Air Waste Manage. Assoc.* **1990,** *40*, 1403-1409.

(34) Larsson, A.-C.; Einvall, J.; Andersson, A.; Sanati, M. Targeting by Comparison with Laboratory Experiments the SCR Catalyst Deactivation Process by Potassium and Zinc Salts in a Large-Scale Biomass Combustion Boiler. *Energy Fuels* **2006,** *20*, 1398-1405.

(35) Eriksen, K. M.; Fehrmann, R.; Hatem, G.; Gaune-Escard, M.; Lapina, O. B.; Mastikhin, V. M. Conductivity, NMR, Thermal Measurements, and Phase Diagram of the $K_2S_2O_7$–$KHSO_4$ System. *J. Phys. Chem.* **1996,** *100*, 10771-10778.

(36) Knudsen, C. B.; Kalampounias, A. G.; Fehrmann, R.; Boghosian, S. Thermal Dissociation of Molten $KHSO_4$: Temperature Dependence of Raman Spectra and Thermodynamics. *J. Phys. Chem. B* **2008,** *112*, 11996-12000.

FIGURES

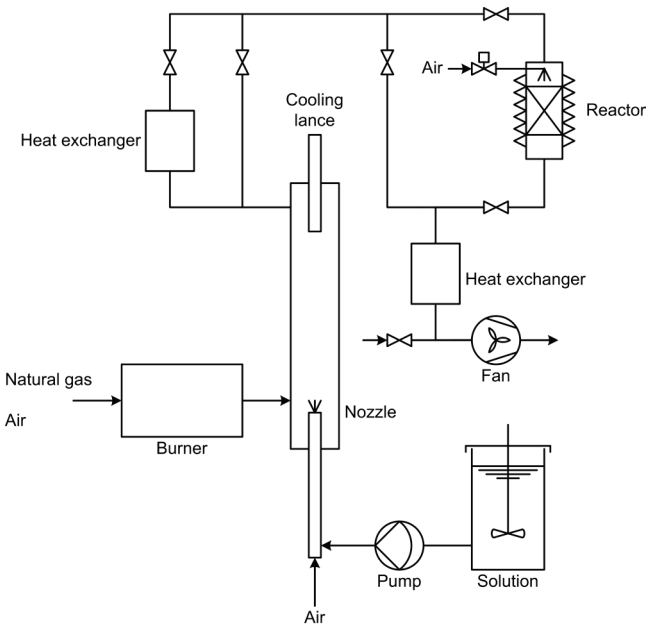

Figure 1. Schematic drawing of the bench-scale setup for aerosol exposure of SCR catalyst plates.

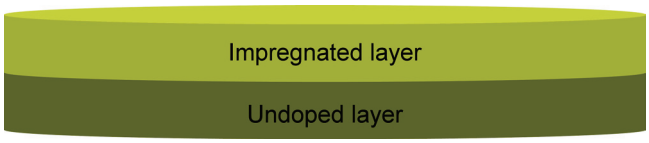

Figure 2. Principle sketch of two-layer pellet.

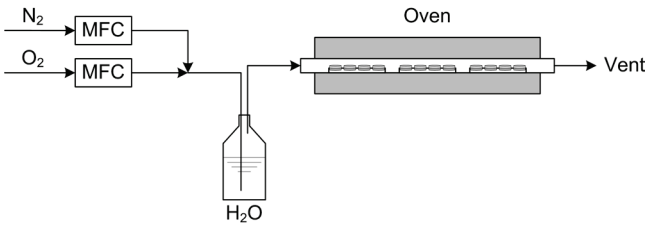

Figure 3. Schematic drawing of the lab-scale setup for exposure of two-layer pellets.

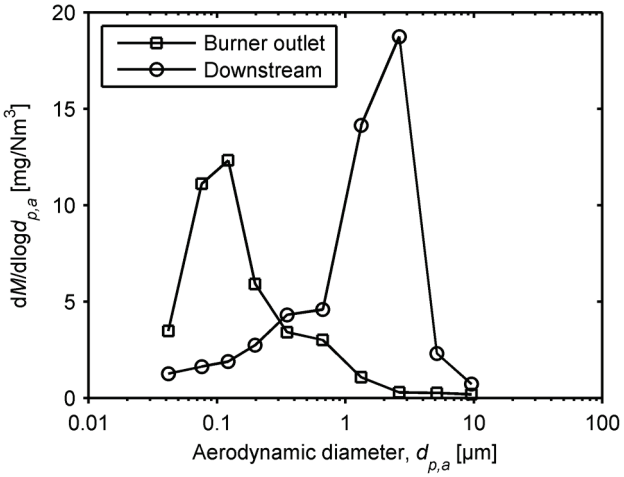

Figure 4. Mass based size distributions obtained during injection of a 0.1 M KCl solution at 420 mL/h at the burner outlet (flue gas temperature ≈ 1075 °C) as well as downstream the burner (flue gas temperature ≈ 550 °C).

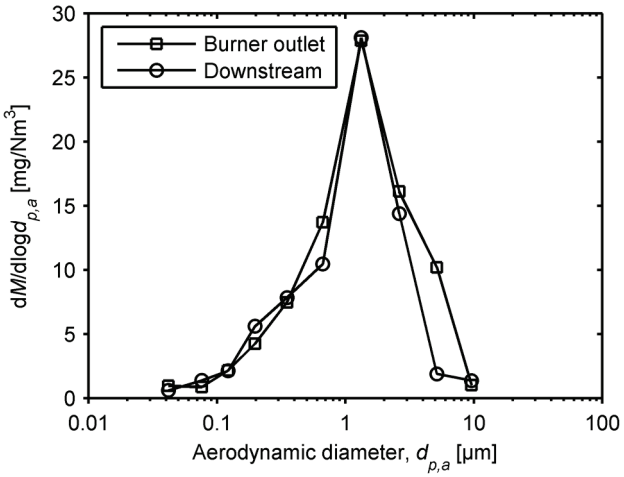

Figure 5. Mass based size distributions obtained during injection of a 0.05 M K_2SO_4 solution at 420 mL/h at the burner outlet (flue gas temperature ≈ 1075 °C) as well as downstream the burner (flue gas temperature ≈ 550 °C).

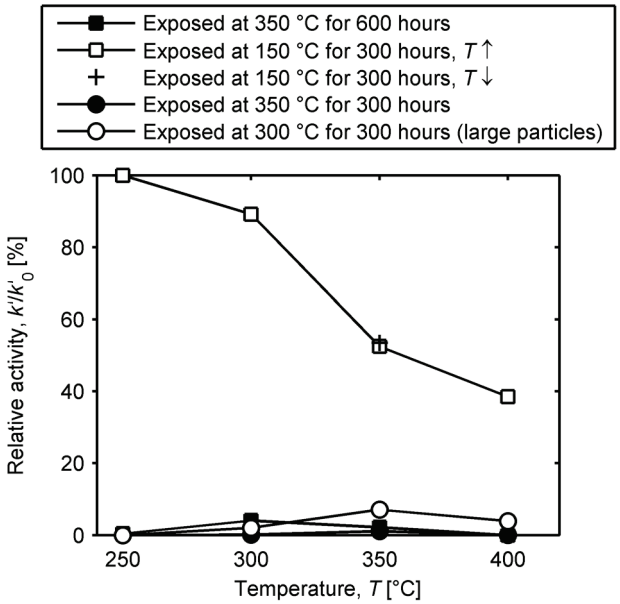

Figure 6. Relative catalytic activities of KCl exposed 3%V_2O_5-7%WO_3/TiO_2 catalysts as functions of temperature. Measurement conditions: [NO] = 500 ppmv, [NH_3] = 600 ppmv, [O_2] = 5 vol.%, [H_2O] ≈ 1.4 vol.%, balance N_2. Total flow = 2800 mL/min.

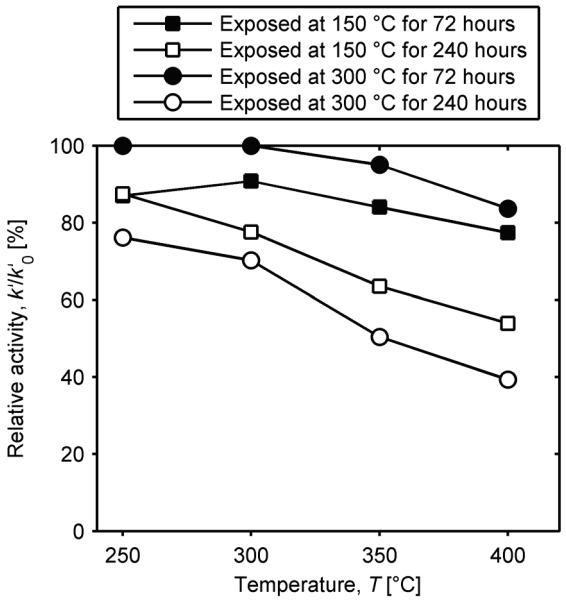

Figure 7. Relative catalytic activities of K_2SO_4 exposed $3\%V_2O_5$-$7\%WO_3/TiO_2$ catalysts as functions of temperature. Measurement conditions: [NO] = 500 ppmv, [NH_3] = 600 ppmv, [O_2] = 5 vol.%, [H_2O] ≈ 1.4 vol.%, balance N_2. Total flow = 2800 mL/min.

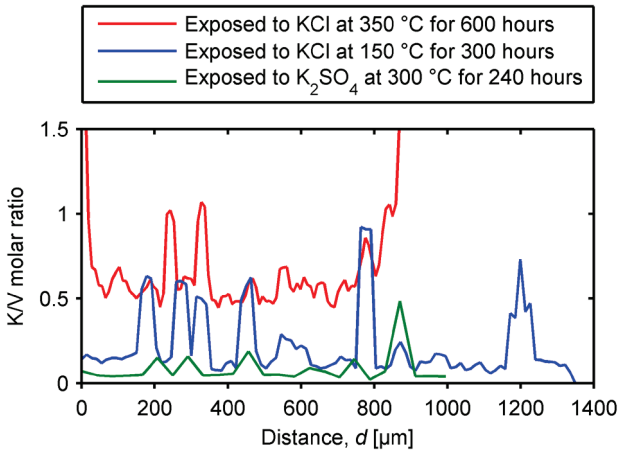

Figure 8. K/V molar ratios across the thickness of $3\%V_2O_5$-$7\%WO_3/TiO_2$ catalyst plates exposed to aerosols of KCl or K_2SO_4.

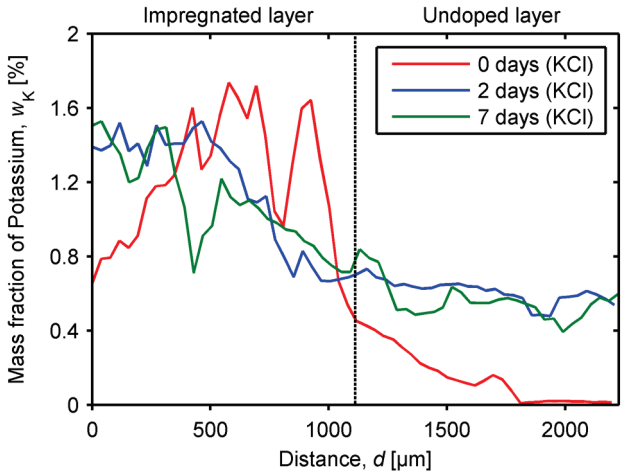

Figure 9. Potassium profiles in KCl impregnated (1.6 wt.% K, nominal) two-layer pellets of 3%V_2O_5-WO_3/TiO_2 catalyst, exposed to a flow (1000 NmL/min) of 6 vol.% O_2 and 3 vol.% H_2O in N_2 at 350 °C for 0-7 days.

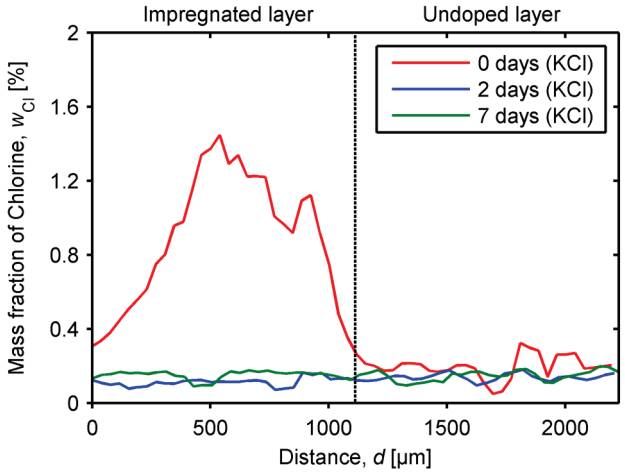

Figure 10. Chlorine profiles in KCl impregnated (1.6 wt.% K, nominal) two-layer pellets of 3%V_2O_5-WO_3/TiO_2 catalyst, exposed to a flow (1000 NmL/min) of 6 vol.% O_2 and 3 vol.% H_2O in N_2 at 350 °C for 0-7 days.

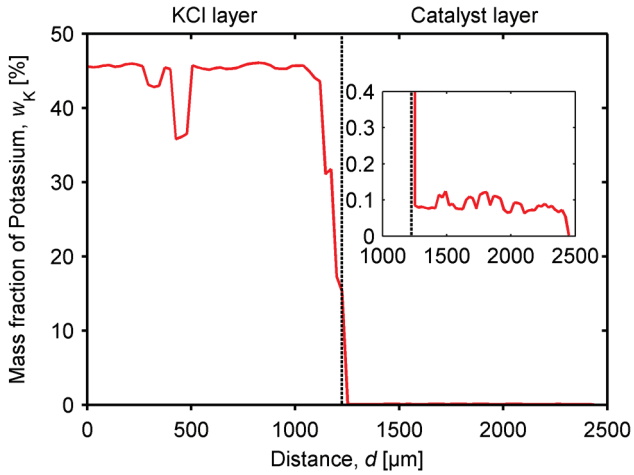

Figure 11. Potassium profiles in a two-layer pellet containing a layer of pure KCl and a layer of a 3%V_2O_5-7WO_3/TiO_2 catalyst, exposed to a flow (1000 NmL/min) of 6 vol.% O_2 and 3 vol.% H_2O in N_2 at 350 °C for 7 days.

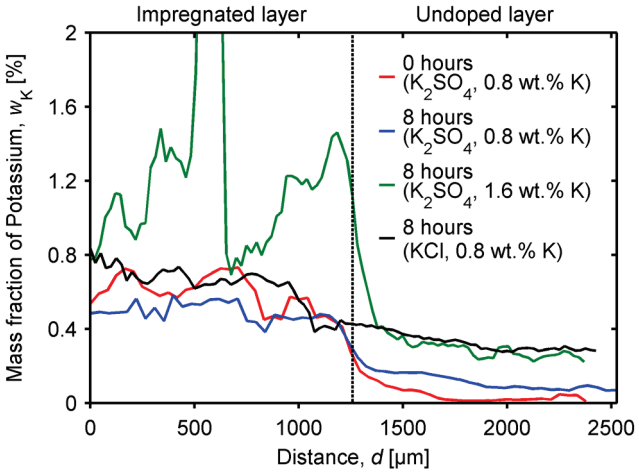

Figure 12. Potassium profiles in K_2SO_4 or KCl impregnated (0.8-1.6 wt.% K, nominal) two-layer pellets of 3%V_2O_5-WO_3/TiO_2 catalyst, exposed to a flow (1000 NmL/min) of 6 vol.% O_2 and 3 vol.% H_2O in N_2 at 350 °C for 0-8 hours.

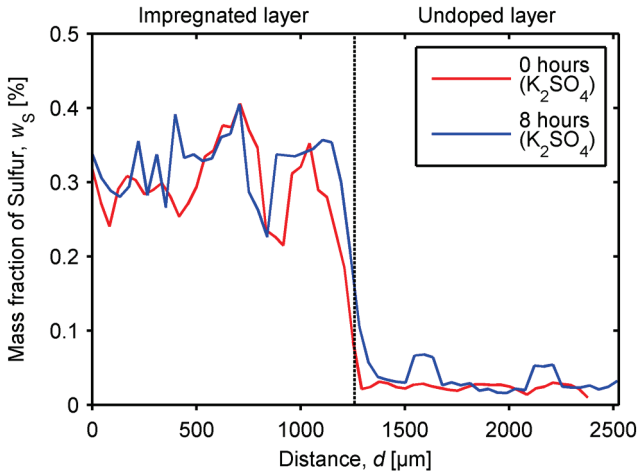

Figure 13. Sulfur profiles in K_2SO_4 impregnated (0.8 wt.% K, nominal) two-layer pellets of 3%V_2O_5-WO_3/TiO_2 catalyst, exposed to a flow (1000 NmL/min) of 6 vol.% O_2 and 3 vol.% H_2O in N_2 at 350 °C for 0-8 hours.

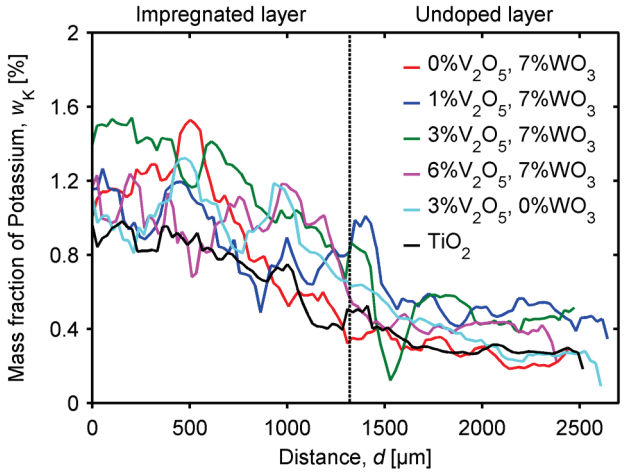

Figure 14. Potassium profiles in KCl impregnated (1.6 wt.% K, nominal) two-layer pellets of V_2O_5-(WO_3)/TiO_2 catalysts, exposed to a flow (1000 NmL/min) of 6 vol.% O_2 and 3 vol.% H_2O in N_2 at 350 °C for 7 days.

TABLES

Table 1. NH_3 chemisorption capacities of V_2O_5-(WO_3)/TiO_2 catalysts measured at 250 °C.

V_2O_5 content [wt. %]	NH_3 chemisorption capacity [μmol/g]	
	0 wt.% WO_3	7 wt.% WO_3
1	41	81
3	66	66
6	70	81

Table 2. Exposure conditions and relative activities of V_2O_5-(WO_3)/TiO_2 catalysts.

Entry no.	V_2O_5 content [wt. %]	Potassium source	Temperature [°C]	Time [h]	Aerosol distribution mode [µm]	Relative activity at 350 °C [%]	
						a) 0 wt.% WO_3	b) 7 wt.% WO_3
1	1	KCl	350	600	0.12	24	11
2	3	KCl	350	600	0.12	19	2
3	6	KCl	350	600	0.12	1	4
4	1	KCl	150	300	0.12	77	29
5	3	KCl	150	300	0.12	32	52
6	6	KCl	150	300	0.12	47	34
7	1	KCl	350	300	0.12	0	6
8	3	KCl	350	300	0.12	14	1
9	6	KCl	350	300	0.12	2	3
10	3	KCl	300	300	2.6	n.p.[a]	7
11	6	KCl	300	300	2.6	n.p.	1
12	3	K_2SO_4	150	72	1.3	n.p.	84
13	3	K_2SO_4	150	240	1.3	77	64
14	3	K_2SO_4	300	72	1.3	n.p.	95
15	3	K_2SO_4	300	240	1.3	37	50

[a] *n.p.:* Experiment not performed.